OPG's DEEP GEOLOGIC

REPOSITORY

FOR LOW & INTERMEDIATE LEVEL WASTE

Postclosure Safety Assessment: Data

March 2011

Prepared by: Quintessa Ltd. and Geofirma Engineering Ltd.

NWMO DGR-TR-2011-32

Quintessa Geofirma Engineering Ltd

OPG's DEEP GEOLOGIC

REPOSITORY

FOR LOW & INTERMEDIATE LEVEL WASTE

Postclosure Safety Assessment: Data

March 2011

Prepared by: Quintessa Ltd. and Geofirma Engineering Ltd.

NWMO DGR-TR-2011-32

THIS PAGE HAS BEEN LEFT BLANK INTENTIONALLY

Document History

Title:	Postclosure Safety Assessment: Data		
Report Number:	NWMO DGR-TR-2011-32		
Revision:	R000	**Date:**	March 2011
Quintessa Ltd. and Geofirma Engineering Ltd.[1]			
Prepared by:	R. Walke, P. Humphreys, F. King, R. Little, R. Metcalfe, J. Penfold, G. Towler, R. Walsh, J. Wilson		
Reviewed by:	M. Thorne and R. Jackson		
Approved by:	R. Little		
Nuclear Waste Management Organization			
Reviewed by:	H. Leung, K. Sedor		
Accepted by:	P. Gierszewski		

[1] Previously known as Intera Engineering Ltd.

THIS PAGE HAS BEEN LEFT BLANK INTENTIONALLY

EXECUTIVE SUMMARY

Ontario Power Generation (OPG) is proposing to build a Deep Geologic Repository (DGR) for Low and Intermediate Level Waste (L&ILW) near the existing Western Waste Management Facility at the Bruce nuclear site in the Municipality of Kincardine, Ontario. The Nuclear Waste Management Organization, on behalf of OPG, is preparing the Environmental Impact Statement (EIS) and Preliminary Safety Report (PSR) for the proposed repository.

The postclosure safety assessment (SA) evaluates the long-term safety of the proposed facility and provides supporting information for the EIS and PSR.

The present report provides a collation of reference information for the assessment of the Normal Evolution Scenario in a clear and well-documented manner. The report includes waste, repository, geosphere, biosphere and exposure data. The data presented in this report are the reference data for the Normal Evolution Scenario. Data specific to Disruptive Scenarios are presented in the reports where those scenarios are assessed.

The assessment has adopted scientifically informed, physically realistic point values for data that can be justified on the basis of the results of research and investigation. Where there are high levels of uncertainty and/or variability associated with data, conservative but physically plausible assumptions have been adopted to allow the impacts of uncertainties/variability to be bounded. Uncertainties and variability in data for some parameters are accounted for through the use of probability distribution functions (PDFs). The biosphere model adopts a deterministic approach, based on 95th percentile characteristics of the critical group consistent with the guidance from the Canadian Standards Association.

While a wide range of data sources has been used to populate the report, key data compilations have been used for each component of the DGR system, including:

- Waste data from the Inventory report for L&ILW;
- Repository data from the preliminary design given in the PSR;
- Geosphere data from the Geosynthesis and Descriptive Site Model reports; and
- Biosphere and exposure data from the latest relevant Bruce nuclear site environmental assessment and derived release limit reports.

THIS PAGE HAS BEEN LEFT BLANK INTENTIONALLY

TABLE OF CONTENTS

LIST OF TABLES

Page

LIST OF FIGURES

Page

1. INTRODUCTION

Ontario Power Generation (OPG) is proposing to build a Deep Geologic Repository (DGR) for Low and Intermediate Level Waste (L&ILW) near the existing Western Waste Management Facility (WWMF) at the Bruce nuclear site in the Municipality of Kincardine, Ontario (Figure 1.1). The Nuclear Waste Management Organization, on behalf of OPG, is preparing the Environmental Impact Statement (EIS) and Preliminary Safety Report (PSR) for the proposed repository.

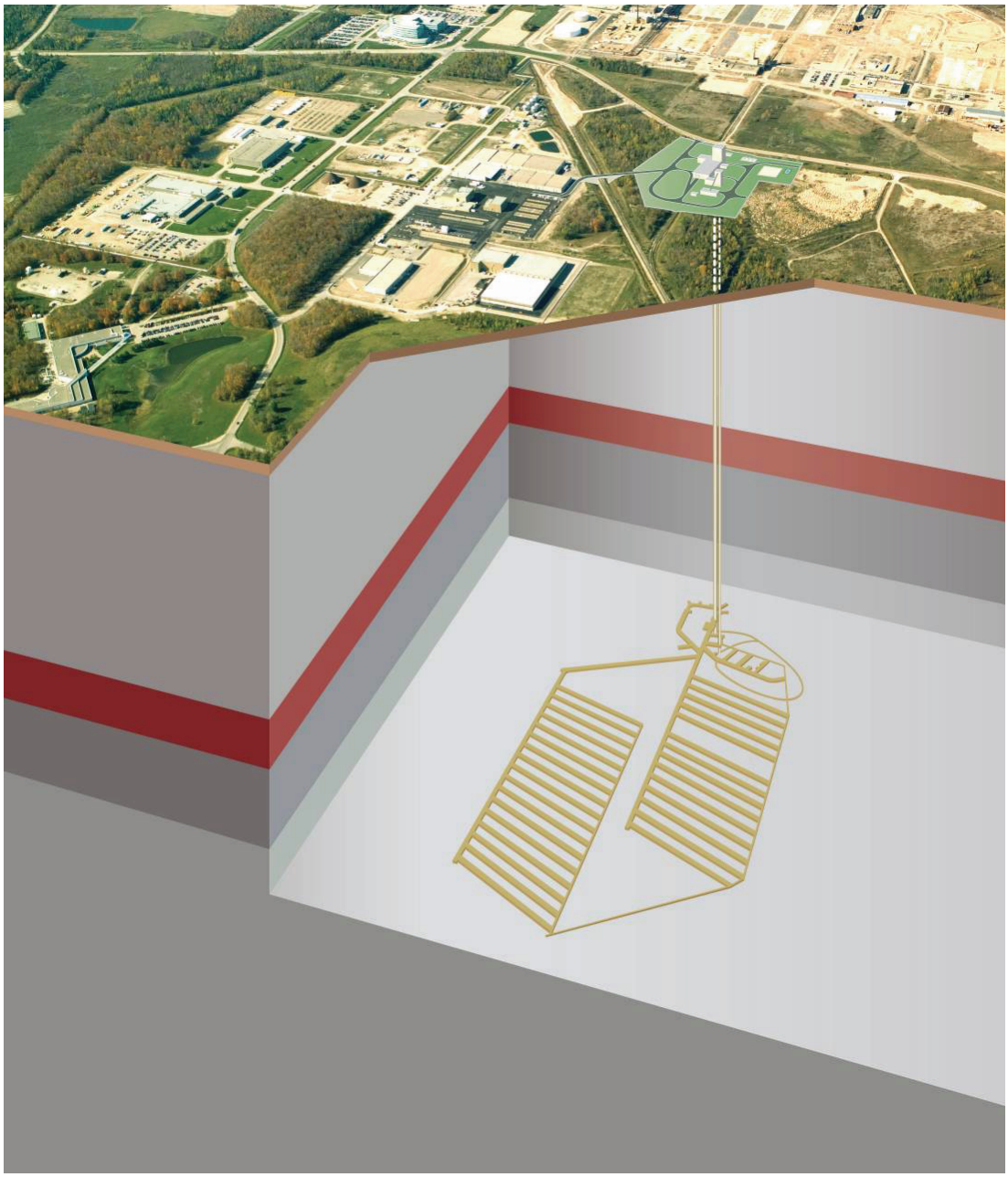

Figure 1.1: The DGR Concept at the Bruce Nuclear Site

The postclosure safety assessment (SA) evaluates the long-term safety of the proposed facility and provides supporting information for the EIS (OPG 2011a) and PSR (OPG 2011b).

This report (Data) is one of a suite of documents that presents the postclosure safety assessment (Figure 1.2), which also includes the Postclosure SA main report (QUINTESSA et al. 2011a), the Normal Evolution Scenario Analysis report (QUINTESSA 2011a), the Human Intrusion and Other Disruptive Scenarios Analysis report (QUINTESSA and SENES 2011), the System and Its Evolution report (QUINTESSA 2011b), the Features, Events and Processes report (QUINTESSA et al. 2011b), the Groundwater Modelling report (GEOFIRMA 2011), and the Gas Modelling report (GEOFIRMA and QUINTESSA 2011).

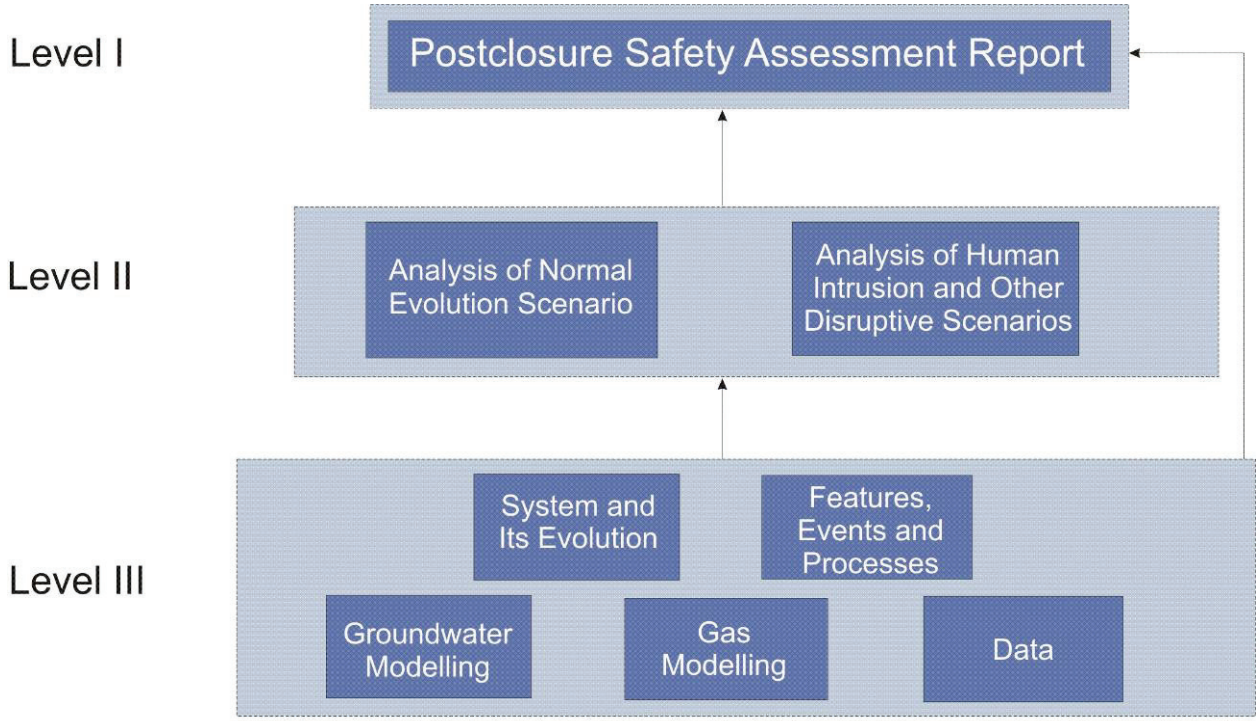

Figure 1.2: Document Structure for the Postclosure Safety Assessment

1.1 Purpose and Scope

The purpose of this report is to provide a collation of reference information for the assessment of the Normal Evolution Scenario in a clear and well-documented manner. The data presented in this report are the reference data for the Normal Evolution Scenario. Data specific to particular calculation cases and for Disruptive Scenarios are presented in other reports as needed.

The emphasis is on the collation of data for safety assessment calculations, rather than for site characterization or repository design purposes. The information in the report has been used to support screening, assessment and detailed calculations relating to the Normal Evolution Scenario.

1.2 Report Outline

The report is organized as follows:

- Chapter 2 provides an overview of the approach that has been used for data selection;
- Chapter 3 describes the waste data, including the waste categories, containers, conditioning and physical, radiological and chemical characteristics;
- Chapter 4 describes the repository data, including its layout, waste handling and emplacement, engineered barriers, flow paths, and water and gas flow and transport parameters in the repository;
- Chapter 5 describes the geosphere data, including the geological setting, the characteristics of the damaged zone around the repository and its shafts, the geosphere and geosphere-biosphere interface, flow paths, and water and gas flow and transport parameters in the geosphere;
- Chapter 6 describes the biosphere data, including surface water, soil and sediment, atmosphere, plant, and animal parameters;
- Chapter 7 describes the exposure data, including information concerning potential critical groups, human dose and intake coefficients, and non-human biota; and
- Chapter 8 provides a brief summary, describing the key updates since the previous data report (Walke et al. 2009).

The report has been written for a technical audience that is familiar with: the scope and objectives of the DGR project; the Bruce nuclear site; and the process of assessing the long-term safety of radioactive waste disposal.

2. APPROACH TO DATA SELECTION

2.1 Data Sources

A wide range of data sources has been used in the report; full details are provided in the relevant sections. Nevertheless, it is possible to identify certain key data compilations for each component of the DGR system:

- Waste and waste packaging – the Reference L&ILW Inventory Report (OPG 2010);
- Repository – Chapter 6 (Facility Description) of the PSR (OPG 2011b);
- Geosphere – the Descriptive Geosphere Site Model report (INTERA 2011); and
- Biosphere – the Technical Support Documents supporting the Environmental Assessment (EA) for the DGR (GOLDER 2011a to g and AMEC NSS 2011) and the EA Study Report for the WWMF (OPG 2005a).

In general, preference has been given to the use of data from site-specific sources (i.e., from studies undertaken locally to the Bruce nuclear site), where they exist. In the absence of site-specific data, regional sources have been used instead or, in their absence, "generic" sources, such as international or other national studies.

It should be noted that the postclosure safety assessment was initiated based on an original preliminary design documented in NWMO (2010a). The change to the final preliminary design was made after the present assessment was largely complete and so information relating to both designs are presented in this report.

2.2 Parameter Uncertainty and Variability

Parameter uncertainty and variability need to be taken into account when recommending parameter values for use in assessment calculations. **Uncertainty** arises due to incomplete or imprecise knowledge of processes and conditions, for example, uncertainty in the estimation of repository and geosphere solubility limits and sorption coefficients due to incomplete knowledge of evolving geochemical conditions. In contrast, **variability** arises from processes and features considered varying naturally in time and/or space across the system being considered, for example, variation in corrosion rates between different packages or at different times.

2.2.1 Uncertainty

It is helpful to recognize the potential sources of parameter uncertainty when reviewing information on which to base recommendations for parameter values/distributions. Parameter uncertainty can arise for a number of reasons, including:

- Many parameters are known on a purely empirical basis, and their range of applicability may be uncertain;
- Macroscopic processes made up of complex lower scale processes are frequently represented using coarse grained or lumped parameters, which approximate the process;
- Values obtained from observational data will contain measurement errors; and
- Observational data may be lacking.

The complexity of issues that arise in addressing uncertainty when making parameter recommendations is highlighted by the overlap between parameter uncertainty and future

uncertainty, given that uncertainty in parameters describing processes that undergo environmental or cultural change is likely to increase as the calculations are extended further and further into the future.

2.2.2 Variability

Temporal variability can be taken into account in a number of ways.

- Through explicit representation of time-dependency by including time-dependent parameters - Some parameters may change significantly over the time period relevant to the assessment, for example, hydraulic conductivity of concrete engineering structures will change as the chemical conditions evolve over hundreds of years after construction. Such changes can be explicitly represented through the adoption of time-dependent parameters in an assessment model. Information concerning the time-dependency would therefore be required in the parameter data report.
- Through adopting a suitable time-averaged value - Many parameters are likely to fluctuate over relatively short timescales in relation to the overall assessment. An assessment-level model is unlikely to need to represent this small-scale temporal variability explicitly in calculations, and a time-averaged value/distribution could be applied based on a minimum time period for averaging.
- Through the use of steady-state values from the range of possible time-dependent values to either bound or test sensitivity to time-dependence.

Spatial variability will exist on almost any scale that is considered in the system being assessed. It is also an example of the strong link between the conceptual model, mathematical model and the parameter requirements given that the way spatial variability is modelled will be influenced by the scale of discretization of system components. Assessments will typically aim to use representative properties at a particular scale for the spatially varying media modelled, looking to adopt average properties at that scale. The averaging scale used will be influenced by practical considerations in the modelling but also by data availability. In each case, the way variability is handled, including the choice of the scale used for averaging, should be described, and, if necessary, the uncertainty in results that arises from the adopted approach can be explored through deterministic or probabilistic calculations.

2.2.3 Treatment of Uncertainty and Variability

The assessment has adopted scientifically informed, physically realistic assumptions for data that are understood and can be justified on the basis of the results of research and investigation. Where there are high levels of uncertainty and/or variability associated with data (e.g., the habits and characteristics for representative persons from potential critical groups), conservative, but physically plausible, assumptions have been adopted to allow the impacts of uncertainties/variability to be bounded. Uncertainties and variability in data are accounted for through the use of probability distribution functions (PDFs). These functions reflect the full uncertainty and variability of the parameter, and not just the uncertainty associated with a best estimate value.

Mishra (2002) provides guidance on assigning probability distributions to input parameters. The approach described in Mishra (2002) of using subjective distributions based on expert judgement has been used to assign PDFs for most uncertain/variable parameters. The impact of key uncertain parameters can be tested through probabilistic and deterministic sensitivity studies.

3. WASTE DATA

3.1 Waste Categories

The proposed DGR will accept Low & Intermediate Level waste (L&ILW) from the operation and refurbishment of nuclear power stations owned by Ontario Power Generation. The DGR will not accept used nuclear fuel.

A description of the L&ILW wastes proposed for emplacement in the DGR is presented in the Reference L&ILW Inventory Report (OPG 2010). This presents the summary information on waste categories as well as the constituent materials, radioactivity content and non-radioactive species content. The categorization of the wastes is consistent with that used to track the wastes in the OPG Integrated Waste Tracking System, and is based on 10 operational LLW categories, 7 operational ILW categories, and 5 refurbishment L&ILW waste categories.

The waste categories for postclosure safety assessment are discussed further below.

3.1.1 LLW

The LLW classification scheme used here is based on that used by OPG (2010). However, it does not distinguish between ash from the old and more recently installed incinerator, and feeder pipes have been categorized with non-processible (other) wastes. This is because not all data distinguish these categories (e.g., bulk material inventory) and they are not significantly different from other similar wastes.

The number of resultant LLW categories, 10, is similar to those often considered by other safety assessment studies (e.g., the SAFE project for the Swedish SFR repository, Riggare and Johansson 2001). Further amalgamation of the waste categories would mean that information on distinct physical and/or radiological characteristics would be lost. In addition, it is likely to be of interest to distinguish between waste categories in terms of their contribution to postclosure safety (for example, whether one waste category dominates).

The LLW categories used in the Postclosure safety assessment are summarized in Table 3.1, based on OPG (2010) Tables 2.2 and 3.1.

3.1.2 ILW

The inventory of OPG's ILW wastes is derived from Tables 2.3 and 3.1 of OPG (2010), which gives information on volume arisings for moderator resins, Primary Heat Transport (PHT) resins, miscellaneous resins, irradiated core components, filters & filter elements, ion exchange (IX) columns and re-tube fuel channel wastes. OPG (2010) distinguishes between pressure tubes, end fittings, calandria tubes and calandria tube inserts in the retube waste inventory. The ILW waste categories are suitable for consideration in safety assessment modelling and are summarized in Table 3.2.

Table 3.1: Low Level Waste Categories

Waste Category	Description
Bottom ash	Heterogeneous ash and clinker from waste incineration.
Baghouse ash	Fine homogeneous ash from waste incineration.
Compacted wastes (bales)	Compacted empty waste drums, rubber hoses, rubber area floor matting, light gauge metals, welding rods, plastic conduit, fire blankets and fire retardant material, metal cans, insulation, ventilation filters, air hoses, metal mop buckets and presses, electric cable (<1/4" dia), lathe turnings, metal filings, glass, plastic suits (Mark III/IV), rubbers, Vicraft hoods, rubber gloves, etc.
Compacted wastes (boxes)	Same as compact bales.
Non-Processible (boxes)	Respirator filters, heavy gauge metal (e.g., beams, IX vessels, angle iron, plate metal), concrete and cement blocks, metal components (e.g., pipe, scaffolding pipes, metal planks, motors, flanges, valves), wire cables and slings, electric cables (>1/4" dia), tools, paper, plastic, absorbent products, laboratory sealed sources, etc. Also includes feeder pipes for the purposes of the safety assessment.
Non-Processible (drums)	Floor sweepings, Dust Bane, Stay Dry, metal filings, glassware, light bulbs, bituminized low-level waste, etc.
Non-Processible (other)	Large and irregularly shaped objects such as heat exchangers, encapsulated tile holes, shield plugs, and other miscellaneous large objects (e.g., fume hoods, glove boxes, processing equipment).
LL/ALW Resins	Spent IX resin arising from light water auxiliary system and from Active Liquid Waste (ALW) Treatment Systems.
ALW sludges	Sludge containing clay sorbent arising from liquid effluent treatment plant at Bruce A.
Steam generators	Redundant steam generators from refurbishment. The steam generators consist of Inconel 600 tubes, carbon steel shell and shroud, and head and tubesheet.

Table 3.2: Intermediate Level Waste Categories

Waste Category	Description
CANDECON resins	Spent ion exchange (IX) resin from chemical decontamination process for nuclear heat transport systems.
Moderator resins	Spent IX resin arising from moderator purification systems.
PHT resins	Spent IX resin arising from PHT purification systems.
Misc. Resins	Spent IX resin arising from station auxiliary systems (e.g., heavy water upgraders).
Irradiated core components	Various replaced core components, notably flux detectors and liquid zone control rods.
Filters and filter elements	Filters and filter elements from various station process systems.
IX columns	Spent IX resin mainly arising from Pickering PHT purification system, comes as package with steel container.
Retube - Pressure Tubes	Zircaloy fuel channel waste from large scale retube.
Retube - End Fittings	Stainless steel fuel channel waste from large scale retube.
Retube - Calandria Tubes	Zircaloy fuel channel waste from large scale retube.
Retube - Calandria Tube Inserts	Fuel channel waste from large scale retube.

3.2 Waste Packaging

Waste packages (i.e., waste, containers and overpacks) used by OPG for storage of L&ILW at WWMF are described in Appendix E of the Reference L&ILW Inventory Report (OPG 2010) and are summarized below.

The inventory report identifies reference containers and overpacks used with the major waste categories, although it is recognized that there may be a few other waste container types associated with each category. For LLW and most ILW, the containers and overpacks are primarily designed for operational and storage reasons, with limited intention that they provide a long-term barrier to contaminant release. Therefore, representative waste containers and overpacks are sufficient for each waste category.

3.2.1 LLW Containers and Overpacks

Much of the operational raw waste is paper, plastic, rubber, cotton, etc., that is contained in plastic bags or wrapped in plastic sheeting. These wastes are then typically either incinerated, or baled/compacted.

Carbon steel **ash bins** are used for bottom ash and baghouse ash. These are galvanized and have a tubular frame with sheet steel sides. **Drums** have also been used for old baghouse ash.

OPG (2010, Table 2.1) notes that ash bins will be overpacked in a DGR-ready **LLW sheet metal overpack**.

Historically, compacted wastes were 'baled'. Bales consist of compacted material in a large cardboard box, wrapped in plastic and held together with steel bands. Bales were then stored in mild steel **bale racks**, which each hold four bales (Appendix E, OPG 2010). Bales have not been produced since 1993 but a significant stock of these wastes exists. OPG (2010, Table 2.1) assumes that about 25% of the bales are incinerated and the remainder transferred to the DGR in a metal overpack, assumed here to be created by covering the open sides and top of the bale rack with a simple sheet metal **cover**.

Compacted material generated since 1993 is held in B25 **compactor boxes**. These are constructed of painted mild steel panels over a steel channel and tube frame. They are expected to be transferred directly to the DGR without any overpack (Table 2.1, OPG 2010).

Non-processible wastes are stored in a family of **non-pro boxes** having a standard footprint and differing in height (and therefore volume capacity). The boxes are of painted sheet metal, and generally open topped. Lids will be provided when they are transferred (without any overpack) for emplacement in the DGR. The boxes can be stacked 4, 5 or 6 high. The reference container for non-processible wastes has been taken in this data report to be the NPB47 (Appendix E, OPG 2010).

Standard painted carbon steel **drums** are also used for a variety of non-processible wastes. Separate carbon steel **drum racks** have been used to hold six drums for stacking (Appendix E, OPG 2010) and about 14% of raw non-processible wastes are contained in drums (Table 2.1, OPG 2010). Table 2.1 of OPG (2010) notes that about 90% of the drum racks will be placed in the DGR without an overpack, the remainder will be placed in an LLW sheet metal overpack. Carbon steel **drum bins** will also be used to hold six drums and will be transferred directly to the DGR without any overpack (Appendix E and Table 2.1, OPG 2010).

LL and ALW resins are mainly stored in resin totes (**pallet tanks** – steel framed with a plastic tank) (Appendix E, OPG 2010). To avoid flammable packages, it is expected that these pallet tanks will be transferred to the DGR in a metal overpack, assumed here to be created by covering the open sides and top of the tanks with a simple sheet metal cover. Some LL resins are stored in galvanized mild steel resin boxes (80 boxes in total) that will be placed in LLW sheet metal overpacks prior to consignment to the DGR (Table 2.1, OPG 2010).

ALW sludges are stored in carbon steel **sludge boxes**, which will be placed in LLW sheet metal overpacks prior to consignment to the DGR (Appendix E and Table 2.1, OPG 2010).

Large irregular objects such as heat exchangers and large refurbishment wastes will be emplaced "**as is**" in the DGR, without any container. These objects are in a variety of sizes, but will be size-reduced where necessary to fit the DGR cage. Another option for handling of steam generators is being considered which would retain all the radioactivity but reduce the amount of uncontaminated steel; however, the reference assumption here is that the steam generators are size-reduced only.

The characteristics of the LLW reference packaging used in the safety assessment calculations are summarized in Table 3.3. All packages are lidded or closed, but these are not regarded as sealed and they would be water accessible.

Table 3.3: LLW Reference Container and Overpack Characteristics

	Bottom Ash	Baghouse Ash	Compacted Waste (Bales) [a]	Compacted Waste (Boxes)	Non-Pro. (Drums)	Non-Pro. (Boxes)	LL /ALW Resins[a]	ALW Sludges	Steam Generators[b]	LLW Overpack
Container (Identifier)	New Ash Bin (AIBN)	New Ash Bin (AIBN)	Bale Rack (BRACK) with sheet metal cover	Compactor Box (B25)	Drum Bin (DBIN)	Non-pro Container (NPB47)	Pallet Tank (RTK) with sheet metal cover	ALW Sludge Box (NPBSB)	Cut Segments	LLW overpack (BINOPK)
External Width (m)	1.32	1.32	1.22	1.12	1.32	1.32	1.24	1.32	1.8 – 3.6 (O.D.)	1.78
External Depth (m)	1.32	1.32	2.29	1.84	1.96	1.96	1.24	1.96	1.8 – 3.6 (O.D.)	2.54
External Height (m)	1.4	1.4	1.2	1.3	1.03	1.19	1.68	1.03	2.2 – 4.5 (O.L.)	1.88
Geometry	Box	Box	Box	Box	Box with six drums	Box	Box	Box	Segment	Box
Closure	Bolted lid	Bolted lid	Cover around box frame	Clipped gasketed lid	Bolted lid	Lid	Cover around box frame	Lid	Welded steel plate	Lid
Material	Carbon steel	Carbon steel	Carbon steel	Mild steel	Carbon steel	Steel tubular frame and sheet metal	Carbon steel	Carbon steel	Carbon steel shell	Carbon steel
Wall thickness (mm)	3.4	3.4	1.6	4.6	6.5	2.8	1.6	2.7	75	3.4
Coating	Zn galvanized	Zn galvanized	Paint	Paint	Paint	Paint	Paint	Paint	None	Paint
Internal Volume (m^3)	1.8	1.8	1.64	2.3	1.2	2.5	1.5	2.2	Variable	6.56
External Volume (m^3)	2.5	2.5	3.4	2.8	2.8	3.2	2.7	2.7	Variable (12-21)	8.5
External Surface Area (m^2)	10.9	10.9	14.0	11.8	11.9	13.0	11.4	11.9	Variable (30-44)	25.1

Notes: From Appendix E of OPG (2010). These 'reference containers and overpacks' are for consideration in determining the performance of waste packaging in the repository, and not in the calculation of inventory volumes (see Section 3.4 for these assumptions).

a 1.6-mm carbon-steel cover assumed.

b Data from the Nuclear Waste Management Organization (NWMO) (2010a).

3.2.2 ILW Containers and Overpacks

In the past, ILW resins were stored in a 3 m^3 mild steel **resin liner**, coated with coal tar epoxy paint (Appendix E of OPG 2010). Most of these old resin liners have subsequently been placed inside a **stainless steel overpack**. Current ILW resins are stored in stainless steel liners with dimensions similar to the 3 m^3 mild steel resin liner.

For operational radiation protection purposes, most resin liners will be overpacked in **cylindrical concrete shields**. Each overpack will contain one or two resin liners, depending on the specific design. The reference concrete overpack has a concrete wall thickness of 0.25 m (Appendix E of OPG 2010). Variant concrete overpacks will also be used where greater shielding is needed (one with a wall thickness of 0.35 m, and one with wall thickness of 0.35 m and a 40 mm thick steel insert).

Higher activity operational waste, notably ion exchange columns, filters & filter canisters, and irradiated core components were historically placed in **tile hole liners** for storage of other ILW. The most common tile hole liners were approximately 0.6 m in overall diameter and 3.4 m high (Appendix E, OPG 2010). When full, the liner was backfilled with poured concrete forming a monolith, referred to as an "encapsulated tile hole".

Subsequently, these were replaced with two types of **'tile hole equivalent' (T-H-E) liners** - IC-2 and IC-18 T-H-E liners. These are 7.6 m or 10.7 m long lengths of carbon steel pipe placed vertically in ground, and not grouted. For transfer to the DGR, the plan for the original preliminary design was for each liner to be filled at the top with concrete to allow retrieval, and the liner to be transported to the DGR and placed horizontally in holes in a thick concrete array in an emplacement room (NWMO 2010a). This emplacement option has been replaced for the final preliminary design with an option that involves the wastes within the current liners being transferred to a new DGR-ready steel container approximately the size of a current resin liner (OPG 2010). These **Alternative Tile Hole Equivalent Liners (ATHEL)** may be transferred as-is or in cylindrical concrete shields, similar to the resin liners. In the future, such wastes will be placed directly in a new **ILW Shield** container. The details for the ATHEL and ILW Shield containers are not yet defined.

Retube wastes, such as pressure tubes, calandria tubes, end fittings, shield plugs, and spacers resulting from reactor refurbishment will be stored in **retube waste containers**. These containers are rectilinear in shape and constructed of concrete, lined internally and externally with stainless steel. Somewhat different retube container designs (e.g., amount of steel shielding) are used for the different components, and for containers from the different stations. The reference container design adopted in this safety assessment is based on the containers currently used to store Bruce A pressure tube and calandria retube wastes (Appendix E, OPG 2010).

The characteristics of the ILW reference packaging for use in safety assessment calculations are summarized in Table 3.4. For the safety assessment calculations, it is assumed that all ILW resins are contained in the reference RSHLD1 concrete shield. For the assessment of the original preliminary design, filters, ion exchange columns, and core components are assumed to be stored in IC-18 T-H-E inner liners; for the assessment of the final preliminary design, they are assumed to be placed in ILW shields. All packages are closed, and the retube containers in particular are welded shut. The content would not generally be water accessible until the packages corrode or are overtopped with water.

Table 3.4: ILW Reference Container and Overpack Characteristics

	CANDECON, Moderator, PHT and Misc. Resins	Resin Shields [a]	Filters & Elements	Irradiated Core Comp-onents	IX Columns	Retube Waste Containers (End Fittings)	Retube Waste Containers (Others)
Container (Identifier)	Resin Liner (RLSS)	Resin liner shield 1 (RLSHLD1)	IC-18 T-H-E Liner (THLIC18) [b] ILW Shield [c]			End fitting container (RWC(EF))	Pressure tube container (RWC(PT))
External Width (m)	1.63 (O.D.)	2.2 (OD)	0.55 (O.D.) [b] 1.0 (O.D.) [c]			1.70	1.85
External Depth (m)	1.63 (O.D.)	2.2 (OD)	0.55 (O.D.) [b] 1.0 (O.D.) [c]			3.35	1.85
External Height (m)	1.8	4.25	10.7 [b] 1.7 [c]			1.92	2.25
Geometry	Cylinder	Cylinder	Cylinder			Box	Box
Material	Stainless steel	Concrete	Carbon steel [b] Concrete and steel [c]			Steel-concrete-steel	Steel-concrete-steel
Wall thickness (mm)	6.3	250	10 [b] Not given [c]			350	475
Coating	None	None	Galvanized [b] None [c]			Stainless steel lined	Stainless steel lined
Internal Volume (m^3)	3	6	2.5 [b] 0.25 [c]			2.7	0.8
External Volume (m^3)	3.8	16.2	2.6 [b] 1.3 [c]			10.9	7.7
External Surface Area (m^2)	13.4	37	20.8 [b] 6.9 [c]			30.8	23.5

Notes:
Data from NWMO (2010a) and Appendix E of OPG (2010).
These reference containers and overpacks are used in determining the performance of waste packaging in the repository, and not in the calculation of inventory volumes (see Section 3.4 for these assumptions).

a Concrete Resin Liner Shield of 250 mm thickness is assumed. Two alternative concrete shields are also available, and a stainless steel overpack. However, the 250 mm shield will be most common, see OPG (2010).
b For the original preliminary design, it has been assumed that these wastes are emplaced in IC-18 T-H-E liners.
c For the final preliminary design, it has been assumed that these wastes are emplaced in ILW shields.

3.3 Waste Conditioning

Certain wastes will be conditioned prior to being sent to the DGR. This affects the characteristics of the wastes in the DGR, and therefore is summarized below.

The main waste conditioning practices undertaken by OPG are incineration (resulting in the generation of the bottom ash and baghouse ash) and compaction (resulting in the generation of compacted waste bales and boxes). Some wastes have been immobilized in bitumen and some have had clay-based and organic absorbents added. In addition, the reference assumption for steam generators is that they will be filled with grout, segmented into smaller sizes, capped with metal plates, and then shipped to the DGR (Table 3.5, OPG 2010). These practices are accounted for here.

Some LLW has historically been grouting with cement, and some ILW will be partially grouted to facilitate retrieval from storage. However, the proportion of wastes subject to this treatment is small, and such conditioning is not taken into account here.

The conditioning assumptions for L&ILW in safety assessment studies are presented in Table 3.5, based primarily on information in Tables 2.1, 2.2 and 3.1 of OPG (2010).

Table 3.5: Waste Conditioning Assumptions

LLW Waste Category	Conditioning	ILW Waste Category	Conditioning
Bottom Ash	Incineration	CANDECON Resins	None
Baghouse Ash	Incineration	Moderator Resins	None
Compacted Boxes	Compaction	PHT Resins	None
Compacted Bales	Compaction	Miscellaneous Resins	None
Non-Processible – Drums	Some bituminized	Irradiated Core Components	None
Non-Processible – Boxes	None	Filters and Filter Elements	None
Non-Processible – Other	None	IX Columns	None
LL/ALW Resins	None	Retube Wastes (Pressure Tubes)	None
		Retube Wastes (End Fittings)	None
ALW Sludge	Immobilized in clay-based material	Retube Wastes (Calandria Tubes)	None
Steam Generators	Grouted	Retube Wastes (Calandria Inserts)	None

Note: Prior to arrival at the DGR Facility.

3.4 Physical Characteristics

3.4.1 Materials

Safety assessment studies require information on the physical characteristics of the materials present in the waste. This includes the general types of material present (e.g., steel, plastic or glass) as well as physical properties such as density, porosity, moisture content and hydraulic conductivity.

Mass and surface area data for LLW wastes are presented in Table 3.6, with data on the contribution of LLW containers in Table 3.7. The mass of metals and organic material in the LLW has been based on data presented in Table 2.11 of the Reference L&ILW Inventory Report (OPG 2010). Data for the steam generators waste category are presented under containers (see Table 3.7) as the steam generator itself acts as the waste container. The nature of ash wastes is such that they do not contain any cellulosics, rubber or plastic, or significant amounts of concrete or steel, so ash is not included in the table.

OPG (2010) does not present surface areas of bulk LLW. A general value of 0.05 m^2 kg^{-1} has been used to derive the surface area values in Table 3.6. This value assumes metals are typically 5 mm thick steel plate with a density of 7900 kg m^{-3} and two main faces.

Table 3.6: Mass and Surface Area of LLW

Waste Category	Mass (kg)						Surface Area (m^2)	
	Cellulosics and Other Organics	Rubber & Plastic	Dry Resins	Concrete	Carbon Steel	Stainless Steel	Carbon Steel	Stainless Steel
Compacted Bales	5.4E+05	7.6E+05	-	-	2.6E+05~	-	1.3E+04~	-
Compacted Boxes	4.4E+06	6.2E+06	-	-	2.1E+06~	-	1.1E+05~	-
Non-Processible – Drums	8.2E+05	3.3E+05	-	2.8E+05	4.7E+05^	4.7E+05	2.4E+04^	2.4E+04
Non-Processible – Boxes	2.5E+06	9.0E+05 *	-	7.7E+05	1.3E+06^	4.8E+06**	6.5E+04^	2.4E+05
Non-Processible – Other	-	-	1.6E+04	-	4.8E+03~	-	2.4E+02~	-
LL/ALW Resins	-	-	1.5E+06	-	-	-	-	-
ALW Sludge	-	-	-	-	-	-	-	-

Notes:
Ash and inorganic materials are not included as they are considered to have low degradation/gas generation potential; steam generator data are considered under "containers" below. Dry resins do not include bound water.

~ Non-passivated due to absence of concrete in waste.
^ Passivated due to presence of concrete in waste.
* Includes bituminized waste of 1.9E+05 kg.
** Includes "other metals".
\- Indicates not significant amount in waste category, no value given in OPG (2010).

Table 3.7 presents the mass and surface area of LLW containers associated with each waste category, taken from Table 2.9 of OPG (2010). Data for containers and overpacks have been combined, where appropriate.

Table 3.7: Mass and Surface Area of Materials in LLW Containers and Overpacks

Waste Category	Mass (kg)				Surface Area (m^2)	
	Carbon Steel	Stainless Steel	Plastics	Concrete	Carbon Steel	Stainless Steel
Bottom Ash	1.8E+06~	-	-	-	3.3E+04~	-
Baghouse Ash	4.3E+05~	-	-	-	8.2E+03~	-
Compacted Bales	4.6E+05~	-	-	-	2.3E+04~	-
Compacted Boxes	3.0E+06~	-	-	-	7.2E+04~	-
Non-Processible – Drums	4.5E+06~	-	-	-	1.6E+05~	-
Non-Processible – Boxes	8.5E+06~	-	-	-	3.1E+05~	-
Non-Processible – Other&	2.8E+06~~	-	-	1.5E+06	1.0E+05~~	-
LL/ALW Resins	9.8E+05~	-	2.1E+05	-	3.5E+04~	-
ALW Sludge	3.4E+06~	-	-	-	6.3E+04~	-
Steam Generators	8.5E+06^	2.8E+06*	-	2.0E+06	1.1E+04^	2.4E+05

Notes:
~ Non-passivated due to absence of concrete in packaging.
~~ Conservatively taken to be non-passivated due to concrete being only associated with some packages. Includes contribution of copper alloy heat exchangers.
^ Passivated due to presence of grouting.
& Non-processible (other) includes heat exchangers and encapsulated tile holes.
* Inconel 600.
- Indicates not significant amount for waste category; no value given in OPG (2010).

Data for ILW wastes are presented in Table 3.8. Data have been derived for specific waste categories from the data in Table 2.12 of OPG (2010). Data on steel and zirconium content for retube wastes are based on the mass of relevant elements given in Table 3.4 of OPG (2010).

OPG (2010) does not present specific surface area data for ILW. For ILW, the specific surface area is estimated as 0.05 m^2 kg^{-1} for all metallic items except pressure and calandria tubes, using the same rationale as for LLW. These retube wastes have a specific geometry and are therefore estimated to have a specific surface area of 0.0615 m^2 kg^{-1} based on the inner and outer surfaces for tubes, a mean wall thickness of 5 mm and a density for Zr of 6500 kg m^{-3}.

Table 3.8: Mass and Surface Area of ILW

Waste Category	Mass (kg)				Surface Area (m^2)		
	Dry Resins [a]	Carbon Steel	Stainless Steel	Zirconium	Carbon Steel	Stainless Steel	Zirconium
CANDECON resins	1.1E+06	-	-	-	-	-	-
Moderator resins	9.7E+05	-	-	-	-	-	-
PHT resins	6.8E+05	-	-	-	-	-	-
Misc. resins	9.1E+05	-	-	-	-	-	-
Irradiated core components	-	1.3E+04[b]	4.8E+02	-	6.5E+02 [b]	2.4E+01	-
Filters and filter elements	1.7E+05[c]	5.0E+05[b]	9.2E+04	-	2.5E+04 [b]	4.6E+03	-
IX columns	3.1E+05	4.0E+05[b]	-	-	2.0E+04 [b]	-	-
Retube Wastes (Pressure Tubes)	-	-	-	4.3E+05	-	-	2.6E+04
Retube Wastes (End Fittings)	-	-	2.3E+06	-	-	1.1E+05	-
Retube Wastes (Calandria Tubes)	-	-	-	1.7E+05	-	-	1.0E+04
Retube Wastes (Calandria Tube Inserts)	-	-	2.1E+04	-	-	1.0E+03	-

Notes:
- a Resin only, does not include free or bound water.
- b Passivated due to presence of concrete in ILW Shield container.
- c Conservatively includes mass of glass fibre, polypropylene and low density polyethylene given in Table 2.12 of OPG (2010) .
- \- Indicates not significant for waste category; no value given in OPG (2010).

Data for containers and overpacks for ILW are presented in Table 3.9. These have been determined using data from Table 2.10 of OPG (2010) and the same assumptions applied to calculate the mass and surface area of ILW. Note that the surface area data for carbon steels in retube waste containers is derived using 0.04 m^2 kg^{-1}. This value is based on the presence of 0.013 m (0.5 inch) diameter steel reinforcing bars.

Table 3.9: Mass and Surface Area of ILW Containers and Overpacks

Waste Category	Mass (kg)			Surface Area (m^2)	
	Carbon Steel	Stainless Steel	Concrete	Carbon Steel	Stainless Steel
CANDECON resins	2.8E+05^	6.1E+05	5.8E+06	2.8E+03	9.1E+03
Moderator resins	2.4E+05^	5.2E+05	5.0E+06	2.4E+03	7.8E+03
PHT resins	1.7E+05^	3.6E+05	3.5E+06	1.7E+03	5.5E+03
Misc. resins	2.3E+05^	4.9E+05	4.7E+06	2.2E+03	7.3E+03
Irradiated core components	9.5E+03^[a] 5.4E+03^[b]	-[a] 3.0E+03[b]	1.1E+05[a] 2.0E+05[b]	1.1E+02[a] 1.8E+01[b]	-[a] 5.6E+01[b]
Filters and filter elements	4.7E+05^[a] 2.7E+05^[b]	-[a] 1.5E+05[b]	5.5E+06[a] 9.9E+06[b]	5.3E+03[a] 9.1E+02[b]	-[a] 2.8E+03[b]
IX columns	1.9E+05^[a] 1.1E+05^[b]	-[a] 6.0E+04[b]	2.2E+06[a] 4.0E+06[b]	2.1E+03[a] 3.7E+02[b]	-[a] 1.1E+03[b]
Retube Wastes (Pressure Tubes)	1.3E+05^	1.1E+06	5.2E+06	5.2E+03	5.7E+03
Retube Wastes (End Fittings)	5.3E+05^	5.8E+06	2.0E+07	2.1E+04	2.1E+04
Retube Wastes (Calandria Tubes)	8.9E+04^	7.5E+05	3.6E+06	3.6E+03	3.9E+03
Retube Wastes (Calandria Tube Inserts)	2.4E+04^	2.0E+05	9.7E+05	9.6E+02	1.1E+03

Notes:
- a Original preliminary design (NWMO 2010a).
- b Final preliminary design (OPG 2010).
- ^ Passivated due to presence of concrete in ILW Shield container.
- - Indicates not significant for waste category; no value given in NWMO (2010a).

Waste density and physical porosity are listed in Table 3.10, based on Table C.7 of OPG (2010). Values for retube wastes were calculated directly from the waste and container volume (Tables 3.1 and 3.4 of OPG 2010). The information is believed to be adequately characterized for postclosure safety assessment, where repository average is more important than the per-container values. Information on variability is not available, but is expected to be small for most waste packages, with the exception of the Non-Processible LLW wastes and the ILW in ATHEL containers (e.g., Filters and Elements, Irradiated Core Components and IX Columns).

The moisture content in most waste streams is small, consistent with the DGR waste acceptance criteria limit on the amount of free water. The main exception is stored resins, which contain between about 40% moisture by weight as bound water, and typically 3% free water by volume in the container bottom. Sludges are dewatered, but contain residual moisture in the gel of 1%. Details of moisture content are summarized in Table 3.10, from Table C.7 of OPG (2010).

The moisture content and density estimates in Table 3.10 can be combined with the volume estimates (see Table 3.11) to determine a total mass of (free and bound) water associated with wastes of 4.2×10^6 kg. The total amount of free water associated with wastes in the repository emplacement rooms is:

- Panel 1: 2.6×10^5 kg; and
- Panel 2: 2.4×10^5 kg.

The majority of this water (55%) is associated with resins. No account is taken for evaporation or outgassing of the water from the wastes during the surface storage or the emplacement period. Water bound in resins is not included in the above calculation of free water, but could account for a further 3.7×10^6 kg of water (2.0×10^6 kg in Panel 1 and 1.7×10^6 kg in Panel 2).

There is at present insufficient information on waste characteristics to reliably define ranges for the data presented in Table 3.10. However, it is unlikely that these parameters will have a significant effect on overall postclosure impacts, and the reference values are selected to be cautious estimates.

The densities of plain and galvanized C-steel, for passivated C-steel, for the passive stainless steels and Ni-based alloys, and for the Zr alloys are: 7860 kg m^{-3}, 7860 kg m^{-3}, 8100 kg m^{-3}, and 6500 kg m^{-3}, respectively (ASTM 1999). The value for the passive alloys is a weighted mean of that for the 300-series stainless steel and Ni alloys.

Table 3.10: Physical Properties of Raw Wastes

Parameter	Bulk Density (kg m^{-3})	Physical Porosity/ Void Fraction (-)	Moisture Content (kg water/ kg waste)
Bottom Ash	550	0.3	0.01 [d]
Baghouse Ash	390	0.3	0.001 [e]
Compacted Waste - Boxes	1000	0.5	0.001 [e]
Compacted Wastes - Bales	770	0.5	0.001 [e]
Non-processible – Drums	500	0.4 [c]	0.001 [e]
Non-processible – Boxes	230	0.9	0.001 [e]
Non-processible – Other	1070 [a]	0.8 [b]	0.001 [e]
LL/ALW Resins	750 [j]	0.4 [i]	0.03 [f]
ALW Sludges	1120	0.3	0.01 [g]
Steam Generators	1730 [k]	0.8 [k]	0.001 [e]
CANDECON Resins	850 [j]	0.4 [i]	0.03 [f]
Moderator Resins	850 [j]	0.4 [i]	0.03 [f]
PHT Resins	850 [j]	0.4 [i]	0.03 [f]
Misc. Resins	850 [j]	0.4 [i]	0.03 [f]
Irradiated Core Hardware	880	0.9	0.001 [e]
Filters and Filter Elements	880	0.9	0.1 [h]
IX Columns	880 [l]	0.5 [m]	0.03 [f]
Retube Waste (Pressure Tubes)	2290 [o]	0.7 [n]	0.001 [e]
Retube Waste (End Fittings)	970 [p]	0.9 [n]	0.001 [e]
Retube Waste (Calandria Tubes)	1270 [q]	0.8 [n]	0.001 [e]
Retube Waste (Calandria Tube Inserts)	580 [r]	0.9 [n]	0.001 [e]

Notes:
Data based on assumptions described in OPG (2010), in particular, Table C-7.

a Averaged value calculated using data from Tables 2.1, C-7 and Appendix E of OPG (2010) to derive a 53:47 split between the mass of items such as heat exchangers and the mass of items such as encapsulated tile holes.
b Averaged value calculated using data from Tables 2.1, C-7 and Appendix E of OPG (2010) to derive a 85:15 split between the porosity of items such as heat exchangers and the porosity of items such as encapsulated tile holes.
c Contains granular fills and therefore has fewer voids than the other non-processible wastes.
d May contain some moisture, because water is sprayed onto the ashes during loading into the bins to cool the ashes. Some of the moisture may evaporate during storage.
e Waste would normally be dry; this represents trace amounts of water in the package.
f Bound (bead) water not included. Free water is drained from the resins during transfer to the resin liners at the stations, but some water remains on the bottom of the liners, typically 3%.
g Water content is immobilized with polymer gel.
h Expect some moisture retention on filters.
i Typical physical porosity of resins, from standard technical specifications.
j Includes bound water.

k Based on ungrouted porosity of 0.9 (Table C-7 of OPG 2010), a nominal grout porosity of ~30%, an ungrouted bulk density of 1500 kg m^{-3} (midpoint of values in Table C-7 of OPG 2010), and grout grain density of 2560 kg m^{-3} (Table 4.26).
l Taken to be the same as filters and filter elements.
m No data given in OPG (2010). Value of 0.5 adopted for the current assessment.
n Calculated using (1 – Bulk Density/True Density). The Bulk Density is the density of the wastes as packaged, and the True Density is the density of the solid metal that makes up the items. True Density data are taken from Tables C-2 to C-5 of OPG (2010).
o Based on weight of 61 kg per pressure tube and 30 pressure tubes per box (Table 3.4 of OPG 2010) and 242 boxes with net volume of 193 m^3 (Table 3.1 of OPG 2010).
p Based on weight of 163 kg per end fitting and 16 end fittings per box (Table 3.4 of OPG 2010) and 899 boxes with net volume of 2429 m^3 (Table 3.1 of OPG 2010).
q Based on weight of 23 kg per Calandria tube and 44 Calandria tubes per box (Table 3.4 of OPG 2010) and 167 boxes with net volume of 133 m^3 (Table 3.1 of OPG 2010).
r Based on weight of 1.2 kg per Calandria tube insert and 384 Calandria tube inserts per box (Table 3.4 of OPG 2010) and 45 boxes with net volume of 36 m^3 (Table 3.1 of OPG 2010).

3.4.2 Volumes

Both LLW and ILW volumes have been estimated by OPG according to several scenarios, capturing the influence on waste arising from key decisions concerning the potential operating life of reactors at Bruce, Pickering and Darlington. The most recent estimates are presented by NWMO (2010a) and OPG (2010) in Tables 2.1 and 3.1 and are adopted here.

The estimated volumes are presented in Table 3.11. The raw or net volume refers to the waste material itself and the emplaced volume is the volume occupied in the repository including an allowance for additional shielding and overpacks for the DGR.

The waste volumes are considered to be relatively adequately characterized. The estimates include actual current volumes in stock, and future projections that are based on sound information and experience with waste arisings in the past. The main uncertainties are with respect to future plans for the refurbishment of the stations, and for possible off-site volume reduction of the steam generators. It is therefore expected that the total volume of raw waste may differ from the estimates by about 20%. The total emplaced waste volume will be limited by the excavated volume of the repository.

Table 3.11: Reference Waste Volumes

Waste Categories	Raw (Net) Volume (m^3)	Number of DGR Containers	Emplaced Volume (m^3)
LLW			
Bottom ash	2,033	882	7,497
Baghouse ash	364	218	1,853
Compacted wastes (bales)	2,268	1,383	4,702
Compacted wastes (boxes)	14,110	6,135	17,177
Non-processible (drums)	9,408	7,840	25,532
Non-processible (boxes)	56,713	24,190	73,792
Non-processible (other)	3,279	164	3,279
LLW and ALW resins	3,393	2,165	6,307
ALW sludges	3,569	1,709	14,527
Steam generators	8,387	512	8,387
Sub-total LLW	*103,524*	*45,198*	*163,053*
ILW			
Moderator resins	1,929	430	4,779
PHT resins	1,348	301	3,340
Misc. resins	1,808	403	4,480
CANDECON resins	2,257	503	5,592
Irradiated core components	27	4,459 [a] 4,453 [b]	6,101 [a] 9,453 [b]
Filters and filter elements	1,344		
IX columns	544		
Retube Wastes (Pressure Tubes)	193	242	1,860
Retube Wastes (End Fittings)	2,429	899	9,804
Retube Wastes (Calandria Tubes)	133	167	1,285
Retube Wastes (Calandria Tube Inserts)	36	45	349
Sub-total ILW	*12,048*	*7,449 [a]* *7,443 [b]*	*37,590 [a]* *40,942 [b]*
Total	115,572	52,647 [a] 52,641 [b]	200,643 [a] 203,995 [b]

Notes:
Data from Tables 2.1 and 3.1 of OPG (2010).
a Based on waste packages proposed in original preliminary design (NWMO 2010a).
b Based on waste packages in final preliminary design (OPG 2010).

3.5 Radiological Characteristics

3.5.1 Key Radionuclides

A large number of radionuclides are present in wastes initially (e.g., Appendix B of the Reference L&ILW Inventory Report, OPG 2010); however most are short-lived or only present in very small amounts. Screening calculations have been conducted for the L&ILW DGR inventory, to identify potentially important radionuclides for consideration in the long-term safety assessment (Appendix A). Only those identified as being of potential significance are considered in this section, however the list has been supplemented with radionuclides that are not present at emplacement, but will ingrow through radioactive decay. The resulting list of radionuclides is presented in Table 3.12. The list includes all radionuclides typically expected to be important in postclosure safety assessments of other L&ILW facilities (e.g., SKB 2008, NIREX 2003).

Half-life data have been obtained from the electronic database supplied with International Commission on Radiological Protection (ICRP) (2008). The radioactive decay schemes and secular equilibrium assumptions are presented in Table 3.13 and Table 3.14, respectively. These are consistent with other safety assessments such as for Drigg (BNFL 2002) and the International Atomic Energy Agency (IAEA) (2003).

3.5.2 Radionuclide Inventories

The total inventories for each of the waste categories are presented in Table 3.15 and Table 3.16 for the key long-term radionuclides. These values are based on OPG (2010) for all radionuclides and obtained from Tables 2.5, 2.7 and 3.3 of that report. The inventories are presented at 2062, which is the assumed date of closure of the repository adopted in this assessment.

Uncertainties in the concentration of radionuclides in the wastes are discussed in Appendix D of OPG (2010). In general, the package-to-package Log-dispersion variability (which is defined as the Antilog of the standard deviation of the Log of the data) is within a factor of five. Over a large number of packages, the total amount is much less uncertain. A reasonable upper estimate of total inventory is a factor of ten increase for each radionuclide.

The radionuclide concentrations in the wastes can be derived from the inventory and volume data.

Table 3.12: Potentially Important Radionuclides and their Half-Lives

Radionuclide	Half-life (a)	Decay Constant (a^{-1})
H-3	1.23E+01	5.63E-02
C-14	5.70E+03	1.22E-04
Cl-36	3.01E+05	2.30E-06
Ni-59	1.01E+05	6.86E-06
Ni-63	1.00E+02	6.92E-03
Se-79	2.95E+05	2.35E-06
Sr-90[a]	2.88E+01	2.41E-02
Nb-93m	1.61E+01	4.30E-02
Mo-93	4.00E+03	1.73E-04
Zr-93	1.53E+06	4.53E-07
Nb-94	2.03E+04	3.41E-05
Tc-99	2.11E+05	3.28E-06
Ag-108m[a]	4.18E+02	1.66E-03
Sn-121m[a]	4.39E+01	1.58E-02
I-129	1.57E+07	4.41E-08
Cs-137[a]	3.02E+01	2.30E-02
Ir-192	2.02E-01	3.43E+00
Ir-192m	2.41E+02	2.88E-03
Pt-193	5.00E+01	1.39E-02
Pb-210[a]	2.22E+01	3.12E-02
Po-210	3.79E-01	1.83E+00
Rn-222[b]	1.05E-02	6.62E+01
Ra-226[a]	1.60E+03	4.33E-04
Ra-228[a]	5.75E+00	1.21E-01
Th-228[a]	1.91E+00	3.63E-01
Th-229[a]	7.34E+03	9.44E-05
Th-230	7.54E+04	9.20E-06
Th-232	1.41E+10	4.93E-11
Ac-227[a]	2.18E+01	3.18E-02
Pa-231	3.28E+04	2.12E-05
Pa-233	7.38E-02	9.39E+00

Radionuclide	Half-life (a)	Decay Constant (a^{-1})
U-232	6.89E+01	1.01E-02
U-233	1.59E+05	4.35E-06
U-234	2.46E+05	2.82E-06
U-235[a]	7.04E+08	9.85E-10
U-236	2.34E+07	2.96E-08
U-238[a]	4.47E+09	1.55E-10
Np-237	2.14E+06	3.23E-07
Pu-238	8.77E+01	7.90E-03
Pu-239	2.41E+04	2.87E-05
Pu-240	6.56E+03	1.06E-04
Pu-241[a]	1.44E+01	4.83E-02
Pu-242	3.75E+05	1.85E-06
Am-241	4.32E+02	1.60E-03
Am-242m[a]	1.41E+02	4.92E-03
Am-243[a]	7.37E+03	9.40E-05
Cm-242	4.46E-01	1.56E+00
Cm-243	2.91E+01	2.38E-02
Cm-244	1.81E+01	3.83E-02

Notes: Half-lives from the electronic database supplied with ICRP (2008).
a Short-lived daughters taken to be in secular equilibrium.
b Short-lived daughter of Ra-226, modelled explicitly in the biosphere.

Table 3.13: Radionuclide Decay Schemes

Radio-nuclide	Explicitly Modelled Decay Chain
Mo-93	→ (0.8800) Nb-93m
Ir-192m	→ Ir-192
U-232	→ Th-228
Pu-241	→ Am-241 → Np-237 → Pa-233 → U-233 → Th-229
Am-242m	→ (0.1722) Pu-242 → U-238 → U-234 ↘
	→ (0.8233) Cm-242 → Pu-238 → U-234 → Th-230 → Ra-226 → Pb-210 → Po-210 → (0.0045) Pu-238 ↗
Cm-243	→ (0.0024) Am-243 → Pu-239 → U-235 → Pa-231 → Ac-227 → (0.9976) Pu-239 ↗
Cm-244	Pu-240 → U-236 → Th-232 → Ra-228 → Th-228

Notes: Branching ratios for radioactive progeny are indicated in brackets preceding the progeny. If none is indicated, the branching ratio is 1. Short-lived radioactive progeny (e.g., with half-life of a few tens of days) have been taken to be in secular equilibrium with their long-lived parent (see Table 3.14).

Table 3.14: Radionuclides with Progeny in Secular Equilibrium

Radio-nuclide	Progeny in Secular Equilibrium
Sr-90	→ Y-90
Ag-108m	→ (8.700E-2) Ag-108
Sn-121m	→ (7.760E-1) Sn-121
Cs-137	→ (9.440E-1) Ba-137m
Pb-210	→ Bi-210
Ra-226	→ Rn-222 → Po-218 → (9.998E-1) Pb-214 → Bi-214 → (9.998E-1) Po-214 → (2.000E-4) At-218 ↗
Ra-228	→ Ac-228
Th-228	→ Ra-224 → Rn-220 → Po-216 → Pb-212 → Bi-212 → (6.406E-1) Po-212 → (3.594E-1) Tl-208
Th-229	→ Ra-225 → Ac-225 → Fr-221 → At-217 → Bi-213 → (9.791E-1) Po-213 → Pb-209 → (2.090E-2) Tl-209 ↗
Ac-227	→ (9.862E-1) Th-227 → Ra-223→ Rn-219 → Po-215 → Pb-211 → Bi-211 → (9.972E-1) Tl-207 → (1.380E-2) Fr-223 ↗ → (2.760E-3) Po-211
U-235	→ Th-231
U-238	→ Th-234 → Pa-234m → (1.600E-3) Pa-234
Pu-241	→ (2.450E-5) U-237
Am-242m	→ (0.9955) Am-242 → (0.0045) Np-238
Am-243	→ Np-239

Note:
Branching ratios for radioactive progeny have been indicated in brackets preceding the progeny. If none is indicated, the branching ratio is 1.

Table 3.15: Total Activity of the Emplaced LLW (at 2062) (Bq)

Radio-nuclide	Bottom Ash	Baghouse Ash	Compacted Wastes (bales)	Compacted Wastes (boxes)	Non-Pro. (drums)	Non-Pro (boxes)	Non-Pro. (other)	LL/ALW Resins	ALW Sludge	Steam Generators
H-3	4.5E+09	-	3.3E+12	2.8E+14	4.2E+14	1.4E+14	3.2E+12	6.6E+10	1.5E+12	4.8E+11
C-14	6.4E+10	4.6E+08	1.3E+10	9.4E+10	1.4E+11	1.1E+12	3.7E+09	2.1E+10	7.8E+09	1.0E+12
Cl-36	5.9E+05	4.8E+04	1.5E+05	1.1E+06	4.0E+05	5.4E+08	6.8E+04	3.7E+04	1.9E+04	5.7E+07
Ni-59	2.6E+08	4.8E+06	1.0E+07	8.2E+07	5.2E+07	1.7E+09	1.8E+07	6.1E+06	3.2E+06	4.8E+10
Ni-63	2.5E+10	4.3E+08	8.3E+08	8.0E+09	4.9E+09	2.0E+11	1.7E+09	6.7E+08	3.5E+08	4.8E+12
Se-79	3.1E+03	2.6E+03	2.5E+03	1.9E+04	1.5E+04	1.5E+06	5.4E+03	1.2E+03	9.6E+02	6.1E+03
Sr-90	2.0E+10	3.0E+08	9.2E+08	1.4E+10	4.6E+10	2.9E+12	1.0E+09	1.9E+09	5.4E+08	6.0E+12
Zr-93	4.0E+04	2.0E+02	7.9E+03	5.7E+04	6.7E+03	1.5E+06	7.5E+03	-	1.4E+03	2.9E+06
Nb-94	5.2E+09	7.2E+06	1.9E+09	1.4E+10	1.0E+09	2.1E+07	-	-	1.5E+08	2.3E+09
Tc-99	8.3E+04	1.2E+03	3.2E+04	2.3E+05	8.2E+04	5.1E+07	1.3E+04	7.5E+03	3.9E+03	1.1E+07
Ag-108m	6.6E+05	5.4E+05	5.0E+05	4.1E+06	3.2E+06	2.2E+07	1.2E+06	3.0E+05	2.2E+05	1.4E+06
I-129	1.0E+04	1.1E+04	2.7E+02	8.8E+04	1.4E+05	8.9E+05	5.8E+02	1.2E+04	9.6E+01	6.0E+04
Cs-137	4.8E+10	3.2E+10	2.6E+10	3.4E+11	2.4E+11	1.2E+13	8.6E+10	2.8E+10	2.2E+10	1.1E+11
Pb-210	-	-	-	-	-	3.2E+10	-	-	-	-
Ra-226	-	-	-	-	-	3.8E+09	-	-	-	-
U-232	-	-	-	-	-	4.9E+06	-	-	-	2.2E+08
U-233	-	-	-	-	-	6.6E+06	-	-	-	3.0E+08
U-234	1.4E+06	2.4E+04	1.7E+05	2.0E+06	1.7E+02	3.2E+07	4.7E+04	3.4E+04	1.5E+04	1.3E+09
U-235	2.2E+04	4.0E+02	2.9E+03	3.3E+04	2.8E+00	5.1E+05	8.1E+02	5.4E+02	2.5E+02	2.1E+07
U-236	2.5E+05	4.6E+03	3.2E+04	3.7E+05	3.2E+01	5.8E+06	9.2E+03	6.1E+03	2.8E+03	2.5E+08
U-238	1.7E+06	3.0E+04	2.2E+05	2.5E+06	2.2E+02	4.2E+09	6.1E+04	4.1E+04	1.9E+04	1.7E+09
Np-237	1.3E+05	2.4E+03	1.6E+04	1.9E+05	1.6E+01	2.9E+06	4.8E+03	3.2E+03	1.4E+03	1.2E+08

Radio-nuclide	Bottom Ash	Baghouse Ash	Compacted Wastes (bales)	Compacted Wastes (boxes)	Non-Pro. (drums)	Non-Pro (boxes)	Non-Pro. (other)	LL/ALW Resins	ALW Sludge	Steam Generators
Pu-238	6.3E+08	8.2E+06	2.9E+07	4.2E+08	2.2E+04	7.4E+09	9.4E+06	7.7E+06	3.4E+06	4.6E+11
Pu-239	8.4E+08	1.5E+07	1.1E+08	1.3E+09	1.1E+05	2.0E+10	3.0E+07	2.1E+07	9.3E+06	8.1E+11
Pu-240	1.2E+09	2.2E+07	1.5E+08	1.8E+09	1.5E+05	2.7E+10	4.4E+07	2.9E+07	1.3E+07	1.2E+12
Pu-241	8.2E+09	4.3E+07	1.1E+08	6.4E+09	4.8E+05	5.2E+10	1.2E+08	1.7E+08	7.5E+07	[a]
Pu-242	1.2E+06	2.2E+04	1.6E+05	1.8E+06	1.5E+02	2.9E+07	4.4E+04	3.0E+04	1.4E+04	1.2E+09
Am-241	3.0E+09	5.0E+07	2.0E+08	2.7E+09	2.0E+05	4.9E+10	6.8E+07	4.5E+08	1.9E+07	2.1E+12
Am-242m	-	-	-	-	-	5.1E+07	-	-	-	2.3E+09
Am-243	2.7E+06	4.8E+04	3.4E+05	3.9E+06	3.4E+02	6.1E+07	9.5E+04	6.4E+04	3.0E+04	2.6E+09
Cm-243	-	-	-	-	-	-	-	-	-	2.7E+09
Cm-244	1.1E+08	8.1E+05	6.3E+06	2.5E+08	4.9E+03	2.3E+09	2.9E+06	3.5E+06	1.7E+06	1.9E+11

Notes:
Mo-93, Nb-93m, Sn-121m, Ir-192m and Pt-193 have not been included as OPG (2010) does not specify inventories for these in any LLW category.
a No value given in draft version of the Reference L&ILW Inventory Report at the time of the data freeze for the safety assessment calculations (summer 2010). Value in final version of this report (OPG 2010) is 2.8E+12 Bq.
- indicates not expected to be present in significant amounts in waste category; no value given in OPG (2010).

Table 3.16: Total Activity of the Emplaced ILW (at 2062) (Bq)

Radio-nuclide	Moderator Resins	PHT Resins	Misc. Resins	CANDECON Resins	Irradiated Core Compo-nents	Filters and Filter Elements	IX Columns	Retube Wastes (Pressure Tubes)	Retube Wastes (End Fittings)	Retube Wastes (Calandria Tubes)	Retube Wastes (Calandria Tube Inserts)
H-3	3.1E+13	1.7E+13	8.3E+13	1.4E+13	6.5E+08	-	6.8E+12	2.4E+11	4.0E+12	6.4E+10	5.5E+10
C-14	5.2E+15	1.2E+14	2.7E+13	2.2E+11	2.1E+12	1.5E+13	4.8E+13	5.5E+14	6.6E+13	3.6E+13	3.5E+12
Cl-36	6.6E+08	4.0E+06	4.9E+07	1.5E+07	-	9.3E+06	1.6E+06	1.3E+12	6.2E+09	1.1E+11	2.9E+08
Ni-59	2.7E+10	7.9E+07	2.9E+10	3.4E+10	2.7E+11	3.5E+09	3.2E+07	2.7E+11	3.2E+13	2.5E+12	1.2E+12
Ni-63	2.8E+12	8.0E+09	3.3E+12	3.6E+12	2.9E+13	3.7E+11	3.1E+09	7.5E+13	3.0E+15	7.0E+14	1.4E+14
Se-79	2.1E+04	2.6E+06	8.9E+05	1.0E+04	-	7.4E+03	1.0E+06	3.2E+09	5.8E+08	8.7E+09	5.5E+07
Sr-90	1.9E+10	2.8E+11	1.4E+12	4.0E+13	2.6E+09	7.8E+10	1.1E+11	2.4E+12	3.2E+05	9.2E+11	4.4E+06
Mo-93	-	-	-	-	4.5E+08	-	-	3.2E+10	9.2E+11	1.9E+10	3.3E+10
Zr-93	8.7E+05	2.6E+06	1.2E+05	1.0E+07	6.7E+11	1.5E+06	1.0E+06	1.5E+14	1.9E+08	6.2E+13	8.3E+06
Nb-93m	-	-	-	-	2.9E+10	-	-	6.5E+12	3.4E+10	2.7E+12	1.2E+09
Nb-94	-	1.5E+10	2.7E+08	3.8E+09	5.6E+06	9.8E+10	6.0E+09	4.6E+15	7.4E+11	2.8E+11	2.6E+10
Tc-99	-	2.8E+08	9.8E+06	3.2E+06	4.3E+08	1.9E+06	1.1E+08	2.4E+10	2.6E+10	9.4E+09	7.5E+08
Ag-108m	-	5.9E+08	2.0E+08	2.1E+07	-	1.7E+06	2.3E+08	1.2E+13	7.2E+11	6.9E+12	2.9E+10
Sn-121m	-	-	-	-	5.9E+11	-	-	2.1E+11	7.4E+11	7.6E+13	2.7E+10
I-129	-	8.8E+07	8.5E+06	1.0E+05	-	5.2E+04	3.5E+07	3.6E+05	5.4E+04	5.4E+05	1.9E+03
Cs-137	2.6E+11	5.4E+13	1.7E+13	1.9E+12	-	1.6E+11	2.0E+13	6.6E+09	1.1E+05	4.2E+11	5.0E+06
Ir-192m	-	-	-	-	4.9E+07	-	-	1.1E+10	1.2E+07	3.6E+08	1.5E+06
Pt-193	-	-	-	-	3.1E+09	-	-	1.1E+13	7.4E+10	3.8E+11	3.0E+09
U-232	-	-	-	-	-	-	-	2.2E+06	-	5.5E+06	5.5E+03
U-233	-	-	-	-	-	-	-	2.9E+06	-	5.9E+06	8.1E+04
U-234	-	8.5E+05	3.1E+07	6.1E+07	-	2.1E+07	3.4E+05	1.4E+07	-	2.1E+06	-
U-235	-	1.3E+04	5.2E+05	9.7E+05	-	3.6E+05	5.4E+03	2.1E+05	-	1.6E+02	-

Radio-nuclide	Moderator Resins	PHT Resins	Misc. Resins	CANDECON Resins	Irradiated Core Compo-nents	Filters and Filter Elements	IX Columns	Retube Wastes (Pressure Tubes)	Retube Wastes (End Fittings)	Retube Wastes (Calandria Tubes)	Retube Wastes (Calandria Tube Inserts)
U-236	-	1.6E+05	5.8E+06	1.1E+07	-	4.1E+06	6.5E+04	2.6E+06	-	4.5E+04	9.1E+00
U-238	-	1.1E+06	4.0E+07	7.4E+07	-	2.7E+07	4.2E+05	1.7E+07	-	2.4E+05	-
Np-237	-	8.0E+04	2.9E+06	5.6E+06	-	2.0E+06	3.2E+04	-	-	5.4E+04	-
Pu-238	1.8E+06	2.7E+08	8.7E+09	1.1E+10	-	7.2E+09	1.0E+08	[a]	-	4.7E+08	3.0E+04
Pu-239	2.5E+06	5.1E+08	2.7E+10	3.6E+10	-	1.3E+10	2.1E+08	8.3E+09	-	8.7E+07	5.5E+04
Pu-240	3.6E+06	7.4E+08	4.0E+10	5.2E+10	-	1.9E+10	3.0E+08	1.1E+10	-	7.2E+08	4.7E+04
Pu-241	7.2E+06	2.2E+08	1.0E+12	5.6E+11	-	1.2E+10	8.7E+07	1.9E+11	-	2.0E+09	-
Pu-242	3.7E+03	7.5E+05	2.9E+07	5.4E+07	-	1.9E+07	3.0E+05	1.3E+07	-	1.0E+07	-
Am-241	-	1.3E+08	4.7E+10	1.4E+11	-	2.8E+10	5.0E+07	1.4E+10	-	5.4E+08	8.1E+04
Am-242m	-	-	-	-	-	-	-	2.3E+07	-	9.0E+05	1.8E+03
Am-243	-	1.6E+06	6.1E+06	1.2E+08	-	4.3E+07	6.5E+05	-	-	2.6E+08	9.5E+01
Cm-243	-	-	-	-	-	-	-	2.7E+07	-	2.8E+06	2.5E+01
Cm-244	-	1.3E+09	1.8E+09	1.2E+10	-	5.4E+10	5.0E+08	-	-	2.9E+10	2.5E+02

Notes:
Pb-210 and Ra-226 have not been included as OPG (2010) does not specify inventories for these in any ILW category (they are included in assessment through ingrowth).

a No value given in draft version of the Reference L&ILW Inventory Report at the time of the data freeze for the safety assessment calculations (summer 2010). Value in final version of this report (OPG 2010) is 4.6E+09 Bq.

- indicates not expected to be present in significant amounts in waste category; no value given in OPG (2010).

3.6 Chemical Characteristics

3.6.1 Amounts and Concentrations of Non-radioactive Species

The total inventories of non-radioactive species are presented in Table 3.17 for LLW and Table 3.18 for ILW. These contain data presented in Tables 2.8, 3.4 and C.2 – C.5 of the Reference L&ILW Inventory Report (OPG 2010). Only elements and chemicals determined to be potentially of significance by screening analyses (Appendix A) are included in these tables.

Appendix D of OPG (2010) discusses the main sources of uncertainty in the estimates. The concentration in individual waste packages may vary significantly because the characteristics of a single waste package may be dominated by wastes arising from a specific operation or activity, and therefore could deviate substantially from the mean. However, the repository total inventory is less variable because it is averaged over many packages. It is recommended that the maximum total inventory values be set at a factor of up to 10 times greater than the reference values. This value is a nominal estimate of uncertainty consistent with the uncertainty described in OPG (2010).

The volumetric concentrations of non-radioactive species can be calculated by applying the reference volumes presented in Table 3.11.

Table 3.17: Total Inventory of Non-radioactive Species in LLW Waste Streams (kg)

Species	Bottom Ash	Baghouse Ash	Compacted Wastes (Bales)[a]	Compacted Wastes (Boxes)[a]	Non-Pro. (Drums)[a]	Non-Pro. (Boxes)[a]	Non-Pro. (Other)[a]	LLW and ALW Resins	ALW Sludge	Steam Generators
Antimony	1.4E+03	1.2E+02	1.7E+02	1.0E+03	6.8E+01	4.1E+02	3.6E+00	8.7E-02	3.2E-01	-
Arsenic	7.2E+01	5.3E-01	2.1E+01	1.3E+02	8.5E+00	5.1E+01	4.5E-01	3.6E-01	8.0E-02	-
Barium	4.0E+03	6.0E+00	5.3E+02	3.3E+03	2.1E+02	1.3E+03	1.1E+01	6.6E+01	5.2E+01	-
Beryllium	8.8E-01	1.0E-01	-	-	1.6E+01	9.4E+01	8.3E-01	3.1E-01	8.0E-02	-
Boron	5.4E+02	4.2E+00	9.3E+01	5.8E+02	3.8E+01	2.3E+02	1.0E+01	1.3E+00	3.6E+01	-
Bromine	-	-	-	-	-	-	-	1.3E+02	-	-
Cadmium	1.2E+01	2.4E+00	1.1E+03	6.9E+03	4.5E+02	2.7E+03	2.4E+01	5.9E-01	1.5E-01	-
Chromium	6.3E+03	1.2E+01	1.2E+03	7.3E+03	5.5E+04	3.3E+05	3.2E+03	2.8E+00	1.1E+00	3.8E+05
Cobalt	1.3E+02	5.3E-01	2.1E+01	1.3E+02	8.2E+00	4.9E+01	4.4E-01	1.8E+00	1.3E-01	-
Copper	1.8E+04	2.4E+01	3.9E+03	2.4E+04	2.7E+05	1.6E+06	1.4E+06	1.6E+02	4.8E+00	-
Iodine	-	-	-	-	-	-	-	6.6E+01	-	-
Lead	7.7E+03	6.0E+01	2.2E+03	1.4E+04	2.1E+05	1.3E+06	1.2E+04	7.9E+00	3.0E+00	-
Lithium	4.1E+01	9.4E-01	-	-	-	-	-	2.0E+00	7.6E-01	-
Manganese	3.2E+03	1.1E+01	6.1E+03	3.8E+04	3.5E+03	2.1E+04	6.1E+05	4.1E+01	1.0E+01	1.5E+05
Mercury	1.2E+01	5.2E-02	4.7E+00	2.9E+01	3.1E+00	1.9E+01	1.7E-01	3.1E-01	8.0E-02	-
Molybdenum	2.1E+02	3.0E+00	-	-	-	-	-	2.2E+00	1.1E-01	-
Nickel	2.1E+03	1.0E+01	3.5E+02	2.2E+03	3.5E+03	2.1E+04	9.8E+02	3.8E+01	9.6E+00	1.6E+06
Niobium	2.2E+01	-	7.9E+00	4.9E+01	3.2E+00	2.0E+01	1.7E-01	-	-	-
Scandium	2.3E+01	-	-	-	-	-	-	-	-	-
Selenium	-	-	7.9E+00	4.9E+01	3.2E+00	2.0E+01	1.7E-01	7.9E-01	5.6E-01	-
Silver	3.8E+00	2.9E-01	-	-	-	-	-	9.4E-01	1.0E-01	-
Strontium	8.5E+02	1.8E+01	1.7E+02	1.0E+03	8.5E+01	5.1E+02	4.5E+00	5.6E+02	1.3E+01	-
Tellurium	4.9E+01	-	1.5E+01	9.5E+01	6.2E+00	3.7E+01	3.3E-01	-	-	-

Species	Bottom Ash	Baghouse Ash	Compacted Wastes (Bales)[a]	Compacted Wastes (Boxes)[a]	Non-Pro. (Drums)[a]	Non-Pro. (Boxes)[a]	Non-Pro. (Other)[a]	LLW and ALW Resins	ALW Sludge	Steam Generators
Thallium	1.0E-01	2.3E-02	-	-	-	-	-	3.8E-02	8.0E-02	-
Tin	1.3E+02	6.1E+00	-	-	-	-	-	6.1E-01	2.6E-01	-
Tungsten	-	-	-	-	-	-	-	1.1E+00	8.0E-02	-
Uranium	3.1E+00	2.3E-01	-	-	4.7E+01	2.8E+02	2.5E+00	2.8E-01	8.0E-02	-
Vanadium	8.1E+01	8.3E+00	-	-	-	-	-	2.8E-01	8.0E-02	-
Zinc	3.4E+04	1.4E+03	7.1E+03	4.4E+04	6.2E+03	3.7E+04	1.6E+04	1.3E+02	1.2E+02	-
Zirconium	2.7E+02	8.6E-01	4.6E+01	2.8E+02	2.0E+01	1.2E+02	1.1E+00	4.1E-01	3.8E-01	-
PAH	1.4E+00	2.0E+00	-	-	-	-	-	-	-	-
Cl-Benzenes & Cl-Phenols	2.1E+00	6.4E-01	-	-	-	-	-	-	-	-
Dioxins & Furans	7.3E-02	2.0E-02	-	-	-	-	-	-	-	-
PCB	1.3E-01	5.2E-03	-	-	-	-	-	-	-	-

Notes:

a Derived pro-rata on the basis of raw waste inventories from amalgamated data in OPG (2010).

- indicates no value given for waste category in OPG (2010).

Gadolinium and Hafnium have not been included as OPG (2010) does not specify inventories for these elements in any LLW category.

Table 3.18: Total Inventory of Non-radioactive Species in ILW Waste Streams (kg)

Species	Moderator Resin	PHT Resin*	Misc Resin	CAN-DECON Resin	Core Components	Filters & Elements	IX columns*	Retube Wastes			
								Pressure Tubes^	End Fittings^	Calandria Tubes^	Calandria Tube Inserts
Antimony	7.1E-01	5.6E-01	3.7E-01	1.1E-01	-	-	2.3E-01	4.4E-01	2.1E+01	2.3E-01	1.9E-01
Arsenic	4.6E-01	6.0E+00	2.3E+00	1.2E+00	-	-	2.4E+00	1.8E-02	1.3E+02	1.4E-01	1.2E+00
Barium	9.7E+00	9.3E+01	1.9E+01	5.2E-01	-	-	3.7E+01	1.3E-03	9.2E-03	7.7E-04	8.4E-05
Beryllium	8.2E-01	1.4E+01	5.2E-01	6.9E-01	-	-	5.5E+00	4.4E-04	4.6E-03	1.1E-04	4.2E-05
Boron	6.9E+02	2.8E+01	2.4E+02	7.8E+01	-	4.2E+03	1.2E+01	3.1E-02	2.3E+00	6.8E-03	2.1E-02
Bromine	-	-	2.2E-01	2.0E-01	-	-	-	1.8E-02	2.3E-02	1.5E-03	2.1E-04
Cadmium	1.2E+01	7.8E-02	2.7E+00	4.0E+00	-	-	3.2E-02	4.4E-01	2.3E-01	1.1E-01	2.1E-03
Chromium	2.1E+01	1.9E+01	1.1E+01	1.7E+01	4.8E+03	3.1E+04	7.5E+00	2.1E+01	1.6E+05	6.2E+01	1.5E+03
Cobalt	1.0E+00	1.7E-01	3.1E+00	1.8E+01	-	-	6.9E-02	1.3E-01	2.8E+02	5.1E-02	2.5E+00
Copper	7.4E+02	1.6E+01	3.1E+03	1.3E+02	-	-	6.6E+00	3.1E+00	3.0E+03	6.0E-01	2.7E+01
Gadolinium	4.4E+03	7.1E+02	8.3E+00	1.3E-01	-	-	2.9E+02	-	-	-	-
Hafnium	-	-	-	-	-	-	-	1.7E+01	2.3E+02	9.5E+00	2.1E+00
Iodine	-	-	6.2E-02	4.8E-02	-	-	-	1.3E-03	6.9E-03	5.1E-04	6.3E-05
Lead	9.2E+01	7.8E+00	9.6E+01	8.2E+01	-	-	3.2E+00	8.8E-01	2.3E+00	6.0E-01	2.1E-02
Lithium	3.9E+02	3.8E+03	1.9E+02	1.3E+01	-	-	1.5E+03	8.8E-04	1.2E-02	1.9E-04	1.1E-04
Manganese	2.5E+01	6.4E+01	7.6E+01	5.2E+02	-	5.5E+03	2.6E+01	1.3E+00	1.1E+04	2.3E-01	9.9E+01
Mercury	6.2E-02	7.8E-02	3.3E-02	8.1E-02	-	-	3.2E-02	1.3E-02	6.9E-02	4.0E-03	6.3E-04
Molybdenum	2.6E+00	2.8E+01	3.8E+00	2.8E+00	-	-	1.1E+01	8.8E-01	9.2E+02	5.1E-01	8.4E+00
Nickel	4.6E+03	7.8E+00	3.3E+02	4.3E+03	1.7E+04	1.9E+04	3.2E+00	4.4E+00	3.9E+03	4.3E+01	3.6E+01
Niobium	-	-	-	-	-	-	-	1.1E+04	3.5E+01	6.5E-01	3.2E-01
Scandium	5.6E-02	-	-	-	-	-	-	4.4E-01	4.6E-02	7.4E-02	4.2E-04
Selenium	8.2E-01	5.7E-01	2.6E+00	6.6E-01	-	-	2.3E-01	1.8E-02	1.6E-01	4.3E-03	1.5E-03
Silver	4.6E-01	1.3E-01	2.2E-01	1.1E-01	-	-	5.2E-02	4.4E-01	4.6E-01	2.6E-01	4.2E-03
Strontium	5.4E-01	1.1E+00	3.1E+01	1.7E-01	-	-	4.6E-01	2.6E-02	1.4E-01	2.8E-03	1.3E-03
Tellurium	-	-	-	-	-	-	-	1.8E-02	4.6E-02	2.3E-03	4.2E-04

Species	Moderator Resin	PHT Resin*	Misc Resin	CAN-DECON Resin	Core Components	Filters & Elements	IX columns*	Retube Wastes			
								Pressure Tubes^	End Fittings^	Calandria Tubes^	Calandria Tube Inserts
Thallium	8.2E-02	5.7E-02	3.0E-02	8.9E-02	-	-	2.3E-02	3.1E-03	1.8E-02	1.2E-03	1.7E-04
Tin	1.6E+00	3.8E+00	1.4E+00	7.5E+00	-	-	1.5E+00	4.8E+00	6.4E+02	1.7E+03	5.9E+00
Tungsten	1.6E-01	5.7E+00	1.8E+00	1.4E-01	-	-	2.3E+00	3.1E+00	1.3E+02	9.4E-02	1.2E+00
Uranium	9.2E-02	1.3E+00	1.6E+00	2.1E+01	-	-	5.2E-01	1.3E-01	6.9E-03	2.3E-01	6.3E-05
Vanadium	8.2E-02	1.6E+00	1.9E+00	5.5E-02	-	-	6.6E-01	2.2E-01	9.4E+02	6.8E-02	8.6E+00
Zinc	4.1E+02	4.3E+01	1.5E+03	6.8E+01	-	-	1.8E+01	3.1E-02	1.6E+01	3.5E-02	1.5E-01
Zirconium	2.3E-01	1.3E-01	7.5E-01	6.2E-02	-	-	5.2E-02	4.3E+05	3.0E+01	1.7E+05	2.7E-01

Notes:
* Derived pro-rata on the basis of raw waste inventories from amalgamated data in OPG (2010).
^ Data for retube wastes are derived from the elemental compositions given in OPG (2010).
- indicates no value given for waste category in OPG (2010).
PAH, Cl-Benzenes & Cl-Phenols, Dioxins & Furans and PCB have not been included as OPG (2010) does not specify inventories for these elements in any ILW category.

3.6.2 Water Composition

Once closed, the DGR will gradually re-saturate with porewater from the surrounding rock. The chemistry of this water is an important factor controlling the evolution of the repository (due to its impact on processes such as corrosion and microbial degradation) and the dissolution of radionuclides and non-radioactive species.

Based on information in the Descriptive Geological Site Model (DGSM) report (INTERA 2011, Section 4.6) (and summarized in Table 5.4), the natural porewater geochemistry at the depth of the DGR:

- Is anaerobic;
- Has pH within the range 5.0 – 6.5;
- Has a total dissolved solids content of 240 – 365 g L^{-1}; and
- Has a chloride concentration of 170 – 215 g L^{-1}.

The water chemistry in the repository will also be affected by the bulk materials present in the waste packages, as well as the concrete used for floors and seals in the repository. In particular, cement will condition water to high pH (see QUINTESSA 2011b Section 4.5.3 and Appendix E5). As a result, the water composition in the repository will evolve with time and the pH is expected to evolve generally as described in Berner (1990), Karlsson et al. (1999) and Metcalfe and Walker (2004). In the LLW rooms the pH is expected to be similar to background (~up to pH 6.5) with potential increase in pH due to degradation of cement on ceilings, walls and floors and in wastes being offset by decrease caused by acidity induced by H_2, CO_2 and/or organic acids from waste package degradation. In the ILW rooms, pH is likely to be slightly higher than in the LLW rooms, due to increased amount of concrete associated with waste packaging. Local to cementitious waste packages, higher pH conditions can be expected to develop. Within structural concrete, initially there will be an increase to pH > 13 in concrete pore fluids, decreasing to ~12.5 and then to pH ~10 and eventually to pH closer to that of ambient groundwater. However, the time taken for these changes is likely to be extremely long. Although the pH will decrease to around 12.5 over a period of a few hundred years, thereafter it is expected to remain at this value for several hundred thousand years. It is expected to take much longer than the assessment period of 1 million years for natural pH to be attained; alkaline conditions will continue throughout the assessment period. In the Low Heat, High Performance Cement (LHHPC) of the shaft monolith and seals, the initial pH of pore fluids will be ~10, after which it will decrease slowly to that of ambient groundwater in a similar fashion to structural concrete.

The initial amounts/concentrations of nitrate (NO_3^-), sulphate (SO_4^{2-}) and Fe(III) in the water are potentially important with respect to microbial reactions. Nitrate (NO_3^-) would primarily be present from the waste, and the initial amount is determined by the mass of nitrate in the waste (1.2×10^5 kg, Table 2.8 of the Reference L&ILW Inventory Report, OPG 2010). It is expected that under the reducing (anoxic) conditions that would be established following closure of the DGR, nitrate would be reduced progressively to nitrite (NO_2), nitrogen gas (N_2) and ultimately ammonia (NH_3). Most likely the reduction process will be microbiologically mediated and possibly could be catalyzed by metal surfaces; the rate at which reduction will occur and the controlling mechanism is a subject of on-going research (e.g., JAEA 2007 and references therein).

Sulphate (SO_4^{2-}) would be determined by groundwater composition. Its concentration is estimated at c.2 kg m^{-3}, which was obtained by simulating equilibrium between a Cobourg

porewater composition reported in the Descriptive Geological Site Model (INTERA 2011, Section 4.6) and anhydrite (see Appendix C, Section C.2.1). For comparison, the lowest reported concentration among opportunistic groundwater samples from the Deep Bedrock Groundwater Zone (Table 5.4) is 0.35 kg m^{-3} at a depth of 860 m (INTERA 2011, Section 4.5.2). Some SO_4^{2-} could potentially be released to the water by the degradation of ion exchange resins, which are composed of polystyrene molecules that contain sulphonic acid functional groups. However, the breakdown of the resin is expected to be microbially mediated and is more likely to involve reduction of SO_4^{2-}. Additionally, provided that the precipitation of anhydrite is sufficiently fast compared with the addition of SO_4^{2-} from resin degradation, equilibrium between the water and anhydrite will place an upper limit on the aqueous SO_4^{2-} concentration. For these reasons, resin breakdown is not expected to contribute significant SO_4^{2-} to the water.

Dissolved Fe(III) will be at extremely low concentrations owing to the reducing conditions that will be established following closure. As a result Fe-reducing bacteria will be insignificant within the water. However, these micro-organisms may potentially occur within solid Fe(III)-oxides, for example corrosion products on metal surfaces. If active, the micro-organisms could potentially reduce the solid Fe(III) to the more soluble Fe(II) form, thereby increasing the dissolved Fe concentration.

The initial amounts of biomass, as well as iron corrosion products, within the repository are expected to be minor compared to the initial amounts of organic materials in the waste and the uncorroded steel material.

3.6.3 Solubility

3.6.3.1 Gases

Solubility constants (also referred to as Henry's Law Constants) defining the distribution of O_2, N_2, H_2, CO_2, H_2S, CH_4 and He between aqueous and gas phases are given in Table 3.19. Based on a literature review summarized in Appendix B, these values are given at 20-25 ^oC and the salinity of brine (i.e., a total dissolved solids of greater than 100 g L^{-1}).

Table 3.19: Solubility Constants for Gaseous Species in Brine at 20-25^{o}C

Gas	Solubility Constant (mol L^{-1} MPa^{-1})
O_2	9.0E-03
N_2	2.9E-03
H_2	2.2E-03
CO_2	6.9E-02
H_2S	5.1E-01
CH_4	4.0E-03
He	1.2E-03

3.6.3.2 Solids

Limits on the solubility of elements in repository water can constrain the rate of release of contaminants from the waste.

The extent to which elements and chemicals are soluble in the repository water will be affected by the characteristics of incoming rock porewater (including stable isotopes), and its conditioning by waste and waste package degradation products.

- The inflowing water is highly saline, with a high concentration of dissolved solids. The nature of the dissolved minerals will have an important bearing on the potential for elements and chemicals in the waste to dissolve.
- The waste degradation products can affect the water chemistry directly, for example organics may degrade to form weak acids. Also, organic degradation products can form colloids and increase the solubility of radionuclides, as cellulose is known to increase the solubility of actinides. Among the elements of interest to the current assessment, U, Pu, Ni and Cd may form complexes with isosaccharinic acid, an important breakdown product of cellulose.
- The pH of the porewater at the depth of the DGR is near neutral, however locally raised pH might occur where waste packages with substantial quantities of cement are present. The pH does not generally influence solubility significantly, given the range expected under repository conditions, although for some specific elements it may be relevant.
- The porewater at the DGR depth is anaerobic and reducing. This affects which valence state is most likely for some elements and radionuclides, and therefore their solubility. For example, uranium is likely to be in a less soluble form under reducing conditions.

The derivation of solubility-limiting solids and corresponding solubility limits for several key elements is described in Appendix C. In order to undertake solubility limit calculations, representative water compositions were chosen for aqueous speciation calculations, the results of which were used as input for the construction of solubility diagrams that provide an indication of possible stable and metastable solid compounds that may limit contaminant solubilities.

Two water compositions were adopted for the solubility limit calculations: (1) a ‘model’ Cobourg limestone porewater, with a relatively low redox potential (pe = -2), a pH of 6.5 and a high salinity (ionic strength of 3.8); and (2) a modelled fresh cement-equilibrated Cobourg limestone porewater (Appendix C.2.1). Some additional calculations were also undertaken to demonstrate the possible effect of salinity and carbonate species activities on calculated solubility limits. It was assumed that the cement-equilibrated composition would have solute activities that corresponded to equilibrium with phases such as high CSH gel and portlandite (i.e., that the cement is relatively fresh and has not undergone extensive leaching/carbonation). The calculations required the use of a Pitzer geochemical database (Appendix C.2.1), given the high ionic strengths of the representative water compositions. The database chosen was deemed to be the best available, although it does lack data for some elements and compounds (Appendix C.2.1).

The solubility limits for the Cobourg porewater and the cement-equilibrated Cobourg porewater could be used to inform the derivation of solubility limits for the waste packages. However, there are a number of uncertainties associated with such an approach. For a number of elements (e.g., cadmium, nickel and lead) there is a lack of data in the Pitzer database. Additionally, organic complexing could increase solubility limits for certain elements such as uranium and plutonium in those packages containing cellulose-bearing wastes. Therefore,

conservatively, the solubility of all elements, except carbon, is taken to be unlimited in all packages. In contrast to other elements, the solubility limit for inorganic carbon is governed by carbonate mineral equilibria and a solubility limit of 6×10^{-1} mol m^{-3} is used for both cementitious and non-cementitious waste packages, although it may be an order of magnitude lower for cementitious waste packages (Appendix C.3.1).

3.6.4 Sorption

Elements partition between solid and liquid phases according to a range of processes such as ion exchange and surface-complexation processes. Sorption is generally described with an empirical relationship that defines the distribution of contaminants between solid and liquid in a medium that contains both:

$$Kd = \frac{S}{C} \tag{3.1}$$

Where:

Kd is the sorption coefficient;

S is the sorbed concentration of the element of the sorbate of interest in mol kg^{-1}; and

C is the aqueous concentration of the sorbate in mol m^{-3}.

The value of Kd is generally based on measurements with reference sorption values being derived for equilibrium conditions. The low rate of ingress/egress of groundwater from the DGR indicates that equilibrium conditions are likely to become established, and that use of equilibrium Kd values is reasonable.

It is useful to distinguish between cementitious and non-cementitious wasteforms since the high pH conditions in porewater of cement-conditioned wasteforms alters significantly the sorption behaviour of some key elements such as uranium. Although much of the waste anticipated to be emplaced in the DGR is expected to be ungrouted, some wastes have been/will be encapsulated in cement (steam generators) and some wastes will be placed in concrete overpacks (most ILW wastes).

As part of the present dataset, a review of sorption values has been undertaken for several potentially important elements: carbon, chlorine, chromium, nickel, copper, zirconium, niobium, cadmium, iodine, lead, radium, uranium, neptunium and plutonium. Specific consideration was given to the geochemical conditions at the repository horizon and the likely materials present that could alter sorption behaviour. The review is presented in Appendix D.

The review indicates an absence of sorption values relevant to the evolving repository conditions, and so sorption is conservatively neglected for all elements in all wasteforms (be they cementitious or non-cementitious).

3.6.5 Corrosion

Corrosion of metals in the DGR is an important process as it:

- Provides a process by which wastes in sealed watertight containers can ultimately be contacted by water (through the breach of the container as a result of corrosion);

- Provides a process by which radionuclides and non-radioactive species in the 'matrix' of metallic wastes can become available for dissolution in groundwater;
- Can influence the water chemistry;
- Can result in the generation of gas which can affect the conditions in the repository and the potential pathways from it; and
- Can result in the structural collapse of containers which could impact the release of radionuclides.

The rate of corrosion of metallic containers and waste forms is expressed in terms of the average rate at which metal corrodes (m a^{-1}), and is dependent upon the local chemical conditions. A key factor is the distinction between aerobic and anaerobic conditions. Oxygen is important as it acts as an oxidant and directly supports the corrosion reaction. In the absence of oxygen, water can act as an oxidant for certain metallic materials (including all of the materials considered here), but is also required to provide a conducting electrolyte to support the electrochemical reactions that constitute the overall corrosion reaction.

Due to the potentially long period where the repository is unsaturated but contains humid gas, the corrosion rates considered here also make a distinction between waste that is subject to water saturated (i.e., submerged in water) and water unsaturated (i.e., in the vapour phase) conditions.

The other important corrosion characteristic of the repository environment is the salinity of the groundwater. Although chloride ions (Cl^-) are not themselves oxidants that directly support the corrosion of metallic materials, Cl^- does affect the solubility and stability of protective surface layers that would otherwise form. The effects of salinity are accounted for in the corrosion rates.

Therefore corrosion rates will differ for the following three phases of the DGR's evolution:

- Phase 1 - aerobic humid conditions (prior to complete resaturation, and before corrosion and aerobic microbial respiration has exhausted oxygen in the repository atmosphere);
- Phase 2 - anaerobic humid conditions (prior to complete resaturation, after corrosion and aerobic microbial respiration has exhausted oxygen in the repository atmosphere); and
- Phase 3 - anaerobic saline saturated conditions.

3.6.5.1 Corrosion Rates

The most common metals in the repository are carbon steel followed by stainless steel. There are also notable quantities of nickel and zirconium based alloys.

Corrosion rates are presented in Table 3.20 for these metals. These data are based on a review of information presented in literature studies which is described in Appendix E. The review found that there is a large amount of data for the important carbon steel material. There is less data in the literature for the other alloys under DGR conditions. For carbon steel, there are so many data that the range of reported rates is large, reflecting the diversity of materials, environments, experimental methods, etc. that have been used.

Data for passivated steels relate to the presence of cement (pH 12-13). Elevated chloride would tend to induce localized corrosion. This would be relevant to early failure of the containers, but not to the overall degradation of the carbon steel and the overall rate of H_2 evolution, especially after anaerobic conditions are established. Provided the high pH is maintained, de-passivation is not expected.

The data provided in Appendix E represent a best estimate for a range of likely repository conditions. The recommended values are appropriate for neutral pH (other than for passivated steel), but the higher end of the range should be selected if conditions reach pH 5-6. The range of values also reflects the effect of the range of possible groundwater salinity on the corrosion rate.

The review of recommended values indicated that the most appropriate distribution to adopt for corrosion rates is a log uniform distribution, with the maximum and minimum used to define the limits to the distribution.

Table 3.20: Corrosion Rates for Metals

Conditions	Metal	Corrosion Rate (m a^{-1})			
		Best Estimate	Probability Distribution Function		
			Distribution	Minimum	Maximum
Aerobic humid conditions (Phase 1)	Un-passivated C-steel and galvanized steel	1E-05	log uniform	1E-06	1E-04
	Passivated C-steel, stainless steel and Ni-alloys	1E-07	log uniform	5E-08	5E-06
	Zirconium based alloys	1E-08	log uniform	5E-09	5E-08
Anaerobic humid conditions (Phase 2)	Un-passivated C-steel and galvanized steel	1E-06	log uniform	1E-07	1E-05
	Passivated C-steel, stainless steel and Ni-alloys	1E-07	log uniform	1E-08	1E-06
	Zirconium based alloys	1E-08	log uniform	5E-09	5E-08
Anaerobic saline saturated conditions (Phase 3)	Un-passivated C-steel and galvanized steel	2E-06	log uniform	1E-07	1E-05
	Passivated C-steel, stainless steel and Ni-alloys	1E-07	log uniform	1E-08	1E-06
	Zirconium based alloys	1E-08	log uniform	5E-09	5E-08

Notes: The rates in the above table are appropriate for the expected repository environment: pH 5.0-6.5 (except pH 12-13 for the passivated C-steel), temperature of ~ 20 ^{o}C, and a Na-Ca-Cl salinity of 170-215 g L^{-1}.

3.6.5.2 Carbon Dioxide Enhanced Corrosion

The presence of CO_2 increases the rate of corrosion of C-steel and passive materials by lowering the pH (ASM 1987, 2003, 2005; de Waard and Lotz 1993; de Waard and Milliams 1976; de Waard et al. 1991, 1995). The corrosion of C-steel in CO_2 environments has been studied both empirical and mechanistically. A number of models have been developed to predict the rate of corrosion as a function of the partial pressure of CO_2, P_{CO2}.

A simple enhancement factor (F) can be used to account for the effect of CO_2:

$$F = 1 + \left(\frac{P_{CO2}}{P_{CO2}^{ref}} \right)^{q} \quad (3.2)$$

where P_{CO2}^{ref} is a reference CO_2 partial pressure at which the corrosion rate is twice that in the absence of CO_2 and q is the reaction order with respect to the CO_2 concentration. Based on data from de Waard and Lotz (1993), de Waard and Milliams (1976), and de Waard et al. (1991, 1995), an appropriate value for q is

$$q = 0.67 \quad (3.3)$$

The value of q is taken directly from the dependence of the corrosion rate on the partial pressure of CO_2 reported by de Waard and Milliams (1976). However, the corrosion rate expression provided by these authors cannot be used directly to estimate the value of P_{CO2}^{ref} since it does not predict the corrosion rate in the absence of CO_2. King (2008) has summarized the observed time-dependence of the anaerobic corrosion rate of C-steel in various environments. Extrapolating these data to shorter times, i.e., prior to the development of a protective surface film corresponding to the conditions studied by de Waard and Milliams (1976), suggests an initial corrosion rate of the order of 50-100 μm a^{-1}. Using a value of 100 μm a^{-1}, de Waard and Milliams' corrosion rate expression can be used to predict the CO_2 partial pressure at which the corrosion rate would be 200 μm a^{-1}, which corresponds to the value of P_{CO2}^{ref} in Equation (3.2). For a repository temperature of 20°C, the corresponding CO_2 partial pressure is 0.025 MPa.

This enhancement factor may be used for both saturated and unsaturated conditions, but only in the absence of O_2, which otherwise acts as the major oxidant. The same enhancement factor is assumed to also apply for the passive alloys.

3.6.5.3 Effective Molar Masses of Metals

The extent of corrosion can be tracked in terms of the number of moles of each material. The effective molecular mass of C-steel (plain, galvanized, and passivated) can be taken to be the same as iron (0.0559 kg mol^{-1}) (CRC 2006). The effective molar mass for stainless steel (which can be taken as representative of the passive alloys) is 0.0555 kg mol^{-1}, based on a composition of a typical 316L stainless steel with 65.5% Fe,17% Cr and 12% Ni, 2.5% Mo, 2% Mn, 1% Si (by weight) (ASM 1987). The effective molar mass of the Zr alloys can be taken to be 0.0913 kg mol^{-1}, based on a composition of 97.5% Zr and 2.5% Nb (by weight) (ASM 1987).

3.6.5.4 Threshold Relative Humidity for Corrosion Under Humid Conditions

In general, metal corrosion occurs in unsaturated conditions above a threshold relative humidity of 60-80% (Leygraf and Graedel 2000, Shreir et al. 1993), corresponding approximately to the relative humidity at which NaCl deliquesces at room temperature. It is appropriate to use a range for the threshold relative humidity as the condensation of water is also affected by the porosity of surface deposits (capillary condensation), which is likely to vary over the surface of the metallic wastes and container materials, and the presence of other deliquescent salts. In the model, the corrosion rate is assumed to be zero below 60% relative humidity, at the value

for fully saturated conditions at 80% relative humidity, and to vary smoothly between the two limits.

3.6.6 Microbial Degradation

The waste inventory for the DGR includes a significant mass of organic material including cellulose (paper, cotton, wood, and other organics), plastics (especially the resins), and rubber and other organics (Section 3.4.1). These materials will degrade under both aerobic and anaerobic conditions as a result of microbial action. Like corrosion, microbial degradation can therefore:

- Result in the generation of gas which can affect the conditions in the repository and the potential pathways from it;
- Provide a process by which radionuclides can become available for dissolution in groundwater; and
- Influence the water chemistry.

The primary data required to model microbial degradation and gas generation in the present study are:

- Cellulose and ion exchange resin degradation rates; and
- Microbial hydrogen consumption rates.

In addition, the model considers the production and degradation of biomass and requires the following additional data:

- Yield coefficients for each microbial degradation reaction;
- Biomass decay rates; and
- The fraction of biomass that is recyclable.

3.6.6.1 Organic Degradation Rates

The most important data required are the degradation rates of cellulose and ion exchange resins. In order to obtain these data, a literature review has been carried out specifically targeting waste degradation experiments. The review is documented in Appendix F.

Recommended degradation rate constants for cellulose and ion exchange resins for aerobic and anaerobic processes are given in Table 3.21. These reactions assume that sufficient water is available - microbial activity ceases if the water vapour activity (or relative humidity) drops below 0.6. Note that the categorization of denitrification in this table as an aerobic rather than anaerobic process is deliberate since nitrate reduction is considered to be anoxic rather than truly anaerobic. It occurs in an oxidising environment but not in an oxygen based one.

Table 3.21: Degradation Rates for Cellulose and Ion Exchange Resins (20-25°C)

Microbial Processes	Organic Materials	Degradation Rate (a^{-1})			
		Best Estimate	Probability Distribution Function		
			Distribution	Minimum	Maximum
Aerobic processes (aerobic metabolism, denitrification)	Cellulose	1.5E-03	log uniform	1.5E-04	1.5E-02
	Ion Exchange Resins	5E-04	log uniform	1E-04	1E-03
Anaerobic processes (fermentation, iron reduction, sulphate reduction, methanogenesis)	Cellulose	5E-04	log uniform	5E-05	5E-03
	Ion Exchange Resins	5E-05	log uniform	5E-06	5E-04

These degradation reactions can be expected to occur in a well-defined sequence, beginning with aerobic respiration, followed by denitrification, iron reduction, sulphate reduction, and methanogenesis, depending on the availability of the terminal electron acceptor (O_2, NO_3^-, Fe(III), or SO_4^{2-}). In the absence of a particular terminal electron acceptor, the relevant process does not take place. An exception to this rule is methanogenesis, for which CO_2 is not required to be present for degradation to take place.

Cellulose is treated as a polymeric material with the formula $(C_6H_{10}O_5)_n$ with a cellulose monomer molecular mass of 0.162 kg mol^{-1}. Ion exchange resins are polystyrene based, and are basically represented as polystyrene, for which the monomer molecular mass is 0.104 kg mol^{-1}. Other plastics and rubbers are present in the DGR and will have a diverse composition (e.g., polyethylene - $(C_2H_4)_n$, rubber - $(C_5H_8)_n$), but are also represented in this study as polystyrene $(C_8H_8)_n$ for estimating their CO_2 and CH_4 gas generation potential.

More specifically, ion exchange resins are polystyrene-divinyl-benzene with sulfonic acid groups on the cation and quaternary ammonium groups on the anion. Based on the chemical structural formula, the molecular mass of the "dry" cation and anion resins are 0.184 and 0.193 kg mol^{-1} respectively. Assuming equal moles of cation and anion resins used, the molecular mass of the combined "dry" resins is 0.1885 kg mol^{-1}. There are 10 moles of carbon in 1 mole of dry resins, compared to 8 moles of carbon in 1 mole of polystyrene. Therefore, in order to ensure that the number of moles of carbon modelled is equal to the total amount available in the resins, the molar mass is multiplied by a factor 8/10, resulting in an equivalent mass of resin per mole of styrene monomer of 0.1508 kg mol^{-1}.

3.6.6.2 Hydrogen Consumption Rate

The microbial hydrogen reactions can proceed when a suitable terminal electron acceptor (Fe(III), SO_4^{2-}, or CO_2) is present in the system and other more oxidising reactants have been depleted. There is some uncertainty over the microbial hydrogen consumption rates and much of the data in the literature are expressed in units that are incompatible with the first order rate constants used in the present model. However, it is expected that the rates of microbial consumption of hydrogen will be fast compared with its rate of generation from metal corrosion (Grant et al. 1997, Pedersen 2000), consistent with the observation that although corrosion happens in many microbially active environments, hydrogen does not accumulate to any

significant extent. Therefore the model results are not sensitive to the exact rate, but rather to whether the reaction occurs or not.

Harris et al. (2007) provides first order rate constants for hydrogen consuming denitrifying (0.05 h^{-1}), iron reducing (0.18 h^{-1}) and sulphate reducing (1.2 h^{-1}) communities. A rate of 250 a^{-1} (0.03 h^{-1}) is adopted for all the microbial hydrogen reactions, including methanogenesis. This is consistent with microbially active conditions, assuming suitable electron acceptors are present.

3.6.6.3 Biomass Yield Coefficients

Each microbial degradation reaction is characterized by a microbial yield which describes the partitioning of the substrate between biomass production and substrate oxidation. Microbial yield coefficients (i.e., the fraction going to biomass production) have been taken from Rittmann and McCarty (2001) (Table 3.22).

Table 3.22: Biomass Yield Coefficients

Microbial Process	Yield Coefficient
Aerobic metabolism (a)	0.6
Denitrification (b)	0.5
Fermentation and iron reduction (c)	0.23
Fermentation and sulphate reduction (c)	0.23
Fermentation and methanogenesis (c)	0.23

Notes:
- a Value given for "other" biological oxygen demand for aerobic heterotrophs.
- b Value for biological oxygen demand for denitrifiers.
- c Sum of value for fermenters (0.18) and methanogens from the acetate reaction (0.05).

A single yield for all three anaerobic reactions is used since the dominant reaction is the methanogenic reaction.

3.6.6.4 Biomass Decay Rate

Biomass also dies and decays. Biomass decay rates in the literature show a wide degree of variation. Rittmann and McCarty (2001) suggest that typical rates vary between 110 a^{-1} and 18 a^{-1}. An even greater degree of variation (35 to 0.09 a^{-1}) is employed by Agg et al. (2002) in gas generation modelling studies using the code GAMMON. Yim and Simonson (1997) quote a lower range (1.2 to 0.18 a^{-1}) in modelling studies for the US. Electric Power Research Institute although they do acknowledge the wide variation seen in values available in the literature.

A single biomass decay rate is assigned to all microbial populations modelled and a rate of 10 a^{-1} with a range of 0.1 a^{-1} to 100 a^{-1} has been chosen.

3.6.6.5 Fraction of Biomass that is Recyclable

Some dead biomass is amenable to further microbial degradation, while a certain fraction of biomass will be recalcitrant. In order to allow biomass degradation and carbon recycle, biomass degradation is modelled as equivalent to the cellulose degradation pathway, which is already included in the model. Biomass recycle is controlled by setting the fraction of biomass which is recyclable. A wide variety of biodegradation fractions can be found in the literature (Appendix F). A recycle fraction of 0.9 is recommended for use in modelling studies. This is at the upper end of the data values available, however this takes into account the longer time frames considered in this postclosure safety assessment.

3.6.7 Other Gas Parameters

3.6.7.1 Initial Partial Pressures

The initial partial pressures for the gases relevant to consider in the DGR are given in Table 3.23 and are taken from Chemical Rubber Company (CRC) (2006) for air at atmospheric pressure.

When the individual gas components are represented as a single bulk phase, an equivalent molar mass of air can be used, 0.02897 kg mol^{-1}, where the total number of moles of bulk gas is represented as the sum of the number of moles of the individual gas components.

Table 3.23: Initial Partial Pressure for Repository Atmosphere on Closure

Gas	Partial Pressure (MPa)
O_2	2.12E-02
N_2	7.91E-02
CO_2	3.18E-05
H_2	5.07E-08
CH_4	2.03E-07
H_2S	0.00E+00
He	5.31E-07

Notes:
Partial pressure is calculated from composition reported for a U.S. Standard Atmosphere at 1 bar pressure (i.e., sea level) in CRC (2006). The analysis in CRC (2006) is expressed as the volume % of each gaseous component and has been expressed in terms of partial pressures by taking the atmosphere to behave as an ideal gas and 1 bar to have a pressure of 101,325 Pa.

3.6.7.2 Iron Sulphide Precipitation Rate

A first-order rate law can be used to simulate the precipitation of FeS. Rickard (1995) has reported the kinetics of FeS precipitation, and describes the process as fast (on the timescale of

interest for the DGR). Based on the study of Rickard (1995), the first-order rate constant for the precipitation of FeS is defined as 90 s^{-1}.

3.6.7.3 FeOOH Reduction Rate

The reductive dissolution of FeOOH under anaerobic conditions can be modelled based on a first-order reaction with a rate constant of 10^{-8} s^{-1}. This rate constant is equivalent to a half-life for FeOOH under anaerobic conditions of 2.2 years. This value was selected because, although the charge transfer reaction is likely to be fast, the overall reaction will be limited by the slow rate of dissolution of the FeOOH species.

3.6.7.4 Gas-Water Partition Coefficients for Volatile Contaminants

I, Cl and Se released from the wastes will dissolve in water in the repository. These radionuclides may subsequently be volatilized, and enter the gas phase prior to resaturation of the repository. Gas-water partition coefficients are given in Table 3.24 based on the literature review presented in Appendix G.

Table 3.24: Gas-Water Partition Coefficients for Volatile Radionuclides

Gas	Partition Coefficient (-)
Cl	1E-06
I	1E-04
Se	1E-04

Note:
Partition coefficient is defined as the concentration in gas (moles per m^3 gas) over the concentration in water (moles per m^3 water).

4. REPOSITORY DATA

4.1 Preliminary Design Basis

The final preliminary design for the repository is described in Chapter 6 of the Preliminary Safety Report (OPG 2011b). The underground layout is shown in Figure 4.1.

However, the postclosure safety assessment was initiated based on an original preliminary design shown in Figure 4.2 (NWMO 2010a). The change from the original to the final preliminary design was made after the present assessment was largely complete. The key changes are summarized in Table 4.1. It should be noted that these changes have been made for operational safety and reliability reasons rather than postclosure safety reasons.

The design is likely to evolve further prior to the construction of the DGR, as the detailed design is prepared. Since the primary barrier is the geosphere and since long-term safety is a design requirement, it is expected that any changes would not substantively affect the postclosure safety conclusions.

The key features of the repository design relevant to postclosure safety assessment are described in the subsections below. Changes from the original to final version of the preliminary design are noted where applicable.

Table 4.1: Summary of Changes from the Original to the Final Preliminary Design

Feature	Change	Comment
Waste Capacity	Not changed	-
Surface structures	Not changed	-
Shafts	Not changed	-
Shaft Service Area	Rearranged for better air flow. Lower height	More excavated volume. Lower height tunnels are more stable
Access Tunnels	No ventilation duct. Lower height	Less excavated volume. No ventilation duct maintenance, Easier tunnel roof maintenance. Better for tunnel excavation and stability
Emplacement Rooms	Ventilation duct removed Dimensions not changed Capacity not changed Backwall connects to return air drift	Simpler air flow No ventilation duct lifetime limit
T-H-E placement	Changed from horizontal concrete arrays in rooms, to steel & concrete packages similar to resin liners.	Easier handling
Ventilation drifts	Added	Increased excavated volume
Panel closure	Added closure plugs	Added on ventilation drifts
Monolith	Extended into new services area to north east of ventilation shaft	Consistent with the change in shaft service area
Shaft seal	Not changed	-

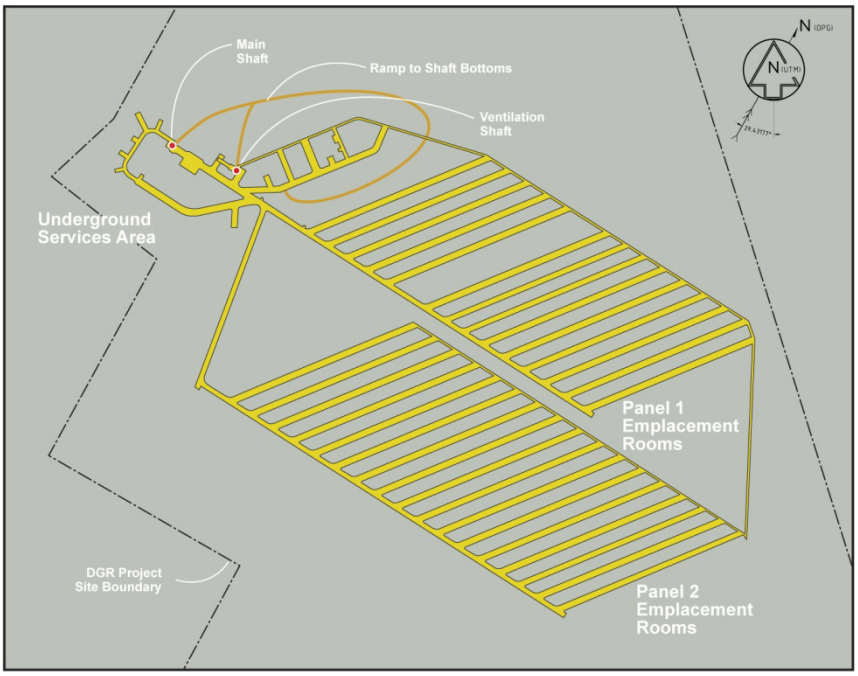

Note: Figure 6-7 from OPG (2011b).

Figure 4.1: General Layout of the Final Preliminary Repository Design

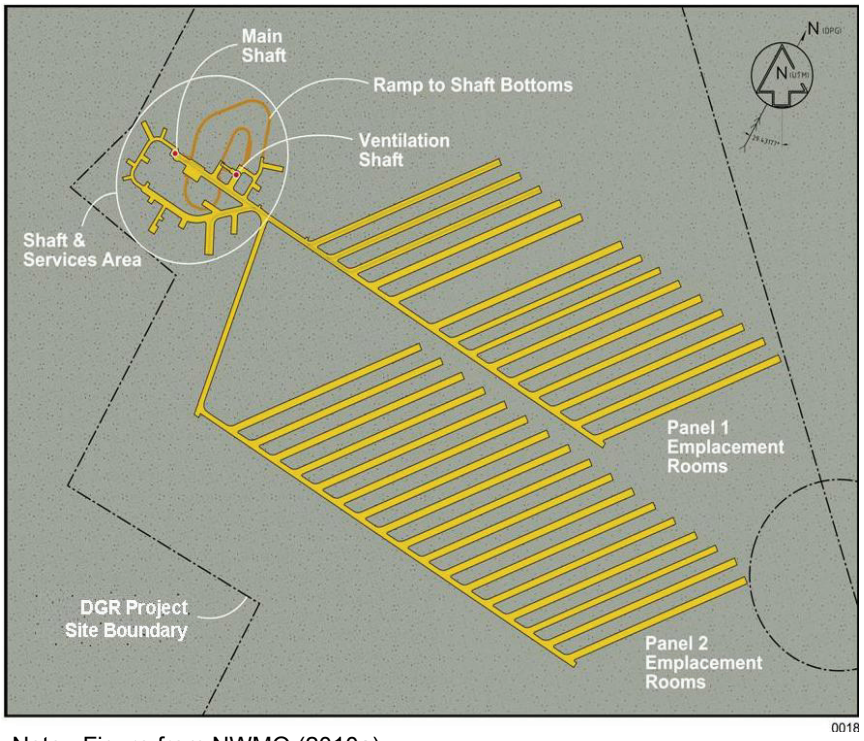

Note: Figure from NWMO (2010a).

Figure 4.2: General Layout of the Original Preliminary Repository Design

4.2 Physical Layout

The underground layout will have a slight grade, and its depth will vary slightly also with local surface topology. However, for postclosure safety assessment, this small variation is ignored and the repository floor is taken to be 6 m above the top of Sherman Falls (which is at 688.1 m, Table 5.1). Therefore, for postclosure safety assessment, the repository floor is located at a nominal depth of 682.1 m below ground surface (mBGS) within the Cobourg formation. The main features of the repository are discussed in Chapter 6 of the PSR (OPG 2011b) and are summarized below and in Figure 4.3 and Figure 4.4.

The underground layout of the repository has two vertical shafts (the main and ventilation shafts) as an islanded arrangement with a shaft and services area. A main access tunnel extends from the main shaft to the east, passing the ventilation shaft and then proceeding towards the two panels of waste emplacement rooms. The emplacement rooms are all aligned with the assumed direction of the major principal horizontal stresses of the rock mass in the Cobourg formation (i.e., east-north-east) to minimize the risks of rockfall, especially during the period in which the repository is open but also postclosure. The main access tunnel running from the main shaft continues straight into the “Panel 1” access tunnel, while a branch tunnel to the south leads to the “Panel 2” access tunnel.

Panel 1 has 14 emplacement rooms; Panel 2 has 17 emplacement rooms. The reference schedule is for Panel 2 to be filled first, primarily with wastes from storage at WWMF. This will likely take 5 to 10 years. Panel 2 will therefore contain mostly LLW rooms. Subsequently Panel 1 will be filled in two stages. The reference allocation of wastes to the emplacement rooms adopted for the current assessment is summarized in Table 4.2.

The preliminary dimensions and derived areas of the emplacement rooms and access tunnels, and the shafts are summarized in Table 4.3, and Table 4.4, respectively. The associated volumes of the emplacement rooms, access tunnels, ventilation (return air) drifts, and the shafts and services area, are presented in Table 4.5. The number of containers and volumes of waste to be emplaced in each panel are given in Table 4.6.

Table 4.2: Number of Emplacement Rooms Occupied by Each Waste Category in the Repository Panels

Waste Category	Panel 1		Panel 2 (Rooms 1 – 17)
	Rooms 1 – 5	Rooms 6 – 14	
LLW Non-Processible (other)	1	-	-
LLW Steam generators	-	1	1 (1)
All other LLW categories	1	3	13
All ILW categories	3	5	4

Note:
1. Emplaced in same room as ILW.

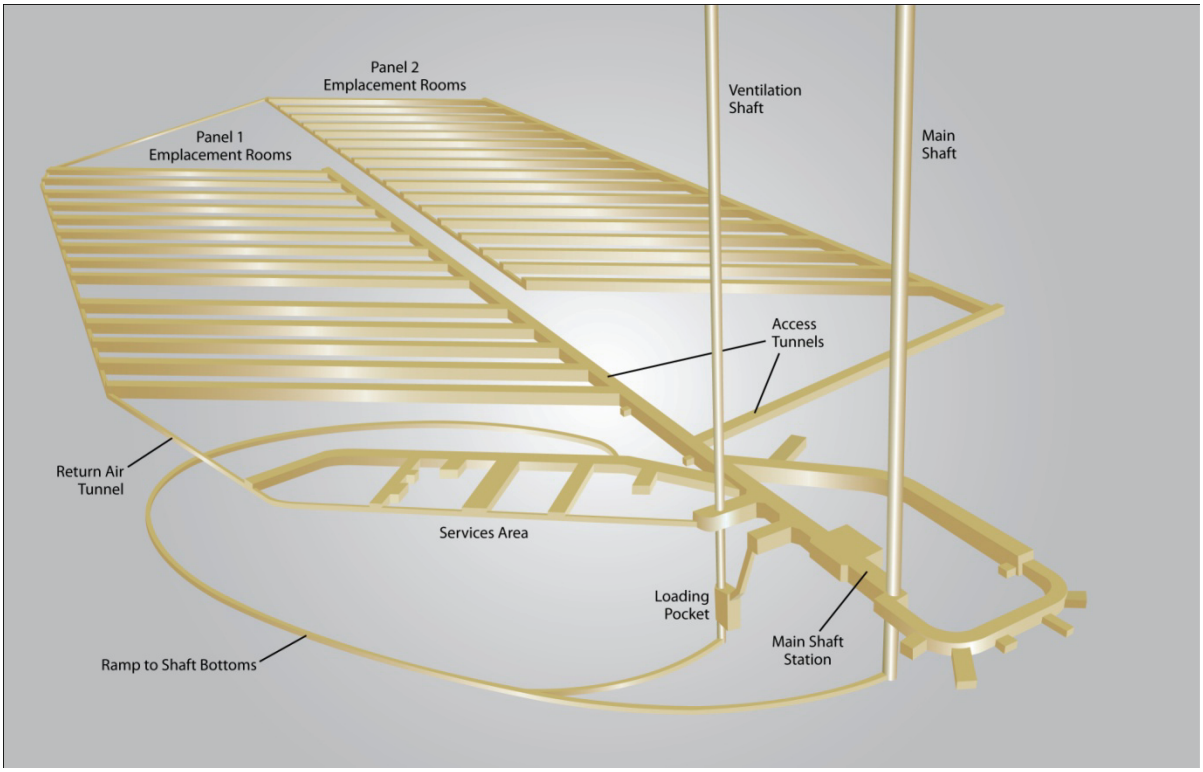

Note: Figure 6-6 in OPG (2011b).

Figure 4.3: Perspective View of the Repository

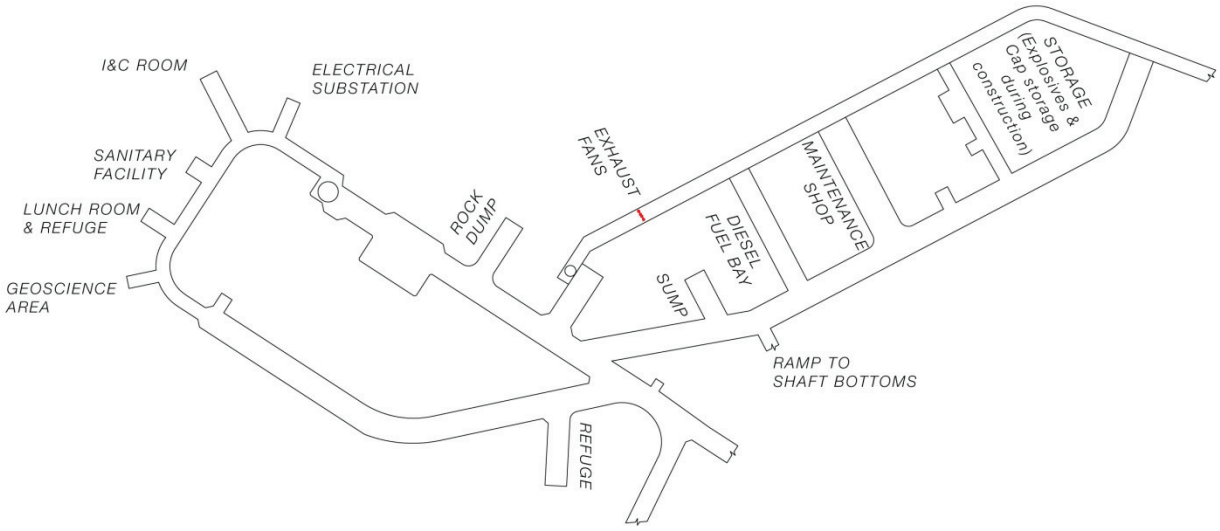

Note: Figure 6-14 in OPG (2011b).

Figure 4.4: Layout of the Shaft and Services Area

Table 4.3: Excavated Dimensions and Areas of Emplacement Rooms and Access Tunnels

Parameters	Panel 1						Panel 2						Total
Emplacement Rooms:													
Depth (m) (1)	682.1						682.1						
Emplacement Room ID (2)	P1	P2	P3	P4	P5	P6	P1	P2	P3	P4	P5	P6	
Number of Emplacement Rooms (2)	4	0	3	2	2	3	13	1	2	1	0	0	31
Length of each room (m) (2)	250	250	250	250	250	250	250	250	250	250	250	250	
Width of each room (m) (2)	8.6	8.6	8.4	7.4	8.4	8.1	8.6	8.6	8.4	7.4	8.4	8.1	
Height of each room (m) (2)	7	6.35	5.8	6.5	6.2	7.2	7	6.35	5.8	6.5	6.2	7.2	
Total Roof Area (m^2)	28,875						36,150						65,025
Access Tunnels (outside shaft and services area):													
Length (m) (2)	514 (2) / 510 (3)						809 (2) / 820 (3)						
Width (m) x Height (m)	5.4 x 8.15 (2) / 5.4 x 6.4 (3)						5.9 x 8.15 (2) / 5.4 x 6.4 (3)						
Roof Area (m^2)	2,812 (2) / 2,780 (3)						4,773 (2) / 4,600 (3)						7,585 (2) / 7,380 (3)
Ventilation (Return Air) Drifts:													
Length (m)	None (2) / 520 (3)						None (2) / 795 (3)						
Width x Height (m)	None (2) / 5 x 5 (3)						None (2) / 5 x 5 (3)						
Roof Area (m^2)	- (2) / 2,600 (3)						- (2) / 4,000 (3)						- (2) / 6,600 (3)
Panel (from first emplacement room):													
Length (m) (2)	250 (2) / 260 (3)						250 (2) / 260 (3)						
Width (m) (2)	441 (2) / 440 (3)						515 (2) / 515 (3)						
Footprint (m^2)	110,250 (2) / 114,000 (3)						128,750 (2) / 134,000 (3)						239,000 (2) / 248,000 (3)

Notes:
1. For the Postclosure Safety Assessment, the repository floor elevation is taken to be -496.3 m above sea level (mASL) (i.e., a depth of 682.1 mBGS) based on ground surface elevation of 185.84 mASL at DGR-2. This is 6 m above top of Sherman Falls (Section 4.2).
2. Data from NWMO (2010a) for the original preliminary design.
3. Data from NWMO (2010b) for the final preliminary design.

Table 4.4: Dimensions and Cross-sectional Areas of Shafts at Closure

	Main Shaft	Ventilation Shaft
Surficial Groundwater Zone:		
Length (m) (1)	20	20
Excavated Diameter (m) (1)	9.4	7.7
Finished Diameter (m) (2)	6.5	5
Excavated cross-sectional area (m^2)	69.40	46.57
Finished cross-sectional area (m^2)	33.18	19.63
Liner thickness (m)	1.45	1.35
Shallow Bedrock Groundwater Zone:		
Length (m) (1)	158.6	158.6
Excavated Diameter (m) (1)	8.15	6.45
Finished Diameter (m) (2)	6.5	5
Excavated cross-sectional area (m^2)	52.17	32.67
Finished cross-sectional area (m^2)	33.18	19.63
Liner thickness (m)	0.83	0.73
Intermediate Bedrock Groundwater Zone:		
Length (m) (1)	269.1	269.1
Diameter (m) (3)	9.15	7.45
Cross-sectional area (m^2)	65.76	43.59
Liner thickness (m)	0	0
Deep Bedrock Groundwater Zone:		
Length to top of monolith (m) (1)	214.4	214.4
Diameter (m) (4)	9.15	7.45
Cross-sectional area (m^2)	65.76	43.59
Liner thickness (m)	0	0

Notes:
1. Data from NWMO (2010a).
2. Liner and highly damaged zone (HDZ) around shafts in Surficial and Shallow Bedrock Groundwater Zones are not removed at closure (NWMO 2010a).
3. Data from NWMO (2010a). Shaft liners in Intermediate Bedrock Groundwater Zone are removed at closure and 0.5 m thickness of HDZ removed (NWMO 2010a) from around the shafts. The diameter given is the diameter of the shaft once the liner and HDZ have been removed.
4. Data from NWMO (2010a). Shaft liners above the level of the DGR are removed at closure and 0.5 m thickness of HDZ removed (NWMO 2010a) from around the shafts. The diameter given is the diameter of the shaft once the liner and HDZ have been removed.

Table 4.5: Repository Volumes

	Panel 1	Panel 2	Total
ORIGINAL PRELIMINARY DESIGN			
Excavated Volumes (m^3):			
Emplacement Rooms (1)	1.91E+05	2.46E+05	4.37E+05
Access Tunnel (outside shaft and services area) (1)	2.26E+04	3.89E+04	6.15E+04
Shaft and Services Area (2)			3.53E+04
Total	**2.13E+05**	**2.85E+05**	**5.33E+05**
Void Volume (m^3):			
Emplacement Rooms (3)	1.55E+05	1.99E+05	3.53E+05
Access Tunnel (outside shaft and services area) (4)	1.93E+04	3.63E+04	5.56E+04
Shaft and Services Area (5)			9.18E+03
Total	**1.74E+05**	**2.35E+05**	**4.18E+05**
FINAL PRELIMINARY DESIGN			
Excavated Volumes (m^3):			
Emplacement Rooms (1)	1.91E+05	2.46E+05	4.37E+05
Access Tunnel (outside shaft and services area) and Ventilation Drifts (1)	3.06E+04	4.90E+04	7.96E+04
Shaft and Services Area (2)			4.79E+04
Total	**2.22E+05**	**2.95E+05**	**5.65E+05**
Void Volume (m^3):			
Emplacement Rooms (3)	1.63E+05	2.02E+05	3.65E+05
Access Tunnel (outside shaft and services area) and Ventilation Drifts (4)	2.50E+04	4.40E+04	6.90E+04
Shaft and Services Area (5)			1.54E+04
Total	**1.88E+05**	**2.46E+05**	**4.49E+05**

Notes:
1. Derived from dimensions given in Table 4.3. Includes volume that will be filled by room and closure walls.
2. Data from NWMO (2010a) for original preliminary design, and NWMO (2010b) for final preliminary design. Includes volume that will be filled by concrete monolith at base of main and ventilation shafts but does not include ramps down to shaft sumps.
3. Derived by subtracting emplaced waste volume given in Table 4.6 from excavated volume with allowance for volume of concrete in rooms, waste voidage (Table 3.10) and packaging voidage (Appendix H).
4. Allowance made for volume of concrete in tunnels and drifts.
5. Allowance made for volume of concrete in shaft and services area (including concrete monolith (Figure 4.5 for final preliminary design, and Figure 4.6 for original preliminary design). Allowance also made for volume of concrete and steel decommissioned ventilation shaft, and equipment used in the DGR (e.g., forklifts and cranes) which is to be left in the South and West Service Tunnels.

Table 4.6: Numbers of Containers and Volumes of Waste in Each Panel

Waste Categories	Panel 1		Panel 2	
	Number of Containers	Emplaced Volume (m^3)	Number of Containers	Emplaced Volume (m^3)
LLW				
Bottom ash	208	1,764	674	5,733
Baghouse ash	51	436	167	1,417
Compacted wastes (bales)	325	1,106	1,058	3,596
Compacted wastes (boxes)	1,444	4,042	4,691	13,135
Non-processible (drums)	1,845	6,008	5,995	19,524
Non-processible (boxes)	5,692	17,363	18,498	56,429
Non-processible (other)	164	3,279	0	0
LLW resins	509	1,484	1,656	4,823
ALW resins				
ALW sludges	402	3,418	1,307	11,109
Steam generators	256	4,194	256	4,194
Sub-total LLW	***10,896***	***43,093***	***34,302***	***119,960***
ILW				
CANDECON resins	335	3,728	168	1,864
Moderator resins	287	3,186	143	1,593
PHT resins	201	2,227	100	1,113
Misc. resins	269	2,987	134	1,493
Irradiated core components	2,973 (1) 2,969 (2)	4,067 (1) 6,302 (2)	1,486 (1) 1,484 (2)	2,034 (1) 3,151 (2)
Filters and filter elements				
IX columns				
Retube Wastes (Pressure Tubes)	161	1,240	81	620
Retube Wastes (End Fittings)	599	6,536	300	3,268
Retube Wastes (Calandria Tubes)	111	857	56	428
Retube Wastes (Calandria Tube Inserts)	30	233	15	116
Sub-total ILW	***4,966 (1)*** ***4,962 (2)***	***25,060 (1)*** ***27,295 (2)***	***2,483 (1)*** ***2,481 (2)***	***12,530 (1)*** ***13,647 (2)***
Total	**15,862 (1)** **15,858 (2)**	**68,153 (1)** **70,388 (2)**	**36,785 (1)** **36,783 (2)**	**132,490 (1)** **133,607 (2)**

Note:

Values calculated using container and waste data from Table 3.11 and waste allocation given in Table 4.2.

1. Data from NWMO (2010a) for the original preliminary design.
2. Data from NWMO (2010b) for the final preliminary design.

4.3 Repository Closure

4.3.1 Repository Level

Partial closure of emplacement rooms during DGR operations is planned as rooms are filled, with a wall (a room wall) constructed at the entrance to individual emplacement rooms (NWMO 2010a). Room walls may consist of a reinforced concrete block wall that extends above the waste package height within the room, but not to the roof. The thickness of the concrete in the room walls is taken to be 0.4 m with a width equal to the room width (NWMO 2010a).

After a group of emplacement rooms have been filled with waste packages, closure walls will be constructed in the access tunnel and ventilation drift to isolate this group of rooms (Section 6.13 of the PSR, OPG 2011b). It is expected that there may be three closure walls in the preliminary design (NWMO 2010b) and six closure walls in the final preliminary design (NWMO 2010a) in place at the end of repository operations. The thickness of the concrete in the closure walls is taken to be 20 m, with a width equal to the access tunnel/ventilation tunnel width.

The shaft base will be filled on closure with a concrete monolith at the foot of each shaft (see Section 13.6.2 of the PSR, OPG 2011b). Each monolith provides long-term support for the shaft seals and for the rock around the shafts. The concrete will be placed in mass (i.e., without structural reinforcement). Once completed, the monolith will extend from each shaft's base (taken to be 719.1 mBGS for the main shaft and 746.4 mBGS for the ventilation shaft) to 662.1 mBGS in both shafts (NWMO 2010a). The monoliths will extend into the repository tunnels to form a single monolith at repository level (Figure 4.5 and Figure 4.6). Bulkheads (to contain the monolith's concrete) will be located to ensure support to a minimum distance of 60 m from each of the shafts. There will be no removal of the damaged zone in the tunnels. The resulting dimensions, areas and volumes of the monoliths are presented in Table 4.7.

Concrete and steel will be used in the construction and closure of the repository. The estimated amounts of concrete and steel (excluding waste packages and the shaft sealing materials other than the concrete monoliths) are given in Table 4.8 and Table 4.9, respectively. These data can be combined with the data on the amounts of organics, concrete and metals in the wastes and their packaging (presented in Section 3.4.1) to derive total amounts of organics, concrete and metals in the repository (excluding the shaft sealing materials other than the concrete monoliths). The resulting amounts are presented in Table 4.10, Table 4.11 and Table 4.12. Table 4.13 presents the surface area of metallic materials required for the calculation of the total O_2 consumption and the H_2 generation rates.

Table 4.7: Dimensions, Areas and Volumes of Monoliths

	Main Shaft	Ventilation Shaft
Monoliths (in shaft):		
Vertical length in shaft above DGR floor (m) (1)	20.0	20.0
Vertical length in shaft below DGR floor (m) (1)	37.0	64.3
Diameter in shaft above DGR floor (m) (2)	9.15	7.45
Diameter in shaft below DGR floor (m) (3)	8.15	6.45
Cross-sectional area above DGR floor (m^2)	65.8	43.6
Cross-sectional area below DGR floor (m^2)	52.2	32.7
Total volume (m^3)	1,740	1,083
Monolith (in tunnels) (4):		
Roof area (m^2)	2,708 (5) / 3,360 (6)	
Volume (m^3) (7)	21,666 (5) / 20,200 (6)	

Notes:
1. Both shafts are taken to have a top at 662.1 mBGS. Base of monolith is 719.1 mBGS in main shaft and 746.4 mBGS in ventilation shaft and DGR floor is taken to be at 682.1 mBGS (Table 4.3).
2. See Table 4.4. The concrete liner and HDZ are removed above repository floor level (NWMO 2010a).
3. The concrete liner and HDZ are not removed below repository floor level (NWMO 2010a). Concrete liner is included in the diameter of the shaft below repository floor level. The 0.5 m thick HDZ is not.
4. See Figure 4.5 (final preliminary design) and Figure 4.6 (original preliminary design).
5. Data from NWMO (2010a) for the original preliminary design.
6. Data from NWMO (2010b) for the final preliminary design.
7. Takes into account an average overbreak of 9.7% to account for the assumption of 150 mm overbreak on the perimeter of all excavations (NWMO 2010a).

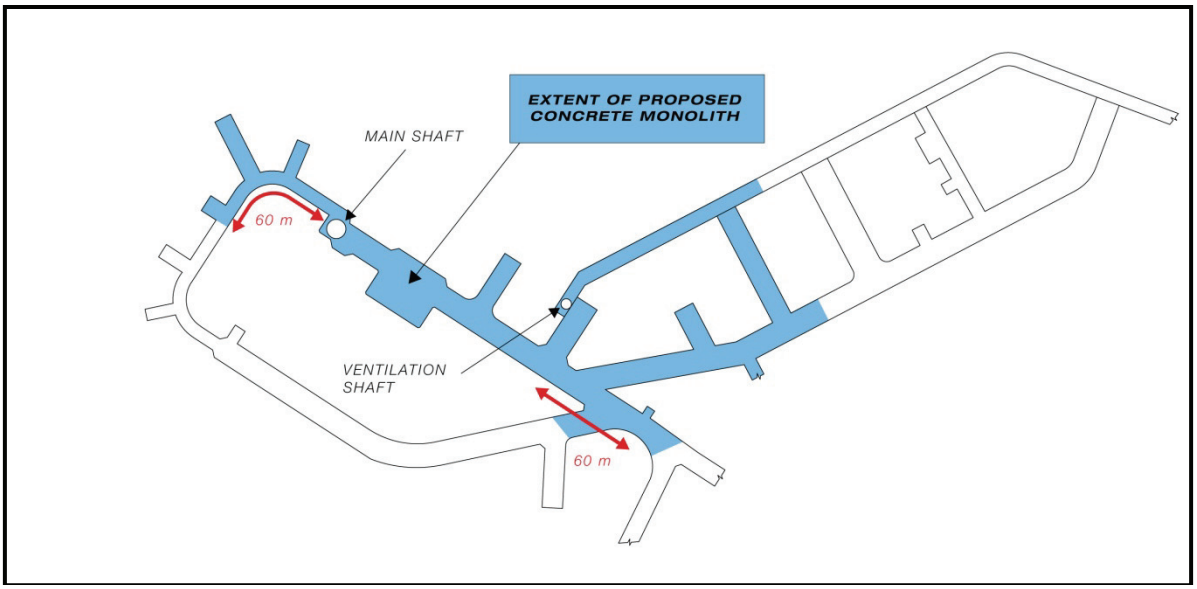

Note: Figure 13-1 in OPG (2011b).

Figure 4.5: Location of Monolith in Repository Tunnels for Final Preliminary Design

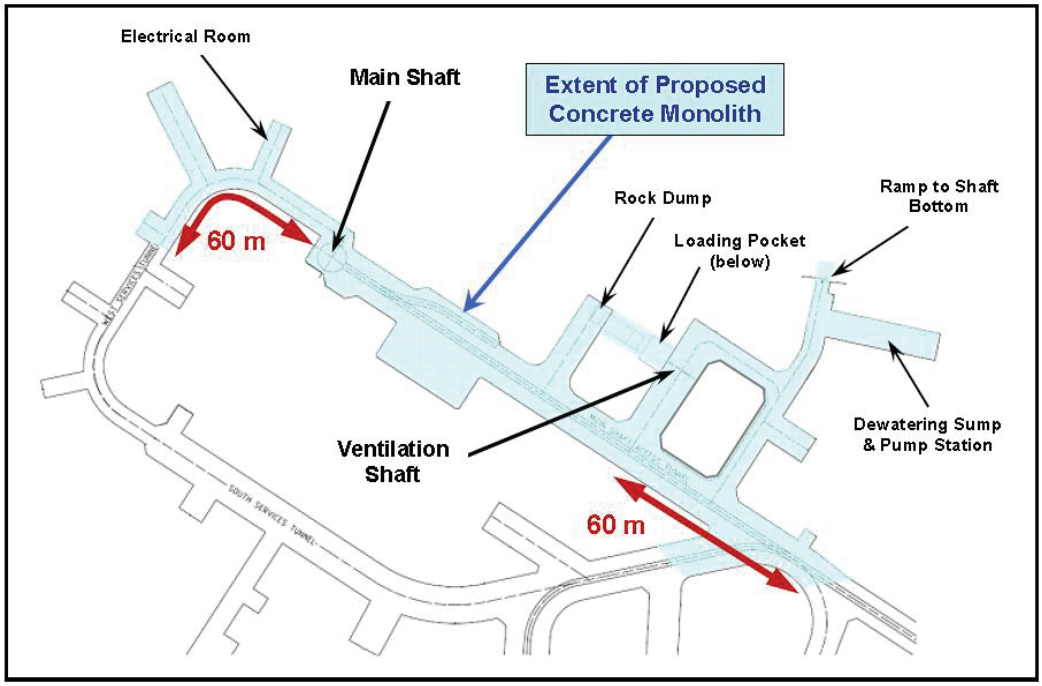

Note: Figure in NWMO (2010a).

Figure 4.6: Location of Monolith in Repository Tunnels for Original Preliminary Design

Table 4.8: Estimated Amount of Concrete in the Repository (excluding waste packages and shaft seals)

	Amount of Concrete (kg) (1)						
	Panel 1 Rooms	**Panel 1 Access Tunnel (and Vent. Drift)**	**Panel 2 Rooms**	**Panel 2 Access Tunnel (and Vent. Drift)**	**Shaft and Services Area**	**Monolith in Tunnel and Shafts**	**Total**
ORIGINAL PRELIMINARY DESIGN							
Concrete Floor (2)	1.4E+07	1.4E+06	1.8E+07	2.4E+06	2.5E+06	-	**3.9E+07**
Shotcrete Walls and Ceilings (3)	7.4E+06	1.0E+06	9.4E+06	1.7E+06	9.2E+05	-	**2.0E+07**
T-H-E Disposal Arrays (4)	1.8E+07	-	-	-	-	-	**1.8E+07**
Room and Closure Walls (5)	7.0E+05	4.1E+06	9.0E+05	2.2E+06	-	-	**7.9E+06**
Removed Ventilation Shaft Liner (6)	-	-	-	-	1.1E+07	-	**1.1E+07**
Total	**4.0E+07**	**6.5E+06**	**2.8E+07**	**6.3E+06**	**1.5E+07**	**5.9E+7**	**1.6E+08**
FINAL PRELIMINARY DESIGN							
Concrete Floor (2)	1.4E+07	2.7E+06	1.8E+07	4.2E+06	4.0E+06	-	**4.3E+07**
Shotcrete Walls and Ceilings (3)	7.5E+06	1.5E+06	9.4E+06	2.4E+06	1.6E+06	-	**2.2E+07**
Room and Closure Walls (5)	7.0E+05	5.5E+06	9.0E+05	2.8E+06	-	-	**9.9E+06**
Removed Ventilation Shaft Liner (6)	-	-	-	-	1.1E+07	-	**1.1E+07**
Total	**2.3E+07**	**9.7E+06**	**2.8E+07**	**9.4E+06**	**1.7E+07**	**5.6E+7**	**1.4E+08**

Notes:

1. Bulk density of 2278 kg m^{-3} given in Table 4.26 for structural concrete is adopted for all items except for monolith. Bulk density of 2425 kg m^{-3} adopted for LHHPC used for monolith (Table 4.26).
2. Concrete floor is 0.2 m thick (NWMO 2010a). Area of floor calculated from dimensions given in Table 4.3 (for emplacement rooms and access tunnel) and floor area of 5.07 x 10^3 m^2 for the shaft and services area for the original preliminary design (NWMO 2010a) and 7.90 x 10^3 m^2 for the final preliminary design. Allowance made for 9.7% overbreak to account for the assumption of 150 mm overbreak on the perimeter of all excavations (NWMO 2010a).
3. 0.05 m thick shotcrete applied to ceiling and extends down to 1.5 m above floor (NWMO 2010a). Area of walls and ceiling calculated from dimensions given in Table 4.3 and NWMO (2010a) for original preliminary design, and Table 4.3 and NWMO (2010b) for final preliminary design.
4. 16 T-H-E disposal arrays each 11.8 m long with 30 pipes of 0.69 m diameter (NWMO 2010a).
5. NWMO (2010a) gives thickness of the room and closure walls as 0.4 m and 20 m, respectively. Room walls are assumed to extend to around 1 m from the emplacement room ceiling (NWMO 2010a). Allowance made for increase tunnel/room dimensions due to overbreak. Three closure walls for original preliminary design (NWMO 2010a), and six for final preliminary design (NWMO 2010b).
6. As part of the repository closure process, the concrete liner in the ventilation shaft will be removed from the top of the Salina F formation down to the repository floor (see Section 13.6.3.1 of the PSR, OPG 2011b). The current assessment assumes that the removed liner material (~ 4900 m^3) is placed in the repository (NWMO 2010a). The main shaft liner will be disposed elsewhere as the repository will be no longer accessible as the liner is being removed.

Table 4.9: Estimated Amount of Steel in the Repository (excluding waste packages and shaft seals)

	Amount of Steel (kg) (1)						
	Panel 1 Rooms	**Panel 1 Access Tunnel (and Vent. Drift)**	**Panel 2 Rooms**	**Panel 2 Access Tunnel (and Vent. Drift)**	**Shaft and Services Area**	**Monolith in Tunnel and Shafts (9)**	**Total**
ORIGINAL PRELIMINARY DESIGN							
Concrete Floor (2)	-	4.8E+04	-	8.2E+04	8.7E+04	-	**2.2E+05**
Walls and Ceilings (3)	1.3E+05	1.8E+04	1.6E+05	2.9E+04	1.6E+04	-	**3.5E+05**
T-H-E Disposal Arrays (2) (4)	2.0E+04	-	-	-	-	-	**2.0E+04**
Concrete Room and Closure Walls (2)	2.4E+04	-	3.1E+04	-	-	-	**5.5E+04**
Rockbolts (5)	4.9E+05	7.5E+04	6.2E+05	1.3E+05	8.4E+04	-	**1.4E+06**
Ventilation Ducts (6)	1.7E+05	4.1E+04	1.6E+05	6.4E+04	1.3E+04	-	**4.4E+05**
Rails (7)	1.3E+05	4.3E+04	-	-	1.8E+04	-	**1.9E+05**
Other equipment and metals (8)	-	-	-	-	8.7E+05	-	**8.7E+05**
Total	**9.6E+05**	**2.3E+05**	**9.6E+05**	**3.0E+05**	**1.1E+06**	**-**	**3.5E+06**
FINAL PRELIMINARY DESIGN							
Concrete Floor (2)	-	4.7E+04	-	7.6E+04	1.4E+05	-	**2.6E+05**
Walls and Ceilings (3)	1.3E+05	2.6E+04	1.6E+05	4.1E+04	2.7E+04	-	**3.9E+05**
Concrete Room and Closure Walls (2)	2.4E+04	-	3.1E+04	-	-	-	**5.5E+04**
Rockbolts (5)	4.9E+05	1.3E+05	6.2E+05	2.1E+05	1.3E+05	-	**1.6E+06**
Rails (7)	1.3E+05	4.3E+04	-	-	1.8E+04	-	**1.9E+05**
Other equipment and metals (8)	-	-	-	-	8.7E+05	-	**8.7E+05**
Total	**7.7E+05**	**2.4E+05**	**8.1E+05**	**3.2E+05**	**1.2E+06**	**-**	**3.3E+06**

Notes:

1. Based on steel density of 7860 kg m^{-3} (see Section 3.4.1). Steel taken to be carbon steel.
2. Volume of steel reinforcement to volume of concrete in floor, T-H-E disposal arrays, and room and closure walls taken to be 0.01. Volume of concrete derived from Table 4.8. Floor not reinforced in emplacement rooms (see NWMO 2010a).
3. Volume of steel to volume of concrete walls and ceilings taken to be 0.005 (consistent with shotcrete reinforcing concentrations of 40 kg m^{-3}). Volume of concrete derived from Table 4.8.
4. Thickness of each T-H-E concrete pipe and lattice support taken to be 0.05 m and cross-sectional area of lattice support taken to be 0.0025 m^2. Length of each lattice support is 0.2 m (NWMO 2010a) and 245 lattice supports taken to be in one array. 16 T-H-E disposal arrays each 11.8 m long with 30 pipes of 0.7 m diameter (NWMO 2010a).
5. Rock bolt dimensions and spacing as per NWMO (2010a) (bolt length: 3.6 m; bolt diameter: 0.025 m; plate thickness: 0.01 m; plate width/length: 0.15 m; rock bolt spacing: 1.5 m centre-to-centre spaced longitudinally and transversely; height from floor to which bolts extend down wall from ceiling: 2 m). Area of ceiling and walls calculated from Table 4.3 and NWMO (2010a) with allowance made for increase tunnel/room dimensions due to overbreak (NWMO 2010a).
6. Details of ventilation ducts taken from NWMO (2010a). Assumes steel thickness of 0.002 m in ducting and no ducting in West or South Service Tunnels.
7. Adopts 42.2 kg steel per m of length of rail. Length of rail calculated from Table 4.3 and NWMO (2010a).
8. As part of the repository closure process, the steel work and reinforced concrete liner in the ventilation shaft will be removed (see Section 13.6.3.1 of the PSR, OPG 2011b). The current assessment assumes that the removed steel work (accounting for ~ 350,000 kg C-steel) and liner material (accounting for ~ 190,000 kg C-steel) is placed in the repository (NWMO 2010a). In addition, it is assumed that metal equipment used in the DGR, such as forklifts and cranes, will be left in repository (accounting for ~ 330,000 kg C-steel) (NWMO 2010a). The steel work and reinforced concrete liner from the main shaft liner will be disposed elsewhere as the repository will be no longer accessible as the shaft is being decommissioned.
9. No reinforcement in the monolith, see Section 13.6.2 of the PSR (OPG 2011b).

Table 4.10: Estimated Amount of Organic Material in the Repository (including wastes, packaging and engineered features)

Organic Material	Mass (kg)		
	Panel 1	Panel 2	Total
Cellulosics (wood, paper and cotton)	1.9E+06	6.3E+06	8.2E+06
Dry ion exchange resins	3.2E+06	2.5E+06	5.7E+06
Plastics and rubbers	2.0E+06	6.4E+06	8.4E+06

Note:
Derived from data on mass of organics in waste (Table 3.6 and Table 3.8) and packaging (Table 3.7 and Table 3.9), and adopting waste allocation given in Table 4.2. Values are the same for the original and draft preliminary designs.

Table 4.11: Estimated Amount of Concrete in the Repository (including wastes, packaging and engineered features but excluding shaft seals)

Location	Mass for Original Preliminary Design (kg)	Mass for Final Preliminary Design (kg)
Panel 1	8.1E+07	7.7E+07
Panel 2	4.9E+07	6.0E+07
Shaft and Services Area (including monolith)	7.4E+07	7.3E+07
Total	2.0E+08	2.1E+08

Note:
Derived from data on mass of concrete in waste (Table 3.6 and Table 3.8), packaging (Table 3.7 and Table 3.9) and engineered features (Table 4.8), and adopting waste allocation given in Table 4.2.

4.3.2 Shafts

The preliminary design of the shaft seals is based on durable materials and is consistent with international practice (Section 13.6.3.1 of the PSR, OPG 2011b). This design concept is summarized below.

- A **concrete monolith** will be constructed at the base of each shaft (see Section 4.3.1).
- **Concrete bulkheads** will be placed in each shaft at specific points. These will provide immediate permeability control as well as structural support. One bulkhead will be located towards the top of the Silurian rock formations at the boundary between the saline lower rock formations and the upper freshwater formations. Two other bulkheads will be located around the two more permeable zones in the Silurian rock formations. Other bulkheads may be added for further structural support, or if needed to separate the bentonite/sand and asphalt seals.
- The shaft will be sealed with durable materials. A **bentonite/sand** mix will be used for the majority of seals, especially in the lower Ordovician formations. An **asphalt mastic mix** will be used in one section to provide a different low-permeable material barrier. The shaft in the upper formations will be filled with compacted **engineered fill** such as sand.
- A **concrete cap** will be constructed at the top of each shaft.

The sequence of sealing materials in the preliminary shaft seal design is summarized in Table 4.14 and illustrated in Figure 4.7. The amounts and volumes of seal materials are given in Table 4.15. Their chemical composition is discussed in Section 4.4.

Table 4.12: Estimated Amount of Metal in the Repository (including wastes, packaging and engineered features)

Metal	Mass (kg)			
	Panel 1	Panel 2	Shaft and Services Area	Total
ORIGINAL PRELIMINARY DESIGN				
Unpassivated C-steel	9.0E+06	2.0E+07	6.9E+05	2.9E+07
Passivated C-steel	7.8E+06	7.7E+06	4.0E+05	1.6E+07
Passivated alloys	1.1E+07	9.5E+06	-	2.0E+07
Zircaloy	4.0E+05	2.0E+05	-	6.0E+05
FINAL PRELIMINARY DESIGN				
Unpassivated C-steel	8.8E+06	1.9E+07	6.8E+05	2.9E+07
Passivated C-steel	7.7E+06	7.7E+06	5.0E+05	1.6E+07
Passivated alloys	1.1E+07	9.6E+06	-	2.0E+07
Zircaloy	4.0E+05	2.0E+05	-	6.0E+05

Notes:
Derived from data on mass of metals in waste (Table 3.6 and Table 3.8), packaging (Table 3.7 and Table 3.9) and engineered features (Table 4.9), and waste allocation given in Table 4.2. All reinforced concrete engineered features assumed to contain passivated C-steel.

Table 4.13: Estimated Surface Area of Metal in the Repository (including wastes, packaging and engineered features)

Metal	Surface Area (m^2)			
	Panel 1	Panel 2	Shaft and Services Area	Total
ORIGINAL PRELIMINARY DESIGN				
Unpassivated C-steel	3.2E+05	6.6E+05	2.0E+04	1.0E+06
Passivated C-steel	1.2E+06	1.6E+06	1.5E+06	4.3E+06
Passivated alloys	3.0E+05	3.8E+05	-	6.9E+05
Zircaloy	2.5E+04	1.2E+04	-	3.7E+04
FINAL PRELIMINARY DESIGN				
Unpassivated C-steel	3.0E+05	6.3E+05	1.9E+04	9.5E+06
Passivated C-steel	1.2E+06	1.7E+06	1.8E+06	4.7E+06
Passivated alloys	3.1E+05	3.8E+05	-	6.9E+05
Zircaloy	2.5E+04	1.2E+04	-	3.7E+04

Note:
Derived from data on surface area of metals in waste (Table 3.6 and Table 3.8), packaging (Table 3.7 and Table 3.9) and engineered features (Table 4.9), and waste allocation given in Table 4.2. All reinforced concrete engineered features assumed to contain passivated C-steel, with specific surface area of rails being 0.006 m^2 kg^{-1}, of rock bolts being 0.02 m^2 kg^{-1} and steel reinforcement in floors, walls and ceilings being 5 m^2 kg^{-1}.

Table 4.14: Sequence of Shaft Sealing Materials

Sealing Material ID	Depth of Top (mBGS)	Depth of Base (mBGS)	Vertical Length (m)	Diameter (m)		Comment
				Main Shaft	Ventilation Shaft	
CC	0.0	20.0	20.0	6.50	5.00	Concrete cap
S6	20.0	178.6	158.6	6.50	5.00	Engineered fill. Shaft liner and HDZ not removed.
B3	178.6	190.6	12.0	13.23	10.68	Concrete bulkhead keyed into rock to distance equal to 0.5*shaft radius. Shaft liner and HDZ removed prior to emplacement of shaft seal.
S5	190.6	322.8	132.2	9.15	7.45	Bentonite/sand mix. Shaft liner and HDZ removed prior to emplacement of shaft seal.
B2	322.8	340.8	6.0 (straight) 12.0 (keyed-in)	9.15 (straight) 13.23 (keyed-in)	7.45 (straight) 10.68 (keyed-in)	Lower 12 m of concrete bulkhead keyed into rock to distance equal to 0.5*shaft radius. Shaft liner and HDZ removed prior to emplacement of shaft seal.
S4	340.8	372.6	31.8	9.15	7.45	Bentonite/sand mix. Shaft liner and HDZ removed prior to emplacement of shaft seal.
B1	372.6	390.6	6.0 (straight) 12.0 (keyed-in)	9.15 (straight) 13.23 (keyed-in)	7.45 (straight) 10.68 (keyed-in)	Lower 12 m of concrete bulkhead keyed into rock to distance equal to 0.5*shaft radius. Shaft liner and HDZ removed prior to emplacement of shaft seal.
S3	390.6	506.6	116.0	9.15	7.45	Bentonite/sand mix. Shaft liner and HDZ removed prior to emplacement of shaft seal.
S2	506.6	567.5	60.9	9.15	7.45	Asphalt Mastic Mix. Shaft liner and HDZ removed prior to emplacement of shaft seal.
S1	567.5	662.1	94.6	9.15	7.45	Bentonite/sand mix. Shaft liner and HDZ removed prior to emplacement of shaft seal.
Shaft Monolith above DGR floor	662.1	682.1	20	9.15	7.45	Concrete. Shaft liner and shaft HDZ above DGR floor removed prior to emplacement of shaft seal.
Shaft Monolith below DGR floor (1)	682.1	719.1/746.4	37/64.3	8.15	6.45	Shaft liner and shaft HDZ below DGR floor not removed prior to emplacement of shaft seal. Thickness of liner included in diameter value

Note:
1 Base of monolith in main shaft is at 719.1 m and in ventilation shaft is at 746.4 m.

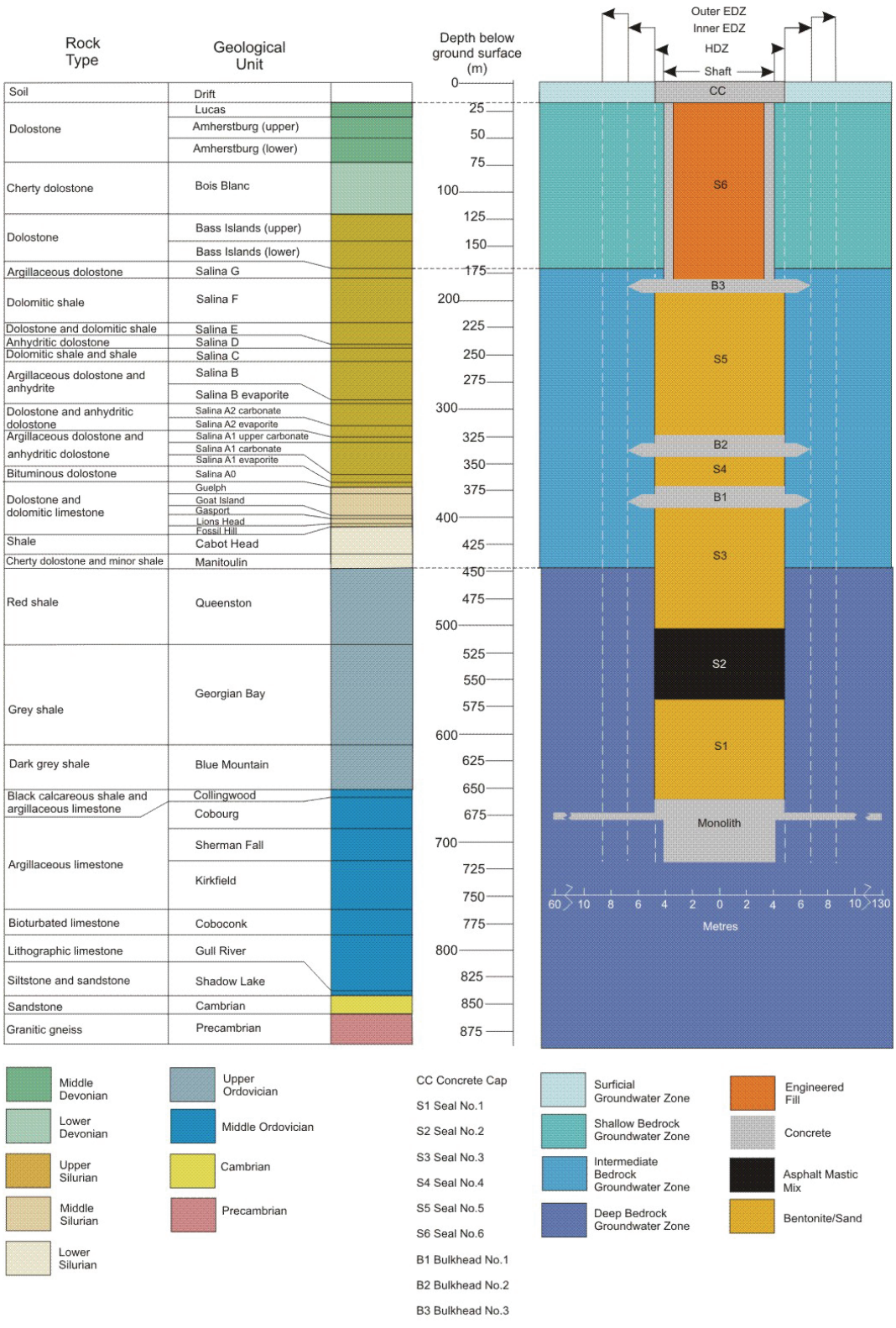

Figure 4.7: Sequence of Shaft Sealing Materials

Table 4.15: Mass and Volume of Shaft Sealing Materials

Sealing Material ID	Sealing Material Type	Main Shaft		Ventilation Shaft		Total Volume (m^3) (1)	Total Mass (kg) (2)
		Volume (m^3) (1)	Mass (kg) (2)	Volume (m^3) (1)	Mass (kg) (2)		
CC	Concrete	6.6E+02	1.6E+06	3.9E+02	9.5E+05	1.1E+03	2.6E+06
S6	Engineered fill	5.3E+03	1.0E+07	3.1E+03	6.2E+06	8.4E+03	1.7E+07
B3	Concrete	1.6E+03	4.0E+06	1.1E+03	2.6E+06	2.7E+03	6.6E+06
S5	Bentonite/sand	8.7E+03	1.4E+07	5.8E+03	9.2E+06	1.4E+04	2.3E+07
B2	Concrete	2.0E+03	5.0E+06	1.3E+03	3.2E+06	3.4E+03	8.2E+06
S4	Bentonite/sand	2.1E+03	3.3E+06	1.4E+03	2.2E+06	3.5E+03	5.6E+06
B1	Concrete	2.0E+03	5.0E+06	1.3E+03	3.2E+06	3.4E+03	8.2E+06
S3	Bentonite/sand	7.6E+03	1.2E+07	5.1E+03	8.1E+06	1.3E+04	2.0E+07
S2	Asphalt Mastic Mix	4.0E+03	8.0E+06	2.7E+03	5.3E+06	6.7E+03	1.3E+07
S1	Bentonite/sand	6.2E+03	1.0E+07	4.1E+03	6.6E+06	1.0E+04	1.7E+07
Monolith	Concrete	Included in calculation of repository concrete in Table 4.7 and Table 4.8					
Total (excl. monolith)	**Engineered fill**	**5.3E+03**	**1.0E+07**	**3.1E+03**	**6.2E+06**	**8.4E+03**	**1.7E+07**
	Concrete (3)	**1.0E+04**	**2.5E+07**	**6.7E+03**	**1.6E+07**	**1.7E+04**	**4.1E+07**
	Bentonite/Sand	**2.5E+04**	**3.9E+07**	**1.6E+04**	**2.6E+07**	**4.1E+04**	**6.6E+07**
	Asphalt Mastic Mix	**4.0E+03**	**8.0E+06**	**2.7E+03**	**5.3E+06**	**6.7E+03**	**1.3E+07**

Notes:
1. Calculated from dimensions given in Table 4.14.
2. Derived using bulk densities given in Table 4.26. Includes liner in Surficial and Shallow Bedrock Groundwater Zones.
3. Includes concrete liners in shafts in Surficial and Shallow Bedrock Groundwater Zones.

4.3.3 Other Excavations

The preliminary design for the DGR includes excavations below repository level for rock handling and ramp access to the shaft bottoms (Section 6.3.7 of the PSR, OPG 2011b). The rock handling excavations are estimated to have a volume of around 250 m^3 and the volume of the ramp is around 3,950 m^3.

It is envisaged that the rock handling and ramp excavations will be backfilled with concrete at closure and there will be no removal of any associated damaged zone. Around 1 x 10^7 kg of concrete will be required to fill the 4,200 m^3 void (adopting a concrete bulk density of 2,430 kg m^{-3} - see Table 4.26).

4.4 Repository Materials

4.4.1 Concrete

Concrete will be used for a number of purposes: the floors, walls and ceilings of the tunnels/emplacement rooms; the repository room and closure walls; and the monoliths, bulkheads, liners and surficial cap (Chapters 6 and 13, PSR, OPG 2011b).

The concrete used for all structures, other than the monoliths and bulkheads (and backfilling the rock handling and ramp excavations), is taken to use Canadian Standards Association (CSA) Type 10 (GU) Portland cement, or similar, and is described as "**structural concrete**". In the case of the surficial cap, closure walls and emplacement room floors, it will be placed in mass (i.e., without structural reinforcement). The concrete used for the access tunnel floors, room walls and shaft liners will be reinforced with rebars, while the shotcrete used for the walls and ceilings will be reinforced with steel fibre.

The chemical composition of the CSA Type 10 (GU) Portland cement is based on that provided in Gillott and Quinn (2003) (Table 4.16). The concrete structures in the DGR will comprise specific mixtures of the cement with aggregate and water. The typical range of compositions for concrete based on Portland cement is given in Table 4.17 (CPCA 1995). For the postclosure safety assessment, the proportions are assumed as per SFR (Sweden) given in Höglund (2001), with the same air content as per the Low Heat High Performance Cement (Table 4.17).

The concrete used for the monoliths and bulkheads (and the rock handling and ramp excavations) will be placed in mass (i.e., without structural reinforcement). The concrete will use sulphate-resistant Portland cement and will be expansive with a low permeability and a low heat of hydration. This concrete is taken to have the characteristics of the **LHHPC** developed by Atomic Energy of Canada Limited (AECL), which uses CSA Type 50 Portland Cement (Dixon et al. 2009). The chemical composition of the cement used in LHHPC is given in Table 4.18 based on data in Gillott and Quinn (2003). The mixing proportions are taken from Dixon et al. (2009) and are given in Table 4.19.

Table 4.16: Chemical Composition of Cement used in Structural Concrete

Major Component	wt%
CaO	63.2
SiO_2	20.5
Al_2O_3	4.1
Fe_2O_3	2.7
MgO	4.5
Na_2O	0.55
SO_3	2.4
Loss on Ignition at 1050 °C	2.8
Insoluble residue	0.14
Anhydrous Cement Phases	**wt%**
C_3S (Alite, 3 CaO • SiO_2)	62.8
C_2S (Belite, 2 CaO • SiO_2)	11.5
C_3A (Aluminate 3 CaO • Al_2O_3)	6.3
C_4AF (Ferrite 4 CaO • Al_2O_3 • Fe_2O_3)	8.3

Table 4.17: Mixing Proportions for Structural Concrete

Component	Typical range (vol. %)	Reference (kg m^{-3})
Cement (Type 10)	7-15	350
Fine aggregate (<8 mm)	24-30	920
Coarse aggregate	31-51	909
Water	14-18	164.5
Air	0.5-8	3.2 (vol %)

Table 4.18: Chemical Composition of Cement used in LHHPC

Major Component	wt%
CaO	62.5
SiO_2	21.4
Al_2O_3	3.3
Fe_2O_3	3.8
MgO	4.5
Na_2O	0.56
SO_3	2.2
Loss on Ignition	1.0
Insoluble Residue	0.1
Anhydrous Cement Phases	**wt%**
C_3S (Alite, 3 CaO • SiO_2)	58.0
C_2S (Belite, 2 CaO • SiO_2)	17.7
C_3A (Aluminate 3 CaO • Al_2O_3)	2.3
C_4AF (Ferrite 4 CaO • Al_2O_3 • Fe_2O_3)	11.4

Table 4.19: Mixing Proportions for LHHPC

Component	Amount (kg m^{-3})
Cement (Type 50)	95.6
Silica fume	95.6
Silica flour	190.9
Sand	881
Coarse aggregate	1024
Superplasticizer (dry mass) (1)	10.16
Added water	127.27
Air content (volume %)	3.2

Note:
1. Superplasticizer is a sodium naphthalene sulphonate based material.

The hydration of the cement will result in the formation of a number of phases typical of Ordinary Portland Cement (OPC) blends, including C_3S, C_2S, C_3A and C_4AF as shown in Table 4.16 and Table 4.18 above. However, the actual phase compositions used in the current assessment are calculated from the bulk cement compositions for the specific DGR conditions using the latest thermodynamic data (e.g., Lothenbach et al. 2008) and therefore may differ from the phase compositions tabulated above.

4.4.2 Bentonite/Sand

The reference clay seal is bentonite mixed with sand to a 70:30 mix (by weight) (Section 13.6.3.1 of the PSR, OPG 2011b). The reference bentonite is Wyoming Type Sodium Bentonite (MX80), which is a montmorillonite-based clay material. The reference sand component will be a washed, silica-based material with particle sizes no greater than 2.5 mm. Alternatives that may be considered for the final design include use of a higher clay fraction, and also the use of finely crushed limestone sand rather than silica sand.

It has been assumed that the bentonite/sand mixture will be placed loose and compacted in situ using vibratory compaction equipment. Using this compaction method results in an emplaced dry density of around 1600 kg m^{-3} (Section 13.6.3.1 of the PSR, OPG 2011b). With MX80 clay, the resulting effective montmorillonite dry density (EMDD) would be about 1215 kg m^{-3}.

The chemical composition of the bentonite is based on that from Karnland et al. (2006) (Table 4.20).

Table 4.20: Chemical Composition of MX80 Bentonite

Component	wt%
Montmorillonite	82
Quartz	3
Feldspar and Mica	8
Cristobalite/tridymite	4
Others (minor impurities)	3

4.4.3 Asphalt Mastic Mix

The asphalt mastic mix is taken to have the same composition at that proposed for use in the shaft seal for the Waste Isolation Pilot Plant (WIPP 2009). It will contain 70% (by weight) silica sand (with a maximum diameter of 2.36 mm), 20% (by weight) asphalt and 10% (by weight) hydrated lime. The asphalt used is AR-4000, a graded asphalt of intermediate viscosity.

Asphalt consists mainly of four components (Pettersson and Elert 2001):

- Saturated hydrocarbons;
- Aromatic hydrocarbons;
- Resins; and
- Asphaltenes.

Typically the aromatic hydrocarbons comprise the most abundant component, while the asphaltenes comprise the least abundant component (Pettersson and Elert 2001) (Table 4.21).

Table 4.21: Chemical Composition of Asphalts

Component	Asphalt Grade 80/100	Asphalt Grade 90/40	"Averaged"
	wt%	wt%	wt%
Aromatic hydrocarbons	72.5	53.0	63
Saturated hydrocarbons	5.4	21.0	13
Resins	15.5	14.9	15
Asphaltenes	6.6	11.1	9

4.4.4 Engineered Fill

The engineered fill is taken to be compacted clean sand screened to a maximum particle dimension of 2 mm, and graded and placed to achieve a nominal hydraulic conductivity of 10^{-4} m s^{-1}.

4.5 Hydraulic Parameters

The relevant hydraulic parameters for the different wastes in the repository are given in Section 3.4.1, in particular Table 3.10. The relevant parameters for the other materials within the repository (and its shafts) are discussed below and summarized in Table 4.22.

Table 4.22: Hydraulic Conductivities and Porosities for Repository Materials

Parameter	Material		Undegraded	Degraded
Vertical and Horizontal Hydraulic Conductivity ($m\ s^{-1}$) (1)	Structural Concrete	Ref. value	1E-10	1E-8
		PDF values	Min: 1E-11 /Max: 1E-9	Min: 1E-9 /Max: 1E-7
		PDF type	Log-triangular	Log-triangular
	LHHPC	Ref. value	2E-12	1E-10
		PDF values	Min: 2E-13Max: 2E-11	Min: 1E-11 /Max: 1E-9
		PDF type	Log-triangular	Log-triangular
	Bentonite/ sand	Ref. value	1E-11	
		PDF values	Min: 1E-14 /Max: 1E-9	
		PDF type	Log-triangular	
	Asphalt Mastic Mix	Ref. value	1E-12	
		PDF values	Min: 1E-14 /Max: 1E-11	
		PDF type	Log-triangular	
	Engineered Fill	Ref. value	1E-4	
		PDF values	Min: 1E-6 /Max: 1E-2	
		PDF type	Log-triangular	
Diffusion and Transport Porosities (-)	Structural Concrete	Ref. value	0.11	0.25
		PDF values	Min: 0.08 /Max: 0.14	Min: 0.2 /Max: 0.3
		PDF type	Triangular	Triangular
	LHHPC	Ref. value	0.05	0.1
		PDF values	Min: 0.04 /Max: 0.1	Min: 0.05 /Max: 0.15
		PDF type	Triangular	Triangular
	Bentonite/ sand	Ref. value	0.29	
		PDF values	Min: 0.25 /Max: 0.33	
		PDF type	Triangular	
	Asphalt	Ref. value	0.02	
		PDF values	Min: 0.01 /Max: 0.04	
		PDF type	Triangular	
	Engineered Fill	Ref. value	0.25	
		PDF values	Min: 0.2 /Max: 0.3	
		PDF type	Triangular	

Note:
1. Slightly lower values (less than a factor of two) can be expected for saline conditions due to greater density and viscosity of water. However, this data report adopts freshwater hydraulic conductivity values irrespective of salinity conditions.

4.5.1 Transport Path Lengths and Areas

Path lengths and areas for contaminant transport can be derived from the repository dimensions given in Section 4.2 and Section 4.3.

4.5.2 Hydraulic Conductivities and Permeabilities

The hydraulic conductivity and permeability of a given porous medium are typically (e.g., Fetter 1994) related by:

$$K = \frac{\rho_f \, g}{\mu} k \tag{4.1}$$

where:

K is the hydraulic conductivity, m s^{-1};

ρ_f is the fluid density, kg m^{-3};

g is the acceleration due to gravity, m s^{-2};

μ is the fluid kinematic viscosity, Pa s (= kg m^{-1} s^{-1}); and

k is the permeability, m^2.

Using the data given in Table 5.3, values for the $\rho_f g / \mu$ term of 8.6 x 10^6 and 5.1 x 10^6 m^{-1} s^{-1} can be derived for fresh and saline water, respectively.

4.5.2.1 Concrete

Structural concrete will be used for the waste packaging, the shaft lining, the floors, walls and ceilings of tunnels/emplacement rooms, and the closure and room walls (Section 4.4.1). The Swiss safety assessment of the proposed L&ILW repository at the Wellenberg site (NAGRA 1994) used a range for the hydraulic conductivity of structural concrete of 1 x 10^{-10} to 1 x 10^{-8} m s^{-1}, depending on the degree of physical degradation.

A low heat high performance concrete such as AECL's **LHHPC** will be used for the DGR shaft monoliths, ramp backfill, and bulkheads. Guo (2004) adopts a permeability value of 3 x 10^{-21} m^2 (approximately 3 x 10^{-14} m s^{-1}) for numerical simulation of the LHHPC used in the tunnel sealing experiment at the AECL's underground research laboratory (URL). A permeability range of 2 x 10^{-21} to 1 x 10^{-17} m^2 (approximately 2 x 10^{-14} to 1 x 10^{-10} m s^{-1}) is given in WIPP (2009) for the concrete to be used in the shaft seal for the Waste Isolation Pilot Plant, which in turn was derived from an experimental program review by Hurtado et al. (1997). Russell and Simmons (2003) and Garisto et al. (2004) have proposed values of 1 x 10^{-12} and 2 x 10^{-12} m s^{-1}, respectively, for such concrete. This is consistent with the value of 1 x 10^{-19} m^2 given in NAGRA (2008) for the permeability of high performance concrete.

As discussed in Section 4.5.3 of the System and Its Evolution report (QUINTESSA 2011b), it is expected that there will be some physical and chemical degradation of the structural concrete and LHHPC over the long timescales of the assessment. NAGRA (1994) gives a hydraulic conductivity of degraded structural concrete of 1 x 10^{-8} m s^{-1}. Since the extent of LHHPC

degradation is expected to be limited (Section 4.5.3 of QUINTESSA 2011b), a hydraulic conductivity at the upper end of the range given above (i.e., 1 x 10^{-10} m s^{-1}) is adopted for degraded LHHPC. Consistent with the above review, reference values and ranges for the hydraulic conductivities of undegraded and degraded structural concrete and LHHPC adopted for the current assessment are given in Table 4.22. For probabilistic calculations, a log-triangular distribution is adopted with a range of an order of magnitude about the reference value.

4.5.2.2 Bentonite/Sand

The hydraulic conductivity of bentonite/sand mixes is a function of the dry density of the bentonite, the salinity of the water, and sand content (see for example Dixon et al. 2001, Baumgartner 2006, and Russell and Simmons 2003). Hydraulic conductivity decreases as the dry density increases, whereas it increases with increasing salinity and sand content (once the sand content in the mix is greater than 50% by dry weight). Figure 3 of Baumgartner (2006) shows that the saturated hydraulic conductivity can range between 1 x 10^{-14} and 1 x 10^{-9} m s^{-1} for salinity ranges from 0 to 350 mg L^{-1} NaCl and effective montmorillonite dry densities (EMDDs) of between 1000 and 1500 kg m^{-3}. This range is broadly comparable with ranges given in Dixon et al. (2001), Russell and Simmons (2003) and WIPP (2009) for a range of different densities, salinities and sand contents. Baumgartner (2006) provides a series of empirical fitting equations which relate the hydraulic conductivity to the EMDD of the mix at four different salinities (Figure 4.8).

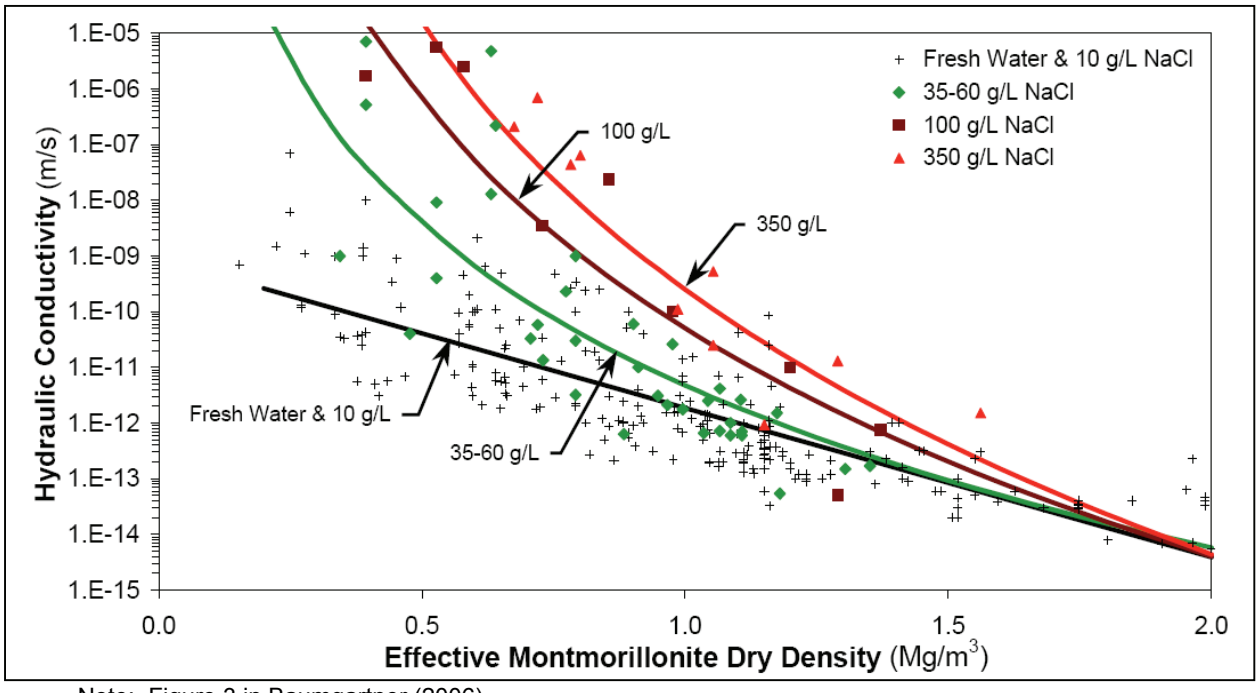

Note: Figure 3 in Baumgartner (2006).

Figure 4.8: Hydraulic Conductivity as a Function of EMDD and Total Dissolved Solids

For the DGR, the reference material is a 70/30 bentonite/sand mixture (Section 13.6.3.1 of the PSR, OPG 2011b), compacted in-situ or placed as blocks. For compacted in-situ, a reasonable target is a dry density of 1600 kg m^{-3} (see Figure 4.9). At groundwater salinities of 100 and 350 mg L^{-1} and an EMDD of around 1215 kg m^{-3} (consistent with a dry density of 1600 kg m^{-3}), the hydraulic conductivities are 4 x 10^{-12} and 1 x 10^{-11} m s^{-1}.

As discussed in Section 4.5.4 of the System and Its Evolution report (QUINTESSA 2011b) some degradation of the bentonite/sand material is possible, although it will be limited in spatial extent (a few tens of cm) and to areas near concrete in particular. Given that total dissolved solid concentrations of up to 375 g L^{-1} (250 g L^{-1} NaCl) occur at the Bruce nuclear site (Table 5.4), a reference value towards the upper end of the range derived from Baumgartner (2006) is cautiously adopted (i.e., 1 x 10^{-11} m s^{-1}) throughout the length of the shafts. For probabilistic calculations, a log-triangular distribution is recommended with a peak of 1 x 10^{-11} m s^{-1} and lower and upper limits of 1 x 10^{-14} m s^{-1} and 1 x 10^{-9} m s^{-1}, respectively.

4.5.2.3 Asphalt Mastic Mix

WIPP (2009) gives a permeability range of 1 x 10^{-21} to 1 x 10^{-18} m^2 for the asphalt mastic mix to be used in the shaft seal for the Waste Isolation Pilot Plant. This is consistent with that given in Hurtado et al. (1997), which in turn was derived from a literature review, and approximately equates to a hydraulic conductivity of 1 x 10^{-14} to 1 x 10^{-11} m s^{-1}. This range is also comparable with the range of hydraulic conductivities given in Bowders et al. (2001) for asphalt concrete barriers.

Section 4.5.5 of the System and Its Evolution report (QUINTESSA 2011b) notes that some degradation of the mix is possible although it is likely to be limited in spatial extent. Therefore a reference value towards the upper end of the range given in WIPP (2009) is adopted of 1 x 10^{-12} m s^{-1}. This is consistent with the average hydraulic conductivity given in Bowders et al. (2001) for an asphalt concrete barrier. For probabilistic calculations a log-triangular distribution is recommended with a peak of 1 x 10^{-12} m s^{-1} and lower and upper limits of 1 x 10^{-14} m s^{-1} and 1 x 10^{-11} m s^{-1}, respectively.

4.5.2.4 Engineered Fill

The reference engineered fill is a graded clean sand, emplaced for a long-term hydraulic conductivity of 1 x 10^{-4} m s^{-1}. The hydraulic conductivity range given in Freeze and Cherry (1979) for clean sand is 1 x 10^{-6} to 1 x 10^{-2} m s^{-1}. Therefore, a log-triangular probabilistic distribution is adopted with a range of 1 x 10^{-6} to 1 x 10^{-2} m s^{-1} and a peak of 1 x 10^{-4} m s^{-1}.

4.5.3 Hydraulic Gradient

Horizontal hydraulic gradients are taken to be the same as those for the surrounding geosphere (see Section 5.4.1.1). Vertical hydraulic gradients in the shafts are determined from detailed groundwater modelling (GEOFIRMA 2011).

4.5.4 Porosities

The transport (effective) porosity values are expected to be the same as the diffusion (accessible) porosity values for all materials, since the porosities are not very low and isolated porosity is not expected.

4.5.4.1 Concrete

The air content of the concrete at emplacement in the monoliths and bulkheads (i.e., the LHHPC) is taken to be 0.02 and for the concrete in the surficial cap (i.e., the structural concrete) as 0.04 to 0.07. Dixon et al. (2009) give an air content of 0.032 for LHHPC with a water to cement ratio of 0.63. Assuming an initial saturation of 50% (Russell and Simmons 2003), these air contents equate to porosities of 0.04 to 0.06 for LHHPC and 0.08 to 0.14 for the structural concrete. Hurtado et al. (1997) give a best estimate value of 0.05 for the porosity of the concrete to be used in the shaft seal for the Waste Isolation Pilot Plant, while Guo (2004) adopts a value of 0.1 for the numerical simulation of the concrete bulkhead in the AECL Tunnel Sealing Experiment. NAGRA (2008) gives a porosity of 0.15 for concretes with a water-cement mixing ratio of around 0.4 (mass ratio) but notes that long-term studies have shown that porosities are reduced by 20 – 30%. Therefore for undegraded **LHHPC**, a reference porosity of 0.05 with a range of 0.04 to 0.1 is adopted. A triangular probabilistic distribution is adopted with a range of 0.04 to 0.1 and a peak of 0.05. For undegraded **structural cement**, a reference porosity of 0.11 with a range of 0.08 to 0.14 is adopted. A triangular probabilistic distribution is adopted with a range of 0.08 to 0.14 and a peak of 0.11.

Consistent with the discussion on hydraulic conductivities (Section 4.5.2.1), the porosity of concrete increases due to degradation of the concrete. The Swedish SFR database (Savage and Stenhouse 2002) proposes a value of 0.25 for degraded structural concrete. A value at the upper end of the range given above (i.e., 0.1) is adopted for degraded LHHPC. A triangular distribution is adopted with a range of ±0.05 about the reference value for both the structural concrete and the LHHPC.

4.5.4.2 Bentonite/Sand

Dixon et al. (2009) provides a graph that indicates that a (sodium) bentonite/sand mix with an emplaced dry density of around 1600 kg m^{-3} can be expected to have a porosity of around 0.29 (Figure 4.9). This is higher than the reference value of 0.24 given by Hurtado et al. (1997) for the porosity of the clay to be used in the shaft seal for the Waste Isolation Pilot Plant, which has a higher emplaced dry density of between 1800 and 2000 kg m^{-3}. A triangular distribution is adopted with a range of ± 0.04 about the reference value of 0.29, consistent with the range given in Hurtado et al. (1997). Limited degradation of the bentonite/sand material is expected (see Section 4.5.4 of the System and Its Evolution report, QUINTESSA 2011b), mostly in the vicinity of concrete bulkheads and monolith, and therefore no impact on overall porosity is expected.

4.5.4.3 Asphalt Mastic Mix

The air content of the asphalt mastic mix at emplacement is taken to be 0.02. This is consistent with WIPP (2009), which states that air voids should be less than 0.02 to ensure that the WIPP asphalt mastic mix seal has low permeability. This value is taken here as the reference value for asphalt mastic mix porosity with an upper limit of 0.04 (taken from Bowders et al. 2001) and lower limit of 0.01 (taken from Hurtado et al. 1997). Limited degradation of the mix is expected (see Section 4.5.5 of the System and Its Evolution report, QUINTESSA 2011b) and therefore no impact on average porosities is expected. For probabilistic calculations a triangular distribution is recommended with a peak of 0.02 and lower and upper limits of 0.01 and 0.04, respectively.

4.5.4.4 Engineered Fill

The engineered fill is expected to have a porosity of around 0.25. This is at the lower end of range given in Freeze and Cherry (1979) for sand due to the compacted nature of fill. A triangular probabilistic distribution is adopted with a peak at 0.25 and a range of ± 0.05 about the peak.

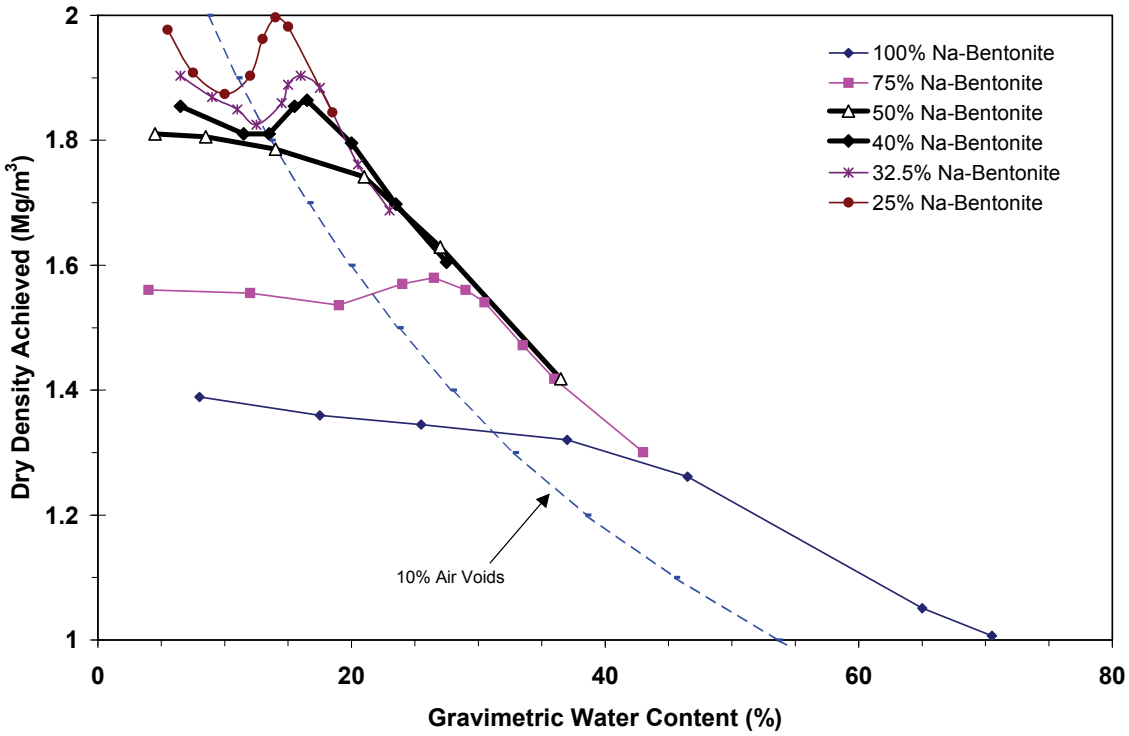

Note: Figure 9 in Dixon et al. (2009).

Figure 4.9: Dry Density – Water Content Relationships for Bentonite-Sand Mixtures

4.5.5 Specific Storage

Representative specific storage values for shaft sealing components have been calculated from pore compressibilities published in Hurtado et al. (1997). Using the data provided by Hurtado et al. (1997) the porous medium compressibility was calculated using the following expression:

$$C = \theta\, C_p \tag{4.2}$$

where:

C is the porous medium compressibility, Pa^{-1};

θ is the physical porosity (unitless); and

C_p is the pore compressibility, Pa^{-1}.

Using this compressibility, the specific storage was calculated as (Freeze and Cherry 1979):

$$S = \rho_f g(C + \theta C_f) \quad (4.3)$$

where:

S is the specific storage, m^{-1};

ρ_f is the fluid density, kg m^{-3};

g is the gravitational acceleration, m s^{-2}; and

C_f is the fluid compressibility, Pa^{-1}.

Fluid parameters appropriate to the saline waters of the Silurian and Ordovician sequences were used. Namely, a value of 1185 kg m^{-3} was used for fluid density and 3.3 x10^{-10} Pa^{-1} for the fluid compressibility (see Table 5.3). For the porous medium compressibility, the porosity values reported in Hurtado et al. (1997) were used. However, the storage coefficient calculation used porosity values given in Table 4.22. This assumes that the pore compressibilities reported in Hurtado et al. (1997) are derived from the measured porous medium compressibility, and that a change in porosity will not have a large effect on the porous medium compressibility. The resulting specific storage values are summarized in Table 4.23.

Table 4.23: Specific Storage Values for Repository Materials

Material	Specific Storage (m^{-1})	
	Undegraded	Degraded
Structural concrete	1.1E-06	1.7E-06
LHHPC	8.9E-07	1.1E-06
Bentonite/sand	6.1E-06	
Asphalt	3.5E-06	
Engineered fill	1.2E-04	

4.6 Transport Parameters

Contaminants may be transported through the following repository materials:

- Waste;
- Concrete associated with waste packaging, tunnels/emplacement rooms (floors, walls, ceilings and closure walls), monoliths, bulkheads, and shaft liners;
- Bentonite/sand in the shafts;
- Asphalt in the shafts; and
- Engineered fill in the shaft.

Groundwater transport parameters for the wastes are given in Section 3.6. Parameters for the other materials are discussed below.

4.6.1 Water Composition

The water composition in the emplacement rooms, access tunnels and ring tunnel is discussed in Section 3.6.2.

The geochemical processes related to the degradation of shaft materials and their impact on the water composition in the shaft are described in the System and Its Evolution report (Section 4.5 of the System and Its Evolution report, QUINTESSA 2011b).

4.6.2 Solubility Limits

Solubility limits of key elements are discussed in detail in Appendix C and are summarized below for the various engineered barriers.

Consistent with the approach adopted for the cementitious waste packages (Section 3.6.3.2), the solubility for **structural concrete** in the repository is taken to be to be unlimited for all elements other than carbon. For carbon, a solubility limit of 1×10^{-2} mol m^{-3} has been calculated for Cobourg porewater equilibrated with cement (Appendix C.3.1). However, in the long-term the concrete is expected to degrade to a certain extent both physically and chemically (Section 4.5.3 of the System and Its Evolution report, QUINTESSA 2011b) and so a Cobourg porewater solubility limit of 6×10^{-1} mol m^{-3} is used.

The **LHHPC**, that is to be used for shaft monoliths and bulkheads, has a composition for which relatively little is understood in terms of the long-term evolution of hydrated phases (especially in saline water). It may be the case that the low amount of CaO present in the initial blend prevents the formation of Portlandite, leading to the growth of calcium silicate hydrate phases (possibly with a low Ca:Si ratio) that will act as the primary pH buffer (producing an pH of approximately 10 to 11). There are a number of other potential candidate phases that could form during cement hydration, the subsequent dissolution of which would result in changes in porewater chemistry. Therefore, given these uncertainties, a conservative approach has been adopted, whereby all elements except carbon are considered to have an unlimited solubility in the LHHPC. For carbon, a solubility limit of 6×10^{-1} mol m^{-3} is adopted consistent with that used for structural concrete.

With regard to solubility limits in **bentonite-sand**, recent modelling work (Savage et al. 2010) suggests that the dominant control over equilibrium bentonite porewater pH (using conventional models, that ignore mineral hydrolysis and alteration) is the prevailing $pCO_{2(g)}$ with smectite ion exchange and surface protonation reactions being of secondary importance. Therefore, it is assumed that infiltrating porewaters will equilibrate with bentonite minerals such that a relatively minor change in pH will occur. Given the high salinity of the porewaters associated with the host rock, the montmorillonite present in the bentonite is likely to remain largely in the Na^+ exchanged form. It is therefore assumed that bentonite-sand porewater compositions will be broadly similar to, and can be represented by, Cobourg Limestone (repository host porewater) and higher salinity Guelph water (for upper levels) (Table 5.4). Solubility limits have been calculated for these two water compositions (see Appendix C). To introduce conservatism, the higher of the solubility limits for the two water compositions can be adopted and are summarized in Table 4.24.

Solubility limits have not been determined for **asphalt** given the paucity of available data. Instead, a conservative approach has been adopted, where it is assumed that all elements have unlimited solubilities in water in this material.

Table 4.24: Solubility Limits to Elemental Aqueous Concentrations and Solubility-Limiting Solid Phases for Bentonite-Sand

Element	Total Conc. (mol m^{-3}) (1,6)	Solubility-limiting Phase (2)
C (3)	6E-01	Carbonate equilibria
Cl (4)	7E+03	Halite (NaCl)
Cr	9E-03	$Cr_2(OH)_3$ (YMP)
Ni	Unlimited (5)	-
Cu	Unlimited (5)	-
Zr	6E-07	Baddelyite (ZrO_2)
Nb	Unlimited (5)	-
Cd	Unlimited (5)	-
I	Unlimited (5)	-
Pb	Unlimited (5)	-
Ra	Unlimited (5)	-
U	3E-04	$U(OH)_4$(am) (YMP)
Np	4E-05	$Np(OH)_4$
Pu	1E-01	$Pu(OH)_4$
All other elements/ substances	Unlimited (5)	-

Notes:
1. Total dissolved concentration of all aqueous species.
2. YMP = thermodynamic data for solid phases taken from "data0.ypf.R2" am = amorphous; cr = crystalline.
3. For dissolved carbon, a total dissolved C concentration was adopted based on carbonate mineral equilibria.
4. It is possible that the Cl^- concentration in the near field may be more similar to that reported for the Cobourg limestone (5 mol kg^{-1}).
5. “Unlimited” means that the solubility is either calculated to be so high that it could never plausibly be attained in a natural system, or else that the solubility is uncertain so that the element is conservatively treated as being non-solubility limited.
6. Adopted higher concentration of calculated solubility limits for Cobourg and Guelph given in Appendix C.

4.6.3 Sorption Coefficients

Retardation of radionuclides within the shaft materials is considered to be controlled by linear, equilibrium, reversible sorption (see Equation 3.1). The sorption model is used to group and

upscale the effects of a variety of different processes such as ion-exchange and adsorption (see Appendix D). The literature review described in Appendix D has proposed conservative (i.e., lower than likely) sorption coefficients for a set of potentially important elements for bentonite/sand. These are presented in Table 4.25. Conservatively, all other element and organic contaminants are assumed not to be retarded through sorption. Owing to a lack of sorption data under relevant conditions, sorption onto concrete and asphalt shaft seals is conservatively taken to be zero. In addition, it is assumed that there is no sorption onto the engineered fill.

Table 4.25: Sorption Coefficients for Bentonite/Sand Shaft Seals (m^3 kg^{-1})

Element	Kd
C	0
Cl	0
Cr	0 (1)
Ni	0
Cu	0 (1)
Zr	0.05
Nb	0.1
Cd	0 (1)
I	0
Pb	0.001
Ra	0
U	0.01
Np	0.004
Pu	0.5
All other elements and organic contaminants	0

Note:
1. Where relevant data is not available, a value of 0 is chosen conservatively.

4.6.4 Densities

Grain and dry bulk densities are related as follows:

$$\rho = \rho_g (1 - \theta) \quad (4.4)$$

where:

ρ is the dry bulk density of the material, kg m^{-3};

ρ_g is the grain density of the material, kg m^{-3}; and
θ is the physical porosity of the material (unitless).

The measured diffusion (accessible) porosity (given in Table 4.22) is expected to provide an adequate value of the physical porosity for these materials.

Values of grain and dry bulk densities for the repository materials are given in Table 4.26. The variation in grain density for a given material is small and so a single reference value is given. Dry bulk densities will show a greater range due to the uncertainty in porosity (see Table 4.22) and so it is recommended for probabilistic calculations that the dry bulk density should be calculated using Equation 4.4.

Table 4.26: Densities for Repository Materials

Parameter	Material	Undegraded	Degraded
Grain Density (kg m^{-3})	Structural Concrete (1)	2560	2650
	LHHPC	2560 (2)	2650 (3)
	Bentonite/Sand	2740 (4)	
	Asphalt	1990 (5)	
	Engineered Fill	2650 (6)	
Dry Bulk Density (kg m^{-3})	Structural Concrete (7)	2280	1990
	LHHPC	2425 (8)	2390 (7)
	Bentonite/Sand	1600 (9)	
	Asphalt	1960 (7)	
	Engineered Fill	1990 (7)	

Notes:
1. Taken to be the same as for LHHPC.
2. Derived from bulk density using Equation 4.4 and porosity value from Table 4.22.
3. Assumed to degrade to have the same grain density as quartz given in CRC (2006).
4. Average grain density for 70:30 mix of MX80 bentonite (2780 kg m^{-3}, Karnland et al. 2008) and quartz sand (2650 kg m^{-3}, CRC 2006).
5. Average grain density for 70:20:10 mix of quartz sand (2650 kg m^{-3}, CRC 2006), asphalt (1035 kg m^{-3}, Pettersson and Elert 2001) and hydrated lime (2200 kg m^{-3}, CRC 2006).
6. Grain density of quartz given in CRC (2006).
7. Derived from grain density using Equation 4.4 and porosity value from Table 4.22.
8. Table 5 of Dixon et al. (2009).
9. See Section 4.4.2.

4.6.5 Effective Diffusion Coefficients

The effective diffusion coefficient is defined as:

$$D_e = D_p \theta_d \tag{4.5}$$

where:

D_e is the effective diffusion coefficient, $m^2\ s^{-1}$;
D_p is the porewater diffusion coefficient, $m^2\ s^{-1}$; and

θ_d is the diffusion (accessible) porosity (unitless).

Values for the effective diffusion coefficient for the repository materials are summarized in Table 4.27 and discussed below.

Table 4.27: Effective Diffusion Coefficients for Repository Materials

Parameter	Material	Undegraded	Degraded
Horizontal and Vertical Effective Diffusion Coefficient ($m^2\ s^{-1}$)	Structural Concrete	2.5E-12	1.25E-10
	LHHPC	3E-13	1.25E-10
	Bentonite/Sand	3E-10	
	Asphalt	1E-13	
	Engineered Fill	2.5E-10	

Note:
No distinction is made between values for anions and other species.

Savage and Stenhouse (2002) summarize effective diffusion coefficient data for a range of concretes. For undegraded **structural concrete**, they suggest a coefficient of 2.5×10^{-12} $m^2\ s^{-1}$. This is within the range suggested in Konecny and Tikalsky (2010) (1×10^{-13} to 2.5×10^{-11} $m^2\ s^{-1}$, with a best estimate of 1×10^{-12} $m^2\ s^{-1}$) and Chisholm and Lee (2001) (1×10^{-12} to 8×10^{-12} $m^2\ s^{-1}$). Savage and Stenhouse (2002) note that effective diffusion coefficients can increase to 1.25×10^{-10} $m^2\ s^{-1}$ as a result of the degradation of structural concrete resulting in an increase in porosity. The lower porosity and permeability of **LHHPC** will result in lower diffusion coefficients than for structural concrete. Mihara and Torii (2009) present results showing that high fly ash silica cements have an effective diffusion coefficient of 3×10^{-13} $m^2\ s^{-1}$, the same value as given in Byfors (1987) for cement with a high silica fume content. In the absence of data for degraded LHHPC, the diffusion coefficient is conservatively taken to be the same as for degraded structural concrete.

Diffusion of liquids in a **bentonite/sand** mix is a function of the bentonite's and hence the mix's density and the ratio of bentonite to sand (see Figure 4.10 and Figure 4.11). JNC (2000) considers a bentonite/sand mix in the ratio of 70:30 with an emplacement dry density of 1600 kg m^{-3}, i.e., the same as in the DGR shafts (Section 4.4.2). Three values are given in JNC (2000) for the effective diffusion coefficient: 2×10^{-10} for Se; 6×10^{-10} $m^2\ s^{-1}$ for Cs; and 3×10^{-10} $m^2\ s^{-1}$ for all other elements. An effective diffusion coefficient of 3×10^{-10} $m^2\ s^{-1}$ has been selected for bentonite/sand for all elements in the current assessment. Limited degradation of the bentonite/sand material is expected (see Section 4.5.4 of the System and Its Evolution report, QUINTESSA 2011b) and therefore no impact on diffusion coefficients is expected.

Petterson and Elert (2001) note that diffusion of radionuclides in bitumen (**asphalt)** is "insignificant". Testa (1995) notes that diffusion experiments on bituminized radioactive wastes indicate effective diffusion coefficients ranging from 1×10^{-17} $m^2\ s^{-1}$ to 1×10^{-14} $m^2\ s^{-1}$. Nakayama et al. (2003) give a value of 1×10^{-13} $m^2\ s^{-1}$ for bituminized radioactive wastes. In the light of these papers, a conservative value of 1×10^{-13} $m^2\ s^{-1}$ is adopted for asphalt.

The value for **engineered fill** is derived using Equation 4.5 with a free water diffusion coefficient of 1×10^{-9} $m^2\ s^{-1}$ (Freeze and Cherry 1979) and the diffusion porosity value given in Table 4.22.

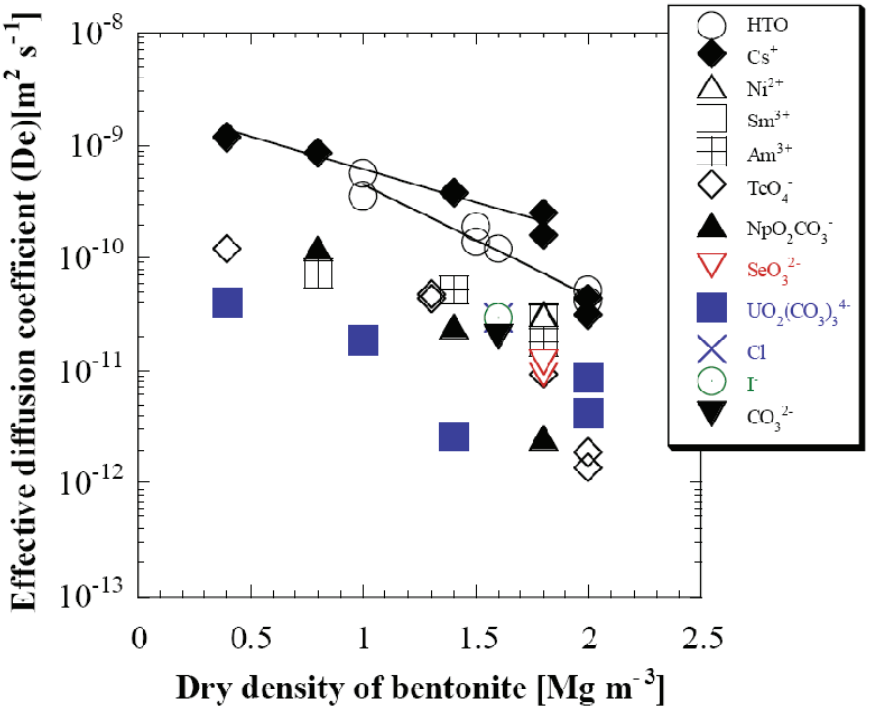

Note: Figure 5.3.1-5 in JNC (2000).

Figure 4.10: Effective Diffusion Coefficients as a Function of Bentonite Dry Density

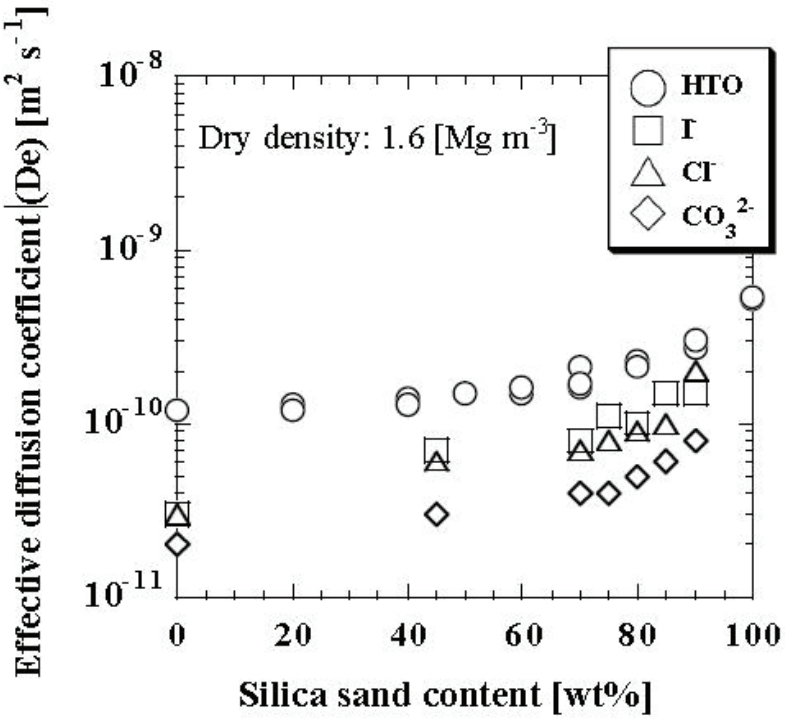

Note: Figure 5.3.1-7 in JNC (2000).

Figure 4.11: Effective Diffusion Coefficients as a Function of Silica Sand Content

4.7 Gas Flow Parameters

Gas flow in a porous rock system is described by two-phase flow behaviour, assuming gas and groundwater are the only fluids in the system. Two-phase flow behaviour can be described using two-phase flow characteristic curves, including capillary pressure as a function of saturation and relative permeability as a function of saturation. **Capillary pressure** is the difference in pressure across the interface between two immiscible fluids, and is defined here as the difference in pressure between the gas phase (non-wetting phase) and the water phase (wetting phase).

While several models are available to describe these characteristic curves, the parameters presented in this data report are based on the widely used van Genuchten model. The van Genuchten capillary pressure curve is given by:

$$P_c = -\frac{1}{\alpha}\left[S_{ec}^{-1/m} - 1\right]^{1/n} \tag{4.6}$$

$$S_{ec} = \frac{S_l - S_{lr}}{1 - S_{lr}} \tag{4.7}$$

The van Genuchten-Mualem-Luckner relative permeability curves are given by:

$$k_{rl} = S_{ek}^{1/2}\left[1 - (1 - S_{ek}^{1/m})^m\right]^2 \tag{4.8}$$

$$k_{rg} = (1 - S_{ek})^{1/3}\left[1 - S_{ek}^{1/m}\right]^{2m} \tag{4.9}$$

$$S_{ek} = \frac{S_l - S_{lr}}{1 - S_{lr} - S_{gr}} \tag{4.10}$$

Finally, the gas or liquid permeability is calculated by multiplication with the relative permeability:

$$k_g = k_{rg} * k \quad \textit{and} \quad k_l = k_{rl} * k \tag{4.11}$$

where:

P_c is the capillary pressure, Pa;
k_{rl} is the liquid phase relative permeability (ratio);
k_{rg} is the gas phase relative permeability (ratio);
k is the intrinsic permeability, m^2;
S_{ec} is the effective saturation for the capillary pressure relationship (volume ratio);
S_{ek} is the effective saturation for the relative permeability relationship (volume ratio);
S_l is the liquid saturation (volume ratio);
S_{lr} is the residual liquid saturation (volume ratio);
S_{gr} is the residual gas saturation (volume ratio);
m is a van Genuchten fitting parameter (unitless);
n is a van Genuchten fitting parameter (unitless); and
α is a van Genuchten fitting parameter, Pa^{-1}.

The van Genuchten parameters for each repository material are summarized in Table 4.28 and are discussed below.

Table 4.28: Two-phase Flow Parameters for Repository Materials

Material	α	m	n	S_{lr}	S_{gr}
	Pa^{-1}	-	-	-	-
Concrete (LPHPC & structural)	Ref: 1.0E-6 Min: 1.0E-7 Max: 3.0E-5	Ref: 0.5 Min: 0.3 Max: 0.6	Ref: 2.0 Min 1.5 Max: 2.3	Ref: 0.20 Min: 0.01 Max: 0.30	Ref: 0.10 Min: 0.00 Max: 0.20
Bentonite/ sand	Ref: 1.0E-7 Min: 3.0E-8 Max: 3.0E-5	Ref: 0.4 Min: 0.25 Max: 0.6	Ref: 1.8 Min 1.25 Max: 2.5	Ref: 0.01 Min: 0.0 Max: 0.60	0.01
Asphalt	Assume zero capillary pressure at all saturations				
Engineered Fill	2E-3	0.5	2.0	0.25	0.0

The reference parameter values listed in Table 4.28 are considered to be applicable to sealing materials affected by limited degradation. It is possible that significant degradation of the sealing materials could increase the intrinsic permeability, and reduce the air entry pressure, meaning that gas could move more easily up the shaft. The possible consequences of significant degradation of the sealing materials is addressed in the Severe Shaft Seal Failure Scenario.

4.7.1 Concrete

In the DGR, concrete is intended primarily as a structural component of the system, but will likely also provide a substantial barrier to gas migration. Sources for van Genuchten parameters for concrete include:

- Senger et al. (2003);
- Burnol et al. (2006);
- Monlouis-Bonnaire et al. (2004);
- Olivella and Alonso (2008);
- Arnedo et al. (2008);
- NAGRA (2008) - which presents data from numerous sources; and
- SANDIA (1996).

Table 4.29 shows the van Genuchten parameters for concrete from these sources. While there were many sources that presented two-phase flow properties for concrete, many referred back to the same original sources, and many used the same or similar values. Nevertheless, it was possible to obtain the range of values for concrete gas flow parameters given in Table 4.28, although the breadth of the available data does not allow for high confidence that the range of values fully characterizes the possible behaviour of concrete. The ranges in Table 4.28

comprise approximately the minimum and maximum values from the literature, rounded to one significant digit. The reference value is the approximate average from Table 4.29, or in some cases the mode value. The values are taken to be applicable to both LPHPC and structural concrete since the literature is not sufficiently large to allow for meaningful differentiation between the two types of concrete. Figure 4.12 shows the reference capillary pressure curve, along with the maximum and minimum capillary pressure curves, and a selection of the capillary curves from Table 4.29. The curve for Monlouis-Bonnaire et al. (2004) was plotted by assuming S_{lr} equal to 0.2, although this information was not provided in the source document.

Table 4.29: Literature Values for Two-phase Flow Parameters in Concrete

Source	Type	α	m	n	S_{lr}	S_{gr}
		Pa^{-1}	-	-	-	-
Senger et al. (2003)	concrete	1.00E-06	0.500	2.00	0.250	-
Monlouis-Bonnaire et al. (2004)	concrete	9.02E-08	0.560	2.27	-	-
Olivella and Alonso (2008)	silo concrete	1.00E-06	0.500	2.00	-	-
SANDIA (1996)	concrete 0-400 years	5.81E-07	-	-	0.200	0.200
SANDIA (1996)	concrete 400-10000 years	2.56E-05	-	-	0.200	0.200
NAGRA (2008)	concrete	5.00E-07	0.351	1.54	-	-
NAGRA (2008)	low permeability concrete barriers	1.15E-05	0.333	1.50	0.160	0.010
NAGRA (2008)	normal concrete	1.00E-05	0.500	2.00	0.300	0.180
NAGRA (2008)	lining invert	2.00E-07	-	-	-	-
NAGRA (2008)	waste package concrete	5.00E-07	0.351	1.54	0.010	0.000
Burnol et al. (2006)	concrete barrier	5.00E-07	0.317	-	-	-

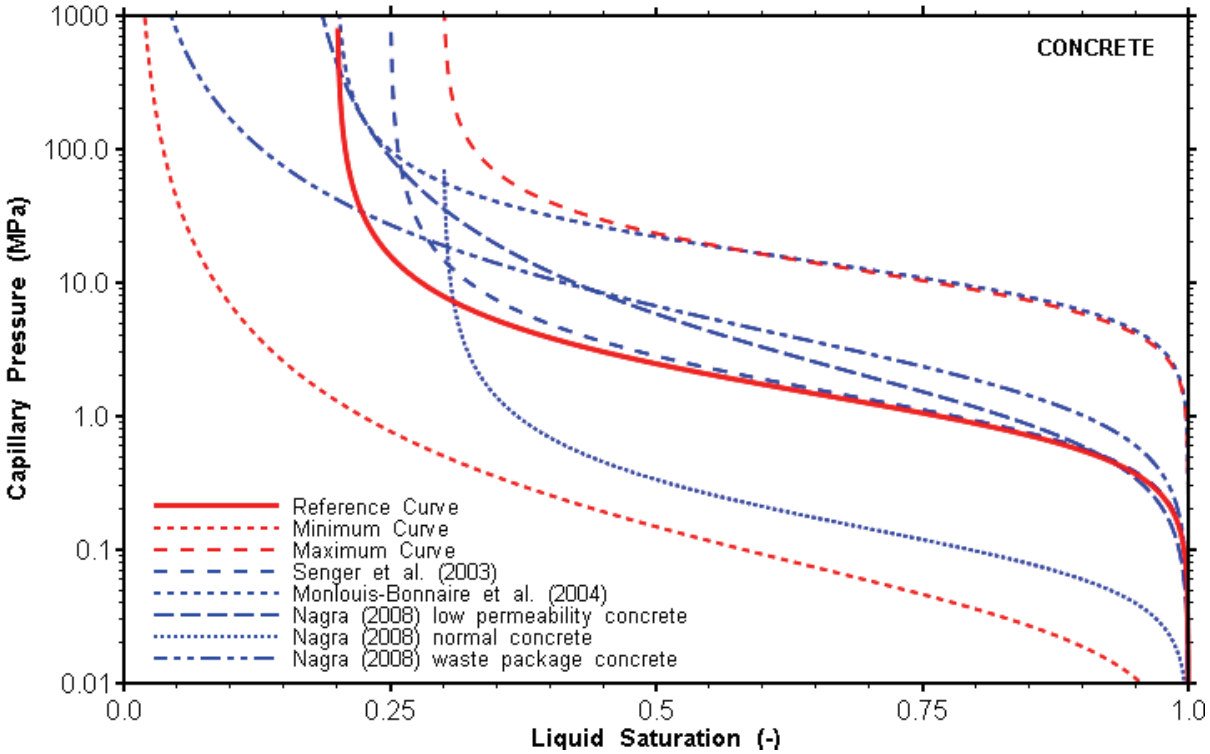

Figure 4.12: Capillary Pressure Curves for Concrete

Monlouis-Bonnaire et al. (2004) reported that they were unable to obtain a good fit to capillary pressure-saturation and relative permeability-saturation curves using the standard van Genuchten model. Rather, they altered the equations by including certain exponents in the relative permeability curve optimization, which are usually not changed. When we attempted a new fit to capillary pressure-saturation and relative permeability-saturation curves available in Lanyon et al. (2001), it was similarly difficult to obtain a good fit to these curves with the traditional van Genuchten model. However, two-phase flow models such as TOUGH2 do not currently allow input of non-standard van Genuchten curves.

4.7.2 Bentonite/Sand

The bentonite-sand mixture proposed in the preliminary design (Section 13.6.3.1 of the PSR, OPG 2011b) has a high bentonite composition, with 70% bentonite and 30% sand. Bentonite-sand is the primary shaft sealing material. Sources for van Genuchten parameters for bentonite/sand include:

- Senger et al. (2003), 20:80 bentonite/sand;
- Olivella and Alonso (2008), 20:80 bentonite/sand;
- Arnedo et al. (2008), 20:80 bentonite/sand;
- NAGRA (2004), 30:70 bentonite/sand; and
- NAGRA (2004), 20:80 bentonite/sand.

Table 4.30 shows the van Genuchten parameters for bentonite/sand and bentonite from these sources. The information in the literature pertains to bentonite-poor mixtures with a mixing ratio of 70-80% sand. Two-phase flow parameters for the bentonite-rich mixture proposed for the DGR could not be found. However, there is a general consensus in the literature that as the clay content increases above around 50%, the aggregate becomes isolated and the properties approximate those of the clay itself. That is, the rich bentonite mixture may behave much more like pure bentonite.

An examination of values for bentonite based on:

- Baumgartner (2006), bentonite;
- Senger and Marschall (2008), bentonite; and
- Burnol et al. (2006), Callovian-Oxfordian clay,

as well as the low bentonite mixtures listed above, was used to obtain the range of probable values for the 70% bentonite mixture given in Table 4.28. It is expected that the van Genuchten parameters will be somewhere between the values for bentonite and the low bentonite/sand mixtures for which information is available. Figure 4.13 shows the reference capillary pressure curve, along with the maximum and minimum capillary pressure curves, and a selection of the capillary curves from Table 4.30. Curves for Olivella and Alonso (2008) and Burnol et al. (2006) were plotted by assuming a residual liquid saturation of zero.

Table 4.30: Literature Values for Two-phase Flow Parameters in Bentonite and Sand-Bentonite

Source	Type	α	m	n	S_{lr}	S_{gr}
		Pa^{-1}	-	-	-	-
Senger et al. (2003)	20:80 bentonite/sand	7.69E-06	0.600	2.50	0.580	-
Arnedo et al. (2008)	20:80 bentonite/sand	2.22E-05	0.200	1.25	0.000	0.010
Olivella and Alonso (2008)	20:80 bentonite/sand	3.33E-05	0.200	1.25	-	-
NAGRA (2008)	20:80 bentonite/sand	1.92E-05	-	-	-	-
NAGRA (2004)	30:70 bentonite/sand	6.67E-07	-	-	-	-
Senger and Marschall (2008)	Bentonite	5.56E-08	0.451	1.82	0.010	0.050
Burnol et al. (2006)	Callovian-Oxfordian clay	6.67E-08	0.317	1.46	-	-

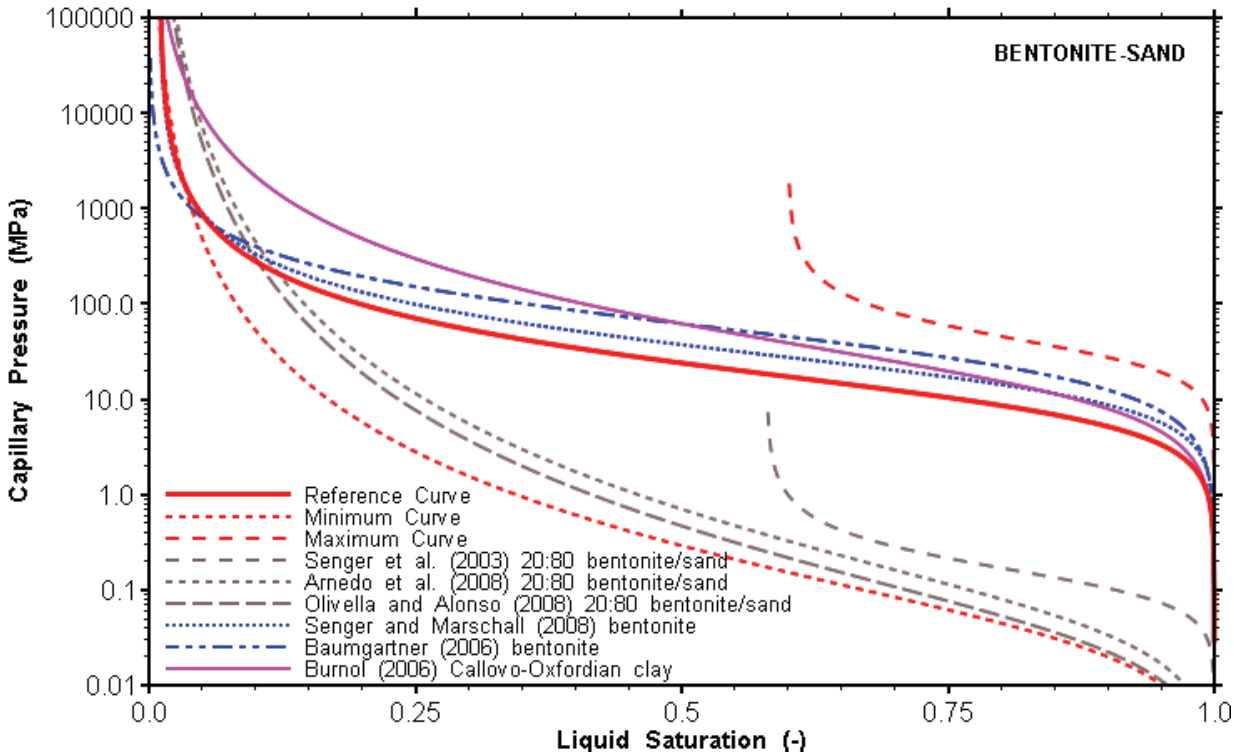

Figure 4.13: Capillary Pressure Curves for Bentonite

4.7.3 Asphalt

No two-phase flow data are available for asphalt. However, Appendix C of the WIPP Seal Report (SANDIA 1996) does discuss two-phase flow in asphalt. As asphalt is hydrophobic, it should not develop any suction pressure, and as a result it will not attract water. SANDIA (1996) recommends a capillary pressure model for asphalt defined by zero capillary pressure at all saturations. In other words, the gas and water pressure are equal at all saturations.

4.7.4 Engineered Fill

Sources for van Genuchten parameters for engineered fill include:

- Senger et al. (2003);
- Olivella and Alonso (2008); and
- SANDIA (1996).

There was very little variability in values used by the authors. As would be expected, all were characterized by relatively low air entry pressures. Values used by Senger et al. (2003) for a sand/gravel backfill are adopted in Table 4.28. The reference engineered fill is a clean sand with a hydraulic conductivity of 10^{-4} m s^{-1}, which may have slightly different gas flow properties to sand/gravel. Using sand-gravel properties is conservative with respect to gas flow, and the relatively minor property differences between sand/gravel and sand will have a negligible effect on the gas flow calculations given that engineered fill is only used to fill the shaft adjacent to relatively high permeability upper rock formations.

4.7.5 Initial Gas Saturations

Gas saturation measures the fraction of the void space filled with gas, as opposed to liquid (water). Initial gas saturations of barrier materials will have an impact on gas flow processes in the shaft sealing system, especially during the first few thousand years after closure. For concrete, the initial gas saturation is set at 50% (Russell and Simmons 2003). Compacted bentonite-sand is expected to have initial gas saturations between 10 and 30% (Dixon et al. 2009; Baumgartner et al. 1996). For safety assessment modelling, a reference value of 20% gas saturation is adopted. Asphalt, a hydrophobic material, is assumed to have an initial gas saturation of 100% (SANDIA 1996). Finally, the engineered fill, which is intended to be used in the upper reaches of the shaft which are surrounded by relatively permeable sandstone, can be reasonably assumed to have an initial gas saturation of 0%.

5. GEOSPHERE DATA

The Geosynthesis Report (NWMO 2011) and the Descriptive Geosphere Site Model (DGSM) report (INTERA 2011) are the primary sources of geosphere data. These reports present site-specific data from the DGR-1, -2, -3, -4, -5 and -6 boreholes and shallow US series boreholes at the Bruce nuclear site, plus data from the wider region. The data have been cross-checked (e.g., use of multiple samples, multiple analytical methods and cross-laboratory comparisons) and extensively analyzed (e.g., through the use of modelling to test the conceptual models developed from the data, and thus check the internal consistency of the dataset).

Site-specific data are not available for a small number of parameters. Where site-specific data are not yet available, data have been drawn from a wider range of sources. These data sources can be described as a hierarchy of decreasing confidence:

- Data from analogous geological formations at the Bruce nuclear site;
- Data from the same geological formations and comparable hydrogeochemical environments across the wider region, e.g., oil and gas wells;
- Literature data for equivalent material types, often selected to be cautiously realistic; and
- Reasonable values that have been adopted in the absence of the above.

The majority of such data extrapolations and assumptions are described in the DGSM report (INTERA 2011) and the Geosynthesis report (NWMO 2011), and the underpinning technical reports, with the key recommended datasets being collated in this report for the purposes of the postclosure safety assessment calculations. Any additional extrapolations and assumptions are described herein.

5.1 Geosphere Characteristics

The understanding of the stratigraphy of the Bruce nuclear site used in the safety assessment is described in the DGSM report (INTERA 2011) and Geosynthesis reports (NWMO 2011). Many of the physical and chemical properties of the geosphere are directly correlated with lithology and hence the stratigraphy. Therefore, the stratigraphy has generally been used as the basis for presenting the geosphere properties. Figure 5.1 shows the geological stratigraphy and the lithologies of the different geological formations, members and units. The depths of the different geological units are given in Table 5.1.

Superimposed on the stratigraphy, distinct hydrogeological zones have been recognized within which different flow and transport processes dominate. These zones can be further sub-divided into a number of hydrostratigraphic units, which have distinct hydrogeological and geochemical conditions (Figure 5.2). The hydrostratigraphic units correlate well with the geology, directly mapping to specific formations, and, in some cases, to formation members or units. The correlations are shown in Table 5.2. In the remainder of this section, geosphere data are presented using the geological units shown in Table 5.2.

The temperature at the proposed DGR horizon was measured to be 22 °C in borehole DGR-3 and 23 °C in borehole DGR-4 (Pehme and Melaney 2010).

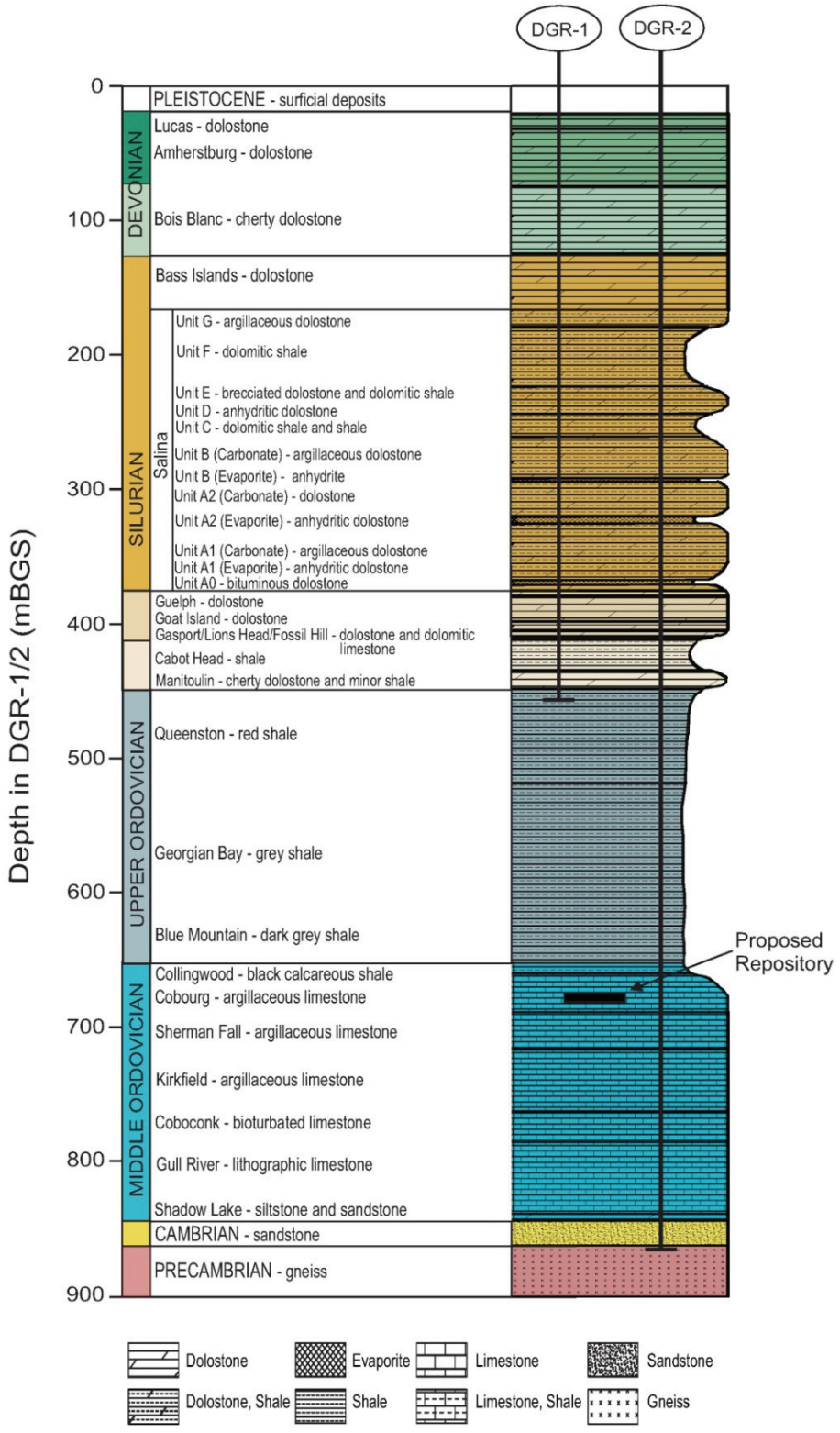

Note: Figure 3.2 in INTERA (2011).

Figure 5.1: Reference Stratigraphic Column at the Bruce Nuclear Site Based on DGR-1 and DGR-2 Borehole Data

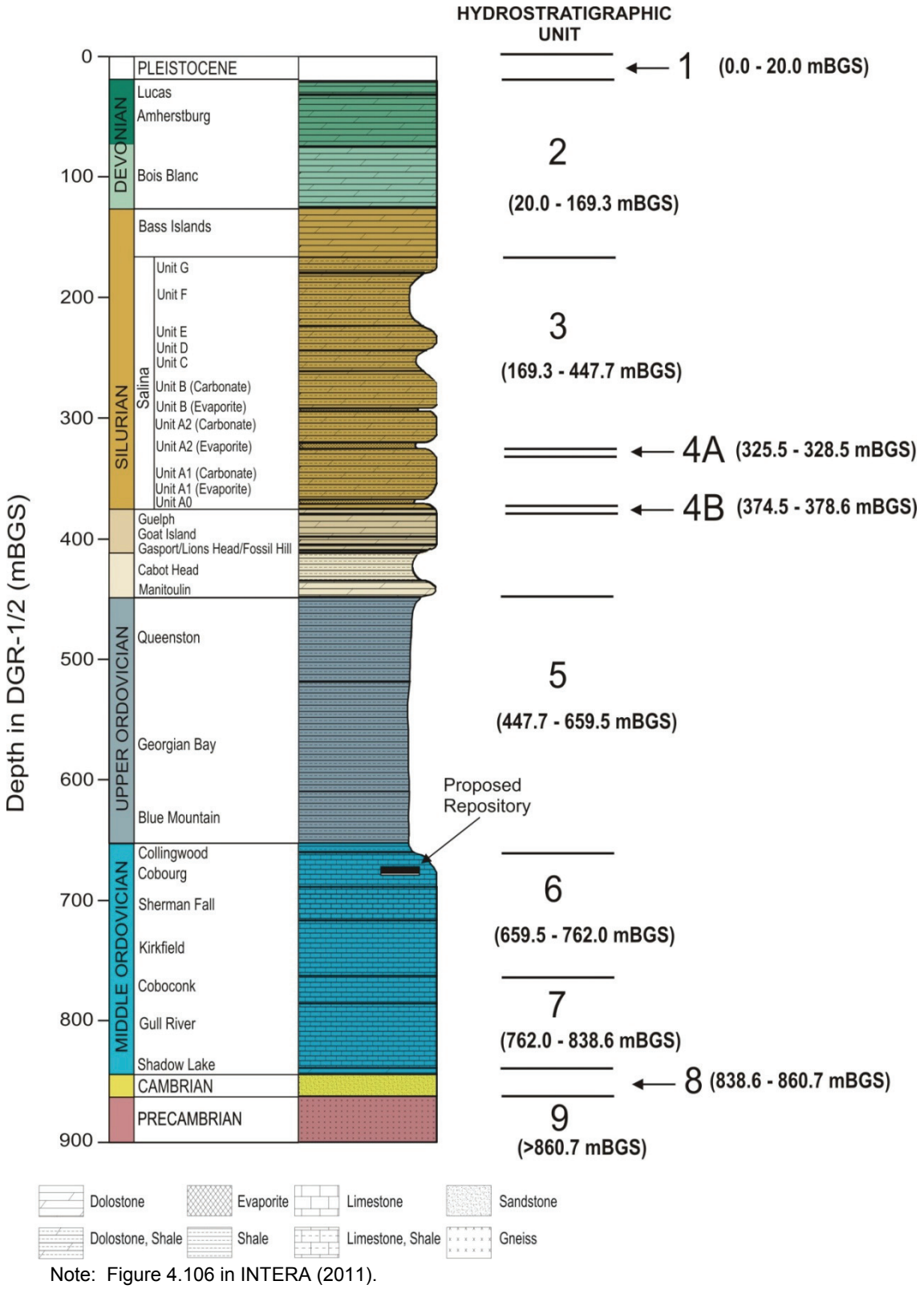

Note: Figure 4.106 in INTERA (2011).

Figure 5.2: Reference Stratigraphic Column Showing Hydrostratigraphic Units at the Bruce Nuclear Site

Table 5.1: Depths to Geological Units (metres below ground surface)

Geological Unit	Depth of Top Unit (mBGS)	Depth at Centre of Stratigraphic Unit (mBGS)
Quaternary	0	10
Lucas	20	25
Amherstburg (upper)	30.4	40
Amherstburg (lower)	50	63
Bois Blanc	75	100
Bass Island (upper)	124	134
Bass Island (lower)	144	157
Salina G	169.3	174
Salina F	178.6	201
Salina E	223	233
Salina D	243	244
Salina C	244.6	252
Salina B	260.3	276
Salina B evaporite	291.2	292
Salina A2 carbonate	293.1	306
Salina A2 evaporite	319.7	323
Salina A1 Upper carbonate	325.5	327
Salina A1 carbonate	328.5	348
Salina A1 evaporite	367	369
Salina A0	370.5	373
Guelph	374.5	377
Goat Island	378.6	388
Gasport	397.4	401
Lions Head	404.25	406
Fossil Hill	408.7	410
Cabot Head	411	423
Manitoulin	434.8	441
Queenston	447.7	483
Georgian Bay	518	563
Blue Mountain	608.9	630
Collingwood	651.6	656
Cobourg	659.5	674
Sherman Fall	688.1	702
Kirkfield	716.1	739
Coboconk	762	774
Gull River	785	812
Shadow Lake	838.6	841
Cambrian	843.8	852
Precambrian	860.7	N/A

Note:
The DGR-1/2 stratigraphy is used as reference. All data from Table 3.1 of the DGSM report (INTERA 2011) except for Amherstburg (lower), Bass Islands (lower) and Salina A1 Upper Carbonate which are from TR-08-10 (Walsh 2011).

Table 5.2: Mapping of the Geological Units to the Hydrogeological Zones and Hydrostratigraphic Units

Geological Unit	Hydrogeological Zones	Hydrostratigraphic Units
Quaternary	Surficial Groundwater Zone	1
Lucas	Shallow Bedrock Groundwater Zone	2
Amherstburg (upper)		
Amherstburg (lower)		
Bois Blanc		
Bass Island (upper)		
Bass Island (lower)		
Salina G	Intermediate Bedrock Groundwater Zone	3
Salina F		
Salina E		
Salina D		
Salina C		
Salina B		
Salina B evaporite		
Salina A2 carbonate		
Salina A2 evaporite		
Salina A1 Upper carbonate		4a
Salina A1 carbonate		3
Salina A1 evaporite		
Salina A0		
Guelph		4b
Goat Island		3
Gasport		
Lions Head		
Fossil Hill		
Cabot Head		
Manitoulin		
Queenston	Deep Bedrock Groundwater Zone	5
Georgian Bay		
Blue Mountain		
Collingwood		
Cobourg		6
Sherman Fall		
Kirkfield		
Coboconk		7
Gull River		
Shadow Lake		8
Cambrian		
Precambrian		9

General characteristic values for water are given in Table 5.3 and chemical compositions are given in Table 5.4.

As is usual for deep groundwater and porewater compositions, those reported in Table 5.4 inevitably differ from actual in-situ water compositions owing to perturbations concerned with sampling and analyses. This is particularly the case for the porewaters, analysis of which involved an extraction procedure that causes water – solid interactions. For example, the Cobourg porewater from DGR-3 has an Mg concentration that is much higher than the Ca concentration. This is an unusual relationship in natural waters and likely is an artefact of perturbations during sampling and/or corrections of raw analytical data for these perturbations. Nevertheless, the selected water compositions are the most appropriate ones reported in INTERA (2011, Sections 4.5.2 and 4.6), taking into account the locations in the DGR at which in-situ compositions need to be estimated to support the current assessment and the desirability of selecting a small number of compositions to bracket the range of actual compositions. The perturbations from actual in-situ compositions are taken into account in the calculations to support the assessment by constructing model in-situ waters using the data in Table 5.4 as a starting point, as described in Appendix C.

Table 5.3: General Characteristic Values for Water

Parameter	**Units**	**Freshwater, 20 ^{o}C, 0.1 MPa (Fetter 1994)**	**Saline Water 25 ^{o}C, 300 g L^{-1} NaCl, 0.1 MPa (Pruess 1991)**
Water Density	kg m^{-3}	998	1185
Compressibility of water	Pa^{-1}	4.6E-10	3.3E-10 (Walsh 2011)
Kinematic viscosity of water	kg m^{-1} s^{-1}	0.00114	0.0023
Molar mass of water	kg mol^{-1}	0.018 (1)	0.0234 (2)

Notes:
Summation of elemental masses for H_2O (H = 1 g; O = 16 g).
Summation of elemental masses for H_2O and 300 g L^{-1} NaCl.

Table 5.4: Sampled Groundwater and Porewater Compositions

Sample	OGW-8	OGW-12	Salina A2	Salina A1	Georgian Bay Shale	Cobourg Limestone
Sample Type	Groundwater	Groundwater	Porewater	Porewater	Porewater	Porewater
Borehole	DGR-3	DGR-4	DGR-4	DGR-3	DGR-3	DGR-3
Depth (mBGS)	337.80-341.51	373.66-381.18	304.05	348.31	581.28	680.46
Formation	Salina Upper A1 Formation	Guelph	Saline A2 Unit - Carb	Salina A1 Unit - Carb	Georgian Bay	Cobourg
Source (INTERA 2011)	Table 4.7 and Table 4.8; Figures 4.53 to 4.57	Table 4.7 and Table 4.8; Figures 4.53 to 4.57	Figures 4.53 to 4.57	Figures 4.53 to 4.57	Figures 4.53 to 4.57	Figures 4.53 to 4.57
% Drill Water Contamination	3.1	0.3	N.D.	N.D.	N.D.	N.D.
pH	7.3	6.5	N.D.	N.D.	N.D.	N.D.
Eh (mV)	-13	-141.9	N.D.	N.D.	N.D.	N.D.
DO (mg L^{-1})	0.3	0.23	N.D.	N.D.	N.D.	N.D.
Sulphide (mg L^{-1})	5	0	N.D.	N.D.	N.D.	N.D.
Calculated TDS (mg L^{-1})	26760	375468	131035	191664	298610	260362
Fluid Density (kg m^{-3})	1019	1210	N.D.	N.D.	N.D.	N.D.
Na (mg L^{-1})	7835	99133	47446	61626	54486	59514
Ca (mg L^{-1})	1003	31597	2208	668	40533	9530
Mg (mg L^{-1})	580.6	7901	2558	8738	12651	22099
K (mg L^{-1})	125.2	3665	545	1407	16159	17303
Sr (mg L^{-1})	17.7	589.3	252	1128	1566	1868
Fe (mg L^{-1})	10	29.6	N.D.	N.D.	N.D.	N.D.
Mn (mg L^{-1})	1.03	4.27	N.D.	N.D.	N.D.	N.D.
Cl (mg L^{-1})	13615	229635	77617	54775	212431	178956
Br (mg L^{-1})	<30	1715	167	30	2371	1824
F (mg L^{-1})	1.9	0.3	N.D.	N.D.	N.D.	N.D.
I (mg L^{-1})	<0.3	0.5	N.D.	N.D.	N.D.	N.D.
Si (mg L^{-1})	2.6	987	N.D.	N.D.	N.D.	N.D.
SO_4 (mg L^{-1})	3568	211	8713	80999	291	1415
NO_3 (mg L^{-1})	<6	<5	N.D.	N.D.	N.D.	N.D.
B (mg L^{-1})	N.D.	N.D.	75	241	182	177
Alkalinity as $CaCO_3$ (mg L^{-1})	180.6	42.5	N.D.	N.D.	N.D.	N.D.

Notes:
These compositions are groundwater and porewater analyses that have been corrected for perturbations due to sampling and analysis where feasible. It is expected that the departure from in-situ conditions will be greatest for the porewaters. Porewater concentrations (apart from TDS) were reported in the original source in units of mmol kg^{-1} water. These concentrations have been converted to mg L^{-1} based on1 kg L^{-1} water density.
N.D. means no data.

5.2 Damaged Zone Characteristics

The envelope of sedimentary rock surrounding underground excavations, including the shafts that connect the DGR with the ground surface, could have enhanced hydraulic conductivity as a consequence of excavation-induced damage due to excavation techniques and stress relief. The Geosynthesis Report (Section 6.3.1 of NWMO 2011) collates information from international mines and Underground Rock Laboratories (URLs) on the properties, extent and temporal evolution of the zone.

The damaged zone can be subdivided into 3 sub-zones (Figure 5.3 and NWMO 2011).

- Highly Damaged Zone (HDZ) where macro-scale fracturing or spalling may occur. The effective permeability of this zone is dominated by the interconnected fracture system.
- Excavation Damaged Zone (EDZ) with hydromechanical and geochemical modifications inducing changes in flow and transport properties.
- Excavation disturbed Zone, or Excavation Influence Zone, (EdZ/EIZ) with possible hydromechanical and geochemical modification, without material changes in flow and transport properties. This zone is not explicitly represented in the safety assessment calculations since there are no changes in flow and transport properties in this zone.

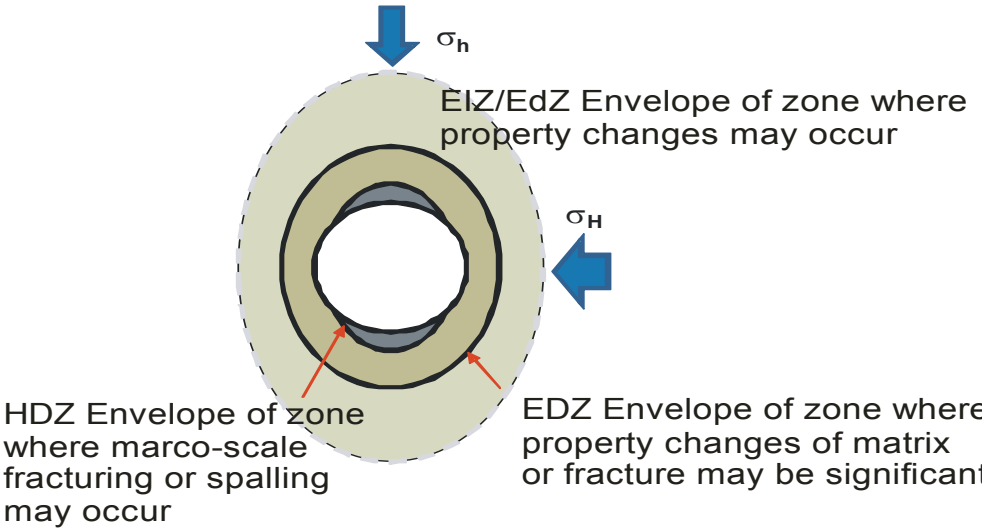

Figure 5.3: Schematic Illustrating Definitions of EdZ (EIZ), EDZ, and HDZ for an Unjointed Rock in an Anisotropic Stress Field

5.2.1 Shafts

The HDZ in the Deep and Intermediate Bedrock Groundwater Zones will be removed from the shaft walls from the level of DGR upwards by means of overexcavation before the shafts are sealed during DGR closure (Section 13.6.3.1 of the PSR, OPG 2011b). The EDZ will remain in place. The HDZ and EDZ will not be removed in the Shallow Bedrock Groundwater Zone and the Surficial Groundwater Zone.

The shaft HDZ and EDZ extent was estimated from numerical modelling using FLAC 3D and Phase 2 codes described in the Geosynthesis report (Section 6.4.3 of NWMO 2011). The results showed that the maximum extent of the HDZ and EDZ, is generally less than 1.1 times the excavated shaft radius. The estimated thickness of the HDZ (from the shaft wall to the outer limit of the HDZ) is approximately 0.5 m, or 0.11 times the radius of the shaft. The extent of the EDZ varies with depth, lithology and excavation method (Figure 5.4). The estimations of the maximum extent of the EDZ from the shaft seal analysis are consistent with observations from URLs.

Because the geosphere horizontal stress field is anisotropic with a ratio ranging between 1 to 1.2 (NWMO 2011), the EDZ could likely take an slightly elliptical shape with axes aligned with the major and minor horizontal stress tensors. However the impact of the actual orientation of the EDZ is not significant. The most important aspect for the DGR is the area of higher permeability around the shafts for vertical transport, which is expected to be covered adequately by conservatively assuming a circular model of one shaft radius in the safety assessment.

There will be a transition in the extent of damage across the EDZ, with the magnitude of damage, and thus the rock permeability, decreasing away from the wall of the excavation. Therefore, the EDZ is subdivided into inner and outer zones. with average assumed permeabilities to facilitate numerical modelling. The thickness of the inner EDZ is taken to be a uniform 0.5r, where r is the radius of the unlined shaft prior to removal of the HDZ. The thickness of the outer EDZ is also taken to be 0.5r. The total thickness of the inner and outer EDZ is therefore r (i.e., 4.075 m for the main shaft and 3.225 m for the ventilation shaft – see Table 4.14).

The stability of the EDZ with time was also modelled (Section 6.4.3 of NWMO 2011), taking into consideration long-term rock strength and concrete bulkhead strength degradation, seismic loading, ice-sheet loading, gas pressure and selected combinations of these factors. In general, the models showed that the majority of the EDZ development occurs during the initial shaft excavation phase. Once the shafts have been sealed they will be significantly stabilized due to increase in confinement. Long-term bulkhead strength degradation and pore pressure evolution will both lead to active mechanical processes within the existing EDZ and some further development of the EDZ adjacent to the bulkheads and bentonite-sand backfill. Due to the vertical geometry of the shaft, glacial loading has only a minor effect on differential ground stresses in the horizontal plane. Consequently, the effect of EDZ increase during glaciations is minor for the shaft. Similarly, pore pressure and seismic loading will not significantly increase the predicted extent of the EDZ around the shaft. These changes are small compared with uncertainty regarding the properties of the EDZ, and when averaged over the shaft sealing system as a whole, the extent of the shaft EDZ is not considered to change significantly over 1 Ma timescales. Therefore, the limited evolution of the EDZ is subsumed into the parameterization of the EDZ.

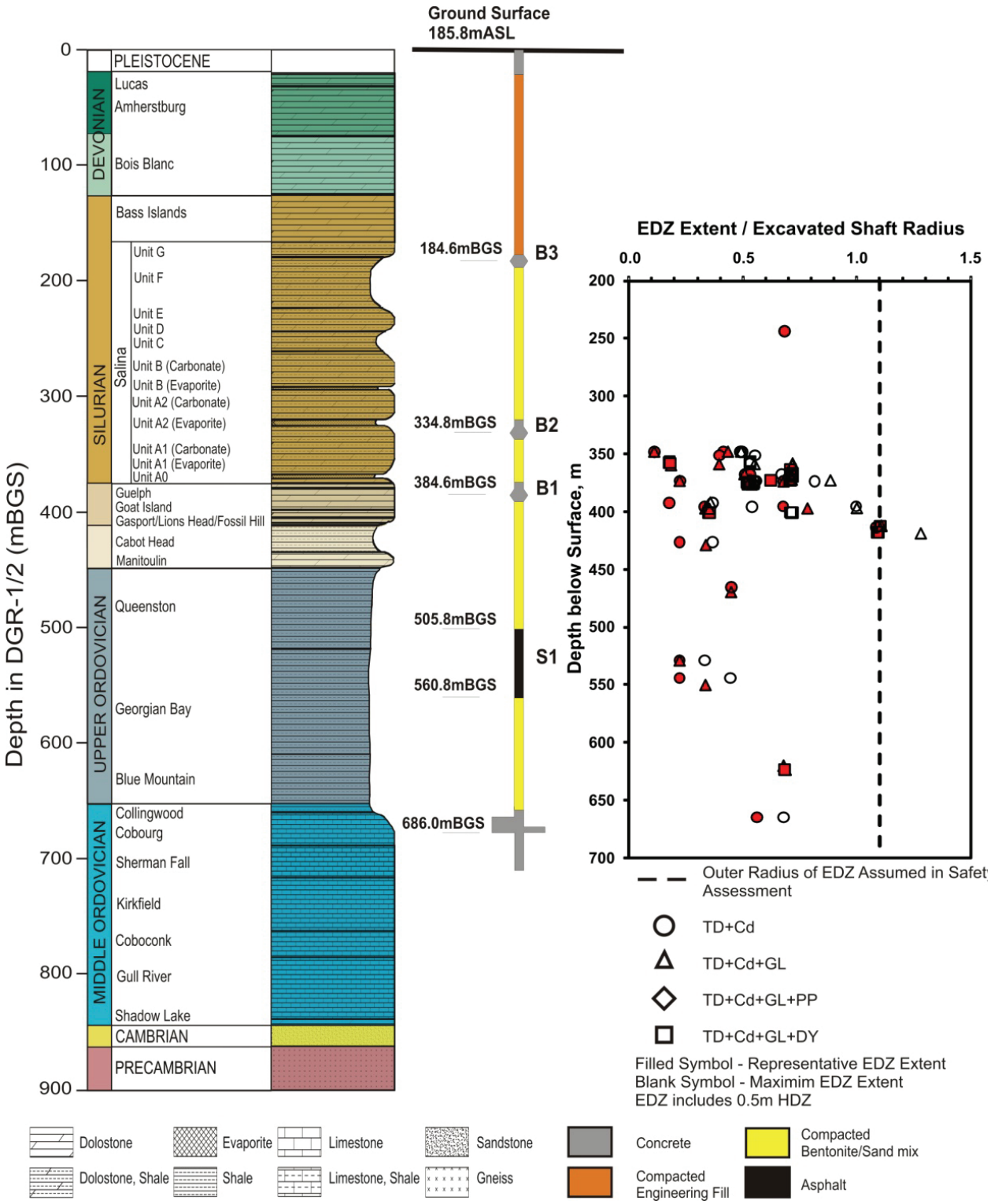

Note: Figure 6.22 in NWMO (2011).

Figure 5.4: Formation Specific Distribution of Representative and Maximum EDZ Extent Along Shaft, Including 0.5 m HDZ

5.2.2 Repository Excavation

An HDZ and EDZ will also form around the repository excavations. The HDZ will be left in place around the emplacement rooms, access tunnels and shaft sump ramps. The HDZ around the emplacement rooms and unsupported access tunnels is assumed to have a similar thickness to the shaft HDZ (0.5 m). For supported access tunnels and the shaft sump ramps, it is assumed to be 2 m above the ceiling and below the floor, and 0.5 m for the walls. The different HDZ thicknesses are derived from two different phases of modelling work presented by NWMO (2011). The modelling results for the unsupported rooms are comprehensive, and there is high confidence in the results. However, uncertainty in the extent for the HDZ adjacent to the open (i.e., not backfilled) tunnels is not important. The modelling results for the supported tunnels, where the extent of the HDZ is important, are from a separate modelling exercise and are very conservative.

In light of modelling results reported in the Geosynthesis report (NWMO 2011), the EDZ around the rooms and unsupported tunnels is estimated to be 8 m thick since they are unsupported in the long term, and 3 m thick around the access tunnels where they are supported by concrete seals as part of the tunnel monolith.

It is also recognized that the roofs of the emplacement rooms and access tunnels will likely collapse over postclosure timescales due to seismic events and ice-sheet loading and unloading. The former loosen and dislodge fractured rock around openings, whereas the later generate new cracks in the host rock. After a roof fall, the EDZ will reform around the new enlarged room boundary.

Within the room, the rockfall plus the waste packages will partially fill the space. The fallen rock will tend to dilate when it breaks up. With a reasonable bulking factor, the fallen rock will completely choke off the cavern and prevent further roof collapse. The frictional properties of the pillar material and the presence of this “backfill” will stabilize the cavern in time, with resultant displacements within the tolerance of the overlying strata of key barrier rock units – the Georgian Bay and Queenston shales. For example, assuming a bulking factor of 1.3, then it can be readily shown that the 7 m high rooms would fill after 20 m of roof fall, taking no credit for the waste packages. Based on the results of detailed modelling of the emplacement rooms described in the Geosynthesis Report (Section 6.4.4 of NWMO 2011), and the anticipated frequency of significant seismic events and glacial cycles, a self-supporting collapse zone is assumed to develop over a period of 300,000 years, due to the combined effects of rockfall from the roof and pillar collapse, with the collapse zone extending approximately 10 m into the roof (Section 4.4.1 of the System and Its Evolution report, QUINTESSA 2011b).

5.3 Flow Paths

Data relating to the representation of the geosphere groundwater and gas pathways within the assessment-level AMBER models are described in the Normal Evolution Scenario report (QUINTESSA 2011a) and the Human Intrusion and Other Disruptive Events report (QUINTESSA and SENES 2011), based on detailed modelling results described in the Groundwater Modelling report (GEOFIRMA 2011) and the Gas Modelling report (GEOFIRMA and QUINTESSA 2011).

5.4 Groundwater Flow Parameters

5.4.1 Geosphere

The parameters used for the geosphere flow properties are:

- Groundwater heads and gradients – Section 5.4.1.1 (Section 4.16.9 of the DGSM report, INTERA 2011);
- Hydraulic conductivity - Table 5.5 (Table 4.19 of the DGSM report, INTERA 2011);
- Specific storage - Table 5.5 (Table 4.19 of the DGSM report, INTERA 2011); and
- Porosity - Table 5.6 (Table 4.18 of the DGSM report, INTERA 2011).

5.4.1.1 Groundwater Heads and Head Gradients

Groundwater hydraulic head and gradient data are available from:

- Shallow boreholes across the region;
- Shallow groundwater boreholes at the Bruce nuclear site ("US series" boreholes);
- DGR site characterization boreholes drilled on the Bruce nuclear site (DGR-1, -2, -3, -4, -5 and -6);
- Intermediate and deep gas exploration boreholes across the wider region; and
- Numerical groundwater simulations conducted at Bruce nuclear site and regional scales (NWMO 2011).

At the Bruce nuclear site, horizontal gradients in the surficial and shallow bedrock groundwater zone are of the order 0.003, directed towards Lake Huron. There is also an upward vertical gradient of 0.001 to 0.01 in this zone (Section 4.12.1 of INTERA 2011). A mean upward vertical gradient of 0.005 is adopted for the postclosure safety assessment.

There are lateral head gradients in the Salina A1 Upper Carbonate, Guelph, and Cambrian units. Table 4.16 of INTERA (2011) details the present day hydraulic gradients as having magnitude 0.0077, 0.0026, and 0.0031 metres per metre in the Salina A1 Upper Carbonate, Guelph and Cambrian units, respectively. Flow directions in the three units are reported as having azimuth 322 (i.e., northwest), 78 (i.e., east), and 89 (i.e., east) degrees clockwise from north, respectively. These gradients might be subject to future change due to changing boundary conditions (e.g., the advance and retreat of ice-sheets). Furthermore, horizontal flow in these formations will act to dilute and disperse radionuclides migrating in the shaft/shaft EDZ. Therefore a conservative assumption for long-term safety assessment calculations is to assume a gradient of zero.

Intermediate and deep zone data from the DGR boreholes show a pattern of hydraulic heads that are out of equilibrium with the present-day surface conditions. The head profile from the site is shown in Figure 5.5[2]. In particular, the Cambrian units are overpressured, while the

[2] The upper figure (head profiles) is derived from Figures 4.99, 4.100 and 4.102 of INTERA (2011). The lower figure (density profile) is taken from the interim version of Figure 4.81 of INTERA (2011) available at the time of the data freeze for safety assessment calculations (summer 2010) ; see Appendix A of INTERA (2011).

Ordovician sediments are underpressured. The existence of these large disequilibrium heads is supporting evidence for the very low hydraulic conductivities in the Ordovician rocks.

The disequilibrium heads, their possible causes, and likely evolution are described in the Geosynthesis report (Section 5.4 of NWMO 2011). The overpressures in the Cambrian group are consistent with the density-dependent hydraulic conditions within the Michigan Basin. The cause of the underpressures in the Ordovician rocks is less established; glaciation is not likely to be the explanation, however, the presence of a gas phase in these rocks could explain the underpressures. It is expected that both of these pressure features (i.e., over and underpressures) will persist over the assessment timescale.

5.4.1.2 Hydraulic Conductivity and Specific Storage

Hydraulic conductivity data for the Bruce nuclear site are provided in Table 4.19 of INTERA (2011). They are presented in Figure 5.6 and Table 5.5. Permeabilities for the purposes of gas migration assessment can be derived from these data using Equation 4.1, Section 4.5.2 and the data in Table 5.3 and Table 5.5.

It may be noted that the measured hydraulic conductivities in the Ordovician formations are very low. The low hydraulic conductivity is also consistent with other site and regional information, as discussed in the Geosynthesis report (NWMO 2011), including for example the natural tracer profiles and the measured disequilibrium hydraulic heads.

Hydraulic conductivity (and hence permeability) is typically characterized as a tensor with values quoted as the magnitude of the tensor along the principal axes (x, y and z). The orientation of the principal axes in space within the reference frame is typically described using angles of rotation about each of these axes. For the Bruce nuclear site, the x and y components of the conductivity tensor are of the same magnitude and oriented sub-horizontally, parallel with sedimentary bedding. The magnitude of the x and y components is referred to as the ‘horizontal hydraulic conductivity’ in this document. The z axis is referred to as the ‘vertical hydraulic conductivity’. The ratio of vertical to horizontal hydraulic conductivity is specified in Table 4.19 of INTERA (2011) and the resulting vertical hydraulic conductivities are given in Table 5.5.

Specific storage data are also presented Table 4.19 of INTERA (2011) and are reproduced in Table 5.5.

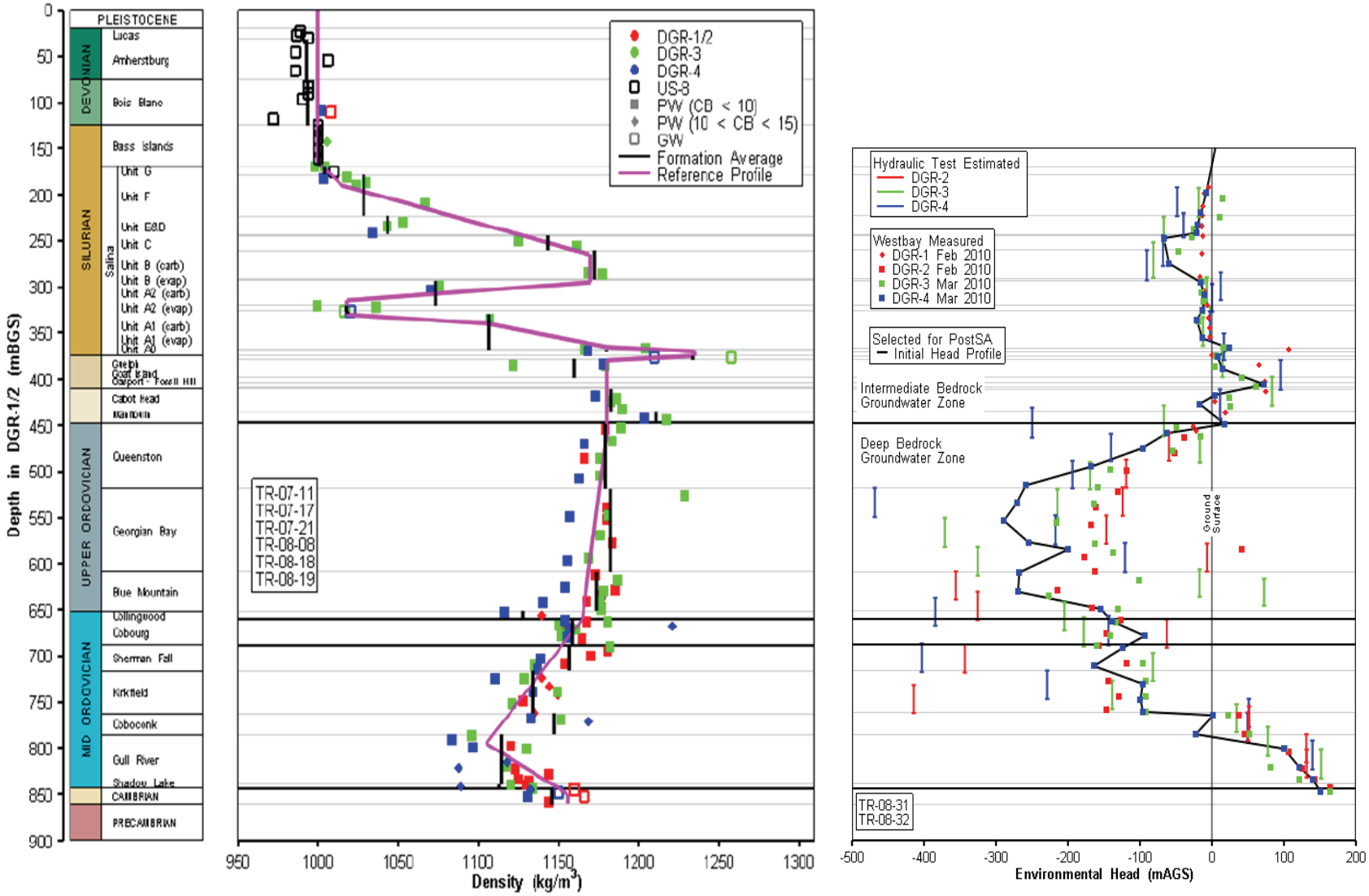

Figure 5.5: Groundwater Vertical Head and Density (Salinity) Profiles

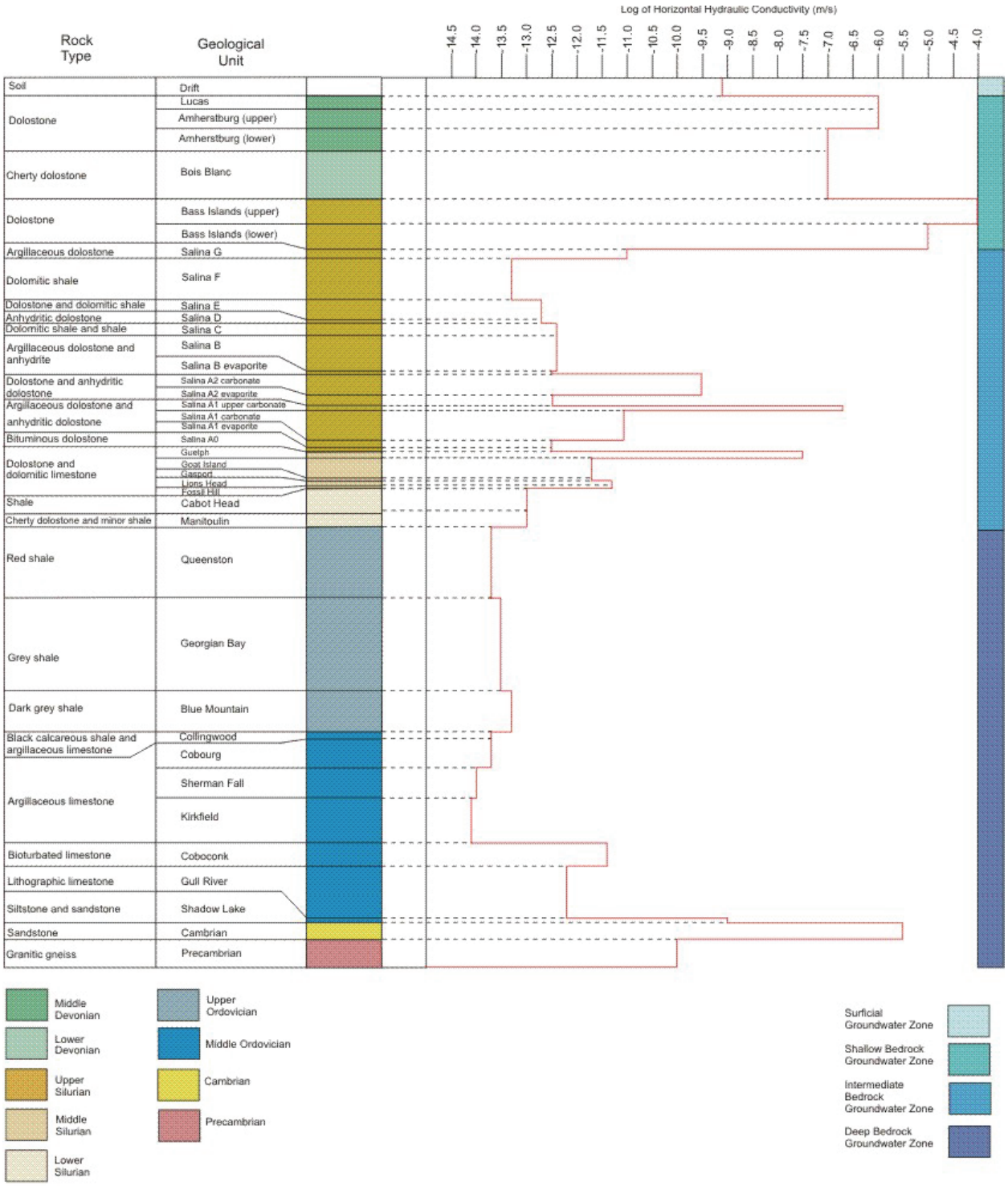

Figure 5.6: Variation of Horizontal Hydraulic Conductivity with Geological Unit

Table 5.5: Geosphere Hydraulic Conductivity and Specific Storage

Geological Unit	Horizontal Hydraulic Conductivity (m s^{-1})	PDF	Vertical Hydraulic Conductivity (m s^{-1})	PDF	Specific Storage (m^{-1})	PDF
Quaternary	8E-10	(1)	4E-10	(1)	1E-3	(2)
Lucas	1E-06	4E-9 to 2E-4 (3)	1E-07	(1)	8E-07^	(2)
Amherstburg (upper)	1E-06	1E-8 to 2E-5 (3)	1E-07	(1)	2E-06	(2)
Amherstburg (lower)	1E-07	1E-8 to 2E-5 (3)	1E-08	(1)	2E-06	(2)
Bois Blanc	1E-07	6E-10 to 1E-4 (3)	1E-08	(1)	1E-06	(2)
Bass Island (upper)	1E-04	1E-5 to 3E-4 (3)	1E-05	(1)	2E-06	(2)
Bass Island (lower)	1E-05	(1)	1E-06	(1)	2E-06	(2)
Salina G	1E-11	(1)	1E-12	(1)	5E-06^	(2)
Salina F	5E-14	(1)	5E-15	(1)	3E-06^	(2)
Salina E	2E-13	(1)	2E-14	(1)	3E-06^	(2)
Salina D	2E-13	(1)	2E-14	(1)	8E-07^	(2)
Salina C	4E-13	(1)	4E-14	(1)	5E-06^	(2)
Salina B	4E-13	(1)	4E-14	(1)	3E-05^	(2)
Salina B evaporite	3E-13	(1)	3E-14	(1)	9E-07^	(2)
Salina A2 carbonate	3E-10	(1)	3E-11	(1)	2E-06	(2)
Salina A2 evaporite	3E-13	(1)	3E-14	(1)	7E-07^	(2)
Salina A1 Upper carbonate	2E-07	(1)	2E-07	(1)	1E-06	(2)
Salina A1 carbonate	9E-12	(1)	9E-13	(1)	1E-06	(2)
Salina A1 evaporite	3E-13	(1)	3E-14	(1)	4E-07	(2)
Salina A0	3E-13	(1)	3E-14	(1)	2E-07^	(2)
Guelph	3E-08	(1)	3E-08	(1)	1E-06	(2)
Goat Island	2E-12	(1)	2E-13	(1)	5E-07	(2)
Gasport	2E-12	(1)	2E-13	(1)	5E-07	(2)

Geological Unit	Horizontal Hydraulic Conductivity (m s^{-1})	PDF	Vertical Hydraulic Conductivity (m s^{-1})	PDF	Specific Storage (m^{-1})	PDF
Lions Head	5E-12	(1)	5E-13	(1)	7E-07	(2)
Fossil Hill	5E-12	(1)	5E-13	(1)	9E-07^	(2)
Cabot Head	9E-14	(1)	9E-15	(1)	3E-05	(2)
Manitoulin	9E-14*	(1)	9E-15*	(1)	2E-06^	(2)
Queenston	2E-14*	(1)	2E-15*	(1)	4E-06^	(2)
Georgian Bay	3E-14	(1)	3E-15	(1)	1E-05	(2)
Blue Mountain	5E-14*	(1)	5E-15*	(1)	1E-05^	(2)
Collingwood	2E-14	(1)	2E-15	(1)	1E-06	(2)
Cobourg	2E-14*	(1)	2E-15*	(1)	7E-07^	(2)
Sherman Fall	1E-14*	(1)	1E-15*	(1)	3E-06^	(2)
Kirkfield	8E-15*	(1)	8E-16*	(1)	2E-06	(2)
Coboconk	4E-12*	(1)	4E-15*	(1)	2E-06^	(2)
Gull River	7E-13*	(1)	7E-16*	(1)	2E-06^	(2)
Shadow Lake	1E-09	(1)	1E-10	(1)	1E-06	(2)
Cambrian	3E-06	(1)	3E-06	(1)	1E-06	(2)
Upper Precambrian	1E-10	(4)	1E-10	(4)	1E-06	(4)

Notes:
Horizontal hydraulic conductivity from Table 4.19 of INTERA (2011).
Vertical hydraulic conductivity calculated using anisotropy given in Table 4.19 of INTERA (2011).
Specific storage from Table 4.19 of INTERA (2011).

1. Log triangular PDF with the minimum/maximum minus/plus 0.699 (i.e., a factor of 5) based on Figure 4.88 of INTERA (2011) compared with Figure 4.90 of INTERA (2011).
2. Log triangular PDF with the minimum minus 1.0 and the maximum plus 0.699 (i.e., a factor of 5) based on Figure 4.94 of INTERA (2011) and the discussion therein.
3. Log triangular PDF with the minimum/maximum values shown here – taken from Table 4.12 of INTERA (2011).
4. Single point value.

* Value from interim version of INTERA (2011) at time of data freeze for safety assessment (summer 2010). Values differ (up/down) by a factor of two or less from those given in the final version, see Appendix A, INTERA (2011).

^ Value from interim version of INTERA (2011) at time of data freeze for safety assessment (summer 2010). Values differ (up/down) by a factor of two or less from those given in the final version, with the exception of the Salina G, Fossil Hill, Coboconk and Gull River for which the value is up to a factor of five higher than the value given in the final version, see Appendix A, INTERA (2011).

5.4.1.3 Porosities

Table 4.18 of INTERA (2011) reports both total and liquid porosities analyzed by four laboratories, using a range of methods. Liquid porosities are used for the purposes of numerical modelling of groundwater flow. Liquid porosities are presented in Table 5.6. These liquid porosities are used for both the physical porosity (i.e., the volume fraction that is not rock) and the transport (effective) porosity (i.e., the volume fraction considering only interconnected pores).

Effective diffusivity (Section 5.5.1.4) is equal to the porewater diffusivity multiplied by the diffusion accessible porosity. Diffusion experiments with sodium iodide tracer (NaI) show that I^- is excluded from some pores relative to tritiated water (HTO, Figure 4.39, INTERA 2011). The diffusion accessible porosity for HTO is generally similar to the liquid porosity, while the diffusion accessible porosity for I^- is generally lower than the liquid porosity (Figure 4.41 and 4.42b, INTERA 2011).

The following relationships apply to the diffusion accessible porosity.

- The HTO diffusion accessible porosity is equal to the liquid porosity.
- The NaI diffusion accessible porosity is a factor of two lower than the HTO diffusion accessible porosity because the NaI effective diffusion coefficients are typically a factor of two lower than the HTO effective diffusion coefficients (Figure 4.39, INTERA 2011).
- The bedding normal diffusion accessible porosity is equal to the bedding parallel diffusion accessible porosity (Figure 4.41, INTERA 2011).
- This indicates that the difference in effective diffusion coefficients parallel and normal to bedding is due to a difference in tortuosity (i.e., effective diffusivity is equal to porewater diffusivity multiplied by diffusion accessible porosity multiplied by tortuosity).

Diffusion accessible porosities for NaI should be applied to radionuclides that are subject to anion exclusion, i.e., I-129, Cl-36, Se-79, while diffusion accessible porosities for HTO should be applied to non-excluded radionuclides.

Table 5.6: Geosphere Porosities

Geological Unit	(Liquid) Porosity (-) [1]	PDF ^ (Fractional Std.Dev)	PDF (min/max) [3]
Quaternary	0.2	0.80	0.04 / 0.36
Lucas	0.07*	0.80	0.014 / 0.13
Amherstburg (upper)	0.07*	0.80	0.014 / 0.13
Amherstburg (lower)	0.07*	0.80	0.014 / 0.13
Bois Blanc	0.077*	0.80	0.015 / 0.14
Bass Island (upper)	0.057*	0.80	0.011 / 0.10
Bass Island (lower)	0.057*	0.80	0.011 / 0.10
Salina G	0.172*	0.80	0.034 / 0.31
Salina F	0.128*	0.80	0.026 / 0.23
Salina E	0.135*	0.80	0.027 / 0.24
Salina D	0.098*	0.80	0.020 / 0.18
Salina C	0.205*	0.80	0.041 / 0.37
Salina B	0.165*	0.80	0.033 / 0.30
Salina B evaporite	0.098*	0.80	0.020 / 0.18
Salina A2 carbonate	0.145*	0.80	0.029 / 0.26
Salina A2 evaporite	0.098*	0.80	0.020 / 0.18
Salina A1 Upper carbonate	0.07*	0.80	0.014 / 0.13
Salina A1 carbonate	0.019*	0.80	0.038 / 0.034
Salina A1 evaporite	0.007*	0.80	0.001 / 0.013
Salina A0	0.027*	0.80	0.005 / 0.049
Guelph	0.057*	0.80	0.011 / 0.10
Goat Island	0.02*	0.80	0.004 / 0.036
Gasport	0.02*	0.80	0.004 / 0.036
Lions Head	0.031*	0.80	0.006 / 0.056
Fossil Hill	0.031*	0.80	0.006 / 0.056
Cabot Head	0.116*	0.80	0.023 / 0.21
Manitoulin	0.028*	0.80	0.006 / 0.050
Queenston	0.073*	0.22	0.057 / 0.089
Georgian Bay	0.071	0.22	0.055 / 0.087
Blue Mountain	0.078*	0.22	0.061 / 0.095
Collingwood	0.012*	1.0	0 / 0.024
Cobourg	0.015*	1.0	0 / 0.030
Sherman Fall	0.016*	1.0	0 / 0.032
Kirkfield	0.021*	1.0	0 / 0.042
Coboconk	0.009	1.0	0 / 0.018
Gull River	0.022	1.0	0 / 0.044
Shadow Lake	0.097*	0.74	0.025 / 0.17
Cambrian	0.071*	0.74	0.018 / 0.12
Upper Precambrian	0.038	0.5 [2]	0.019 / 0.057

Notes:
1. Liquid porosity from Table 4.18 of INTERA (2011).
2. No data in Table 4.3 of INTERA (2011), assumed based on the ranges for units where data are available.

3. Triangular distribution. Min/max equals mean minus/plus one standard deviation.
* Value from interim version of INTERA (2011) at time of data freeze for safety assessment (summer 2010). Values differ (up/down) by a factor of less than two from those given in the final version, with the exception of the Fossil Hill which is about a factor of six higher than the value given in the final version; see Appendix A of INTERA (2011).
^ Value from interim version of INTERA (2011) at time of data freeze for safety assessment (summer 2010). Values differ (up/down) by a factor of less than 1.2 from those given in the final version; see Appendix A of INTERA (2011).

5.4.2 Damaged Zone

Hydraulic conductivities and porosities in the EDZs associated with the repository rooms, tunnels and shafts will be enhanced compared with the undisturbed geosphere. The hydraulic conductivity and porosity enhancement factors are given in Table 5.7 and Figure 5.7 for the shafts, and Table 5.8 and Figure 5.8 for the rooms and tunnels. The hydraulic conductivity enhancement factors are based on the findings of the review documented in the Geosynthesis report (Section 6.3.1 of NWMO 2011), focussed on sedimentary rocks, while the porosity enhancement factors are based on NAGRA (2002). The results are correlated in terms of the EDZ thickness relative to the excavated radius, and the EDZ hydraulic conductivity and porosity relative to the host rock undisturbed hydraulic conductivity and porosity.

The main factors considered in deriving the recommended factors are:

- EDZ effects are most pronounced closest to the excavated wall;
- EDZ measurements typically represent point or punctual estimates, the effective EDZ hydraulic conductivity at distances relevant to transport would be considerably less than maximum reported values;
- The extent of the EDZ varies with lithology, intersection with geological features, in-situ stress magnitude and orientation and excavation methods;
- The HDZ will be removed during shaft sealing; and
- The EDZ values are applied over a thick ring around the shaft, corresponding to an area larger than that of the shaft itself. The dimensions of this ring are based on worst case extension of the EDZ over a million years, considering different shaft locations, lithologies and stress regimes, under different various loading scenarios. The dimension is then applied to the entire length of the shaft and is therefore conservative.

The **shaft** is perpendicular to the bedding planes. Therefore for the shaft EDZ, hydraulic conductivity enhancement factors should be applied to the rock vertical hydraulic conductivity. The EDZ is divided into two regions to better represent the large variation in properties across this region, each of the same thickness. The inner EDZ has the higher hydraulic conductivity, estimated as approximately 100x the host rock hydraulic conductivity averaged over a half-radius thickness and vertically connected. An extreme upper value of 10,000x is recommended for sensitivity studies, based on maximum single point measurements. The reference value for the outer EDZ is 10x the host rock hydraulic conductivity with an upper value of 100x. Within the EDZ, it is assumed that the horizontal and vertical hydraulic conductivities are the same.

It is expected based on experimental observation and numerical simulation that the EDZ forms quickly following excavation. Although there is substantial evidence for self-sealing of the EDZ and fractures in various sedimentary rocks, particularly argillaceous formations, the assumed hydraulic conductivities do not consider the phenomena of self-sealing, which could return EDZ properties to those of the undisturbed rock mass.

The values in Table 5.7 are supported by site-specific evidence from hydraulic conductivity tests on rock core samples. Permeabilities measured from laboratory gas pulse decay testing were higher than those measured from in-situ straddle packer tests. Although laboratory permeability tests were conducted at depth-specific confining stresses intended to simulate in-situ effective stress, the results suggest irrecoverable damage to the cores due to microcrack formation and core disking, particularly for the Ordovician shales and to lesser degree for the Ordovician limestones. The overestimation of actual in-situ permeability from the laboratory gas pulse decay testing is likely about a factor of 10 to 100 for Ordovician limestones and 100 to 1000 for Ordovician shales; see Section 4.9.3 of INTERA (2011) and Figure 4.92 therein. These enhancement factors are comparable to those reported in Section 6.3.1 of NWMO (2011) for URLs.

For the **repository excavation** (i.e., the emplacement rooms, access tunnels and shaft sump ramps), the HDZ is not removed. Damage (fracturing) will preferentially occur along the bedding places, which are co-planar with the excavations. Therefore, the HDZ/EDZ hydraulic conductivity enhancement factors should be applied to the rock horizontal hydraulic conductivity. The EDZ is less important for the tunnels and emplacement rooms than for the shaft because of the presence of the HDZ, and more significantly the open tunnels themselves. Therefore the tunnel and room EDZ is modelled as a single region.

In addition to an increase in hydraulic conductivity within the EDZs, there is anticipated to be an increase in porosity. Previous studies in Canadian Shield granite and in Opalinus Clay (NAGRA 2002) have suggested an increase of about a factor of two averaged over the inner EDZ volume.

For the shafts, the porosity enhancement factor is taken to be a factor of two for the inner EDZ, but there is no enhancement in the outer EDZ. For the DGR rooms and tunnels, the porosity enhancement factor is taken to be a factor of two for the EDZ, and a factor of four for the HDZ. For the both shafts and rooms and tunnels, the porosity enhancement is taken to apply equally to the physical, transport and diffusion (accessible) porosities.

Table 5.7: Hydraulic Properties of the Shaft EDZs

Parameter	Inner EDZ		Outer EDZ	
	Reference Value	PDF (1)	Reference Value	PDF (1)
Thickness (2)	0.5 x r`	-	0.5 x r`	-
Hydraulic Conductivity (3)	100 x geosphere (vertical) (5)	100 to 10,000 x geosphere (vertical)	10 x geosphere (vertical)	10 to 100 x geosphere (vertical)
Total, Transport and Diffusion (Accessible) Porosities (4)	2 x geosphere	-	Geosphere	-

Notes:
1. Taken to be log uniform.
2. r` is the radius of the excavated shaft (i.e., prior to removal of HDZ).
3. Hydraulic conductivity taken to be isotropic in EDZs.
4. Note that this is the matrix porosity, not fracture porosity.
5. 100x is recommended as the reference value to be consistent with the assumed areas of the shaft EDZs.

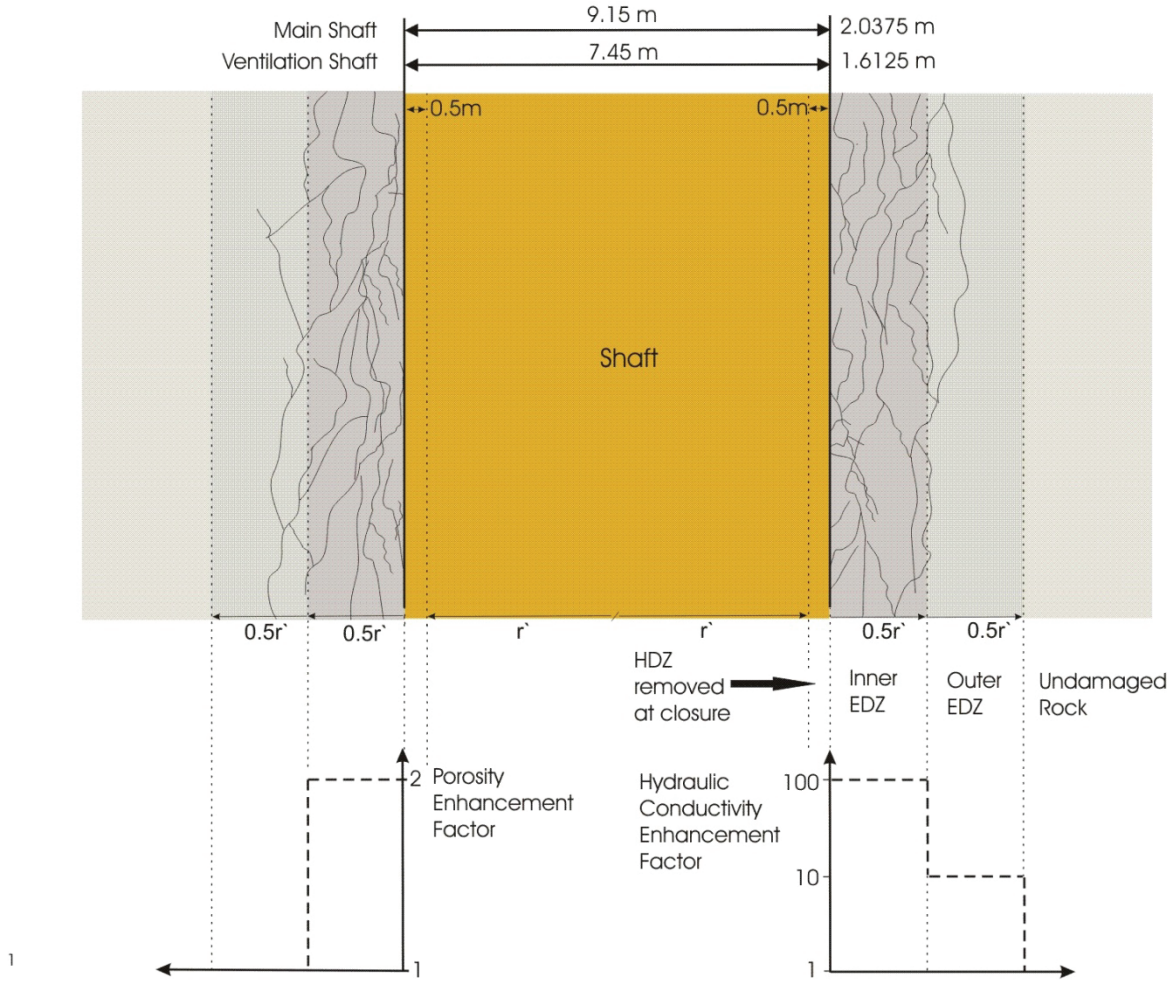

Figure 5.7: Vertical Section through the Shaft EDZs

Table 5.8: Hydraulic Properties of the Repository HDZ and EDZ

Parameter	Emplacement Rooms & Unsupported Access Tunnels				Supported Access Tunnels			
	HDZ		EDZ		HDZ		EDZ	
	Reference Value	PDF	Reference Value	PDF (1)	Reference Value	PDF	Reference Value	PDF (1)
Thickness (m)	0.5	-	8	-	2 (top & bottom) 0.5 (sides)	-	3	-
Hydraulic Conductivity (2)	1E-6 m s^{-1}	-	1,000 x geosphere (horizontal)(4)	100 to 10,000 x geosphere (horizontal)	1E-6 m s^{-1}	-	1,000 x geosphere (horizontal)	100 to 10,000 x geosphere (horizontal)
Total, Transport and Diffusion (Accessible) Porosities (3)	4 x geosphere	-	2 x geosphere	-	4 x geosphere	-	2 x geosphere	-

Notes:
1. Taken to be log uniform.
2. Hydraulic conductivity taken to be isotropic in HDZs and EDZs.
3. Note that this is the matrix porosity, not fracture porosity.
4. Mid-range of the PDF is recommended noting that lateral transport will be dominated by presence of the HDZ and open tunnels.

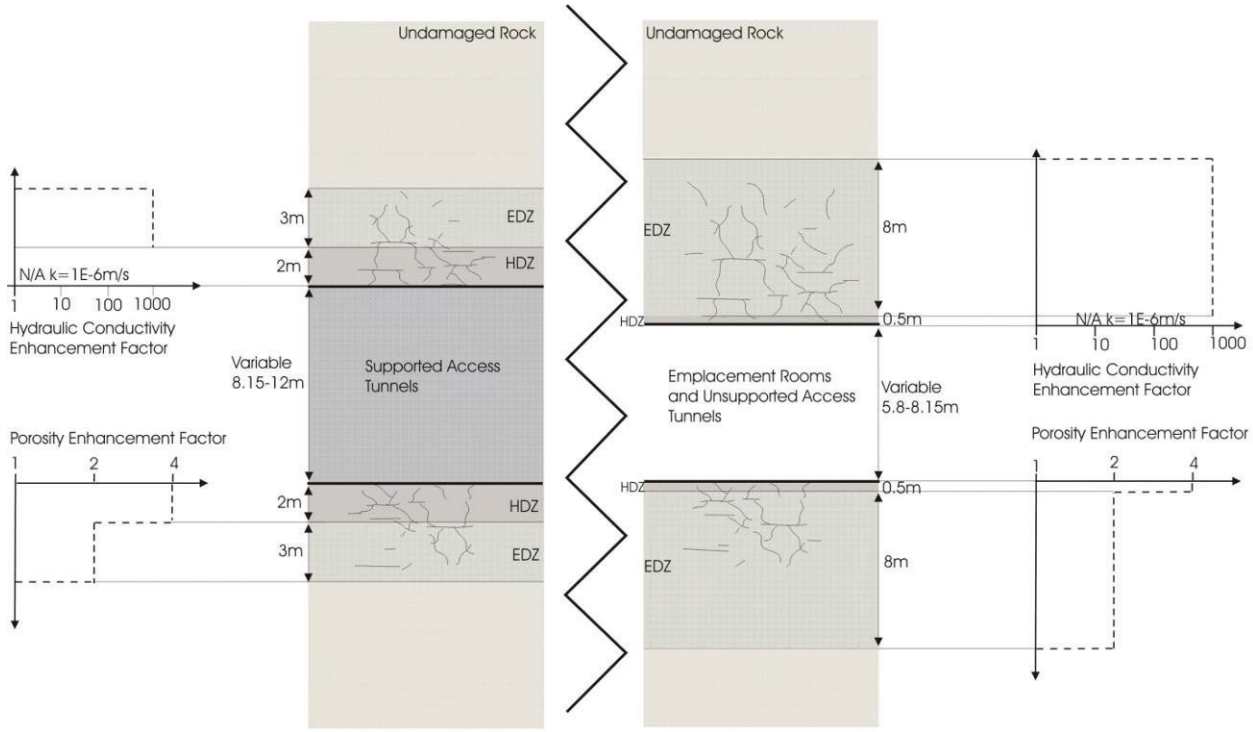

Figure 5.8: Vertical Section through the Repository HDZ and EDZ

5.4.3 Geosphere Biosphere Interface

The main geosphere biosphere interfaces (GBI) are the natural locations of groundwater discharge from the geosphere to the biosphere, and the extraction of contaminated water from a well in the Shallow Bedrock Groundwater Zone. The properties of such a well are detailed in Table 5.9.

Table 5.9: Well Parameters

Parameter	Description	Units	Value	Comments/Notes
Well depth	Depth to bottom of well	mBGS	80	Based on current practices in the area for wells. Deeper wells would reach brackish, non-potable water (Section 4.5.1.1 of INTERA 2011). Assumed to be screened between 40 and 80 m.
Well casing radius	Well casing radius	m	0.0508 (4 inch diameter well)	Adopted as 'representative' value, typical of local groundwater wells.
Well abstraction rate	Well abstraction rate	$m^3\ a^{-1}$	6388	Derived for small self-sufficient farm, as described in Section 6.2.3.
Well location	Distance downstream from the Main Shaft	m	500	An advective flow path of around 500 m is necessary to result in contaminant transport by vertical dispersion into the region from which well water is abstracted.

5.5 Transport Parameters

5.5.1 Geosphere

Transport parameters are presented for each of the geological units. Transport may occur through diffusion of aqueous radionuclides in response to concentration gradients, and/or advection of aqueous radionuclides by groundwater flow.

The parameters used for the geosphere transport models are:

- Densities - Table 5.10 and Table 5.11;
- Solubility limits - Table 5.12;
- Sorption coefficients - Table 5.13; and
- Diffusion coefficients - Table 5.14.

5.5.1.1 Densities

Grain densities and dry bulk densities are shown in Table 5.10 and Table 5.11 respectively. Data are taken from Table 4.18 of the DGSM report (INTERA 2011).

Table 5.10: Geosphere Grain Densities

Geological Unit	Grain Density Values (kg m^{-3})	PDF
Quaternary	2800 (4)	(1)
Lucas	2700*	(2)
Amherstburg (upper)	2700*	(2)
Amherstburg (lower)	2700*	(2)
Bois Blanc	2700*	(2)
Bass Island (upper)	2700*	(2)
Bass Island (lower)	2700*	(2)
Salina G	2700*	(2)
Salina F	2760*	(2)
Salina E	2830*	(2)
Salina D	2930	(2)
Salina C	2750*	(2)
Salina B	2810	(2)
Salina B evaporite	2930	(2)
Salina A2 carbonate	2870*	(2)
Salina A2 evaporite	2930*	(2)
Salina A1 Upper carbonate	2720*	(2)
Salina A1 carbonate	2720*	(2)
Salina A1 evaporite	2930	(2)
Salina A0	2780*	(2)
Guelph	2810	(3)
Goat Island	2730	(3)
Gasport	2730	(3)
Lions Head	2730	(3)
Fossil Hill	2730	(3)
Cabot Head	2800*	(3)
Manitoulin	2730*	(3)
Queenston	2770	(3)
Georgian Bay	2760	(3)
Blue Mountain	2760*	(3)
Collingwood	2690*	(3)
Cobourg	2710	(3)
Sherman Fall	2720	(3)
Kirkfield	2700*	(3)
Coboconk	2690	(3)
Gull River	2730	(3)
Shadow Lake	2750*	(3)
Cambrian	2660*	(3)
Precambrian	2590	(1)

Notes:
1. Assume triangular distribution with min and max -5% and +5% of the mean.
2. Triangular distribution with min and max -5% and +5% of the mean based on Figure 4.1 of INTERA (2011).
3. Triangular distribution with min and max -2.5% and +2.5% of the mean based on Figure 4.1 of INTERA (2011).
4. Nominal value for clay based on illite mineral density (CRC 2006).

* Value from interim version of INTERA (2011) at time of data freeze for safety assessment (summer 2010). Values differ (up/down) by a factor of less than 1.08 from those given in the final version; see App. A of INTERA (2011).

Table 5.11: Geosphere Dry Bulk Densities

Geological Unit	Dry Bulk Density Values (kg m^{-3})	PDF
Quaternary	2240 (1)	(2)
Lucas	2490*	(3)
Amherstburg (upper)	2490*	(3)
Amherstburg (lower)	2490*	(3)
Bois Blanc	2490*	(3)
Bass Island (upper)	2490*	(3)
Bass Island (lower)	2490*	(3)
Salina G	2480*	(3)
Salina F	2300*	(3)
Salina E	2490*	(3)
Salina D	2870*	(3)
Salina C	2290*	(3)
Salina B	2370*	(3)
Salina B evaporite	2870*	(3)
Salina A2 carbonate	2440*	(3)
Salina A2 evaporite	2870	(3)
Salina A1 Upper carbonate	2630*	(3)
Salina A1 carbonate	2630*	(3)
Salina A1 evaporite	2870*	(3)
Salina A0	2600*	(3)
Guelph	2600*	(4)
Goat Island	2600*	(4)
Gasport	2600*	(4)
Lions Head	2600*	(4)
Fossil Hill	2600*	(4)
Cabot Head	2540*	(4)
Manitoulin	2660*	(4)
Queenston	2580*	(4)
Georgian Bay	2610	(4)
Blue Mountain	2560*	(4)
Collingwood	2580*	(4)
Cobourg	2660	(4)
Sherman Fall	2660	(4)
Kirkfield	2640*	(4)
Coboconk	2670	(4)
Gull River	2670	(4)
Shadow Lake	2530*	(4)
Cambrian	2400*	(4)
Precambrian	2490	(2)

Notes:
1. Calculated from grain density in Table 5.10 and the porosity in Table 5.6 using Equation 4.4.
2. Assume triangular distribution with min and max -5% and +5% of the mean.
3. Triangular distribution with min and max -5% and +5% of the mean based on Figure 4.1 of INTERA (2011).
4. Triangular distribution with min and max -2.5% and +2.5% of the mean based on Figure 4.1 of INTERA (2011).

* Value from interim version of INTERA (2011) at time of data freeze for safety assessment (summer 2010). Values differ (up/down) by a factor of less than 1.09 from those given in the final version; see App. A of INTERA (2011).

5.5.1.2 Solubility Limits

Elemental solubility is not expected to be a significant consideration in the geosphere due to the processes of dilution and dispersion which will act to reduce aqueous radionuclide concentrations during transport through the geosphere. Nonetheless, solubility limit calculations have been undertaken for the porewaters in the Cobourg (the repository host rock) and the higher salinity Guelph Formation (see Appendix C). Conservatively, the higher solubility limits of the two water compositions can be adopted for the Deep and Intermediate Bedrock Groundwater Zones and are summarized in Table 5.12. It is conservatively assumed that there is no solubility limitation in the Shallow Bedrock Groundwater Zone.

Table 5.12: Solubility Limits to Elemental Aqueous Concentrations and Solubility-limiting Solid Phases in the Deep and Intermediate Bedrock Groundwater Zones

Element	Total Conc. (mol m^{-3}) (1,6)	Solubility-limiting Phase (2)
C (3)	6E-01	Carbonate equilibria
Cl (4)	7E+03	Halite (NaCl)
Cr	9E-03	$Cr_2(OH)_3$ (YMP)
Ni	Unlimited (5)	-
Cu	Unlimited (5)	-
Zr	6E-07	Baddelyite (ZrO_2) (YMP)
Nb	Unlimited (5)	-
Cd	Unlimited (5)	-
I	Unlimited (5)	-
Pb	Unlimited (5)	-
Ra	Unlimited (5)	-
U	3E-04	$U(OH)_4$(am) (YMP)
Np	4E-05	$Np(OH)_4$
Pu	1E-01	$Pu(OH)_4$
Other elements/ substances	Unlimited (5)	-

Notes:
1. Total dissolved concentration of all aqueous species.
2. YMP = thermodynamic data for solid phases taken from "data0.ypf.R2" am = amorphous.
3. For dissolved carbon, a total dissolved C concentration was adopted based on carbonate mineral equilibria.
4. It is possible that the Cl^- concentration in the near field may be more similar to that reported for the Cobourg limestone (5 mol kg^{-1}).
5. “Unlimited” means that the solubility is either calculated to be so high that it could never plausibly be attained in a natural system, or else that the solubility is uncertain so that the element is conservatively treated as being non-solubility limited.
6. Adopted the higher of the two calculated solubility limits for Cobourg and Guelph given in Appendix C.

5.5.1.3 Sorption Coefficients

Retardation of radionuclides within the geosphere is considered to be represented by linear, equilibrium, reversible sorption (see Equation 3.1). This sorption model is used to group and upscale the effects of a variety of different processes such as ion-exchange and adsorption (see Appendix D). There are presently no published sorption data measured specifically for rock and groundwater conditions at the Bruce nuclear site, but preliminary NWMO results have been taken into account. The literature review described in Appendix D has proposed conservative (i.e., lower than likely) distribution coefficients for a set of potentially important elements. These are presented in Table 5.13. Conservatively, all other elements and organic contaminants are assumed not to be retarded through sorption.

Table 5.13: Geosphere Sorption Coefficients

Element	Limestone and Dolostone (m^3 kg^{-1})	Shale (m^3 kg^{-1}) (2)
C	0	0
Cl	0	0
Cr	0 (1)	0 (1)
Ni	0	0
Cu	0 (1)	0 (1)
Zr	0 (1)	0.01
Nb	0 (1)	0.05
Cd	0 (1)	0.05
I	0	0
Pb	0 (1)	0.03
Ra	0	0
U	0.001	0.001
Np	0.001	0.03
Pu	0.02	0.2
All other elements and organic contaminants	0	0

Notes:
1. No relevant data available, therefore no sorption is conservatively assumed.
2. Geological Units classified as shale are: Salina C and F, Cabot Head, Manitoulin, Queenston, Georgian Bay and Blue Mountain.

5.5.1.4 Effective Diffusion Coefficients

Site-specific geosphere effective diffusion coefficient (D_e) data have been measured using laboratory tests on rock core samples from the DGR boreholes (see Figure 5.9 and INTERA 2011). Effective diffusion coefficients normal to bedding are presented in Table 5.14 based on data taken from Table 4.19 of INTERA (2011).

Diffusion experiments with NaI show that I^- is excluded from some pores relative to HTO (Figure 4.39, INTERA 2011), and that the effective diffusion coefficient parallel to bedding is typically a factor of two higher than normal to bedding (see Table 5.14).

Effective diffusion coefficients for NaI should be applied to radionuclides that are subject to anion exclusion, i.e., I-129, Cl-36 and Sr-79, while effective diffusion coefficients for HTO should be applied to non-excluded radionuclides. Effective diffusion coefficients for radionuclides that are subject to anion exclusion are taken to be a factor of two lower than for radionuclides that are not excluded, based on Figure 4.39 of INTERA (2011).

5.5.2 Damaged Zone

The contaminant transport parameters in the damage zone around the repository excavation and shafts are taken to be the same as in the surrounding geosphere, with the exception of the diffusion coefficient values. These are conservatively taken to be isotropic and are set equal to the maximum (i.e., horizontal) diffusion coefficient value (Table 5.14) multiplied by the relevant porosity enhancement factor (Table 5.7 and Table 5.8).

5.5.3 Geosphere Biosphere Interface

All GBI parameters for transport are already specified through the geosphere/GBI characteristics and the geosphere transport parameters.

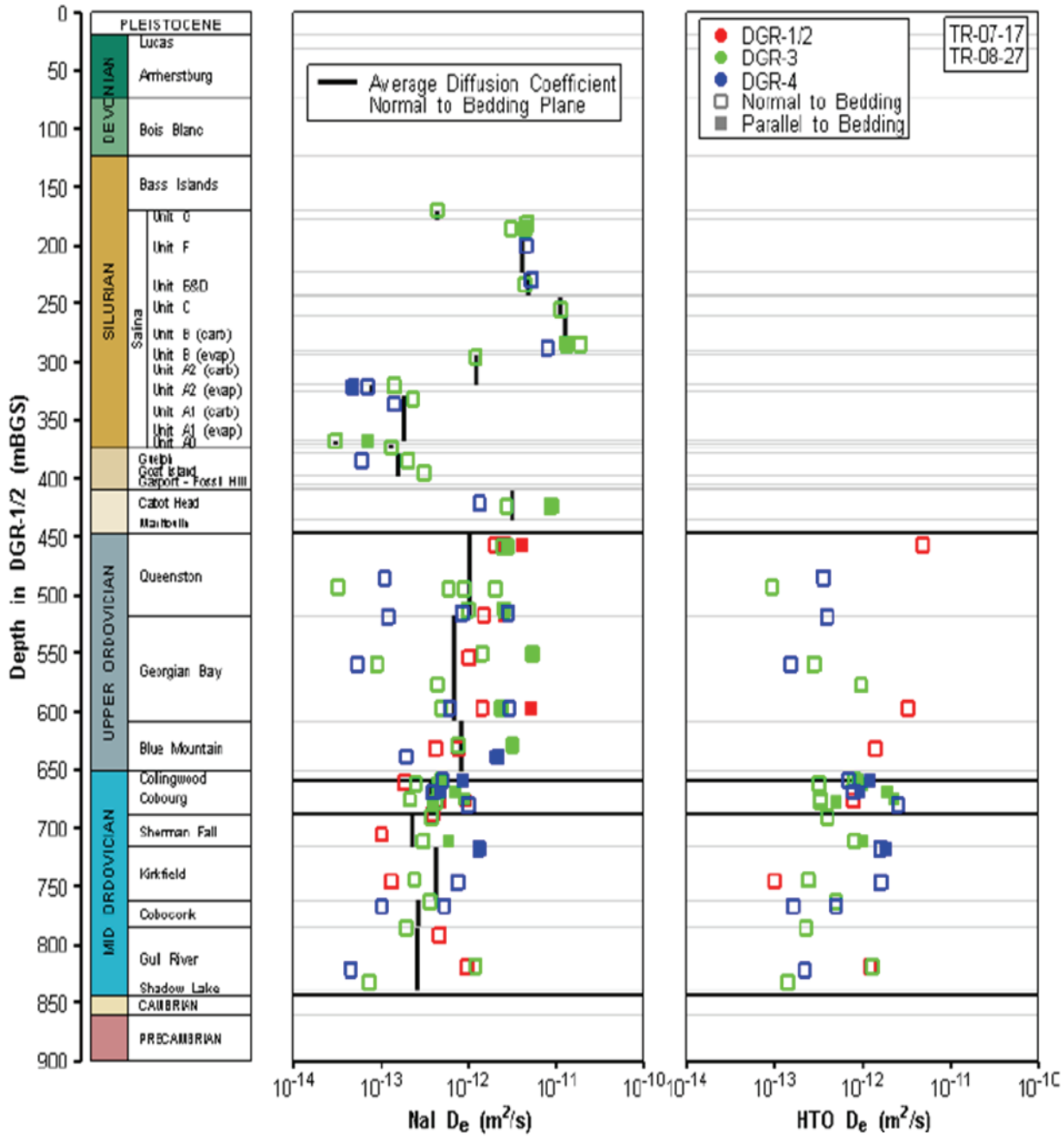

Note: Figure 4.38 in INTERA (2011).

Figure 5.9: Effective Diffusivities from Testing of DGR Cores

Table 5.14: Geosphere Effective Diffusion Coefficients

Geological Unit	D_e NaI Normal to Bedding ($m^2 s^{-1}$) (1)	D_e HTO Normal to Bedding ($m^2 s^{-1}$) (3)	PDF	D_{e-h}:D_{e-v} (-)
Quaternary (2)	6.0E-11	1.2E-10	(2)	1:1
Lucas	6.0E-12*	1.2E-11	(2)	1:1
Amherstburg (upper)	6.0E-12*	1.2E-11	(2)	1:1
Amherstburg (lower)	6.0E-12*	1.2E-11	(2)	1:1
Bois Blanc	6.0E-12*	1.2E-11	(2)	1:1
Bass Island (upper)	1.3E-11*	2.6E-11	(2)	1:1
Bass Island (lower)	1.3E-11*	2.6E-11	(2)	1:1
Salina G	4.3E-13	8.6E-13	(2)	2:1
Salina F	4.1E-12	8.2E-12	(2)	2:1
Salina E	4.7E-12	9.4E-12	(2)	2:1
Salina D	4.7E-12	9.4E-12	(2)	2:1
Salina C	1.1E-11	2.2E-11	(2)	2:1
Salina B	1.2E-11	2.4E-11	(2)	2:1
Salina B evaporite	7.7E-14	1.5E-13	(2)	2:1
Salina A2 carbonate	1.2E-12	2.4E-12	(2)	2:1
Salina A2 evaporite	7.7E-14	1.5E-13	(2)	2:1
Salina A1 Upper carbonate	4.9E-12*	9.8E-12	(2)	1:1
Salina A1 carbonate	1.8E-13	3.6E-13	(2)	2:1
Salina A1 evaporite	3.0E-14	6.0E-14	(2)	2:1
Salina A0	3.0E-14	6.0E-14	(2)	2:1
Guelph	3.2E-12*	6.4E-12	(2)	1:1
Goat Island	1.5E-13	3.0E-13	(2)	2:1
Gasport	1.5E-13	3.0E-13	(2)	2:1
Lions Head	6.2E-12*	1.2E-11	(2)	2:1
Fossil Hill	1.6E-11*	3.2E-11	(2)	2:1
Cabot Head	3.1E-12	6.2E-12	(2)	2:1
Manitoulin	1.5E-13	3.0E-13	(2)	2:1
Queenston	1.0E-12	2.0E-12	(2)	2:1
Georgian Bay	6.8E-13*	1.4E-12	(2)	2:1^
Blue Mountain	8.2E-13	1.6E-12	(2)	2:1
Collingwood	4.9E-13	9.8E-13	(2)	2:1
Cobourg	3.7E-13	7.4E-13	(2)	2:1
Sherman Fall	2.2E-13	4.4E-13	(2)	2:1
Kirkfield	4.2E-13	8.4E-13	(2)	2:1
Coboconk	2.7E-13	5.4E-13	(2)	2:1
Gull River	2.6E-13	5.2E-13	(2)	2:1
Shadow Lake	6.1E-12*	1.2E-11	(2)	2:1
Cambrian	7.7E-12*	1.5E-11	(2)	1:1
Upper Precambrian	3.0E-13	6.0E-13	(2)	1:1

Notes:
1. From Table 4.19 of INTERA (2011).
2. Log-triangular distribution with the minimum/maximum minus/plus 0.699 (i.e., a factor of 5) based on Figure 4.38 of INTERA (2011).
3. A factor of two greater than De Nal normal to bedding.

* Value from interim version of INTERA (2011) at time of data freeze for safety assessment (summer 2010). Values are up to a factor of 30 higher than those given in the final version, except for the Shadow Lake which is a factor of 1.5 lower and the Fossil Hill which is almost a factor of 400 higher than final value; see Appendix A of INTERA (2011).

^ Value from interim version of INTERA (2011) at time of data freeze for safety assessment (summer 2010). Value of 7:1 is given in the final version; see Appendix A of INTERA (2011).

5.6 Gas Flow Parameters

5.6.1 Geosphere

The parameters relevant to gas flow and transport in the geosphere are discussed in the following sections. Gas flow properties in the Ordovician shale and limestone units are of particular importance, as the repository will be located in the Cobourg limestone unit, and the Ordovician shales will act as cap rocks, inhibiting gas flow to overlying formations. The parameters used for the geosphere gas transport properties are:

- Gas permeabilities - Section 5.6.1.1;
- Two-phase flow parameters - Table 5.15; and
- Henry's law constants – Section 5.6.1.2.

5.6.1.1 Gas Permeabilities and Two-Phase Flow Parameters

Gas permeabilities can be calculated from the hydraulic conductivity for the different geological units (Table 5.5) using Equation 4.1, Section 4.5.2. These permeabilities are suitable for application to gas migrating as a fluid through the rock mass, as part of a two-phase flow calculation.

The two-phase flow calculations also require characteristic curve data for the different geosphere units (Equation 4.6 to Equation 4.10). Two-phase flow parameters have been determined for most units in the Ordovician and Silurian sequences by fitting van Genuchten characteristic curves (capillary pressure and relative permeability as a function of saturation – see Section 4.7) to laboratory petrophysics data (TR-08-33, Calder 2011). Two fits were calculated: one fit for the full set of data (referred to as the full fit, Table 5 of TR-08-33, Calder 2011), and the second fit restricted to the data with a liquid saturation (S_l) greater than 0.7 (referred to as the limited fit, Table 6 of TR-08-33, Calder 2011). The limited fit was generated to provide an improved relationship to high liquid saturation data, as two-phase flow in the host rock will likely be under conditions that are highly saturated with liquid. In most cases, the limited fit provided a negligible improvement and for these units the full fit is used. In the Salina E and Salina C, the limited fit provided an improved match to the data, and consequently the limited fit is used for these units. There are no measurements for the Devonian units, but the gas flow modelling is expected to conservatively neglect the transport delay in these more permeable rocks.

The two-phase flow parameters are described in Table 5.15. Where multiple samples from one unit were available, the mean value has been used as the reference value, and the minimum and maximum values are the minimum and maximum fitted parameter values in the unit. For alpha, the reference value was calculated using a geometric mean, while for all other parameters reference values were calculated using the arithmetic mean. It is important to note that while these ranges are provided, all of these parameters interact in the van Genuchten model, and randomly choosing a set of parameters within these ranges might not lead to a parameterization that behaves in a similar way to that measured in the rock. Where there are no measured capillary pressure curves in a given unit, the gas flow parameters are assumed to equal those of adjacent units with similar rock types. Figure 5.10 shows an example of capillary pressure and relative permeability data from the Queenston Shale formation, as well as the fitted curves and the formation average curve. A detailed discussion of the calculation of formation average capillary pressure and relative permeability curves can be found in Calder (2011).

5.6.1.2 Henry's Law Constants

Gas solubility is described by Henry's law. Henry's law constants for the bulk gases of interest are presented in Table 3.19.

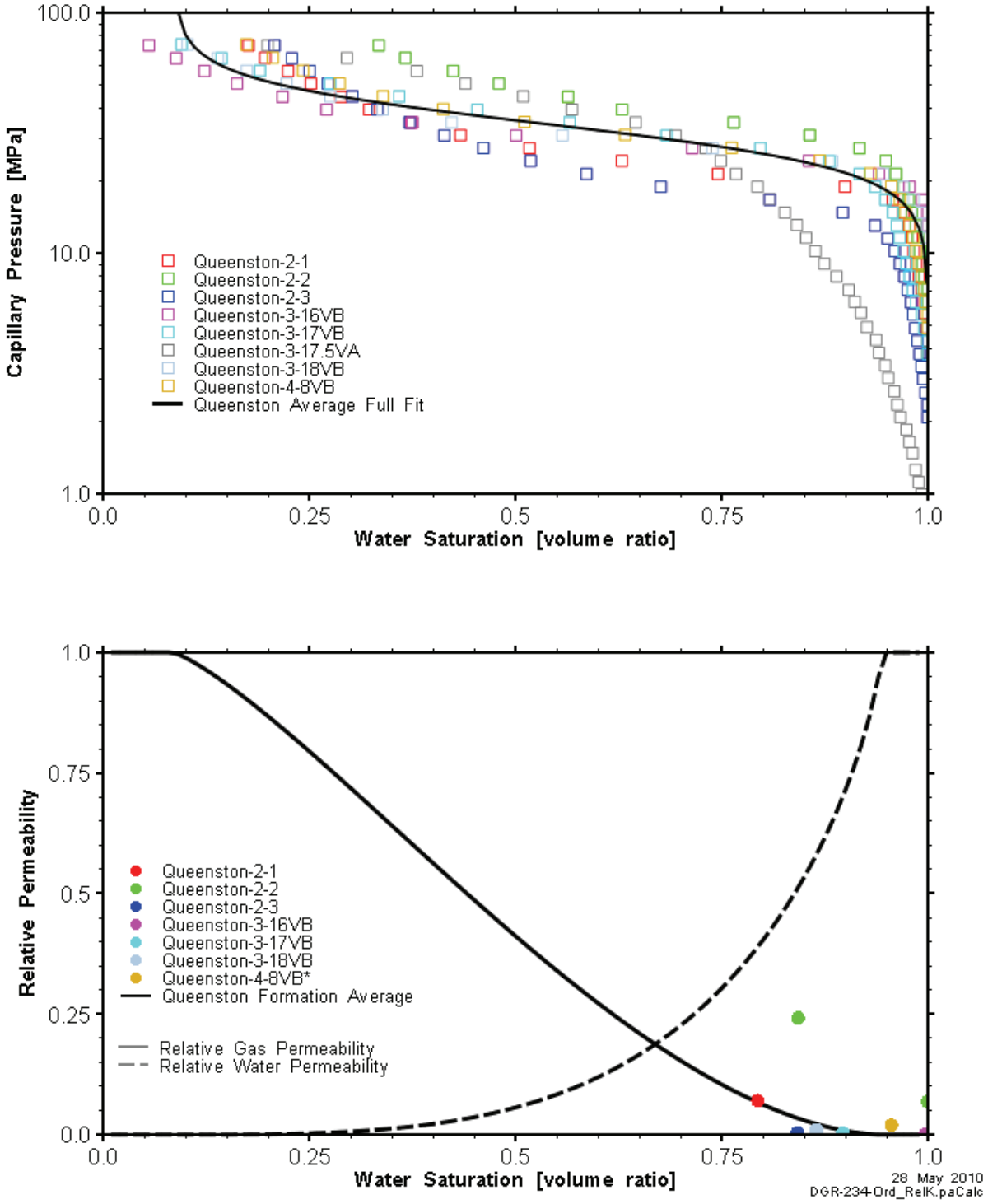

Note: Figure adapted from Appendix B of Calder (2011).

Figure 5.10: Capillary Pressure and Relative Permeability Measurements and Fitted Curves for Samples from the Queenston Shale

Table 5.15: Two-phase Flow Parameters for van Genuchten Model

Geological Unit	Number of Samples	α (Pa^{-1})	m (-)	n (-)	S_{lr} (-)	S_{gr} (-)	Notes/Comments
Shallow Bedrock Groundwater Zone	0	-	-	-	-	-	Not included in gas models
Salina G	0	Ref: 4.11E-08 Min: 3.55E-08 Max: 4.53E-08	Ref: 0.817 Min: 0.356 Max: 1.567	Ref: 3.873 Min: 1.620 Max: 5.520	0.000	Ref: 0.040 Min: 0.000 Max: 0.100	Assume equal to Salina F
Salina F	3	Ref: 4.11E-08 Min: 3.55E-08 Max: 4.53E-08	Ref: 0.817 Min: 0.356 Max: 1.567	Ref: 3.873 Min: 1.620 Max: 5.520	0.000	Ref: 0.040 Min: 0.000 Max: 0.100	
Salina E (1)	1	1.70E-06	0.460	4.310	0.010	0.150	
Salina D	0	1.70E-06	0.460	4.310	0.010	0.150	Salina E
Salina C (1)	2	3.23E-06	0.350	4.220	0.550	0.000	
Salina B	1	1.21E-07	0.931	2.170	0.000	0.035	
Salina B evaporite	0	4.86E-07	0.990	2.280	0.010	0.100	Assume equal to Salina A2 evaporite
Salina A2 carbonate	2	Ref: 1.32E-06 Min: 3.04E-07 Max: 5.76E-06	0.500	Ref: 3.060 Min: 2.420 Max: 3.700	0.000	0.000	m adjusted to achieve improved qualitative fit
Salina A2 evaporite	1	4.86E-07	0.990	2.280	0.010	0.100	
Salina A1 Upper carbonate	0	2.70E-05	0.145	4.890	0.248	0.000	Assume equal to Guelph
Salina A1 carbonate	1	2.57E-08	0.990	2.410	0.000	0.000	
Salina A1 evaporite	1	4.86E-07	0.990	2.280	0.010	0.100	Assume equal to Salina A2 evaporite

Geological Unit	Number of Samples	α (Pa^{-1})	m (-)	n (-)	S_{lr} (-)	S_{gr} (-)	Notes/Comments
Salina A0	2	Ref: 1.70E-07 Min: 1.20E-07 Max: 2.41E-07	Ref: 1.131 Min: 0.990 Max: 1.272	Ref: 2.250 Min: 1.790 Max: 2.710	Ref: 0.002 Min: 0.000 Max: 0.004	Ref: 0.143 Min: 0.020 Max: 0.265	
Guelph	1	2.73E-05	0.145	4.890	0.248	0.000	Based on limited fit for sample 4-5.5 (DGR-4, Salina A0)
Goat Island	3	Ref: 3.58E-08 Min: 9.47E-09 Max: 3.77E-08	Ref: 0.684 Min: 0.527 Max: 15.244	Ref: 6.110 Min: 2.170 Max: 6.540	Ref: 0.025 Min: 0.020 Max: 0.030	0.000	Reference calculation neglects sample 4-6B (DGR-4)
Gasport	0	3.58E-08	0.684	6.110	0.025	0.000	Assume equal to Goat Island
Lions Head	0	3.58E-08	0.684	6.110	0.025	0.000	Assume equal to Goat Island
Fossil Hill	0	3.58E-08	0.684	6.110	0.025	0.000	Assume equal to Goat Island
Cabot Head	1	6.83E-08	0.243	6.820	0.000	0.050	Assume S_{gr} of 0.05
Manitoulin	2	Ref: 2.45E-08 Min: 2.00E-08 Max: 3.00E-08	Ref: 1.305 Min: 0.682 Max: 1.927	Ref: 3.650 Min: 3.430 Max: 3.870	Ref: 0.106 Min: 0.000 Max: 0.211	Ref: 0.050 Min: 0.000 Max: 0.100	
Queenston	7	Ref: 2.81E-08 Min: 1.58E-08 Max: 3.81E-08	Ref: 1.133 Min: 0.429 Max: 2.466	Ref: 4.454 Min: 2.470 Max: 8.840	Ref: 0.086 Min: 0.000 Max: 0.197	Ref: 0.056 Min: 0.000 Max: 0.195	
Georgian Bay	7	Ref: 3.32E-08 Min: 1.34E-08 Max: 4.78E-08	Ref: 1.097 Min: 0.457 Max: 3.195	Ref: 3.813 Min: 2.660 Max: 4.580	Ref: 0.166 Min: 0.000 Max: 0.377	Ref: 0.037 Min: 0.000 Max: 0.120	
Blue Mountain	5	Ref: 2.33E-08 Min: 1.04E-08 Max: 3.80E-08	Ref: 1.089 Min: 0.505 Max: 2.372	Ref: 3.184 Min: 2.380 Max: 3.760	Ref: 0.065 Min: 0.000 Max: 0.155	Ref: 0.010 Min: 0.000 Max: 0.050	Calculated from Calder (2011) by combining Blue Mountain Upper and Lower
Collingwood	1	1.06E-08	2.570	2.140	0.000	0.120	

Geological Unit	Number of Samples	α (Pa^{-1})	m (-)	n (-)	S_{lr} (-)	S_{gr} (-)	Notes/Comments
Cobourg	4	Ref: 1.62E-08 Min: 7.11E-09 Max: 2.69E-08	Ref: 1.689 Min: 0.109 Max: 3.454	Ref: 3.130 Min: 1.520 Max: 7.560	Ref: 0.060 Min: 0.015 Max: 0.171	Ref: 0.025 Min: 0.000 Max: 0.085	
Sherman Fall	2	Ref: 3.54E-08 Min: 2.89E-08 Max: 4.33E-08	Ref: 0.999 Min: 0.791 Max: 1.206	Ref: 2.335 Min: 2.160 Max: 2.510	Ref: 0.170 Min: 0.130 Max: 0.210	Ref: 0.110 Min: 0.000 Max: 0.220	
Kirkfield	1	5.78E-09	7.216	2.170	0.000	0.150	
Coboconk	2	Ref: 1.51E-08 Min: 1.14E-08 Max: 1.99E-08	Ref: 1.732 Min: 0.738 Max: 2.726	Ref: 1.820 Min: 1.700 Max: 1.940	0.000	Ref: 0.025 Min: 0.000 Max: 0.050	
Gull River	1	2.50E-08	0.775	4.060	0.210	0.110	
Shadow Lake	0	4.41E-06	0.583	1.200	0.040	0.000	Assume equal to Cambrian
Cambrian	1	4.41E-06	0.583	1.200	0.040	0.000	
Precambrian	0						Not included in Gas models

Notes:
Data based on limited fit to capillary pressure data with liquid saturations between 0.7 and 1.0.

5.6.2 Damaged Zone

It is well established that capillary pressure and permeability of a rock are not independent parameters, rather they are generally correlated. As the permeability of the rock increases in the damaged zone, one would expect the capillary pressure characteristic function to change as well. NAGRA (2008) used an air entry pressure of 18 MPa for undisturbed Opalinus Clay and 2 MPa for EDZ in the same material, while other parameters for the van Genuchten relative permeability and capillary pressure equations were kept equal for damaged and undamaged rock. The exceptions to this were the liquid and gas residual saturations, which were changed to account for the increased porosity and the presence of fractures. NAGRA (2002) used air entry pressures of 5 and 2 MPa, respectively for undisturbed and disturbed Opalinus clay. Norris (2008) did not look specifically at damaged zones, but rather at gas flow in formations where fracture flow is dominant. For such formations, Norris (2008) assumed a capillary pressure of zero at all saturations. This might be a reasonable approach to take for the HDZ, where flow will presumably occur in well-connected fractures. Davies (1991) provided an expression for air entry pressure (which is often assumed to equal the reciprocal of **α**) as a function of permeability. This expression has the following form:

$$P_o = a\, k^{\,b} \tag{5.1}$$

where:

P_o is the air entry pressure (MPa);
k is the permeability (m^{-2});
a is an empirical fitting parameter (equal to 5.6×10^{-7}); and
b is an empirical fitting parameter (equal to -0.346).

To estimate **α** for the EDZ, the difference between the permeabilities was used, in conjunction with Davies' expression, to scale the **α** values. The resulting scaling factors are 4.92 for the inner EDZ (vertical permeability is 100 times higher) and 2.22 for the outer EDZ (vertical permeability is 10 times higher). The EDZ **α** is obtained by multiplying the intact rock **α** by the scaling factor.

There are no established relationships between permeability and other characteristic curve parameters, therefore these parameters are not changed for the EDZ (i.e., they are taken to be the same as for the geosphere).

5.6.3 Geosphere Biosphere Interface

The GBI for the gas pathways is simply the geosphere media and therefore requires no further parameterization.

6. BIOSPHERE DATA

The biosphere systems relevant to a postclosure safety assessment for the proposed L&ILW facility at the Bruce nuclear site are described in Chapter 6 of the System and Its Evolution report (QUINTESSA 2011b). The recommended parameters and values required to describe these systems are primarily drawn from a few main sources:

- EIS technical support documents for the DGR (GOLDER 2011a, b, c), and WWMF site Environmental Assessment (EA) Study Reports (e.g., OPG 2005a), which provide detailed site-specific information concerning the present-day biosphere in the vicinity of the Bruce nuclear site;
- The guidelines for calculating Derived Release Limits (DRLs) for normal operations of nuclear facilities, prepared by the Canadian Standards Association (CSA 2008);
- The biosphere section of the data report for the 'Third Case Study' assessment for a used fuel repository (Garisto et al. 2004), although this study presents information for the Canadian Shield, it provides useful information regarding alternative biosphere modelling approaches and for less site-specific data; and
- Specific studies undertaken for OPG to investigate parameter values for key elements, including Cl, I, Ra, U and Np (Sheppard et al. 2006). The recommendations arising from these reviews are adopted in preference to other sources.

The biosphere assessment model draws significantly on that developed by the CSA (2008). The recommended model in CSA (2008) is deterministic in nature, therefore point estimate values are presented in CSA (2008) and this section. The parameterization of CSA (2008) is intended to be conservative, but not overly so. This is achieved by a combination of conservative intake and exposure factors with realistic dispersion and partitioning parameters. This approach is taken to provide sufficient conservatism to be protective; use of all factors at conservative values would be excessively restrictive (Clause 4.2.9 of CSA 2008).

The biosphere in the vicinity of the Bruce nuclear site will change over the long timescale under consideration for the postclosure safety assessment. Climate change is a key example of how long-term environmental change may significantly affect the DGR system, particularly the biosphere. In this report, data are presented relevant to the present-day temperate biosphere conditions considered in the Normal Evolution Scenario. Data relevant to a potential future colder 'tundra' climate state are provided in Section 4.4.3 of the Normal Evolution Scenario Analysis report (QUINTESSA 2011a).

The list of biosphere parameters is presented in the following sub-sections:

- Surface water parameters, such as surface run-off, infiltration, stream flows, lake exchange rates and irrigation rates, are presented in Section 6.1;
- Soil and sediment parameters, such as densities, porosities, depths and sorption coefficients, are presented in Section 6.2;
- Atmospheric parameters, such as dust and aerosol concentrations, are presented in Section 6.3;
- Plant parameters, such as crop yields and concentration factors, are presented in Section 6.4; and
- Animal parameters, such as stocking densities, ingestion rates and transfer factors, are presented in Section 6.5.

6.1 Surface Water Parameters

This section provides the data required in order to develop appropriate representations of the movement of water (and thus associated contaminants) through the surface water systems. The information developed thus covers processes including runoff, infiltration, stream flows, and, in particular, exchanges between different sections of Lake Huron.

6.1.1 Description of the Present-Day System

The Bruce nuclear site is situated on the shores of Lake Huron. Lake Huron is a cold, deep oligotrophic lake with low nutrient levels (relative to Lakes Ontario and Erie). There are no major rivers or lakes in the vicinity of the site other than Lake Huron. 'Stream C' drains into the southwest corner of the Baie du Doré to the north (Figure 6.1) and the Little Sauble River discharges into Inverhuron Bay to the south. Stream C is a former tributary of the Little Sauble River that was diverted to Baie du Doré during the initial development of the Bruce nuclear site in the 1960s (GOLDER 2011c).

Baie du Doré comprises a Provincially Significant Wetland, with an area of about 9.5×10^5 m^2, and a bay. Under most prevailing current conditions, there is little circulation in the bay, which appears to be more heavily influenced by wind and wave action than by broad circulation patterns in the lake (OPG 2005b). Water depths in the bay are relatively shallow, with mean depths of approximately 0.4 m to 1.2 m offshore.

The proposed location of the main and ventilation shafts lies on the approximate boundary between the area draining north into MacPherson Bay through drainage ditches and the area draining south into the Railway Ditch (originally excavated parallel to the abandoned rail line) (GOLDER 2011c). The distance adjacent to the proposed location of the shafts to the point at which the Railway Ditch drains into Stream C is approximately 1 km. Stream C flows slowly for another 1 km into the Baie du Doré wetland, which runs for approximately 800 m further before discharging into the Baie du Doré bay.

In addition to receiving surface water drainage, the Railway Ditch also intercepts groundwater and is wet throughout the year, although flow is sluggish and can be stagnant. The ditch[3] is approximately 3 m wide and 1.5 m deep with a mean water depth of 0.15 m. It slopes slightly to the east (0.09% to 0.15% grade) (GOLDER 2011a; OPG 2005a and b).

Near to the site, Stream C has an average depth of approximately 0.25 to 0.5 m (although it can be as shallow as 1 cm, where it flows over rocks, and as deep as 1 m). Downstream, the average depth increases to approximately 0.5 to 1 m until it drains into the Baie du Doré, at which point it has an average depth of approximately 0.2 m.

For safety assessment modelling purposes, Lake Huron is divided into six compartments, which represent the North Channel, Georgian Bay, Mackinac Basin, Central Basin, South Basin, and Saginaw Bay (see Figure 6.2). Both Lake Superior and Lake Michigan drain into Lake Huron, via the St. Mary's River and the Straits of Mackinac, respectively. Lake Huron discharges to the St. Clair River.

---

[3] Based on the ditch to the south of the rail bed.

Note: Adapted from Figure 5.4.3-1 in GOLDER (2011a).

Figure 6.1: Local Watersheds

6.1.2 Postclosure Surface Water System

Although the site area illustrated in Figure 6.1 will differ appreciably in the postclosure period, the general description of the present-day system provided above is the best basis for defining a hypothetical surface water system for the postclosure period that reflects constant temperate conditions.

An agricultural system is envisaged with water inputs via precipitation and irrigation. Water infiltrating through the irrigated soil is directed to the surface water on the basis that the silt tills will divert much of the infiltrating water and as a cautious assumption. The surface water system draining to Lake Huron is represented by a drainage ditch, a stream and a wetland.

This maximizes the range of habitats considered (a cautious assumption for non-human biota assessments) and reflects the present-day system draining via the railway ditch.

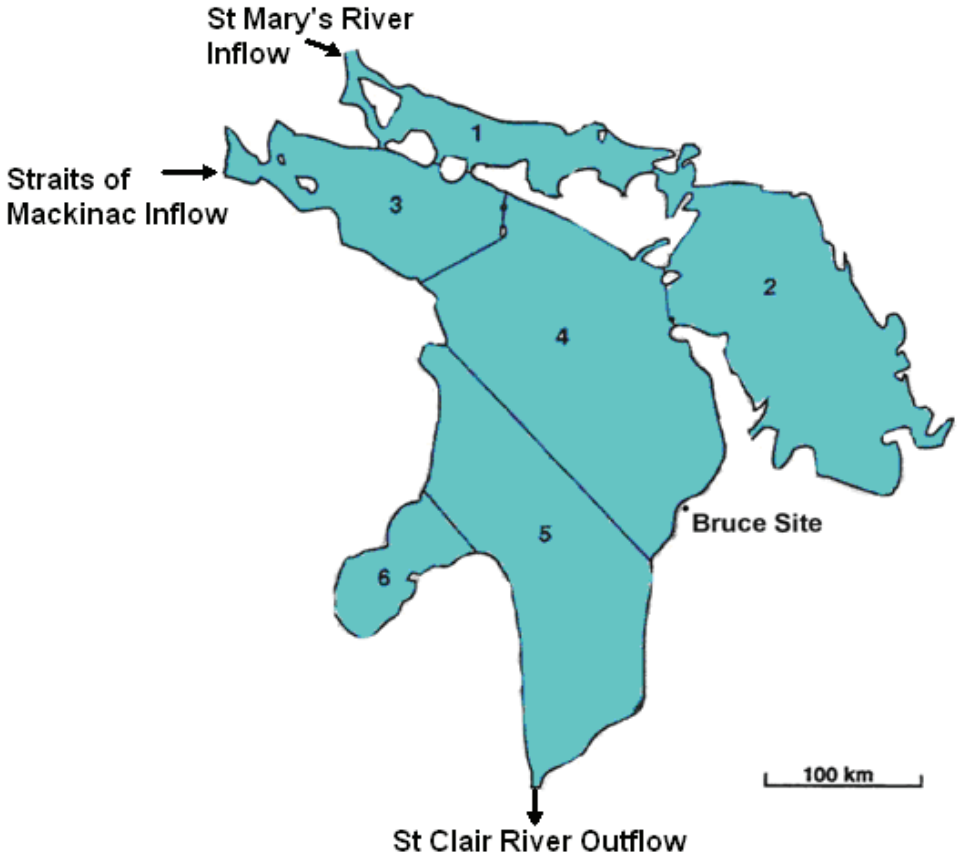

Figure 6.2: Lake Components

The length of the ditch from the irrigated farmland to the stream is taken to be 1 km and the stream is taken to run for approximately 1 km before reaching the wetland. These distances are assessment-level assumptions, but also reflect the approximate lengths of the railway ditch and Stream C.

The wetland is taken to extend for approximately a further 800 m from the point that the stream discharges to the edge of Lake Huron. The area of the wetland through which the stream water passes will be relatively broad and shallow. It is therefore assumed that the water is about 100 m wide and 0.2 m deep.

The dimensions for the Shore region into which the shallow groundwater discharges are taken to be 1000 m along the shore-line and 500 m into the Lake. This area is taken to be the smallest reasonable area within which the potentially contaminated plume might discharge. The average depth along this region is 5 m, based on the bathymetric map of the site area in GOLDER (2008a). The lake circulation runs anti-clockwise along the shoreline in this region at a rate of approximately 0.1 m s^{-1} (GOLDER 2008b).

While basing the surface water system on the present-day biosphere provides confidence that it provides a feasible combination of features, given continuing present-day climate, it is noted that the resulting biosphere system is stylized and that there is considerable uncertainty concerning its characteristics. Should the surface water system be shown to be a significant exposure route, the sensitivity of the model to these features could be investigated through sensitivity studies.

The surface water information identified is divided into four separate tables (see Table 6.1 to Table 6.4 below). Table 6.1 presents general surface water parameters, while Table 6.2 to Table 6.4 present data associated with the model for Lake Huron.

Table 6.1: Terrestrial Surface Water Parameters

Parameter		Reference Value	Note
Biosphere temperatures (°C)		8.2	A
Precipitation rate (m a^{-1})		1.07	B
Runoff (m a^{-1})		0.36	C
Stream/river flow rate (m s^{-1})	Railway Ditch	0.25	D
	Stream C	0.75	
Stream/river depth (m)	Railway Ditch	0.15	E
	Stream C	0.5	
Stream/river width (m)	Railway Ditch	3.0	F
	Stream C	3.0	
Irrigation rate (L m^{-2} s^{-1})		1.1E-5	G
Evapotranspiration rate (m s^{-1})		2.06E-8	H
Domestic water demand per person (m^3 a^{-1})		130	I
Volatilization rate for C (s^{-1})		6.7E-8	J
Dissolved inorganic carbon concentration in surface waters (mg L^{-1})		21.4	K
Mass of stable carbon in dissolved inorganic phase in water, gC L^{-1}		0.0213	L
Fraction of time that precipitation falls (-)		0.23	M
Surface water degassing rate for Rn-222 (m s^{-1})		6.7E-6	N
Degassing fraction for Rn-222 from domestic water (-)		0.52	N

Notes:

A Reference value represents the present-day yearly average daily temperature from Table 5.3.2-1 of GOLDER (2011c). The Table also reports the minimum extreme temperature as –21.1°C and the maximum as 31.8°C.

B Total annual precipitation given in Table 5.3.3-1 of GOLDER (2011c) for the period 2002 to 2005, which indicates a relatively even distribution of precipitation between winter and summer seasons and that about 30% of this falls as snow.

C Clause 6.3.6.3 of CSA (2008). Note that effective precipitation can be calculated from the precipitation rate, minus runoff.

D No clear data available, other than statements that the railway ditch has ‘sluggish’ to ‘stagnant’ flow and Stream C is ‘slow flowing’ (GOLDER 2011a; OPG 2005a and b). Values adopted as reasonable estimates.

E Railway Ditch and Stream C depth range is taken from OPG (2005b).

F Widths taken from OPG (2005a and b).

G Equivalent to 0.35 m a^{-1}, from Clause 7.2.3.2.2 of CSA (2008), which notes that it is a conservative value for an irrigation pathway.
H Table 15 of CSA (2008).
I Consistent with Garisto et al. (2004).
J Recommended in Clause 6.6.2.5 of CSA (2008), which also states that volatilization rates for other radionuclides may be considered to be negligible relative to other loss mechanisms.
K Recommended for pond water in Clause 6.7.4 of CSA (2008) and based on dissolved inorganic carbon concentration in the surface waters of the Great Lakes watershed.
L Clause 7.7.5.3 of CSA (2008).
M Conservative value from Clause 6.3.3.3 of CSA (2008) adopted.
N Based on Table 4 of Sheppard et al. (2006).

Table 6.2: Lake Huron Compartment Characteristics

Lake Compartments	Drainage Area [A] (%)	Compartment Surface Area (km^2)	Compartment Mean Depth (m)	Water Volume (m^3)	Area and Depth Notes
North Channel	25.6	3,950	22	8.7E+10	B
Georgian Bay	34.2	15,108	44	6.6E+11	C
Mackinac Basin	4.1	5,600	80	4.5E+11	D
Central Basin	5.7	17,300	100	1.7E+12	D
South Basin	13.5	14,000	50	7.0E+11	D
Saginaw Bay	16.9	2,960	16	4.7E+10	E
Shore	0	0.5	5	2.5E+6	F
Total		58,918		3.7E+12	

Notes:
A Estimated based on the discretization shown in Figure 6.2 and the drainage basin for Lake Huron (USEPA 2008).
B Area and depth from Sly and Munawar (1988).
C Area and depth from Bennett (1988).
D Areas and depths from interpolated from bathymetric map (NDGC 2010).
E Area and depth from McCormick and Schwab (2008).
F Shore compartment is taken to be too small to be involved in the net basin flows, which includes the contribution of net basin supply via the drainage area.

Table 6.3: Lake Huron Interface Characteristics

Lake Compartments		Interface Width [A] (m)	Interface Depth [A] (m)	Interface Area (m^2)	Circulation Velocity ($m\ s^{-1}$)	Circulation Velocity Notes
North Channel	Georgian Bay	2.0E+3	1.0E+1	2.0E+4	0.03	B
North Channel	Mackinac Basin	1.0E+4	5.0E+1	5.0E+5	0.03	B
Georgian Bay	Central Basin	1.6E+4	4.5E+1	7.2E+5	0.033	C
Mackinac Basin	Central Basin	6.8E+4	8.2E+1	5.6E+6	0.025	C
Central Basin	South Basin	1.6E+5	6.0E+1	9.3E+6	0.025	C
Central Basin	Shore	5.0E+2	5.0E+0	2.5E+3	0.1	D
South Basin	Saginaw Bay	4.2E+4	2.0E+1	8.4E+5	0.016	C

Notes:
A Interpolated from bathymetric map (NDGC 2010).
B Based on Bennett (1988).
C Based on Beletsky et al. (1999).
D Based on GOLDER (2008b).

Table 6.4: Net Water Flows for Lake Huron

Item	Reference Value ($m^3\ a^{-1}$)	Note
Inflow to North Channel from Lake Superior via St Mary's River	7.10E+10	A
Inflow to the Mackinac Basin from Lake Michigan via the Straits of Mackinac	3.72E+10	A
Net basin supply	6.28E+10	B
Outflow from the South Basin via St Clair River	1.71E+11	A

Notes:
A Based on Schertzer et al. (2008).
B Represents surface runoff to the lake, precipitation and evaporation and is based on Schertzer et al. (2008). Note that net flow from the North Channel is split 50:50 to the Mackinac Basin and Georgian Bay.

6.2 Soil and Sediment Parameters

This section provides the data required for modelling the movement of contaminants into, through and out of the soil and surface water sediment, including parameters representing the physical and chemical characteristics of the soil and sediment, such as densities, porosities, vertical and horizontal extents, sedimentation rates, erosion rates, and the mineralogy, sorption coefficients and grain density. Values obtained are based on a range of reference material, including a wide range of site-specific underpinning documentation and generic resources.

6.2.1 Surface Soil Parameters

In general, there is a thin veneer of topsoil and humus (0.3 m) above a surficial sand and gravel unit which itself overlies silt till (GOLDER 2011d). There are occasional regions of peat-like materials. The soils and subsoils are generally firm to stiff and dense. Moisture varies, but the soil is generally moist and often wet or even saturated. Conversion of the land to agriculture is taken to include the introduction of further drainage, reducing soil moisture content in comparison to present-day values.

The lack of clear information regarding the mineralogy associated with the soils means that the assumption taken is that **clay** soils dominate. Sorption is strongest on clay soils in comparison to other soils that are suitable for agriculture (i.e., sand and loam), which will result in greater retention and is therefore cautious with respect to key exposure pathways, such as ingestion of farm produce. While greater retention would also be associated with restricted plant uptake, it is noted that the CSA (2008) model does not distinguish between soil types with respect to soil to plant transfer (see Section 6.4), therefore the adoption of a clay soil remains cautious. However, it is noted that values associated with other soil types can be used for sensitivity studies.

Soil parameters are presented in Table 6.5. Table 6.6 summarizes the adopted soil sorption coefficients. It is noted that review papers recommend geometric standard deviations of 10 for Cl, I and Np and 20 for U, which imply that these parameters are highly uncertain. In the case of Cl and I, there is limited data but clearly limited or no sorption. In the case of U, there are many data and so the uncertainty is likely related to variability with different soil conditions, but in all cases the U is highly sorbed.

Table 6.5: Soil Parameters

Parameter		Reference Value	Note
Depth of top soil (m)		0.2	A
Soil dry bulk density (kg dw m^{-3})	Sand	1500	B
	Loam	1300	
	Clay	1400	
	Organic	400	
Soil water content (m^3 water m^{-3} soil)	Sand	0.1	C
	Loam	0.2	
	Clay	0.3	
	Organic	0.7	
Total porosity (m^3 void space m^{-3} soil)	Sand	0.57	D
	Loam	0.62	
	Clay	0.59	
	Organic	0.75	
Surface erosion rate (kg m^{-2} s^{-1})	Sand	1.5E-8	E
	Loam or Clay	5.0E-8	
	Organic	0	
Volatilization rate (s^{-1})	I	6.7E-10	F
	Se	1.0E-9	
	C	4.3E-7	
Reduction factor for the effect of soil water HTO concentrations being lower than air moisture HTO concentrations (-)		0.68	G
Rn-222 emission rate from the soil (mol_{Rn-222} m^{-2} s^{-1}) per (mol_{Ra-226} kg^{-1} dry soil)		2.7E-9	H
Soil to indoor air transfer factor for Rn-222 (mol_{Rn-222} m^{-3}) per (mol_{Ra-226} kg^{-1} dry soil)		1.0E-5	H
Maximum oxidation rate of CH_4 to CO_2 in soil (mg m^{-2} day^{-1})		4.9	I

Notes:

A While the description of the present-day site describes 0.3 m of topsoil and humus (Section 5.4.1.1 of GOLDER 2011d), the long-term nature of the calculations means that the generic value of 0.2 m recommended in Clause 6.3.1.1 of CSA (2008) is adopted.
B Clause 6.3.2.2 of CSA (2008).
C Clause 6.3.4.3 of CSA (2008) with modification for organic soil to ensure soil water content is slightly less than total porosity.
D Table 8.4 of Garisto et al. (2004).
E Clause 6.3.4.2 of CSA (2008).
F Clause 6.3.5.1 of CSA (2008).
G Consistent with the assumptions made in Table A.5a of CSA (2008).
H Based on Table 4 of Sheppard et al. (2006).
I Highest value from Section 5.4.2 of Thorne and MacKenzie (2005).

Table 6.6: Soil and Sediment Sorption Coefficients (K_d) (m^3 kg^{-1})

Element	Sand	Loam	Clay	Organic	Note
H	-	-	-	-	A
Li	0.0E+00	0.0E+00	0.0E+00	0.0E+00	B
Be	2.4E-01	8.1E-01	1.3E+00	3.0E+00	C
B	0.0E+00	0.0E+00	0.0E+00	0.0E+00	B
C	5.0E-03	2.0E-02	1.0E-03	7.0E-02	D
Cl	1.0E-04	1.0E-04	1.0E-04	2.0E+00	E
Sc	1.4E-01	4.7E-01	7.2E-01	1.7E+00	C
V	3.0E-01	3.0E-01	3.0E-01	3.0E-01	F
Cr	6.7E-02	3.0E-02	1.5E+00	2.7E-01	C
Mn	4.9E-02	7.2E-01	1.8E-01	4.9E-01	C
Co	6.0E-02	1.3E+00	5.4E-01	9.9E-01	C
Ni	4.0E-01	3.0E-01	6.7E-01	1.1E+00	C
Cu	2.7E-01	2.7E-01	2.1E+00	3.2E-01	G
Zn	2.0E-01	1.3E+00	2.4E+00	1.6E+00	C
As	1.0E-03	6.0E-03	1.0E-02	1.0E-02	C
Se	1.5E-01	4.9E-01	7.4E-01	1.8E+00	C
Br	1.5E-02	4.9E-02	7.4E-02	1.8E-01	C
Sr	1.3E-02	2.0E-02	1.1E-01	1.5E-01	C
Zr	6.0E-01	2.2E+00	3.3E+00	7.3E+00	C
Nb	1.6E-01	5.5E-01	9.0E-01	2.0E+00	C
Mo	1.0E-02	1.3E-01	9.0E-02	2.5E-02	C
Tc	1.4E-04	1.0E-04	1.2E-03	1.5E-03	C
Ag	9.0E-02	1.2E-01	1.8E-01	1.5E+01	C
Cd	7.4E-02	4.0E-02	5.4E-01	8.1E-01	H
Sn	1.3E-01	4.5E-01	6.7E-01	1.6E+00	C
Sb	4.5E-02	1.5E-01	2.4E-01	5.4E-01	C
Te	1.3E-01	5.0E-01	7.2E-01	1.9E+00	C
I	8.0E-03	2.0E-02	1.0E-02	8.0E-02	I
Cs	2.7E-01	4.4E+00	1.8E+00	2.7E-01	C
Ba	9.9E-02	3.4E-01	5.2E-01	1.2E+00	C
Gd	9.9E-02	3.4E-01	5.2E-01	1.2E+00	C

Element	Sand	Loam	Clay	Organic	Note
Hf	4.5E-01	1.5E+00	2.4E+00	5.4E+00	C
W	0.0E+00	0.0E+00	0.0E+00	0.0E+00	B
Ir	3.0E-03	3.0E-03	3.0E-03	3.0E-03	J
Pt	2.4E-02	2.4E-02	2.4E-02	2.4E-02	J
Hg	1.6E-02	5.5E-02	8.4E-02	1.9E-01	C
Tl	0.0E+00	0.0E+00	0.0E+00	0.0E+00	B
Pb	2.7E-01	1.6E+01	5.5E-01	2.2E+01	K
Po	1.5E-01	4.0E-01	3.0E+00	7.3E+00	K
Ra	4.7E-02	4.7E-02	4.7E-02	4.7E-02	L
Ac	4.5E-01	1.5E+00	2.4E+00	5.4E+00	K
Th	3.0E+00	3.3E+00	5.4E+00	8.9E+01	C
Pa	5.4E-01	1.8E+00	2.7E+00	6.6E+00	C
U	4.0E-02	2.0E-01	2.0E-01	2.0E+00	M
Np	3.0E-03	1.0E-02	2.0E-02	5.0E-01	E
Pu	5.4E-01	1.2E+00	4.9E+00	1.8E+00	C
Am	2.0E+00	9.6E+00	8.1E+00	1.1E+02	C
Cm	4.0E+00	1.8E+01	5.4E+00	1.2E+01	C
All organics	1.0E+00	1.0E+00	1.0E+00	1.0E+00	O

Notes:

A No sorption values required for H-3 due to specific activity model adopted.
B Assumed in the absence of data to be zero.
C Table G2 of CSA (2008).
D Table G2 of CSA (2008), while sensitivity studies could consider alternative approaches for modelling carbon in soil due to its distinct behaviour in relation to trace elements, particularly in organic soils.
E Geometric mean (GM) from Table 2 of Sheppard et al. (2006), which also recommends a geometric standard deviation (GSD) of 10.
F Arithmetic mean from Table 14 of IAEA (2010). No GM given. Arithmetic mean for all soils used since no specific data for loam, clay and organic soils and only one value for sand.
G GM from Table 14 of IAEA (2010).
H Derived from mean of natural logarithm of the observed values given in Tables A-1 to A-4 of Sheppard and Thibault (1990).
I GM from Table 2 of Sheppard et al. (2006) which also recommends a GSD of 10 for sand, loam and clay soils and a GSD of 22 for organic soils.
J Mean value given in Table 14 of IAEA (2010), which does not distinguish between soil textures.
K Table 8.6 of Garisto et al. (2004).
L GM from Table 2 of Sheppard et al. (2006), which also recommends a GSD of 4.9.
M GM from Table 2 of Sheppard et al. (2006), which also recommends a GSD of 20.
O Assumed to be strongly sorbed.

6.2.2 Sediment Parameters

Parameters are presented for freshwater sediments in Table 6.7, relevant parameters (e.g., sorption coefficients) are based on generic recommendations in CSA (2008).

Table 6.7: Sediment Parameters

Parameter		Reference Value	Note
Sediment dry bulk density (kg m^{-3})		400	A
Sediment porosity (-)		0.85	B
Suspended sediment concentration (kg m^{-3})		0.01	C
Bed and suspended sediment sorption coefficients, K_d (m^3 kg^{-1})	Ditch, Stream & Wetland	5 times loam K_d	A
	Lake Huron	10 times sand K_d	D
Dilution factor for shoreline deposits (-)		1	E
Shore width factor for external irradiation (-)	Lake Huron	0.3	F
	Stream	0.2	

Notes:
- A Based on recommendation for aquatic sediments in Clause 6.6.2.2 of CSA (2008).
- B Derived from bulk density and a grain density of 2650 kg m^{-3}.
- C Represents a reasonable assumption. In the absence of available data, the suspended sediment concentration is defined as being the same throughout the surface water system to help ensure an appropriate sediment balance.
- D Based on recommendation for near-shore freshwater sediments in Clause 7.8.2 of CSA (2008).
- E Conservatively set to 1.
- F Clause 7.9.3 of CSA (2008).

6.2.3 Farmed Land Areas and Water Requirements

For calculations of potential impact, the area of farmland that could be affected can be estimated based on the assumption that the water and food demands are reflected by the requirement of two adults, a child and an infant at the cautious (90^{th} percentile) intake rates recommended in Section 7.1. It is also assumed that water pumped from the well is used for domestic and farming purposes:

- Domestic use includes drinking, cooking and bathing water; and
- Farming use includes irrigation and drinking water for animals. Other farming demand for water, such as for washing animals and machinery, is supplied from non-contaminated sources.

The domestic water demand is 130 m^3 a^{-1} per person (Garisto et al. 2004).

The demand for animal produce is met with one dairy cow, one beef steer, four sheep, two goats, two pigs and twenty chickens. The farm also has two further non-dairy cattle either to

provide surplus produce or as working animals (representative of a more traditional and non-technological way of farming). Cattle, sheep and goats are fed entirely on forage (either as grazing, hay or silage), whereas pigs and poultry feed on grain alone.

These assumptions result in the following characteristics for water requirements:

- Water demand for domestic use: 520 m^3 a^{-1};
- Water demand for animal drinking water: 118 m^3 a^{-1}; and
- Water demand for irrigation of crops for human and animal consumption (based on field areas listed below): 5750 m^3 a^{-1}.

Water demand therefore sums to 6388 m^3 a^{-1}. The well depth and location are discussed in Section 5.4.3.

The following can also be derived as the requirement for the farming area:

- Area required for forage: 286,000 m^2
- Area required for feed crops: 13,450 m^2;
- Area required for crops of human consumption: 2,986 m^2 (comprising 626 m^2 for vegetables, 140 m^2 for potatoes, 508 m^2 for fruit and berries, 1708 m^2 for grain and 4 m^2 for mushrooms).

The total area of the farm is therefore 302,436 m^2, i.e., about 30 hectares. Note that the irrigated area for human food crops occupies about 1% of the total area of the farm. The farm area is therefore sufficient to meet the family's food demands and also produce some surplus for market.

6.3 Atmosphere Parameters

Table 6.8 provides data required for modelling the movement of contaminants into, through and out of the atmosphere in solid and gaseous form.

Table 6.8: Atmosphere Parameters

Parameter		Reference Value	Note
Atmospheric dust concentration (kg m^{-3})		5.9E-8	A
Resuspended water body aerosol concentrations (m^3 water m^{-3} air)		2.9E-10	B
Annual average wind speed (m s^{-1})		3.56	C
Building height (m)		2.4	D
Building area (m^2)		95	E
Household ventilation rates (h^{-1})		0.35	F
Concentration of stable C in air, gC m^{-3}		0.2	G
Ratio of HTO concentration in air moisture to HT concentration in air (Bq L^{-1} per Bq m^{-3})		8	H
Absolute humidity over snow free period (L m^{-3})		0.0089	I
Absolute humidity over growing season (L m^{-3})		0.012	I
Fraction of the year when oxidation may occur (-)		0.75	J
Ratio of the concentration of tritium in air moisture at 1.5 m above ground to concentration of tritium in air moisture at ground level (-)	Area of irrigated field		K
	≤ 10^2 m^2	0.3	
	> 10^2 m^2 and < 10^6 m^2	$(\log_{10} A_f + 1)/10$	
	≥ 10^6 m^2	0.7	
Washout ratio for deposition to plants (-)	Iodine	2.0E+5	L
	All others	6.3E+5	
Washout ratio for deposition to soil and water (-)	Iodine	1.6E+5	L
	All others	5.5E+6	
Effective duration of irrigation deposition (for crops other than forage) (s)		5.2E+6	M
Dry deposition velocity (m s^{-1})	Chlorine	2.0E-2	L
	Iodine	7.5E-3	
	All others	1.4E-3	
Friction velocity (m s^{-1})		0.2	N

Notes:

A Section 3.2.1 of Amiro (1992). Uses cautiously realistic approach to subsume potential volatilization from water. Note that suspended particulate data are available in GOLDER (2011b) however, these relate to particle size of 2.5 µm and above, while the inhalation dose coefficients (Table 7.5) are based on an activity mean aerodynamic diameter of 1 µm.

B Table 8.3 of Garisto et al. (2004).

C Yearly average used for dispersion meteorology for the DGR site from Table 4.1.4-1 of the draft version of GOLDER (2011c) at time of data freeze for safety assessment (summer 2010). Value given in final version of the report is 3.28 m s^{-1} (Table 5.3.4-1 of GOLDER (2011c)).

D Table 9.1 of Garisto et al. (2004).

E Derived from volume and height given in Table 9.1 of Garisto et al. (2004).

F Table 9.1 of Garisto et al. (2004).

G Recommended in Clause 6.4.9.3 of CSA (2008).

H Conservative value adopted from Clause 6.1.6.3 of CSA (2008).

I Value for Southern Ontario from Table 11 of CSA (2008), consistent with Clause 0.3.

J Value for Southern Ontario from Clause 6.1.6.5 of CSA (2008), consistent with Clause 0.3.

K Consistent with Clause 7.2.5.4 of CSA (2008).

L Table 14 of CSA (2008) – value for iodine adopts that for elemental iodine, which is the form that would be released.

M Clause 6.4.5 of CSA (2008) – equivalent to 60 days; note that forage is not irrigated.

N Based on Section A.6 of Limer et al. (2008).

6.4 Plant Parameters

The biosphere description given in Section 2.4 of the System and Its Evolution report (QUINTESSA 2011b) includes areas of farmed land and semi-natural land (wetland). Farmland accounts for around 60% of the land use in the Bruce county, with many cattle farmers, as well as farmers of pigs, sheep and goats, and crops such as oats, barley, canola and hay.

Consistent with CSA (2008), soil-to-plant concentration factors are reported on a dry weight basis (Bq kg^{-1} dry weight plant per Bq kg^{-1} dry weight soil). Sheppard (2003) notes that there is little to distinguish uncertainty about the soil-to-plant concentration factor within a crop species from that between different crop species, therefore a single generic set of values is presented in Table 6.9 for application to all plant types, consistent with CSA (2008). These values can be converted to a fresh weight plant basis by applying the dry:fresh weight ratio for plant products, reported in Table 6.10.

Table 6.9 includes translocation fractions from external contamination to edible portions and concentration ratios from plants to honey are also provided. Interception fractions are presented in Table 6.10 based on the crop canopy approach adopted in CSA (2008). Other plant parameters are provided in Table 6.11.

Plants that may therefore be involved in potential exposure pathways to humans (the primary assessment end point) are:

- Large-scale agricultural crops, in particular oats, barley, canola, wheat and corn;
- Small-scale subsistence crops, such as potatoes, onions, carrots, cabbage, beans and apples;
- Forage crops, principally pasture; and
- Foodstuffs potentially gathered from semi-natural habitats, such as wild berries, mushrooms and nuts.

For this data report, emphasis has been placed on collating information on plants that have been considered in the main literature sources, described at the beginning of Chapter 6.

Table 6.9: Element-Dependent Crop Parameters

Element	Soil to Plant Concentration Ratio, Bq kg^{-1} dw plant per Bq kg^{-1} dw soil		External Plant to Edible Portion Translocation Fraction (-)			Concentration Ratio for Honey, Bq kg^{-1} fresh honey per Bq kg^{-1} dry plant	
			Crops where Foliage is Consumed	Other Crops	Note		
H	-	A	1	1	I	1	L
C	-	A	1	1	I	1	L
Cl	1.5E+1	B	1	1	I	0.1	L
Ni	4.7E-1	C	1	1	I	0.1	L
Se	4.5E-1	C	1	1	I	0.1	L
Sr	8.7E-1	C	1	1	I	0.1	L
Zr	3.2E-3	C	1	0.1	I	0.1	L
Nb	2.9E-2	C	1	0.1	I	0.1	L
Mo	3.6E-1	C	1	1	I	0.1	L
Tc	3.7E+0	C	1	1	I	0.1	L
Ag	2.5E-1	C	1	1	I	0.1	L
Sn	4.1E-1	C	1	1	I	0.1	L
I	3.2E-2	D	1	0.1	I	0.1	L
Cs	5.3E-2	C	1	1	I	0.1	L
Ir	1.1E+0	E	1	1	E	0.1	M
Pt	1.1E+0	E	1	1	E	0.1	M
Pb	4.4E-2	F	1	1	J	0.1	J
Po	2.5E-3	F	1	1	J	0.1	J
Ra	4.0E-2	G	1	1	I	0.1	L
Ac	3.5E-3	F	1	0.01	K	0.1	K
Th	3.3E-3	C	1	0.01	I	0.1	L
Pa	3.8E-2	C	1	0.1	I	0.1	L
U	8.0E-3	D	1	0.1	I	0.1	L
Np	1.2E-2	H	1	0.1	I	0.1	L
Pu	1.4E-4	C	1	0.01	I	0.1	L
Am	6.3E-4	C	1	0.01	I	0.1	L
Cm	2.1E-4	C	1	0.01	I	0.1	L

Notes:
- A Specific activity approach adopted, as recommended by CSA (2008).
- B GM of data for crops for human consumption from Table 2 of Sheppard et al. (2006), converted to dry weight plant basis assuming a moisture content of 75%; the reference recommends a GSD of 5.7.
- C Table G3 of CSA (2008).
- D GM for all plants from Table 2 of Sheppard et al. (2006), converted to dry weight plant basis assuming a moisture content of 75%; the reference recommends a GSD of 10.
- E Based on analogy with Hg, which exhibits a similar degree of soil sorption, from Table G3 of CSA (2008).
- F Geometric mean adopted from Garisto et al. (2004) adopting a dry:fresh weight ratio of 0.25.
- G GM for all plants from Sheppard et al. (2006), converted to dry weight plant basis assuming a moisture content of 75%; the reference recommends a GSD of 11.
- H GM for all plants from Table 2 of Sheppard et al. (2006), converted to dry weight plant basis assuming a moisture content of 75%; the reference recommends a GSD of 5.7.
- I Table G3 of CSA (2008), although the following inconsistencies are noted for consideration in sensitivity studies: (i) transition metals (including Co, Ni, Zr, Nb, Mo, Tc and Ag) would be expected to have similar values; (ii) I and Cl would be expected to have similar values.
- J Pb and Po taken to be analogous to Sn and Se respectively.
- K Taken to be analogous to Th.
- L As recommended in Clause 6.10.5.2 of CSA (2008). Recent data in Sheppard et al. (2009) indicate that this overstates the transfer rate to honey.
- M Based on analogy with Hg and adopting the value for Hg recommended in Clause 6.10.5.2 of CSA (2008).

Table 6.10: Crop Dependent Plant Parameters

Parameter	Forage	Generic Feed Crops	Grain	Generic Fruit & Vegetables	Potatoes	Note
Foliar interception fraction	1	1	1	0.8	0.8	A
Consumable yield, kg (fresh weight) m^{-2} a^{-1}	0.48	0.6	0.4	1	2.1	A
Harvest index, kg (fresh weight product) kg^{-1} (fresh weight above ground biomass)	1	1	0.5	0.8	0.8	A
Dry:fresh weight ratio (-)	0.19	0.86	0.86	0.1	0.21	A
Leaf area index (-)	3	3	3	3	3	A

Notes:
Table G5 of CSA (2008).

Table 6.11: Other Plant Parameters

Parameter		Reference Value	Note
Volume of water retained per unit leaf area, L m^{-2}		0.1	A
Frequency of irrigation events using contaminated water, s^{-1}		3.34E-6	A
Effective duration of deposition, s	Pasture grass	2.6E+6	B
	All other crops	5.2E+6	B
Removal constant from forage and crops, s^{-1}		5.73E-7	C
Cropping frequency, s^{-1}		3.17E-8	D
Nutrient loss (-)		0.05	E
Fraction of plant stable carbon derived from air (-)	Irrigation pathway	0.7	F
	Gas pathway	1.0	G
Mass of stable C per mass of plant, gC kg^{-1} dw		500	G
Fraction of annual input of C-14 leaving the soil surface per annum (-)		1	H
Ratio of total plant yield to the total above-ground yield (total below ground yield for root crops) (-)		2	H
H-3 isotopic discrimination factor for plant metabolism (-)		0.8	I
Water equivalent of the plant dry matter (L kg^{-1} dw)		0.56	J
Oxidation/re-emission/uptake factor for plants, equal to the ratio of HTO concentration in plant water to HT concentration in air, Bq L^{-1} plant HTO per Bq m^{-3} air HT		6	K
Canopy height for crops (m)		0.4	L
Relationship between zero displacement height and canopy height (-)		2/3	M

Notes:

A Clause 7.3.1.2 of CSA (2008); note that CSA (2008) notes that the associated depth of irrigation water is taken to be cautious for the irrigation pathway.

B Clause 6.4.5 of CSA (2008); note that the model includes wet deposition from the atmosphere, hence a value for pasture grass is included, although it is not irrigated.

C Value given in Clause 6.4.4 of CSA (2008).

D Once per year, consistent with Clause 6.3.7.1 of CSA (2008).

E Clause 6.3.7.1 of CSA (2008);

F Clause 7.3.4.3 of CSA (2008) for irrigation pathway; the remaining fraction of plant carbon (i.e., 0.3) is taken to be derived from carbon that has degassed from the soil.

G Clause 6.4.9.3 of CSA (2008) for airborne releases.

H Clause 7.3.4.3 of CSA (2008).

I Clause 6.4.8.4 of CSA (2008).

J Clause 6.4.8.4 of CSA (2008), which notes that the bulk of plant dry matter is cellulose and starch, which have a similar hydrogen content of 10 g H for 162 g organic matter, or 0.062 g H per g dry plant; this is multiplied by 18/2 to give the amount of water per kg dry plant.

K Clause 6.4.7.3 of CSA (2008).

L Value representative of the crop types considered, based on a review of Allen et al. (1998).

M Based on Mölder (1997).

6.5 Animal Parameters

Cattle (beef and dairy), pig, sheep and chicken farming are present in the region around the Bruce nuclear site (Bruce County 2009) and there is potential for goats to be reared. Lake Huron is used locally for fishing for personal consumption, sport and commercial harvesting. A wide range of fish species is found in lake including species of the following sport fish: whitefish, trout, perch, bass, pike, salmon, and carp. Animal parameters for these types of livestock and fish are presented in Table 6.12 to Table 6.15. Data for deer and rabbits are also included in the tables to represent local non-domesticated terrestrial animals.

Table 6.12: Animal Characteristics

Parameter	Dairy cow	Dairy goat	Beef cattle	Pig	Lamb	Poultry	Deer	Rabbit	Note
Body mass at age of use (kg)	600	50	600	110	50	2	80	1.8	A
Feed consumption rate kg dw d^{-1}	19.8	2.6	13.2	3.3	1.7	0.1	2.5	0.11	B
Water consumption rate, L d^{-1}	151	15	31	6.8	3.3	0.1	5.1	0.17	B
Inhalation rate, m^3 d^{-1}	87	13	87	23	13	1	18	1	B
Soil load on feed, kg dw kg^{-1} dw	0.1	0.1	0.1	0.001	0.1	0.001	0.01	0.1	C
Soil consumption rate from other sources, kg dw d^{-1}	0.2	0.02	0.1	0.03	0.02	0.005	0.01	0.006	A
Dry weight fractions for animal produce (-)	0.1	0.1	0.3	0.5	0.3	0.3	0.3	0.3	D
Metabolically derived water ingested as dry weight feed (-)	0.065	0.065	0.074	0.137	0.074	0.151	0.074	0.074	E
Water ingested as water in feed (-)	0.373	0.373	0.412	0.031	0.412	0.035	0.412	0.412	E
Water from inhalation and skin absorption (-)	0.014	0.014	0.019	0.035	0.019	0.024	0.019	0.019	E
Water ingested as drinking water (-)	0.548	0.548	0.495	0.796	0.495	0.79	0.495	0.495	E

Notes:

A Table G6 of CSA (2008). Note that typical values for cows at slaughter range from 400 to 600 kg (Soffe 2003).

B Recommended default values from Table G6 of CSA (2008), based on allometric consideration, although it is noted that the values for beef and dairy cattle are inconsistent from energy balance considerations, since if a beef animal eats less than a dairy animal its inhalation rate would be expected to be lower.

C Table G6 of CSA (2008). Values for harvested feed are recommended for pigs and poultry, which are taken to consume grain products (consistent with footnote 6 to Table G6), values for other animals are based on grazed feed. Sensitivity calculations could address the possibility that pigs and chickens forage for food and have a higher soil intake.

D Clause 6.9.2.4 of CSA (2008), where given; value for dairy goats taken to be the same as for dairy cow, values for lamb, deer and rabbit taken to be the same as for beef cattle.

E Table 16 of CSA (2008), where given; values for lambs, deer and rabbits based on beef. Values expressed as fractions of total water intake.

Table 6.13: Feed to Milk and Meat Transfer Factors

Element	Cow Milk, d L^{-1}	Goat Milk, d L^{-1}	Beef Meat, d kg^{-1}	Beef Liver, d kg^{-1}	Pork, d kg^{-1}	Lamb, d kg^{-1}	Poultry Meat, d kg^{-1}	Eggs, d kg^{-1}	Deer, d kg^{-1}	Rabbit, d kg^{-1}	Note
C	2.7E-2	5.0E-2	8.8E-2	1.2E-1	3.2E-1	1.7E+0	8.5E+0	7.7E+0	6.2E-1	8.9E+0	A
Cl	1.5E-2	1.8E-2	2.0E-2	2.8E-2	6.5E-2	2.6E-1	2.0E+0	2.0E+0	1.4E-1	2.0E+0	B
Ni	1.8E-2	1.8E-2	5.0E-3	5.0E-3	1.2E-2	4.6E-2	3.1E-1	3.7E-1	2.4E-2	3.5E-1	A
Se	1.0E-2	1.0E-2	1.0E-1	1.0E-1	2.3E-1	9.1E-1	9.0E+0	9.0E+0	4.9E-1	6.9E+0	A
Sr	2.0E-3	3.0E-2	2.1E-3	3.0E-4	1.5E-2	3.1E-2	7.6E-2	2.7E-1	4.0E-2	1.9E-1	A
Zr	3.2E-6	6.0E-6	2.1E-5	1.0E-5	3.5E-3	4.5E-5	2.6E-2	3.8E-2	5.0E-5	7.1E-4	A
Nb	4.7E-5	6.0E-6	2.0E-4	1.0E-5	2.0E-4	1.7E-4	1.4E-3	2.3E-3	3.0E-4	4.2E-3	A
Mo	1.5E-3	9.0E-3	2.4E-3	1.0E-1	1.0E-3	5.0E-2	1.9E-1	5.8E-1	1.8E-2	2.5E-1	A
Tc	6.9E-4	1.1E-3	9.6E-4	4.0E-2	2.1E-3	4.7E-3	4.1E-1	1.9E+0	3.4E-3	4.9E-2	A
Ag	3.3E-3	6.0E-2	2.1E-3	4.0E-1	2.7E-2	1.6E-3	4.0E-1	7.9E-2	3.0E-3	4.2E-2	A
Sn	1.1E-3	3.5E-3	1.1E-2	2.2E-2	4.4E-3	1.3E-2	1.2E+0	1.2E+0	2.0E-2	2.8E-1	A
I	7.6E-3	4.0E-1	1.2E-2	2.0E-3	1.2E-2	3.9E-2	7.5E+0	7.5E+0	3.2E-2	4.6E-1	B
Cs	7.3E-3	1.0E-1	3.7E-2	3.0E-2	2.9E-1	4.9E-1	4.4E+0	8.1E-1	1.5E-1	1.1E+2	A
Ir	4.8E-4	1.6E-3	1.0E-2	8.3E-2	2.3E-2	9.1E-2	3.0E-2	3.6E-2	3.6E-2	5.1E-1	C
Pt	4.8E-4	1.6E-3	1.0E-2	8.3E-2	2.3E-2	9.1E-2	3.0E-2	3.6E-2	3.6E-2	5.1E-1	C
Pb	2.6E-4	3.5E-3	4.0E-4	2.2E-2	4.4E-3	1.3E-2	4.0E-2	4.0E-2	2.0E-2	2.8E-1	D
Po	3.4E-4	1.0E-2	4.5E-3	1.0E-1	2.3E-1	9.1E-1	4.5E-1	4.5E-1	4.9E-1	6.9E+0	E
Ra	6.2E-4	1.1E-3	9.0E-4	9.5E-4	2.2E-3	8.6E-3	1.3E-1	1.3E-1	4.6E-3	6.6E-2	B
Ac	2.0E-5	7.7E-5	2.5E-5	6.3E-2	4.6E-3	1.3E-2	2.5E-3	2.5E-3	2.0E-3	2.8E-2	F
Th	2.3E-5	7.7E-5	1.2E-4	6.3E-2	4.6E-3	1.3E-2	1.0E-2	1.0E-2	2.0E-3	2.8E-2	A
Pa	5.0E-6	1.7E-5	1.1E-5	1.1E-3	1.1E-4	3.4E-4	2.0E-3	2.0E-3	9.8E-5	1.4E-3	A
U	3.7E-4	1.4E-3	4.0E-4	6.9E-4	1.9E-2	7.4E-3	1.2E+0	1.2E+0	7.3E-1	4.1E-2	B

Element	Cow Milk, d L^{-1}	Goat Milk, d L^{-1}	Beef Meat, d kg^{-1}	Beef Liver, d kg^{-1}	Pork, d kg^{-1}	Lamb, d kg^{-1}	Poultry Meat, d kg^{-1}	Eggs, d kg^{-1}	Deer, d kg^{-1}	Rabbit, d kg^{-1}	Note
Np	5.0E-6	1.0E-4	2.0E-4	2.0E-2	4.5E-5	4.0E-4	2.0E-2	2.0E-2	6.2E-4	8.9E-3	B
Pu	5.8E-7	9.4E-6	2.1E-5	2.0E-2	2.8E-5	1.1E-3	9.2E-4	3.9E-3	2.5E-4	3.5E-3	A
Am	1.1E-6	1.4E-5	1.6E-5	2.0E-2	7.4E-5	1.3E-3	1.2E-3	7.1E-3	2.3E-4	3.3E-3	A
Cm	9.4E-7	3.1E-6	1.9E-5	2.0E-2	3.4E-5	4.0E-4	8.5E-4	1.8E-2	1.4E-4	2.0E-3	A

Notes:
The biosphere model is based on that described in CSA (2008), which excludes ingestion of lamb's liver and chicken's liver.

A Values from Table G3 of CSA (2008), although it is noted that the value for Cs to rabbit meat looks anomalous in the source reference.
B Values for cows' milk, beef meat and poultry (meat & eggs) based on Table 3 of Sheppard et al. (2006), other values from Table G3 of CSA (2008).
C Values for Hg adopted as an analogue, which gives the highest transfer of the closest analogues available, from Table G3 of CSA (2008).
D Values for cows' milk, beef meat and poultry (used for poultry meat and eggs) adopted from Table 9.11 of Garisto et al. (2004), otherwise values for Sn adopted as an analogue.
E Values for cows' milk, beef meat and poultry (used for poultry meat and eggs) adopted from Table 9.11 of Garisto et al. (2004), otherwise values for Se adopted as an analogue.
F Values for cows' milk, beef meat and poultry (used for poultry meat and eggs) adopted from Table 9.11 of Garisto et al. (2004), otherwise values for Th adopted as an analogue.

Table 6.14: Inhalation/Ingestion Absorption Ratios and Fresh Water to Fish Meat Bioaccumulation Factors

Element	Inhalation/Ingestion Absorption Ratios (-)	Notes for Absorption Ratios	Fresh Water to Fish Meat Bioaccumulation Factor, L kg^{-1} fw	Notes for Bioaccumulation Factors
C	0.02	A	5.7E+3	G
Cl	4.00	B	5.0E+1	H
Ni	2.92	A	1.0E+2	G
Se	0.75	A	2.0E+2	G
Sr	0.91	A	2.0E+0	G
Zr	12.51	A	7.0E+0	G
Nb	12.51	A	3.0E+2	G
Mo	0.63	A	4.6E+2	G
Tc	0.75	A	2.0E+1	G
Ag	2.91	A	5.0E+0	G
Sn	24.2	A	3.0E+3	G
I	0	B	6.0E+0	H
Cs	0.63	A	3.5E+3	G
Ir	24.2	C	1.0E+3	I
Pt	24.2	C	1.0E+3	I
Eu	241	A	5.0E+1	G
Pb	24.2	D	3.0E+2	J
Po	0.75	E	1.0E+2	J
Ra	1.44	B	2.0E+1	H
Ac	101	F	1.5E+1	K
Th	101	A	1.0E+2	G
Pa	241	A	1.0E+1	G
U	15	B	3.0E+0	H
Np	11.1	B	2.0E+2	H
Pu	241	A	3.0E+1	G
Am	241	A	3.0E+1	G
Cm	241	A	3.0E+1	G

Notes:

A Values adopted from Table G7 of CSA (2008).
B Highest of the inhalation transfer/ingestion transfer coefficient ratios based on the data recommended in the ECOMatters reviews for milk, meat and poultry (Sheppard et al. 2002, 2004a, 2004b, 2005a and 2005b).
C Value for Hg adopted as an analogue from Table G7 of CSA (2008).
D Sn value adopted as an analogue.
E Se value adopted as an analogue.
F Th value adopted as an analogue.
G Adopted from Table A25a of CSA (2008), unless otherwise stated.
H Based on Table 2 of Sheppard et al. (2006).
I Value for Hg adopted as an analogue from Table A25a of CSA (2008).
J Based on recommendation of National Council on Radiation Protection and Measurements (NCRP) (1996).
K Value recommended in IAEA (2001).

Table 6.15: Other Animal Parameters

Parameter		Reference Value	Note
Dry weight of freshwater fish meat per total fresh weight, kg dw kg^{-1} fw		0.25	A
Isotopic discrimination factor for animal metabolism (-)		0.8	B
Isotopic discrimination factor for aquatic animal metabolism (-)		0.8	C
Mass of stable carbon in freshwater fish, gC kg^{-1} fw		122	D
Water equivalent of the animal product dry matter, L water kg^{-1} dw product	Cows' milk	0.67	E
	Goats' milk	0.67	
	Beef meat	0.8	
	Beef offal	0.8	
	Pork meat	0.9	
	Lamb meat	0.8	
	Poultry meat	0.8	
	Eggs	0.84	
	Deer meat	0.8	
	Rabbit meat	0.8	
Hold-up time between plant exposure to contamination and feeding, days		1	F

Notes:
- A Clause 7.7.4.2 of CSA (2008).
- B Clause 6.9.3.2 of CSA (2008).
- C Clause 7.7.4.4 of CSA (2008).
- D Table 21 of CSA (2008).
- E Clause 6.9.3.2 of CSA (2008), where given; values for lamb, deer and rabbit taken to be the same as for beef and poultry.
- F Clause 6.10.1.3 of CSA (2008).

7. EXPOSURE DATA

7.1 Potential Critical Group

The Normal Evolution Scenario considers potential exposures arising from existing land uses in the area, including farming, fishing, recreation and dwelling. A 'Site Resident' group has been identified for assessment in the scenario, which is exposed via a wide range of pathways associated with the use of the land for farming, fishing, recreation and dwelling (QUINTESSA 2011a). The use of this Site Resident Group allows the relative importance of each exposure pathway to be examined. Potential exposures for groups that might maximize specific pathways (e.g., consumption of large amounts of deer by hunters or large amounts of fish by a fishing group) can be assessed by scaling the results for the Site Resident Group associated with those particular pathways.

Generic physical characteristics of Canadians are provided in Table 7.1, whereas specific data for the Site Resident Group are presented in Table 7.2 and Table 7.3. Ingestion rates for exposures arising from farming, fishing and hunting are presented in Table 7.2, based on the cautious recommendations of CSA (2008), while occupancy rates are given in Table 7.3. Other exposure related parameters are presented in Table 7.4.

CSA (2008) includes a correction factor that accounts for the location of receptors relative to an irrigated field for the purpose of calculating the concentration of volatilized radionuclides in the air. This is conservatively taken to be unity for the current assessment, consistent with Table A22a of CSA (2008).

Table 7.1: Generic Physical Characteristics of Canadians

Parameter	Age Group			Notes
	Infant	Child	Adult	
Inhalation rate, $m^3\ a^{-1}$	2740	7850	8400	A
Skin surface area, m^2	0.72	1.46	2.19	B
Diffusion rate for water wetted skin, $m^3\ a^{-1}\ m^{-2}$	0.105			B

Notes:

A Recommended default inhalation rates from Clause 6.13.3 and Table 17 of CSA (2008), which reflect 95th percentile values.

B Recommended values from Clause 6.16.2.2 and Table 20 of CSA (2008), based on 95th percentile values.

Table 7.2: Ingestion Rates for the Site Resident Group

Parameter		Local Fraction	Age Group			Notes
			Infant	Child	Adult	
Ingestion rates, g d^{-1}						
	Lake fish	1	1.25	4.25	10.2	A
	Stream fish	1	1.25	4.25	10.2	A
	Cows' milk	1	1016	836	727	B
	Goats' milk	1	102	83.6	72.7	C
	Beef	0.44	28.3	75.2	174.6	D
	Beef Offal	0.44	0.87	2.97	7.19	B
	Pork	0.44	8.64	31.1	79.6	B
	Lamb	0.44	0.03	2.12	2.00	B
	Poultry	0.44	12.5	26.9	53.9	B
	Eggs	0.44	23.0	31.1	82.2	B
	Deer	0.1	0.06	0.15	0.34	B
	Rabbit	1	0.14	0.37	0.85	B
	Grain	0.01	161	441	634	B
	Fruit and berries	0.2	181	255	478	B
	Vegetables	0.25	120	311	642	B
	Mushrooms	1	0.45	2.12	4.11	B
	Potatoes	0.25	64.3	173	285	B
	Honey	1	0.94	2.90	5.60	B
Incidental soil ingestion, g dw d^{-1}		-	0.12	0.33	0.33	E
Drinking water, L d^{-1}		-	0.98	1.4	2.3	F

Notes:

A Total fish consumption rate from Table G9c of CSA (2008) is taken to be split equally between fish from Lake Huron and those from the local stream.

B Recommended default dietary intakes from Table G9c of CSA (2008), which reflect the 90th percentile energy intake.

C No generic Canadian data in CSA (2008), therefore taken to be 10% of cows' milk. It is recognized that this increases the energy intake beyond the 90th percentile, but is considered an appropriate cautious assumption that enables the potential exposure pathway to be considered in this assessment.

D As note B, but veal and beef values combined.

E Recommended 95th percentile values from Clause 6.15.2 and Table 18 of CSA (2008).

F 90th percentile rates from Table 19 of CSA (2008) and recommended in Clause 6.15.3.1.

Table 7.3: Occupancies for the Site Resident Group

Activity/Location	Hours:minutes per day			Fractional		
	Adult	Child	Infant	Adult	Child	Infant
Outdoors, on irrigated land [A]	4:00	2:30	1:00	0.167	0.104	0.042
Outdoors, on grazed land [A]	4:00	-	-	0.167	-	-
Outdoors, by Lake Huron [B]	0:30	0:15	-	0.021	0.010	-
Outdoors, by stream [C]	0:15	-	-	0.010	-	-
Taking a bath [D]	0:20	0:20	0:20	0.014	0.014	0.014
Swimming in Lake Huron [E]	0:20	0:20	-	0.014	0.014	-
Indoors, in contaminated area [F]	14:55	20:55	23:00	0.622	0.872	0.958

Notes:

A The adult spends on average 8 hours working outdoors each day, with half of this time being spent managing the animals on grazing land; children and infants spend on average 2.5 hours and 1 hour outdoors, respectively, in the irrigated area.

B Adults spend on average 30 minutes a day by Lake Huron for activities such as fishing, walking or preparing to swim. Children spend about half as much time by Lake Huron as adults, whereas infants spend no time by the lake.

C Adults spend on average 15 minutes a day by the stream, for activities such as fishing.

D All age groups spend 20 minutes bathing every day (Clause 6.16.1.3 of CSA (2008).

E Consistent with Clause 6.16.1.3 of CSA (2008), adults and children spend on average 20 minutes a day swimming in Lake Huron, equivalent to a 1 hour swim every day during the four summer months, whereas infants do not engage in swimming.

F Accounts for all remaining time for children and infants. Includes time taking a bath.

Table 7.4: Other Critical Group Related Parameters

Parameter		Reference Value	Note
Effective dose correction factor to account for the finite size of a bathtub (-)		0.7	A
Building shielding factor for external irradiation from air from gamma-emitting radionuclides (-)	Gamma emitters	0.5	B
	Essentially pure beta emitters	0	
Building shielding factor for external irradiation from the ground (-)	Gamma emitters	0.2	C
	Essentially pure beta emitters	0	
Modifying factor for external irradiation that takes into account ground roughness (-)		0.7	D

Notes:

A Clause 6.16.1.2 of CSA (2008).

B Clause 6.2.5 of CSA (2008) – C-14, Cl-36, Ni-63, Sr-90 and Tc-99 are taken as essentially pure beta emitters.

C Clause 6.14.3 of CSA (2008) – C-14, Cl-36, Ni-63, Sr-90 and Tc-99 are taken as essentially pure beta emitters.

D Clause 6.14.3 of CSA (2008).

7.2 Radionuclides

7.2.1 Human Dose Coefficients

Table 7.5 to Table 7.10 provide data on ingestion, inhalation and external irradiation dose coefficients. Consistent with CSA (2008), dose coefficients for ingestion and inhalation are primarily based on ICRP (1996) whereas those for external irradiation are primarily based on Eckerman and Ryman (1993) (which is the basis for the dose coefficients reported in Eckerman and Leggett 1996, cited by CSA 2008).

A dose coefficient of 2.4E-9 (Sv h^{-1})/(Bq m^{-3}) is recommended for external irradiation and inhalation of Rn-222 gas based on ICRP (1993). It is noted that this value is for adults, but is adopted for all age groups in the absence of age-specific values.

CSA (2008) includes consideration of the equivalent dose to the skin due to external irradiation because in some cases the ratio of the skin dose coefficient to the effective dose coefficient exceeds the ratio of the relevant dose limits for determining release limits (equivalent dose limit to the skin of 50 mSv a^{-1} versus an effective dose limit of 1 mSv a^{-1})[4]. However, the effective dose limit being considered for the postclosure safety assessment is 0.3 mSv a^{-1} for normal exposure situations (Section 3.4.1 of QUINTESSA et al. 2011a), which is lower than that considered for deriving release limits. The equivalent dose limit for the skin is based on deterministic effects and includes an additional safety factor, therefore the same equivalent dose limit for the skin of 50 mSv a^{-1} would apply in the postclosure period. The increased difference between the effective dose limit and the equivalent dose limit for the skin means that the ratio of equivalent dose coefficient to the skin to the effective dose coefficient would need to exceed 167 for pure beta emitters and 100 for gamma emitters. None of the ratios reported in CSA (2008) exceed these values and it is therefore considered that effective dose represents the limiting exposure calculation for the postclosure period and that the equivalent dose to the skin need not be calculated.

Table 7.5: Human Dose Coefficients for Particulate Inhalation, Sv Bq^{-1}

Parent	Infant	Child	Adult	Notes
C-14	6.6E-9	2.8E-9	2.0E-9	B
Cl-36	2.6E-8	1.0E-8	7.3E-9	B
Ni-59	6.2E-10	2.1E-10	1.3E-10	B
Ni-63	1.9E-9	7.0E-10	4.8E-10	B
Se-79	1.3E-8	5.6E-9	1.1E-9	B
Zr-93	3.1E-9	4.1E-9	1.0E-8	B
Sr-90[A]	1.2E-7	5.4E-8	3.8E-8	B
Nb-93m	2.4E-9	8.2E-10	5.1E-10	B
Nb-94	3.7E-8	1.6E-8	1.1E-8	B
Mo-93	1.8E-9	7.9E-10	5.9E-10	B

[4] See Clause 6.2.7 of CSA (2008).

Parent	Infant	Child	Adult	Notes
Tc-99	1.3E-8	5.7E-9	4.0E-9	B
Ag-108m[A]	2.7E-8	1.1E-8	7.4E-9	B
Sn-121m[A]	1.6E-8	6.7E-9	4.7E-9	B
Sn-126[A]	1.0E-7	4.2E-8	2.8E-8	B
I-129	8.6E-8	6.7E-8	3.6E-8	B
Cs-137[A]	5.4E-9	3.7E-9	4.6E-9	B
Ir-192	2.2E-8	9.5E-9	6.6E-9	B
Ir-192m	9.1E-8	4.5E-8	3.9E-8	B
Pt-193	1.6E-10	4.3E-11	2.1E-11	B
Pb-210[A]	4.0E-6	1.6E-6	1.2E-6	B
Po-210	1.1E-5	4.6E-6	3.3E-6	B
Ra-226[A]	1.1E-5	4.9E-6	3.5E-6	B
Ra-228[A]	1.0E-5	4.7E-6	2.6E-6	B
Th-228[A]	1.4E-4	5.9E-5	4.3E-5	B
Th-229[A]	2.3E-4	1.1E-4	8.6E-5	B
Th-230	3.5E-5	1.6E-5	1.4E-5	B
Th-232	5.0E-5	2.6E-5	2.5E-5	B
Ac-227[A]	1.7E-3	7.4E-4	5.7E-4	B
Pa-231	2.3E-4	1.5E-4	1.4E-4	B
Pa-233	1.3E-8	5.5E-9	3.9E-9	B
U-232	2.4E-5	1.1E-5	7.8E-6	B
U-233	1.1E-5	4.9E-6	3.6E-6	B
U-234	1.1E-5	4.8E-6	3.5E-6	B
U-235[A]	1.0E-5	4.3E-6	3.1E-6	B
U-236	1.0E-5	4.5E-6	3.2E-6	B
U-238[A]	9.4E-6	4.0E-6	2.9E-6	B
Np-237	4.0E-5	2.2E-5	2.3E-5	B
Pu-238	7.4E-5	4.4E-5	4.6E-5	B
Pu-239	7.7E-5	4.8E-5	5.0E-5	B
Pu-240	7.7E-5	4.8E-5	5.0E-5	B
Pu-241[A]	9.7E-7	8.3E-7	9.0E-7	B
Pu-242	7.3E-5	4.5E-5	4.8E-5	B
Am-241	6.9E-5	4.0E-5	4.2E-5	B
Am-242m[A]	5.3E-5	3.4E-5	3.7E-5	B
Am-243[A]	6.8E-5	4.0E-5	4.1E-5	B
Cm-242	1.8E-5	7.3E-6	5.2E-6	B
Cm-243	6.1E-5	3.1E-5	3.1E-5	B
Cm-244	5.7E-5	2.7E-5	2.7E-5	B

Notes:

A Includes contribution from short-lived daughters (see Table 3.14).

B Values from ICRP (1996), adopting the recommended default absorption class, where no recommendation is made, then the most conservative (highest) dose coefficient is adopted from the range of absorption classes reported.

Table 7.6: Human Dose Coefficients for Inhalation of Gases

Radionuclide	Inhalation, Sv Bq^{-1}			Notes
	Infant	Child	Adult	
HTO	8.0E-11	3.8E-11	3.0E-11	A
HT	5.3E-15	2.5E-15	2.0E-15	A
C-14 as CO_2	3.8E-11	1.8E-11	1.2E-11	B
C-14 as CH_4	1.6E-11	8.0E-12	5.8E-12	C
Cl-36	2.6E-9	7.1E-10	3.3E-10	D
Se-79	1.3E-8	5.6E-9	1.1E-9	D
I-129	2.0E-7	1.7E-7	9.6E-8	E

Notes:
A Table C1 of CSA (2008).
B Value for C-14 labelled CO_2 from Table C1 of CSA (2008).
C Values for methane based on ICRP (1998), which are increased by a factor of 2, consistent with the dose coefficient for C-14 as CO_2 based on the assumption that long-term retention should be 2% rather than the 1% assumed by the ICRP.
D In the absence of specific data, the recommended value is the inhalation dose coefficient for the fastest available inhalation class in ICRP (1996).
E Value for elemental iodine as a vapour, Table A.3 of ICRP (1996) and consistent with Table C1 of CSA (2008).

Table 7.7: Human Dose Coefficients for Ingestion, Sv Bq^{-1}

Parent	Infant	Child	Adult	Notes
H-3 (HTO)	5.3E-11	2.5E-11	2.0E-11	B
H-3 (OBT)	1.3E-10	6.3E-11	4.6E-11	B
C-14	1.6E-9	8.0E-10	5.8E-10	B
Cl-36	6.3E-9	1.9E-9	9.3E-10	C
Ni-59	3.4E-10	1.1E-10	6.3E-11	C
Ni-63	8.4E-10	2.8E-10	1.5E-10	C
Se-79	2.8E-8	1.4E-8	2.9E-9	C
Zr-93	7.6E-10	5.8E-10	1.1E-9	C
Sr-90[A]	9.3E-8	6.6E-8	3.1E-8	C
Nb-93m	9.1E-10	2.7E-10	1.2E-10	C
Nb-94	9.7E-9	3.4E-9	1.7E-9	C
Mo-93	6.9E-9	4.0E-9	3.1E-9	C
Tc-99	4.8E-9	1.3E-9	6.4E-10	C
Ag-108m[A]	1.1E-8	4.3E-9	2.3E-9	C
Sn-121m[A]	4.0E-9	1.2E-9	5.6E-10	C
Sn-126[A]	3.2E-8	1.1E-8	5.1E-9	C
I-129	2.2E-7	1.9E-7	1.1E-7	C
Cs-137[A]	1.2E-8	1.0E-8	1.3E-8	C

Parent	Infant	Child	Adult	Notes
Ir-192	8.7E-9	2.8E-9	1.4E-9	C
Ir-192m	1.4E-9	5.5E-10	3.1E-10	C
Pt-193	2.4E-10	6.9E-11	3.1E-11	C
Pb-210[A]	3.6E-6	1.9E-6	6.9E-7	C
Po-210	8.8E-6	2.6E-6	1.2E-6	C
Ra-226[A]	9.6E-7	8.0E-7	2.8E-7	C
Ra-228[A]	5.7E-6	3.9E-6	6.9E-7	C
Th-228[A]	1.1E-6	4.3E-7	1.4E-7	C
Th-229[A]	2.4E-6	1.2E-6	6.1E-7	C
Th-230	4.1E-7	2.4E-7	2.1E-7	C
Th-232	4.5E-7	2.9E-7	2.3E-7	C
Ac-227[A]	4.3E-6	2.0E-6	1.2E-6	C
Pa-231	1.3E-6	9.2E-7	7.1E-7	C
Pa-233	6.2E-9	1.9E-9	8.7E-10	C
U-232	8.2E-7	5.7E-7	3.3E-7	C
U-233	1.4E-7	7.8E-8	5.1E-8	C
U-234	1.3E-7	7.4E-8	4.9E-8	C
U-235[A]	1.3E-7	7.2E-8	4.7E-8	C
U-236	1.3E-7	7.0E-8	4.7E-8	C
U-238[A]	1.5E-7	7.5E-8	4.8E-8	C
Np-237	2.1E-7	1.1E-7	1.1E-7	C
Pu-238	4.0E-7	2.4E-7	2.3E-7	C
Pu-239	4.2E-7	2.7E-7	2.5E-7	C
Pu-240	4.2E-7	2.7E-7	2.5E-7	C
Pu-241[A]	5.7E-9	5.1E-9	4.8E-9	C
Pu-242	4.0E-7	2.6E-7	2.4E-7	C
Am-241	3.7E-7	2.2E-7	2.0E-7	C
Am-242m[A]	3.0E-7	2.0E-7	1.9E-7	C
Am-243[A]	3.8E-7	2.2E-7	2.0E-7	C
Cm-242	7.6E-8	2.4E-8	1.2E-8	C
Cm-243	3.3E-7	1.6E-7	1.5E-7	C
Cm-244	2.9E-7	1.4E-7	1.2E-7	C

Notes:

A Includes contribution from short-lived daughters (see Table 4-11).

B Values from Table C.2 of CSA (2008). Note that values for HTO and OBT differ from those presented in ICRP (1996); the values are increased by 10% to apply the calculated doses to soft tissue mass, rather than whole body mass.

C Consistent with Table C.2 of CSA (2008), values from ICRP (1996).

Table 7.8: Human Dose Coefficients for External Irradiation due to Air and Water Immersion

Parents	Air Immersion [B] (Sv a^{-1}) per (Bq m^{-3})		Water Immersion [B] (Sv a^{-1}) per (Bq m^{-3})	
	Adults & Children	Infants [C]	Adults & Children	Infants [C]
H-3	0.0E+0	0.0E+0	[D]	[D]
C-14	8.2E-11	8.2E-11	9.1E-14	9.1E-14
Cl-36	5.2E-9	5.2E-9	6.2E-12	6.2E-12
Ni-59	0.0E+0	0.0E+0	0.0E+0	0.0E+0
Ni-63	0.0E+0	0.0E+0	0.0E+0	0.0E+0
Se-79	1.2E-10	1.2E-10	1.4E-13	1.4E-13
Zr-93	0.0E+0	0.0E+0	0.0E+0	0.0E+0
Sr-90[A]	2.8E-8	2.8E-8	3.5E-11	3.5E-11
Nb-93m	9.6E-11	1.3E-10	2.3E-13	2.9E-13
Nb-94	2.3E-6	3.0E-6	4.9E-9	6.4E-9
Mo-93	5.5E-10	7.1E-10	1.3E-12	1.7E-12
Tc-99	9.1E-10	9.1E-10	9.9E-13	9.9E-13
Ag-108m[A]	2.3E-6	3.0E-6	5.0E-9	6.4E-9
Sn-121m[A]	2.6E-9	3.1E-9	4.5E-12	5.6E-12
Sn-126[A]	2.8E-6	3.7E-6	6.2E-9	8.0E-9
I-129	8.9E-9	1.2E-8	2.1E-11	2.7E-11
Cs-137[A]	8.1E-7	1.0E-6	1.7E-9	2.3E-9
Ir-192	1.1E-6	1.5E-6	2.5E-9	3.2E-9
Ir-192m	2.2E-7	2.8E-7	4.8E-10	6.2E-10
Pt-193	1.3E-11	1.7E-11	3.0E-14	3.9E-14
Pb-210[A]	9.6E-9	1.2E-8	1.3E-11	1.6E-11
Po-210	1.2E-11	1.6E-11	2.7E-14	3.5E-14
Ra-226[A]	2.6E-6	3.3E-6	5.7E-9	7.2E-9
Ra-228[A]	1.4E-6	1.4E-6	3.1E-9	3.1E-9
Th-228[A]	2.4E-6	2.5E-6	5.2E-9	5.4E-9
Th-229[A]	4.4E-7	5.5E-7	9.5E-10	1.2E-9
Th-230	4.7E-10	6.1E-10	1.1E-12	1.4E-12
Th-232	2.3E-10	3.0E-10	5.2E-13	6.7E-13
Ac-227[A]	5.5E-7	6.9E-7	1.2E-9	1.5E-9
Pa-231	5.0E-8	6.4E-8	1.1E-10	1.4E-10
Pa-233	2.7E-7	2.7E-7	5.9E-10	5.9E-10
U-232	3.7E-10	4.8E-10	8.4E-13	1.1E-12
U-233	4.5E-10	5.8E-10	9.9E-13	1.3E-12
U-234	1.9E-10	2.5E-10	4.4E-13	5.7E-13

Parents	Air Immersion [B] ($Sv\ a^{-1}$) per ($Bq\ m^{-3}$)		Water Immersion [B] ($Sv\ a^{-1}$) per ($Bq\ m^{-3}$)	
	Adults & Children	Infants [C]	Adults & Children	Infants [C]
U-235[A]	2.2E-7	2.8E-7	4.8E-10	6.2E-10
U-236	1.2E-10	1.6E-10	2.8E-13	3.6E-13
U-238[A]	5.7E-8	7.1E-8	1.0E-10	1.3E-10
Np-237	2.8E-8	3.6E-8	6.3E-11	8.2E-11
Pu-238	1.1E-10	1.4E-10	2.6E-13	3.4E-13
Pu-239	1.1E-10	1.4E-10	2.5E-13	3.2E-13
Pu-240	1.1E-10	1.4E-10	2.5E-13	3.3E-13
Pu-241[A]	6.1E-12	6.7E-12	1.3E-14	1.5E-14
Pu-242	9.2E-11	1.2E-10	2.1E-13	2.8E-13
Am-241	2.1E-8	2.8E-8	4.9E-11	6.3E-11
Am-242m[A]	2.4E-8	3.0E-8	5.0E-11	6.3E-11
Am-243[A]	2.8E-7	3.0E-7	6.2E-10	6.5E-10
Cm-242	1.3E-10	1.6E-10	3.0E-13	3.8E-13
Cm-243	1.7E-7	2.2E-7	3.7E-10	4.8E-10
Cm-244	1.1E-10	1.4E-10	2.5E-13	3.3E-13

Notes:

A Includes contribution from short-lived daughters (see Table 4-11).

B Values represent the effective dose rate (identified as "e") from the online version of Eckerman and Ryman (1993), which are based on ICRP 60 (ICRP 1991) tissue weighting factors, http://www.ornl.gov/~wlj/fgr12tab.htm (last accessed March 2010). This source is consistent with Eckerman and Leggett (1996), which is cited in CSA (2008).

C Consistent with CSA (2008), the effective dose coefficients for infants were determined by multiplying the adult dose coefficients by 1.3, except for essentially pure beta emitters for which a scaling factor of unity was used.

D Consistent with CSA (2008), the dose rate due to immersion in water is calculated differently for H-3 due to skin absorption.

Table 7.9: Human Dose Coefficients for External Irradiation from Soil

Parents	External Infinite Soil [B] (Sv a^{-1}) per (Bq m^{-3})		External 5 cm Soil [B] (Sv a^{-1}) per (Bq m^{-3})		External 15 cm Soil [B] (Sv a^{-1}) per (Bq m^{-3})	
	Adults & Children	Infants [C]	Adults & Children	Infants [C]	Adults & Children	Infants [C]
H-3	0.0E+0	0.0E+0	0.0E+0	0.0E+0	0.0E+0	0.0E+0
C-14	1.9E-15	1.9E-15	1.7E-15	1.7E-15	1.9E-15	1.9E-15
Cl-36	4.2E-13	4.2E-13	3.1E-13	3.1E-13	4.0E-13	4.0E-13
Ni-59	0.0E+0	0.0E+00	0.0E+0	0.0E+00	0.0E+0	0.0E+00
Ni-63	0.0E+0	0.0E+00	0.0E+0	0.0E+00	0.0E+0	0.0E+00
Se-79	2.6E-15	2.6E-15	2.4E-15	2.4E-15	2.6E-15	2.6E-15
Zr-93	0.0E+0	0.0E+00	0.0E+0	0.0E+00	0.0E+0	0.0E+00
Sr-90[A]	6.9E-12	6.9E-12	5.6E-12	5.6E-12	6.7E-12	6.7E-12
Nb-93m	1.2E-14	1.6E-14	1.2E-14	1.6E-14	1.2E-14	1.6E-14
Nb-94	1.5E-9	2.0E-09	8.6E-10	1.1E-09	1.4E-9	1.8E-09
Mo-93	7.0E-14	9.1E-14	7.0E-14	9.1E-14	7.0E-14	9.1E-14
Tc-99	1.8E-14	1.8E-14	1.6E-14	1.6E-14	1.8E-14	1.8E-14
Ag-108m[A]	1.5E-9	2.0E-09	8.8E-10	1.1E-09	1.4E-9	1.8E-09
Sn-121m[A]	2.6E-13	3.4E-13	2.6E-13	3.3E-13	2.6E-13	3.4E-13
Sn-126[A]	1.9E-9	2.4E-09	1.1E-9	1.4E-09	1.7E-9	2.2E-09
I-129	1.6E-12	2.1E-12	1.6E-12	2.1E-12	1.6E-12	2.1E-12
Cs-137[A]	5.4E-10	7.0E-10	3.1E-10	4.0E-10	4.8E-10	6.3E-10
Ir-192	7.2E-10	9.4E-10	4.4E-10	5.8E-10	6.7E-10	8.7E-10
Ir-192m	1.2E-10	1.5E-10	8.1E-11	1.1E-10	1.1E-10	1.5E-10
Pt-193	1.1E-15	1.4E-15	1.1E-15	1.4E-15	1.1E-15	1.4E-15
Pb-210[A]	1.3E-12	1.5E-12	1.1E-12	1.3E-12	1.2E-12	1.5E-12
Po-210	8.3E-15	1.1E-14	4.6E-15	6.0E-15	7.3E-15	9.5E-15
Ra-226[A]	1.8E-9	2.3E-09	9.5E-10	1.2E-09	1.5E-9	1.9E-09
Ra-228[A]	9.6E-10	9.6E-10	5.2E-10	5.2E-10	8.3E-10	8.3E-10
Th-228[A]	1.6E-9	1.7E-09	8.1E-10	8.5E-10	1.3E-9	1.4E-09
Th-229[A]	2.5E-10	3.1E-10	1.6E-10	2.0E-10	2.3E-10	2.9E-10
Th-230	1.8E-13	2.4E-13	1.5E-13	1.9E-13	1.8E-13	2.3E-13
Th-232	7.7E-14	1.0E-13	6.5E-14	8.4E-14	7.6E-14	9.9E-14
Ac-227[A]	3.2E-10	3.9E-10	2.0E-10	2.6E-10	3.0E-10	3.7E-10
Pa-231	3.0E-11	3.9E-11	1.9E-11	2.5E-11	2.8E-11	3.6E-11
Pa-233	1.6E-10	1.6E-10	1.0E-10	1.0E-10	1.5E-10	1.5E-10

Parents	External Infinite Soil [B] (Sv a^{-1}) per (Bq m^{-3})		External 5 cm Soil [B] (Sv a^{-1}) per (Bq m^{-3})		External 15 cm Soil [B] (Sv a^{-1}) per (Bq m^{-3})	
	Adults & Children	Infants [C]	Adults & Children	Infants [C]	Adults & Children	Infants [C]
U-232	1.3E-13	1.7E-13	1.1E-13	1.4E-13	1.3E-13	1.7E-13
U-233	2.1E-13	2.8E-13	1.5E-13	2.0E-13	2.1E-13	2.7E-13
U-234	5.8E-14	7.5E-14	4.9E-14	6.4E-14	5.8E-14	7.5E-14
U-235[A]	1.2E-10	1.5E-10	8.2E-11	1.0E-10	1.1E-10	1.5E-10
U-236	3.0E-14	3.9E-14	2.6E-14	3.4E-14	3.0E-14	3.9E-14
U-238[A]	2.6E-11	3.2E-11	1.7E-11	2.1E-11	2.4E-11	2.9E-11
Np-237	1.2E-11	1.5E-11	9.3E-12	1.2E-11	1.2E-11	1.5E-11
Pu-238	2.0E-14	2.6E-14	1.8E-14	2.4E-14	2.0E-14	2.5E-14
Pu-239	4.4E-14	5.8E-14	3.2E-14	4.1E-14	4.3E-14	5.5E-14
Pu-240	1.9E-14	2.5E-14	1.8E-14	2.3E-14	1.9E-14	2.5E-14
Pu-241[A]	2.9E-15	3.2E-15	2.1E-15	2.4E-15	2.8E-15	3.1E-15
Pu-242	1.7E-14	2.2E-14	1.6E-14	2.0E-14	1.7E-14	2.2E-14
Am-241	6.3E-12	8.2E-12	5.8E-12	7.6E-12	6.3E-12	8.2E-12
Am-242m[A]	1.0E-11	1.3E-11	7.5E-12	9.4E-12	1.0E-11	1.2E-11
Am-243[A]	1.4E-10	1.4E-10	9.9E-11	1.0E-10	1.3E-10	1.4E-10
Cm-242	2.2E-14	2.8E-14	2.0E-14	2.6E-14	2.1E-14	2.8E-14
Cm-243	9.0E-11	1.2E-10	6.2E-11	8.1E-11	8.7E-11	1.1E-10
Cm-244	1.5E-14	2.0E-14	1.5E-14	2.0E-14	1.5E-14	2.0E-14

Notes:

A Includes contribution from short-lived daughters (see Table 4-11).

B Values represent the effective dose rate (identified as "e") from the online version of Eckerman and Ryman (1993), which are based on ICRP 60 (ICRP 1991) tissue weighting factors, http://www.ornl.gov/~wlj/fgr12tab.htm (accessed March 2010). This source is consistent with Eckerman and Leggett (1996), which is cited in CSA (2008).

C Consistent with CSA (2008), the effective dose coefficients for infants were determined by multiplying the adult dose coefficients by 1.3, except for essentially pure beta emitters for which a scaling factor of unity was used.

Table 7.10: External Dose Coefficients for Adults from a Point Source

Parents	Mean Gamma Energy MeV [B]	External Dose Coefficient from a Point Source [D] Sv h^{-1} Bq^{-1}
H-3	0.0E+0	0.0E+0
C-14	1.9E-6 [C]	2.6E-19
Cl-36	1.5E-4	2.1E-17
Ni-59	3.0E-4 [C]	4.2E-17
Ni-63	0.0E+0	0.0E+0
Se-79	2.2E-6 [C]	3.1E-19
Zr-93	4.8E-9 [C]	6.7E-22
Sr-90[A]	2.0E-3 [C]	2.8E-16
Nb-93m	0.0E+0 [C]	0.0E+0
Nb-94	1.6E+0	2.2E-13
Mo-93	6.6E-6	9.3E-19
Tc-99	1.2E-5 [C]	1.7E-18
Ag-108m[A]	1.6E+0	2.3E-13
Sn-121m[A]	2.7E-5 [C]	3.8E-18
Sn-126[A]	2.0E+0	2.8E-13
I-129	1.3E-6 [C]	1.8E-19
Cs-137[A]	5.6E-1 [C]	7.8E-14
Ir-192	8.1E-1	1.1E-13
Ir-192m	1.6E-1	2.2E-14
Pt-193	0.0E+0	0.0E+0
Pb-210[A]	3.9E-4	5.4E-17
Po-210	8.5E-6 [C]	1.2E-18
Ra-226[A]	1.7E+0	2.4E-13
Ra-228[A]	9.3E-1 [C]	1.3E-13
Th-228[A]	1.5E+0	2.1E-13
Th-229[A]	3.2E-1	4.5E-14
Th-230	3.8E-4	5.3E-17
Th-232	1.7E-4	2.4E-17
Ac-227[A]	3.8E-1	5.4E-14
Pa-231	3.5E-2	4.8E-15
Pa-233	2.0E-1	2.8E-14
U-232	2.5E-4	3.5E-17

Parents	Mean Gamma Energy MeV [B]	External Dose Coefficient from a Point Source [D] Sv h^{-1} Bq^{-1}
U-233	2.7E-4	3.8E-17
U-234	1.2E-4	1.7E-17
U-235[A]	1.6E-1	2.2E-14
U-236	2.3E-5	3.2E-18
U-238[A]	2.5E-2 [C]	3.5E-15
Np-237	2.1E-2	3.0E-15
Pu-238	7.5E-6	1.0E-18
Pu-239	5.0E-5	7.0E-18
Pu-240	7.3E-6	1.0E-18
Pu-241[A]	4.7E-6	6.6E-19
Pu-242	8.1E-6	1.1E-18
Am-241	2.1E-2	3.0E-15
Am-242m[A]	1.6E-2	2.2E-15
Am-243[A]	2.1E-1	3.0E-14
Cm-242	4.8E-6	6.7E-19
Cm-243	1.2E-1	1.7E-14
Cm-244	0.0E+0	0.0E+0

Notes:
It is recognized that more recent decay data exists (e.g., ICRP 2008), however, the use of ICRP (1983) and Browne and Firestone (1986) as the basis for calculating external dose coefficients from a point source is consistent with the basis of the dose coefficients for external irradiation adopted in CSA (2008).

A Includes contribution from short-lived daughters (see Table 4-11).

B Data are preferentially taken from ICRP 38 (ICRP 1983). Photons with individual energies below 50 keV have not been included because the equation used to calculate the dose coefficient from a point source substantially over-estimates the dose below this value, and the contribution to effective dose equivalent, given the existence of other exposure pathways, would in any event be very small. Where ICRP 38 does not record a nuclide as having photon energies above the threshold of 50 keV, Browne and Firestone (1986) was used, as indicated by Note C. This reference includes low intensity internal bremsstrahlung (IB) emissions, which may nevertheless be quite energetic. These IB emissions were not included in ICRP 38.

C Data are taken from Browne and Firestone (1986).

D Dose factors for objects take a distance of 1 m from a point source and are obtained by multiplying the mean gamma energy in MeV by 1.4×10^{-13} Sv h^{-1} per Bq MeV^{-1} (Smith et al. 1988).

7.2.2 Radiological Screening Criteria for Non-human Biota

Potential radiological impacts on non-human biota are assessed based on dose benchmarks developed for assessment of priority substances in relation to discharges of radionuclides from nuclear facilities. Criteria are expressed as No-Effect Concentrations (NECs) in water, sediment, soil and groundwater. These NECs are derived from Estimated No Effect Values (ENEVs) for indicator species, which are based on several compilations as documented in Garisto et al. (2008). The NECs assessment includes consideration of specific indicator species relevant to the ecosystem, such as benthic lake fish (e.g., white sucker), pelagic lake fish (e.g., round whitefish), muskrat, deer and wild turkey. The ENEVs used were the most cautious values provided from several references. The pathway model and information are described in Garisto et al. (2008).

For every indicator species, the radionuclide concentration that corresponds to the ENEV is calculated for each medium (surface water, soil, sediment and groundwater), assuming zero radionuclide concentration in other media. The lowest concentration in each medium from all species is selected as the NEC. The 'Upper estimate' (most cautious) NECs for the Southern Canadian deciduous forest, representative of the Bruce nuclear site, are shown in Table 7.11.

If NECs are exceeded for the Normal Evolution Scenario, an Ecological Risk Assessment should be carried out for each radionuclide that exceeds its criteria, taking uncertainties and potential need for the effect of several radionuclides to be summed, into account.

Table 7.11: No Effect Concentrations for Non-Human Biota for Southern Canadian Deciduous Forest

Radionuclide	Media			
	Groundwater ($Bq\ L^{-1}$)	Soil ($Bq\ kg^{-1}$)	Surface Water ($Bq\ L^{-1}$)	Sediment ($Bq\ kg^{-1}$)
C-14	1.6E+6	3.5E+2	2.4E-1	2.8E+5
Cl-36	3.0E+5	5.0E+0	3.1E+0	4.1E+4
Zr-93	5.9E+6	2.8E+5	1.8E+0	5.0E+6
Nb-94	3.6E+4	1.3E+2	1.6E-2	2.6E+4
Tc-99	8.1E+5	6.0E+1	8.0E-1	3.0E+6
I-129	9.0E+5	1.9E+4	3.2E+0	1.2E+6
Ra-226	5.9E+2	2.8E+2	5.9E-4	9.3E+2
Np-237	5.8E+2	5.0E+1	5.8E-2	1.1E+3
U-238	5.6E+2	4.9E+1	2.3E-2	6.6E+4
Pb-210	1.8E+5	3.7E+3	5.0E+0	6.3E+3
Po-210	5.4E+2	3.0E+1	7.0E-3	1.1E+5

Note:
Based on the most cautious 'Upper Estimate' NECs in Garisto et al. (2008).

7.3 Non-Radioactive Species

Potential impacts from non-radiological contaminants are assessed based on concentrations in environmental media relevant to human health and environmental protection.

The acceptance criteria are provided in Table 7.12, based on federal and provincial guideline concentrations for groundwater, surface water, soil and sediment. Guideline concentrations for groundwater, soil and sediment are provided primarily by Ontario Ministry of the Environment (MoE) (2009), since these are the most conservative. The most conservative guideline concentration values between Ministry of the Environment and Energy (MoEE) (1994) and Canadian Council of Ministers for the Environment (CCME) (2007) are used for surface waters. For several elements of potential interest, no criteria were provided in MoEE (1994), CCME (2007) or MoE (2009). In these cases, the exposure is evaluated based solely on surface water criteria from Sneller et al. (2000), Suter and Tsao (1996), Oregon Department of Environmental Quality (ODEQ) (2001) and CCOHS (2009).

Table 7.12: Environmental Quality Standards for Non-Radioactive Species

Species	Ground-water ($\mu g\ L^{-1}$)	Note	Soil ($\mu g\ g^{-1}$)	Note	Surface Water ($\mu g\ L^{-1}$)	Note	Sediment ($\mu g\ g^{-1}$)	Note
Ag	0.3	A	0.5	A	0.1	H, P	0.5	A
As	13	A	11	A	5	I, P	6	A
B	1700	A	36	A	200	I	-	B
Ba	610	A	210	A	-	B	-	B
Be	0.5	A	2.5	A	11	J	-	B
Br	-	B	-	B	1700	T	-	B
Cd	0.5	A	1	A	0.017	Q	0.6	A
Chlorobenzene	0.01	C	0.01	C	0.0065	K	0.02	C
Chlorophenol	0.2	D	0.1	D	0.2	L	-	B
Co	3.8	A	19	A	0.9	H	50	A
Cr	11	E	67	E	1	M	26	E
Cu	5	A	62	A	1	J	16	A
Dioxins/Furans	1.5E-5	F	7E-6	F	0.3	N	-	-
Gd	-	B	-	B	7.1	U	-	B
Hf	-	B	-	B	4	V	-	B
Hg	0.1	A	0.16	A	0.004	R	0.2	A
I	-	B	-	B	100	I	-	B
Li	-	B	-	B	2500	S	-	B
Mn	-	B	-	B	200	S	-	B
Mo	23	A	2	A	40	I	-	B
Nb	-	B	-	B	600	W	-	B
Ni	14	A	37	A	25	H	16	A
PAH	0.1	G	0.05	G	0.0008	O	0.22	G

Species	Ground-water ($\mu g\ L^{-1}$)	Note	Soil ($\mu g\ g^{-1}$)	Note	Surface Water ($\mu g\ L^{-1}$)	Note	Sediment ($\mu g\ g^{-1}$)	Note
Pb	1.9	A	45	A	1	J	31	A
PCB	0.2	A	0.3	A	0.001	H	0.07	A
Sb	1.5	A	1	A	20	I	-	B
Sc	-	B	-	B	1.8	X	-	B
Se	5	A	1.2	A	1	P	-	B
Sn	-	B	-	B	73	Y	-	B
Sr	-	B	-	B	1500	Y	-	B
Te	-	B	-	B	20	T	-	B
Tl	0.5	A	1.0	A	0.3	I	-	B
U	8.9	A	1.9	A	5	I	-	B
V	3.9	A	86	A	6	I	-	B
W	-	B	-	B	30	I	-	B
Zn	160	A	290	A	20	J	120	A
Zr	-	B	-	B	4	I	-	B

Notes:

A 'Full depth background site condition standard' for Ontario from MoE (2009).
B No value available.
C As note A; values for hexachlorobenzene used.
D As note A; values for trichlorophenol used.
E As note A; values for total chromium used.
F As note A; values represent standard toxic equivalents (TEQ).
G As note A; values for anthracene used.
H Provincial Water Quality Objective (PWQO) for Ontario from MoEE (1994).
I Interim PWQO from MoEE (1994).
J Lowest PWQO/Interim PWQO conservatively adopted from MoEE (1994).
K PWQO for hexachlorobenzene from MoEE (1994).
L PWQO for dichlorophenols from MoEE (1994).
M PWQO for Cr (VI) from MoEE (1994).
N PWQO for dibenzofuran in MoEE (1994).
O Interim PWQO for anthracene in MoEE (1994).
P Freshwater CEQG from CCME (2007).
Q Cadmium interim freshwater CEQG from CCME (2007).
R Interim freshwater CEQG for methylmercury from CCME (2007).
S Irrigation water value from the Canadian Water Quality Guidelines for the Protection of Agricultural Water Uses from CCME (2007).
T Calculated from minimum of Oral rate/mouse LD50s from CCOHS (2009).
U Maximum Permissible Concentration (MPC) for freshwater from Sneller et al. (2000).
V Value for Zr used.
W Lowest available from ODEQ (2001).
X Lowest available MPC for freshwater for all rare earth elements from Sneller et al. (2000).
Y Tier II secondary chronic value from Suter and Tsao (1996).

8. SUMMARY

OPG is proposing to build a Deep Geologic Repository for Low and Intermediate Level Waste near the existing Western Waste Management Facility at the Bruce nuclear site.

A postclosure safety assessment has been carried out to support the development of the safety case for the DGR. The purpose of the dataset developed in this report is to provide a collation of reference information for the assessment of the Normal Evolution Scenario in a clear and well-documented manner. The report includes waste, repository, geosphere, biosphere and exposure data. It is anticipated that the report will be updated and extended for future assessments. The data presented in this report are the reference data for the Normal Evolution Scenario. Data specific to particular calculation cases and for the Disruptive Scenarios are presented in other reports as needed.

The assessment has adopted scientifically informed, physically realistic point values for data that can be justified on the basis of the results of research and investigation. Where there are high levels of uncertainty and/or variability associated with data, conservative but physically plausible assumptions have been adopted to allow the impacts of uncertainties/variability to be bounded. Uncertainties and variability in data for some parameters are accounted for through the use of probability distribution functions (PDFs). The biosphere model adopts a deterministic approach, based on 95^{th} percentile characteristics of the critical group consistent with the guidance from the Canadian Standards Association.

This version of the report reflects new information that is available since the previous data report (Walke et al. 2009). In particular, the following important data updates are highlighted:

- The list of radionuclides and non-radioactive species has been updated in light of new screening calculations (Appendix A);
- The waste data have been updated to take account of the updated characterization and assumptions regarding L&ILW contained in the Reference L&ILW Inventory report (OPG 2010);
- The repository data have been updated to take account of the modified design presented in Chapters 6 and 13 of the Preliminary Safety Report (OPG 2011b);
- The geosphere data have been updated in light of the updated Geosynthesis report (NWMO 2011) and the Descriptive Geosphere Site Model report (INTERA 2011); and
- The biosphere data have been updated to reflect the EIS technical support documents for the DGR (GOLDER 2011a to g; AMEC NSS 2011).

9. REFERENCES

Agg, P.J., A. Arcus, D. Blackwood, P.L. FitzGerald, G.J. Holtom, T.R. Lineham, A. Rosevear and N.R. Smart. 2002. The Gas Generation Programme GAMMON: I. Model Calibration. UK Nirex Report AEAT/ERRA-0307. Harwell, United Kingdom.

Allen, R.G., L.S. Pereira, D. Raes and M. Smith. 1998. Crop evapotranspiration: Guidelines for computing crop water requirements. Food and Agriculture Organization of the United Nations, Irrigation and drainage paper 56. Rome, Italy.

AMEC NSS. 2011. Radiation and Radioactivity Technical Support Document. AMEC NSS Ltd. report for the Nuclear Waste Management Organization DGR-TR-2011-06 R000. Toronto, Canada.

Amiro, B.D. 1992. The Atmosphere Submodel for the Assessment of Canada's Nuclear Fuel Waste Management Concept. AECL Research report AECL-9889. Pinawa, Canada.

Arnedo, D., E.E. Alonso, S. Olivella and E. Romero. 2008. Gas Injection Tests on Sand/bentonite Mixtures in the Laboratory. Experimental Results and Numerical Modelling. Physics and Chemistry of the Earth 33, S237-S247.

ASM. 1987. Metals Handbook, Ninth edition, Volume 13, Corrosion. American Society for Metals International, Metals Park, USA.

ASM. 2003. ASM Handbook, Volume 13A, Corrosion: Fundamentals, Testing, and Protection. American Society for Metals International, Metals Park, USA.

ASM. 2005. ASM Handbook, Volume 13B, Corrosion: Materials. American Society for Metals International, Metals Park, USA.

ASTM. 1999. Standard Practice for Preparing, Cleaning, and Evaluating Corrosion Test Specimens. ASTM Standard G1-03, West Conshohocken, USA.

Baumgartner, P. 2006. Generic Thermal-Mechanical-Hydraulic (THM) Data for Sealing Materials – Volume 1: Soil-Water Relationships. Ontario Power Generation Report OPG 06819-REP-01300-10122-R00. Toronto, Canada.

Baumgartner, P., D. Dilinsky, Y. Ates, R. Read, J. Crosthwaite and D. Dixon. 1996. Engineering for a Disposal Facility Using the In-room Emplacement Method. Atomic Energy of Canada Ltd. Report, AECL-11595, COG-96-223. Chalk River, Canada.

Beletsky, D., J.H. Saylor and D.J. Schwab. 1999. Mean circulation in the Great Lakes. Journal of Great Lakes Research 25, 78-93.

Bennett, E.B. 1988. On the Physical Limnology of Georgian Bay. Hydrobiologia 163 21-34.

Berner, U.R. 1990. A Thermodynamic Description of the Evolution of Pore Water Chemistry and Uranium Speciation during the Degradation of Cement. Technical Report, NTB 90-12. Nagra, Switzerland.

BNFL. 2002. Drigg Post Closure Safety Case. British Nuclear Fuels Ltd.. Sellafield, United Kingdom.

Bowders, J.J., J.E. Loehr, D. Neupane and A. Bouazza. 2001. Asphalt Barriers for Containment. Proceedings of the International Containment & Remediation Technology Conference, June10-13. Orlando, USA.

Browne, E. and R.B. Firestone. 1986. Table of Radioactive Isotopes. J. Wiley and Sons, New York, USA.

Bruce County. 2009. Agriculture. Accessed 20 May 2010 from http://www.brucecounty.on.ca/agriculture.php

Burnol, A., P. Blanc, T. Xu, N. Spycher and E.C. Gaucher. 2006. Uncertainty in the Reactive Transport Model Response to an Alkaline Perturbation in a Clay Formation. Proceedings, TOUGH2 Symposium. Lawrence Berkeley National Laboratory, Berkeley, USA.

Byfors, K. 1987. Influence of Silica Fume and Flyash on Chloride Diffusion and pH Values in Cement Paste. Cement and Concrete Research 17, 115-130.

Calder, N. 2011. Two-Phase Flow Parameters from DGR-2, DGR-3 and DGR-4 Petrophysics Data. Intera Engineering Ltd. report TR-08-33 R0. Ottawa, Canada.

CCOHS. 2009. Registry of Toxic Effects of Chemical Substances. Canadian Center for Occupational Health and Safety http://ccinfoweb.ccohs.ca/rtecs/search.html. Accessed May 2009.

Chisholm, D.H. and N.P. Lee. 2001. Actual and Effective Diffusion Coefficients of Concrete under Marine Exposure Conditions. Proceedings 20th Biennial Conference of the Concrete Institute of Australia, Perth, Australia.

CRC. 2006. Handbook of Chemistry and Physics. 87th edition, Chemical Rubber Company Press. Boca Raton, USA.

CSA. 2008. Guidelines for Calculating Derived Release Limits for Radioactive Material in Airborne and Liquid Effluents for Normal Operations of Nuclear Facilities. Canadian Standards Association, Standard N288.1-08. Toronto, Canada.

CCME. 2007. Canadian Water Quality Guidelines for the Protection of Aquatic Life. Canadian Council of Ministers for the Environment. Winnipeg, Canada.

CPCA. 1995. Design and Control of Concrete Mixtures. 6th Canadian Edition, Canadian Portland Cement Association. Ottawa, Canada.

Davies, P.B. 1991. Evaluation of the Role of Threshold Pressure in Controlling Flow of Waste-generated Gas into Bedded Salt at the Waste Isolation Pilot Plant. Sandia Report SAND 90-3246, Sandia National Laboratory, Albuquerque, USA.

de Waard, C. and U. Lotz. 1993. Prediction of CO_2 corrosion of carbon steel. In CORROSION/1993, NACE International, Houston, USA.

de Waard, C. and D.E. Milliams. 1976. Prediction of carbonic acid corrosion in natural gas pipelines. Ind. Finish. & Surf. Coatings 1976, 24-28.

de Waard, C., U. Lotz and D.E. Milliams. 1991. Predictive model for CO_2 corrosion engineering in wet natural gas pipelines. Corrosion 47, 976-985.

de Waard, C., U. Lotz and A. Dugstad. 1995. Influence of liquid flow velocity on CO_2 corrosion: a semi-empirical model. In CORROSION/1995. NACE International, Houston, USA.

Dixon, D.A., N.A. Chandler and P.M. Thompson. 2001. The Selection of Sealing System Components in AECL's 1994 Environmental Impact Statement. Ontario Power Generation Report OPG 06819-REP-01200-10074-R00. Toronto, Canada.

Dixon, D.A., J.B. Martino and D.P. Onagi. 2009. Enhanced Sealing Project (ESP): Design, Construction, and Instrumentation Plan. Nuclear Waste Management Organization Report APM-REP-01601-0001. Toronto, Canada.

Eckerman, K.F. and J.C. Ryman. 1993. External Exposures to Radionuclides in Air; Water; and Soil. United States Environmental Protection Agency Federal Guidance Report No. 12. Washington, D.C., USA.

Eckerman, K.F. and R.W. Leggett. 1996. DCFPAK: Dose Coefficient Data File Package for Sandia National Laboratory. Oak Ridge National Laboratory Report ORNL/TM-13347, Oak Ridge National Laboratory. Oak Ridge, USA.

Fetter, C.W. 1994. Applied Hydrogeology (Third Edition). Prentice-Hall, Inc. Englewood Cliffs, USA.

Freeze, R.A. and J.A. Cherry. 1979. Groundwater. Prentice Hill, Englewood Cliffs, New Jersey, USA.

Garisto, F., A. D'Andrea, P. Gierszewski and T. Melnyk. 2004. Third Case Study – Reference Data and Codes. Ontario Power Generation Report OPG 06819-REP-01200-10107-R00. Toronto, Canada.

Garisto N.C., F. Cooper and S.L. Fernandes. 2008. No-Effect Concentrations for Screening Assessment of Radiological Impacts on Non-Human Biota. Nuclear Waste Management Organization Report TR-2008-02. Toronto, Canada.

GEOFIRMA. 2011. Postclosure Safety Assessment: Groundwater Modelling. Geofirma Engineering Ltd. report for the Nuclear Waste Management Organization DGR-TR-2011-30 R000. Toronto, Canada.

GEOFIRMA and QUINTESSA. 2011. Postclosure Safety Assessment: Gas Modelling. Geofirma Engineering Ltd. and Quintessa Ltd. report for the Nuclear Waste Management Organization DGR-TR-2011-31 R000. Toronto, Canada.

Gillott, J.W. and T. Quinn. 2003. Strength and Sulfate Resistance of Concrete Made With High Alumina Cement, Type 10 Portland Cement, Type 10 Portland Cement Plus Fly Ash and Type 50 Portland Cement. Cement, Concrete, and Aggregates, 25, 21-27.

GOLDER. 2008a. Bruce New Nuclear Power Plant Project Environmental Assessment: Hydrology and Water Quality Technical Support Document. Golder Associates report for Bruce Power. Tiverton, Canada.

GOLDER. 2008b. Bruce New Nuclear Power Plant Project Environmental Assessment: Environmental Impact Statement. Golder Associates report for Bruce Power. Tiverton, Canada.

GOLDER. 2011a. Hydrology and Surface Water Quality Technical Support Document. Golder Associates report for the Nuclear Waste Management Organization Report DGR-TR-2011-04 R000. Toronto, Canada.

GOLDER. 2011b. Aquatic Environment Technical Support Document. Golder Associates report for the Nuclear Waste Management Organization Report DGR-TR-2011-01 R000. Toronto, Canada.

GOLDER. 2011c. Atmospheric Environment Technical Support Document. Golder Associates report for the Nuclear Waste Management Organization Report DGR-TR-2011-02 R000. Toronto, Canada.

GOLDER. 2011d. Geology Technical Support Document. Golder Associates report for the Nuclear Waste Management Organization Report DGR-TR-2011-03 R000. Toronto, Canada.

GOLDER. 2011e. Aboriginal Interests Technical Support Document. Golder Associates report for the Nuclear Waste Management Organization Report DGR-TR-2011-09 R000. Toronto, Canada.

GOLDER. 2011f. Socio-economic Environment Technical Support Document. Golder Associates report for the Nuclear Waste Management Organization Report DGR-TR-2011-08 R000. Toronto, Canada.

GOLDER. 2011g. Terrestrial Environment Technical Support Document. Golder Associates report for the Nuclear Waste Management Organization Report DGR-TR-2011-05 R000. Toronto, Canada.

Grant, W.D., G.J. Holtom, A. Rosevear and D. Widdowson. 1997. A Review of Environmental Microbiology Relevant to the Disposal of Radioactive Waste in a Deep Underground Repository. UK Nirex Report NSS R329. Harwell, United Kingdom.

Guo, R. 2004. Application of Numerical Simulation in the Tunnel Sealing Experiment. Ontario Power Generation Report OPG 06819-REP-01200-10137-R00. Toronto, Canada.

Harris, S.H., R.L. Smith and J.M. Suflita. 2007. In Situ Hydrogen Consumption Kinetics as an Indicator of Subsurface Microbial Activity. FEMS Microbiology Ecology 60(2), 220–228.

Höglund, L.O. 2001. Project Safe. Modelling of Long-term Concrete Degradation Processes in the Swedish SFR Repository. Swedish Nuclear Fuel and Waste Management Company Report R-01-08. Stockholm, Sweden.

Hurtado, L.D., M.K. Knowles, V.A. Kelley, T.L. Jones, J.B. Ogintz and T.W. Pfeifle. 1997. WIPP Shaft Seal System Parameters Recommended to Support Compliance Calculations. Sandia National Laboratories Report SAND97-1287. Albuquerque, USA.

IAEA. 2001. Generic Models for Use in Assessing the Impact of Discharges of Radioactive Substances to the Environment. International Atomic Energy Agency Safety Report Series No. 19. Vienna, Austria.

IAEA. 2003. The Use of Safety Assessment in the Derivation of Activity Limits for Disposal of Radioactive Waste to Near Surface Facilities. International Atomic Energy Agency TECDOC-1380. Vienna, Austria.

IAEA. 2010. Handbook of Parameter Values for the Prediction of Radionuclide Transfer in Terrestrial and Freshwater Environments. International Atomic Energy Agency Technical Report Series 472. Vienna, Austria.

ICRP. 1983. Radionuclide Transformations: Energy and Intensity of Emissions. International Commission on Radiological Protection Publication 38, Annals of the ICRP 11-13.

ICRP. 1991. 1990 Recommendations of the International Commission on Radiological Protection. International Commission on Radiological Protection Publication 60, Annals of the ICRP 21(1-3).

ICRP. 1993. Protection against Radon-222 at Home and Work. International Commission on Radiological Protection Publication 65, Annals of the ICRP 23(2).

ICRP. 1996. Age-Dependent Doses to Members of the Public from Intakes of Radionuclides: Part 5 – Compilation of Ingestion and Inhalation Dose Coefficients. International Commission on Radiological Protection Publication 72, Annals of the ICRP 26(1).

ICRP. 1998. Radiation Dose to Patients from Radiopharmaceuticals. Addendum to International Commission on Radiological Protection Publication 53, Addendum 1 to ICRP Publication 72, Annals of the ICRP, 28(3).

ICRP. 2008. Nuclear Decay Data for Dosimetric Calculations. International Commission on Radiological Protection Publication 107, Annals of the ICRP 38(3).

INTERA. 2011. Descriptive Geosphere Site Model, Deep Geologic Repository Bruce Site. Intera Engineering Ltd. report for the Nuclear Waste Management Organization DGR-TR-2011-24 R000. Toronto, Canada.

JAEA. 2007. Second Progress Report on Research and Development for TRU Waste Disposal in Japan: Repository Design, Safety Assessment and Means of Implementation in the Generic Phase. Japan Atomic Energy Agency Report JAEA-Review 2007-010, FEPC TRU-TR2-2007-01, Tokai-mura, Japan.

JNC. 2000. H12: Project to Establish the Scientific and Technical Basis for HLW in Japan. Supporting Report 3: Safety Assessment of the Geological Disposal System. Japan Nuclear Cycle Development Institute Report TN1410 2000-004, Tokai-mura, Japan.

Karnland, O., S. Olsson and U. Nilsson. 2006. Mineralogy and Sealing Properties of Various Bentonites and Smectite-rich Clay Materials. Swedish Nuclear Fuel and Waste Management Company Report R-06-30. Stockholm, Sweden.

Karnland, O., U. Nilsson, H. Weber and P. Wersin. 2008. Sealing Ability of Wyoming Bentonite Pellets Foreseen as Buffer Material – Laboratory Results. Physics and Chemistry of the Earth, Parts A/B/C 33(1), S472-S475.

Karlsson, F., M. Lindgren, K. Skagius, M. Wiborgh and I. Engkvist. 1999. Evolution of Geochemical Conditions in SFL 3-5, SKB Report R-99-15 Swedish Nuclear Fuel and Waste Management Company, Stockholm, Sweden.

King, F. 2008. Corrosion of Carbon Steel under Anaerobic Conditions in a Repository for SF and HLW in Opalinus Clay. Nagra Technical Report NTB 08-12. Wettingen, Switzerland.

Konecny, A.P. and B.P. Tikalsky. 2010. Reliability of Reinforced Concrete Bridge Decks with Respect to ingress of Chlorides. ASRANet-2010, 5th International ASRANet Conference, Edinburgh, United Kingdom.

Lanyon, G.W., P. Marschall, M. Fukaya, J. Croise, S. Yamamoto and G. Mayer. 2001. Laboratory Data Compilation Report. Nagra Project Report NBP-00-20. Wettingen, Switzerland.

Leygraf, C. and T.E. Graedel. 2000. Atmospheric Corrosion. Wiley Interscience. New York, USA.

Limer, L.M.C., P.R. Maul and M.C. Thorne. 2008. A Soil-Plant Model for the Latera Site. Quintessa Ltd. report to the UK Department of Energy and Climate Change QRS-1320B-2. Henley-on-Thames, United Kingdom.

Lothenbach B., T. Matschei, G. Moschner and F.P. Glasser. 2008. Thermodynamic Modelling of the Effect of Temperature on the Hydration and Porosity of Portland Cement. Cement and Concrete Research 38 (1), 1-18.

McCormick, M.J. and D.J. Schwab. 2008. Observations of Currents in Saginaw Bay, Lake Huron. Aquatic Ecosystem Health and Management 11, 182-189.

Metcalfe, R. and C. Walker (eds). 2004. Proceedings of the International Workshop on Bentonite-Cement Interaction in Repository Environments, Tokyo, Japan, 14th – 16th April 2004. NUMO report NUMO-TR-04-05.

Mihara M. and K. Torii. 2009. Study on Pore Structure and Diffusion Coefficient of Chloride Ion in Hardened Low-alkaline Cement. Japan Atomic Energy Agency Research Report 2008-109, Tokai-mura, Japan.

Mishra, S. 2002. Assigning Probability Distributions to Input Parameters of Performance Assessment Models. Swedish Nuclear Fuel and Waste Management Company (SKB) Technical Report TR-02-11. Stockholm, Sweden.

MoE. 2009. Soil, Ground Water and Sediment Standards for Use Under Part XV.1 of the Environmental Protection Act. Ontario Ministry of the Environment. Toronto, Canada.

MoEE. 1994. Provincial Water Quality Objectives. Policies Guidelines of the Ministry of Environment and Energy, Ontario. Toronto, Canada.

Mölder, M. 1997. Parameterization of exchange processes over a barley field. Boundary-Layer Meteorology, 84(3), 341-361.

Monlouis-Bonnaire, J.P., J. Verdier and B. Perrin. 2004. Prediction of the Relative Permeability to Gas Flow of Cement-based Materials. Cement and Concrete Research 34, 737-744.

NAGRA. 1994. Report on Long-Term Safety of the L/ILW Repository at the Wellenberg Site. Nagra Report NTB 94-06. Wettingen, Switzerland.

NAGRA. 2002. Project Opalinus Clay: Models, Codes and Data for Safety Assessment. Nagra Technical Report TR-02-06. Wettingen, Switzerland.

NAGRA. 2004. Effects of Post-disposal Gas Generation in a Repository for Spent Fuel, High-level Waste and Long-lived Intermediate Level Waste Sited in Opalinus Clay. Nagra Technical Report 04-06. Wettingen, Switzerland.

NAGRA. 2008. Effects of Post-disposal Gas Generation in a Repository for Low- and Intermediate-level Waste sited in the Opalinus Clay of Northern Switzerland. Nagra Technical Report TR-08-07. Wettingen, Switzerland.

Nakayama, S., Y. Lida, T. Nagano and T. Akimoto. 2003. Leaching Behaviour of a Simulated Bituminised Radioactive Waste Form under Deep Geological Conditions. Journal of Nuclear Science and Technology 40(4), 227–237.

NCRP. 1996. Screening Models for Releases of Radionuclides to Atmosphere, Surface Water, and Ground. National Council on Radiation Protection and Measurements Report Number 123. Bethesda, USA.

NDGC. 2010. Bathymetry of Lake Huron. National Geophysical Data Center. Accessed: April 2010. http://www.ngdc.noaa.gov/mgg/greatlakes/huron.html.

NIREX. 2003. Generic Repository Studies: Generic Post-closure Performance Assessment. UK Nirex Report N/080. Harwell, United Kingdom.

Norris, S. 2008. Uncertainties Associated with Modelling the Consequences of Gas. Deliverable (D-N°: D2.2.B.2), PAMINA (Performance Assessment Methodologies in Application to Guide the Development of the Safety Case), European Commission Sixth Framework Programme. Brussels, Belgium.

NWMO. 2010a. L&ILW DGR Project Data Clearance Form: Design Information for Postclosure Safety Assessment. Nuclear Waste Management Organization. Filing Number DGR-REF-01929-23483. September 2010. Toronto, Canada.

NWMO. 2010b. L&ILW DGR Project Data Clearance Form: Design Information for Postclosure Safety Assessment. Nuclear Waste Management Organization. Filing Number DGR–REF-01929-23736. December 2010. Toronto, Canada.

NWMO. 2011. Geosynthesis. Nuclear Waste Management Organization Report DGR-TR-2011-11 R000. Toronto, Canada.

Olivella, S. and E. Alonso. 2008. Gas Flow through Clay Barriers. Geotechnique 58(3), 157-176.

ODEQ. 2001. Guidance Ecological Risk Assessments, Levels I, II, III and IV: Level II Screening Level Values. Oregon Department of Environmental Quality, Portland, USA.

OPG. 2005a. Western Waste Management Facility Refurbishment Waste Storage Project: Environmental Assessment Study Report. Ontario Power Generation Report OPG 01098-REP-07701-00002 R01. Toronto, Canada.

OPG. 2005b. Project Description. Deep Geologic Repository for Low and Intermediate Level Radioactive Waste. Ontario Power Generation Report OPG 00216-REP-03902.07-00001. Toronto, Canada.

OPG. 2010. Reference Low and Intermediate Level Waste Inventory for the Deep Geologic Repository. Ontario Power Generation report 00216-REP-03902-00003-R003. Toronto, Canada.

OPG. 2011a. OPG's Deep Geologic Repository for Low and Intermediate Level Waste: Environmental Impact Statement Ontario Power Generation Report 00216-REP-07701-00001 R000. Toronto, Canada.

OPG. 2011b. OPG's Deep Geologic Repository for Low and Intermediate Level Waste: Preliminary Safety Report. Ontario Power Generation Report 00216-SR-01320-00001 R000. Toronto, Canada.

Pedersen, K. 2000. Microbial Processes in Radioactive Waste Disposal. Swedish Nuclear Fuel and Waste Management Company Technical Report TR-00-04. Stockholm, Sweden.

Pehme, P. and M. Melaney. 2010. Borehole Geophysical Logging in DGR-3 and DGR-4. Intera Engineering Ltd. Report TR-08-15 R1. Ottawa, Canada.

Pettersson, M. and M. Elert. 2001. Characterisation of Bitumenised Waste in SFR1. Swedish Nuclear Fuel and Waste Management Company Report R-01-26. Stockholm, Sweden.

Pruess, K. 1991. EOS7, An Equation of State Module for the TOUGH2 Simulator for Two-Phase Flow of Water and Air. Lawrence Berkeley Laboratory Report LBL-31114. Berkeley, USA.

QUINTESSA. 2011a. Postclosure Safety Assessment: Analysis of the Normal Evolution Scenario. Quintessa Ltd. report for the Nuclear Waste Management Organization DGR-TR-2011-26 R000. Toronto, Canada.

QUINTESSA. 2011b. Postclosure Safety Assessment: System and Its Evolution. Quintessa Ltd. report for the Nuclear Waste Management Organization NWMO DGR-TR-2011-28 R000. Toronto, Canada.

QUINTESSA and SENES. 2011. Postclosure Safety Assessment: Analysis of Human Intrusion and Other Disruptive Scenarios. Quintessa Ltd. and SENES Consultants Ltd. report for the Nuclear Waste Management Organization DGR-TR-2011-27 R000. Toronto, Canada.

QUINTESSA, GEOFIRMA and SENES. 2011a. Postclosure Safety Assessment Report. Quintessa Ltd., Geofirma Engineering Ltd. and SENES Consultants Ltd. report for the Nuclear Waste Management Organization DGR-TR-2011-25 R000. Toronto, Canada.

QUINTESSA, SENES and GEOFIRMA. 2011b. Postclosure Safety Assessment: Features, Events and Processes. Quintessa Ltd., SENES Consultants Ltd. and Geofirma Engineering Ltd. report for the Nuclear Waste Management Organization NWMO DGR-TR-2011-29 R000. Toronto, Canada.

Rickard, D. 1995. Kinetics of FeS precipitation: Part 1. Competing reaction mechanisms. Geochimica et Cosmochimica Acta 59, 4367-4379.

Riggare, P. and C. Johansson. 2001. Project SAFE – Low and Intermediate Level Waste in SFR-1. Swedish Nuclear Fuel and Waste Management Company Report R-01-03. Stockholm, Sweden.

Rittmann, B.E. and P.L. McCarty. 2001. Environmental Biotechnology: Principles and Applications. McGraw –Hill Higher Education. New York, USA.

Russell, S.B. and G.R. Simmons. 2003. Engineered Barrier System for a Deep Geologic Repository in Canada. Proceedings, International High Level Radioactive Waste Management Conference. Las Vegas, USA.

SANDIA. 1996. Waste Isolation Pilot Plant Shaft Sealing System Compliance Submittal Design Report Volume 1 of 2: Main Report Appendices A, B, C, and D. SAND96-1326/1, Sandia National Laboratory. Albuquerque, USA.

Savage, D. and M.J. Stenhouse. 2002. SFR Vault Database. Swedish Nuclear Power Inspectorate Report 02:53. Stockholm, Sweden.

Savage, D., R. Arthur, C. Watson and J. Wilson. 2010. An Evaluation of Models of Bentonite Pore Water Evolution. SSM Technical Report 2010-12. Swedish Radiation Safety Authority. Stockholm, Sweden.

Schertzer, W.M., R.A. Assel, D. Beletsky, T.E. Croley, B.M. Lofgren, J.H. Saylor and D.J. Schwab. 2008. Lake Huron Climatology, Inter-lake Exchange and Mean Circulation. Aquatic Ecosystem Health and Management 11, 144-152.

Senger, R. and P. Marschall. 2008. Task Force on EBS/Gas Transport in Buffer Material. Nagra Report NAB-08-24. Wettingen, Switzerland.

Senger, R., B. Lanyon, P. Marschall, S. Vomvoris and K. Ando. 2003. TOUGH2/iTOUGH2 Modeling in Support of the Gas Migration Test (GMT) at the Grimsel Test Site (Switzerland). Proceedings, TOUGH2 Symposium. Lawrence Berkeley National Laboratory, Berkeley USA.

Sheppard, M.I. and D.H. Thibault. 1990. Default Soil Solid/Liquid Partition Coefficients, Kds, for Four Major Soil types: A Compendium. Health Physics 59(4), 471-482.

Sheppard, M.I., S.C. Sheppard and B. Sanipelli. 2002. Recommended Biosphere Model Values for Iodine. Ontario Power Generation Report OPG 06189-REP-01200-10090-R00. Toronto, Canada.

Sheppard, M.I., S.C. Sheppard and B. Sanipelli. 2004a. Recommended Biosphere Model Values for Chlorine. Ontario Power Generation Report OPG 06189-REP-01200-10119-R00. Toronto, Canada.

Sheppard, M.I., S.C. Sheppard and B. Sanipelli. 2004b. Recommended Biosphere Model Values for Neptunium. Ontario Power Generation Report OPG 06189-REP-01200-10120-R00. Toronto, Canada.

Sheppard, M.I., S.C. Sheppard and B. Sanipelli. 2005a. Recommended Biosphere Model Values for Uranium. Ontario Power Generation Report OPG 06189-REP-01200-10088-R00. Toronto, Canada.

Sheppard, M.I., J.C. Tait, B. Sanipelli and S.C. Sheppard. 2005b. Recommended Biosphere Model Values for Radium and Radon. Ontario Power Generation Report OPG 06189-REP-01200-10144-R00. Toronto, Canada.

Sheppard, S.C. 2003. Transfer Parameters – Are On-Site Data Really Better? International Symposium on Radioecology and Environmental Dosimetry. Rokkasho, Japan.

Sheppard, S.C., M.I. Sheppard, J.C. Tait and B.L. Sanipelli. 2006. Revision and meta-analysis of selected biosphere parameter values for chlorine, iodine, neptunium, radium, radon and uranium. Journal of Environmental Radioactivity 89, 115-137.

Sheppard, S., J. Long and B. Sanipelli. 2009. Field Measurements of the Transfer Factors for Iodine and Other Trace Elements. Nuclear Waste Management Organization Report TR-2009-35. Toronto, Canada.

Shreir, L.L., R.A. Jarman and G.T. Burstein. 1993. Corrosion. Volume 1 Metal/Environment Reactions, 3rd Edition. Butterworth-Heinemann. Oxford, United Kingdom.

Sly, P.G. and M. Munawar. 1988. Great Lake Manitoulin: Georgian Bay and the North Channel. Hydrobiologia 163, 1-19.

SKB. 2008. Safety Analysis SFR 1. Long-term Safety. Swedish Nuclear Fuel and Waste Management Company Report R-08-130. Stockholm, Sweden.

Smith, G.M., H.S. Fearn, K.R. Smith, J.P. Davis and R. Klos. 1988. Assessment of the Radiological Impact of Disposal of Solid Radioactive Waste at Drigg. National Radiological Protection Board Memorandum NRPB-M148. Chilton, United Kingdom.

Sneller, F.E.C., D.F. Kalf, L. Weltje and A.P.Van Wezel. 2000. Maximum Permissible Concentrations and Negligible Concentrations for Rare Earth Elements (REEs). Netherlands National Institute of Public Health and the Environment, RIVM Report 601501011. Bilthoven, The Netherlands.

Soffe, R.J. (ed.). 2003. Primrose McConnell's: The Agricultural Notebook. Blackwell Publishing. Oxford, United Kingdom.

Suter, G.W. and C.L. Tsao. 1996. Toxicological Benchmarks for Screening Contaminants of Concern for Effects on Aquatic Biota. Oak Ridge National Laboratory report prepared for the US DOE, ORNL ES/ER/TM-96/R2. Oak Ridge, USA.

Testa, S.M. 1995. Chemical Aspects of Cold-Mix Asphalt incorporating Contaminated Soil. Journal of Soil Contamination 4(2), 191-207.

Thorne, M.C. and J. MacKenzie. 2005. Treatment of Waste-derived Gas in the Biosphere in Nirex Safety and Performance Assessments. Quintessa Ltd. report to United Kingdom Nirex Ltd. QRS-1248A-1. Henley-on-Thames, United Kingdom.

USEPA. 2008. Lake Huron: Physical and Environmental Features of the Lake Huron Basin. United States Environmental Protection Agency. Accessed: May 6, 2010. Last Updated: October 1, 2008. http://www.epa.gov/glnpo/huron.html.

Walke, R., A. Bath, A. Bond, N. Calder, P. Humphreys, F. King, R. Little, R. Metcalfe, J. Penfold, J. Rees, D. Savage, G. Towler and R. Walsh. 2009. Postclosure Safety Assessment (V1): Data. Nuclear Waste Management Organization Report DGR-TR-2009-08-R0. Toronto, Canada.

Walsh, R. 2011. Compilation and Consolidation of Field and Laboratory Data for Hydrogeological Properties. Intera Engineering Ltd. report TR-08-10 R0. Ottawa, Canada.

WIPP. 2009. Waste Isolation Pilot Plant Hazardous Waste Facility Permit Renewal Application September 2009: Appendix A of Appendix I2, Material Specification Shaft Sealing System Compliance Submittal Design Report. Waste Isolation Pilot Plant, U.S. Department of Energy, Carlsbad, USA.

Yim, M.S. and S. Simonson. 1997. Technical Issues and Low Level Waste Performance Assessment: ^{14}C in Disposal Facilities. EPRI Report TR-107995. Palo Alto, USA.

10. ABBREVIATIONS AND ACRONYMS

AECL	Atomic Energy of Canada Limited
ALW	Active Liquid Waste
CCME	Canadian Council of Ministers for the Environment
CCOHS	Canadian Center for Occupational Health and Safety
CRC	Chemical Rubber Company
CSA	Canadian Standards Association
DGR	Deep Geologic Repository
DGSM	Descriptive Geological Site Model
DRL	Derived Release Limits
EA	Environmental Assessment
EDZ	Excavation Damaged Zone
EdZ	Excavation disturbed Zone
EIS	Environmental Impact Statement
EIZ	Excavation Influence Zone
EMDD	Effective Montmorillonite Dry Density
ENEV	Estimated No Effect Values
GBI	Geosphere Biosphere Interface
GM	Geometric Mean
GSD	Geometric Standard Deviation
HDZ	Highly Damaged Zone
IAEA	International Atomic Energy Agency
ICRP	International Commission on Radiological Protection
ILW	Intermediate Level Waste
IX	Ion Exchange
L&ILW	Low and Intermediate Level Waste
LHHPC	Low Heat, High Performance Cement
LLW	Low Level Waste

MoE	Ontario Ministry of the Environment
MoEE	Ministry of Environment and Energy, Ontario
NCRP	National Council on Radiation Protection
NEC	No-Effect Concentration
NWMO	Nuclear Waste Management Organization
ODEQ	Oregon Department of Environmental Quality
OPC	Ordinary Portland Cement
OPG	Ontario Power Generation
PDF	Probability Distribution Function
PHT	Primary Heat Transport
PSR	Preliminary Safety Report
SA	Safety Assessment
TDS	Total Dissolved Solids
T-H-E	Tile Hole Equivalent
WIPP	Waste Isolation Pilot Plant
WWMF	Western Waste Management Facility

APPENDICES

THIS PAGE HAS BEEN LEFT BLANK INTENTIONALLY

APPENDIX A: SELECTION OF CONTAMINANTS FOR ASSESSMENT

A.1 INTRODUCTION

The purpose of this appendix is to present the screening calculations that have been used to identify the list of radioactive and non-radioactive species for consideration in the current safety assessment.

The appendix is structured as follows:

- Appendix A.2 defines the screening approach;
- Appendices A.3 and A.4 describe the implementation of the screening methodology for radioactive and non-radioactive contaminants respectively; and
- Appendix A.5 discusses the results of the screening in comparison with screened lists produced for other assessments.

A.2 SCREENING METHODOLOGY

This section defines the basis for the screening calculations (Appendix A.2.1) and summarizes the approach adopted (Appendix A.2.2).

A.2.1 Basis for Defining a Screening Methodology

The main aims for the DGR screening methodology are as follows.

- The results from applying the screening methodology should be conservative, in the sense that the species screened from further consideration will clearly give rise to negligible risks.
- The methodology should consider all the assessment pathways in the assessment, in this case the groundwater and gas pathways and human intrusion as routes for the release of radioactive and non-radioactive species to humans.
- Screening should be seen as the first part of a three-stage assessment process, with the second being the mainline assessment of all screened-in species, and the third comprising more detailed calculations for those species, if any, that give rise to results around or above regulatory limits and targets.
- The methodology should be straightforward to implement in terms of both data requirements and calculations. There is need to avoid straying into the area of mainline assessments.
- The conservatism of the methodology and its application should be straightforward to communicate both to stakeholders in the DGR project and to the wider public.

A.2.2 The Screening Approach Adopted

The approach adopted for screening potential radiological and non-radiological impacts of disposed species are described in the following sub-sections.

A.2.2.1 Radionuclide Screening

First, radionuclides are screened by the definition of a minimum period for radioactive decay before radioactive species could be released through assessment pathways. For screening purposes, we assume a reference period of 100 years of institutional control for the DGR which is a cautious value. Societal memory and markers would last at least this long. Furthermore, the slow rate of resaturation of the repository would also prevent radionuclides from leaving for at least 100 years following repository closure. This timescale is also applied to the gas

pathway on the basis that any radioactive and toxic gases would be detected during institutional control and remedial measures would be taken.

The screening methodology for radionuclides is therefore as follows.

1. Radionuclides with a half-life of less than one day are screened out, but their contribution to dose rates for longer-lived parent radionuclides is conservatively accounted for by assuming that they are present in secular equilibrium.
2. Radionuclides with half-lives greater than a year are included, together with any progeny that have a half-life greater than a day.
3. For the *groundwater pathway*, radionuclides are screened out on the basis of potential dose rate from consumption of contaminated groundwater as drinking water once any period of institutional control has come to an end. The concentration in groundwater is derived on a conservative basis. The potential dose rates are compared against the 0.3 mSv a^{-1} criterion, plus an additional safety factor of 10 to reflect the fact that more than one radionuclide may contribute to the dose rate at any one time.
4. For the *gas pathway*, potentially gaseous radionuclides are screened through a conservatively derived release scenario commencing once any period of institutional control has come to an end. The potential dose rates are compared against the 0.3 mSv a^{-1} criterion, plus an additional safety factor of 10 to reflect the fact that more than one radionuclide may contribute to the dose rate at any one time.
5. For the *human intrusion scenario*, radionuclides are screened through consideration of potential exposure of an intruder arising from a conservatively derived borehole intrusion scenario which may occur once any period of institutional control has come to an end. The potential dose rates are compared against the 1 mSv a^{-1} criterion, with a safety factor of 10 to reflect the fact that more than one radionuclide may contribute to the dose rate at any one time.

A.2.2.2 Screening Non-Radioactive Species

The screening methodology for non-radioactive species is as follows.

1. Elements that are considered ubiquitous in terms of concentrations in the geosphere, and not notably hazardous, are eliminated. Also, the screening assessment does not consider container materials (mostly steel, concrete and other standard materials), and standard waste materials like paper, wood and plastics that are commonly put into landfills without requiring any special treatment for toxicity.
2. For the *groundwater pathway*, screening of non-radioactive species is on the basis of conservatively derived groundwater concentrations. These can be considered conservative because in practice, sorption may occur in the near field, and contaminated water leaving the repository will be diluted as it mixes with water in the geosphere. In addition, the screening levels are taken to be 10% of the environmental quality standards employed.
3. The chemical substances comprising the waste to be stored in the DGR are unlikely to give rise to significant quantities of toxic gas, and a screening methodology relevant to the *gas pathway* is not therefore required.
4. For the assessment of *human intrusion*, a simplified analysis is adopted, based on the removal of waste material via an intruding borehole and the resuspension/distribution of this material over a relatively small area at the surface. The resulting concentrations are compared against environmental quality standards for air and soil. This methodology is conservative in the sense that the probability of human intrusion is excluded from the

calculation. In addition, the screening levels are taken to be 10% of the environmental quality standards.

A.3 RADIONUCLIDE SCREENING

A.3.1 Radionuclides and Chains

The initial screening of radionuclides by half-life results in 167 radionuclides that need to be explicitly represented in the screening calculations.

ICRP (2008) has been used as the basis for the half-lives and decay schemes considered. Garisto (2002) has been used as the default data base for scaling factors and dose coefficients. The potential for small inconsistencies between the ICRP (2008) decay schemes and those used in Garisto (2002) for determining dose coefficients is recognized, but considered acceptable for the purpose of the screening calculations.

The results are presented for each disposed radionuclide, including the contributions from all of its daughters. For example, the results for U-238 reflect the U-238 disposed plus the contribution from the ingrown Th-234, U-234, Th-230, Ra-226, etc. Similarly, the results for Th-234 reflect the Th-234 disposed plus the contribution from the ingrown U-234, Th-230, Ra-226, etc.

A.3.2 Radionuclide Inventories

Simple conservative screening calculations for the groundwater, gas and human intrusion scenarios are adopted for further screening of the 167 radionuclides. The different scenarios require different types of inventory information:

- The groundwater pathway calculations need the total inventory of all radionuclides in the waste;
- The gas pathway calculations need the total inventory of potentially gaseous radionuclides in the waste; and
- The human intrusion calculations need the highest concentration of radionuclides in the waste.

The inventory information for each radionuclide is adopted from the Reference L&ILW Inventory report (OPG 2010). This inventory report provides information on radionuclides that are measured or calculated, based on their potential importance during handling or emplacement. However it does not provide values for all potential radionuclides.

For completeness in postclosure screening, radionuclides inventories are estimated here for all 167 radionuclides with half-lives longer than 1 year. Where there is no data in the Reference L&ILW Inventory report (at 2062), then the inventory is assumed to be proportional to the uranium content at 2062, at the same ratio as used in assessments for used fuel (Garisto 2002). The total mass of uranium is calculated from the radionuclide inventory reported in OPG (2010)[5].

[5] Note that the amount of uranium used as the basis for the scaling excludes the non-irradiated U-238 in the non-processible boxed waste reported in OPG (2010)

Note that the following waste streams have no or very low inventories of uranium isotopes, such that no scaling was applied: non-processible drums; moderator resins; irradiated core components; and retube end fittings.

Waste volumes and waste densities are taken from OPG (2010). Assumptions are required to provide densities for some wastes, so the full list of densities is given in Table A.1 for clarity.

Table A.1: Waste Stream Densities

Waste Stream	Dry Bulk Density kg m^{-3}
Bottom Ash (Old)	680
Baghouse Ash (Old)	340
Bottom Ash (New)	550 [a]
Baghouse Ash (New)	390 [a]
Compact Bales	770
Box Compacted	1000
Non-processible Boxed	230
Non-processible Other	1070 [b]
Non-processible Drummed	500
Non-processible (Combined)	310 [c]
Heat Exchangers	670
Feeder Pipes	670 [d]
LLW & ALW Resins	750
ALW Sludge	1120
Moderator IX Resin	850
PHT IX Resin	850
Miscellaneous IX Resin	850
CANDECON Resin	850
IX columns	880 [e]
Irradiated core components	880
Filters and filter elements	880
Retube Wastes (Pressure Tubes)	2290
Retube Wastes (End Fittings)	970
Retube Wastes (Calandria Tubes)	1270 [f]
Retube Wastes (Calandria Tube Inserts)	580 [f]
Steam Generators	1730 [g]

Note:
Data from OPG (2010).

a Density of 'new' ash used in screening radionuclides, where the inventory data does not distinguish between old and new ash streams.
b Calculated based on the volumes of heat exchangers and encapsulated tile hole liners that contribute to this waste stream.
c Needed for screening non-radioactive species and calculated based on drummed, boxed, other non-processible waste and feeder pipes; i.e., excluding heat exchangers, which are accounted for separately for the screening of non-radioactive contaminants.
d Based on density of heat exchangers.
e Taken to be the same as filters and filter elements.
f Calculated based on total elemental mass and net volume.
g Value for grouted steam generators.

A.3.3 Screening Calculations

The approaches adopted for the screening calculations are given in the following subsections for the groundwater, gas and human intrusion scenarios.

A.3.3.1 Groundwater Calculations

Calculations for the groundwater pathway are based on the simple assumption that an individual is able to drink contaminated groundwater 100 years after closure. The concentration of radionuclides in the groundwater is conservatively based on the total radionuclide inventory in the repository. The calculation assumes that all of the void-space in the waste packages, containers and emplacement rooms is filled with water, despite the estimated resaturation period of hundreds of thousands of years. The groundwater concentration is then derived assuming that the total inventory is dissolved in the water, i.e., ignoring sorption and solubility limitations, and ignoring the dilution with uncontaminated groundwater that would occur in transport from the DGR to the accessible environment and that which would be required to reduce the salinity of the water to a level that would be acceptable for drinking[6].

The groundwater concentrations, C_{GW} (Bq m^{-3}), are derived using:

$$C_{GW} = \frac{I}{V_R} \tag{A.1}$$

where I (Bq) is the decayed radionuclide inventory in the repository and V_R is the total available void space (i.e., including waste, packaging, overpack and emplacement room void volumes) (m^3).

The annual individual effective dose rate, D_{GW} (Sv a^{-1}), is calculated on the assumption that an individual uses the contaminated water for their entire annual supply of drinking water:

[6] This approach is considered conservative. If dilution to reduce the salinity to a level that would be acceptable for drinking were considered, fewer radionuclides would be screened-in to the assessment, even if additional exposure pathways were considered, e.g., ingestion of plants contaminated by use of the water for irrigation.

$$D_{GW,Chain} = \sum_{Chain} C_{GW}\ GW_{Ing}\ DC_{Ing} \quad (A.2)$$

where GW_{Ing} ($m^3\ a^{-1}$) is the annual consumption rate of drinking water and DC_{Ing} (Sv Bq^{-1}) is the effective dose coefficient for ingestion. Note that the dose rates are summed for each decay chain.

The screening criterion that this calculation is judged against is 10% of the 0.3 mSv a^{-1} criterion, to reflect the fact that at any one time, more than one radionuclide may contribute to potential dose rates.

A.3.3.2 Gas Calculations

The calculations for the gas pathway adopt similarly conservative assumptions. The scenario assumes that a building is constructed above the Main shaft immediately after the period of institutional control comes to an end. It is also assumed that any containment of gas by the host geology is lost at the same time and that it is free to migrate rapidly up the access shaft (i.e., without delay). The calculations assume that in any one year, a tenth of the potentially gaseous radionuclides present in the repository are released from the waste. The concentration in the building can be derived by considering that all of the gas released from the access shaft enters the building and the building's ventilation rate. Dose rates can then be calculated based on inhalation and air immersion[7].

The potentially gaseous radionuclides H-3, C-14 and Rn-222, inert gases (radioactive isotopes of Ar, Kr and Xe) and potentially volatile contaminants (Cl, Se and I) are included in the gas pathway calculations.

The gas concentration in the air of the building, C_{GAS} (Bq m^{-3}), are calculated using:

$$C_{GAS} = \frac{I_{GAS}\ F_{GAS}}{V_H\ \lambda_H} \quad (A.3)$$

where I_{GAS} is the inventory of the gaseous radionuclide in the repository (Bq), F_{GAS} is the assumed fraction of the inventory released into the building each year (a^{-1}), V_H is the volume of the building (m^3) and λ_H is the ventilation rate of the house (a^{-1}).

The annual individual effective dose rate due to inhalation and immersion, D_{GAS} (Sv a^{-1}), can therefore be calculated using:

$$D_{GAS,Chain} = \sum_{Chain} \left(C_{GAS}\ O_{GAS}\ DC_{Imm} \quad + \quad C_{GAS}\ O_{GAS}\ BR_{GAS}\ DC_{Inh} \right) \quad (A.4)$$

where O_{GAS} (-) is the fractional annual occupancy in the building, DC_{Imm} (Sv a^{-1} per Bq m^{-3}) is the dose coefficient due to air immersion, BR_{GAS} ($m^3\ a^{-1}$) is the breathing rate and DC_{Inh} (Sv Bq^{-1}) is

[7] For C-14 in particular, plant uptake may also be of interest, however, C-14 is screened-in via the groundwater pathway, so there is no need to extend the complexity of the screening calculations for the gas pathway to take plant uptake into account.

the dose coefficient due to inhalation; the first component of Equation A.4 addresses the dose rate from air immersion and the second from inhalation.

The screening criterion for this pathway is one tenth of the 0.3 mSv a^{-1} criterion, assuming that more than one radionuclide may be contributing to the total dose at any one time.

A.3.3.3 Intrusion Calculations

The intrusion scenario assumes direct exposure to the waste. It is assumed that the intrusion occurs into the waste stream with the highest concentration for each radionuclide disposed, where C_{HI} (Bq kg^{-1}) is the relevant concentration given by:

$$C_{HI} = \frac{C_{Waste}}{\rho_B} \tag{A.5}$$

where C_{Waste} (Bq m^{-3}) is the radionuclide concentration in the waste and ρ_B (kg m^{-3}) is the dry bulk density of the waste. C_{Waste} is calculated from:

$$C_{Waste} = \frac{I}{V_{raw}} \tag{A.6}$$

Exposure pathways considered for the intrusion scenario include exposure to the waste itself, via external irradiation and inadvertent ingestion, as well as to material suspended into the air from the waste, via inhalation and air immersion. The annual individual effective dose rate due to the human intrusion scenario D_{HI} (Sv a^{-1}) can therefore be calculated using:

$$D_{HI,Chain} = \sum_{Chain} \left(C_{HI}\, O_{HI}\, DC_{Ext} \;+\; C_{HI}\, HI_{Ing}\, O_{HI}\, DC_{Ing} \;+\; C_{HI}\, C_{Dust}\, BR_{HI}\, O_{HI}\, DC_{Inh} \;+\; C_{HI}\, C_{Dust}\, O_{HI}\, DC_{Imm} \right) \tag{A.7}$$

where O_{HI} (-) is the fractional annual occupancy during which exposure takes place, DC_{Ext} (Sv a^{-1} per Bq kg^{-1}) is the dose coefficient due to external irradiation (which conservatively adopts values for external exposure to contamination on an infinite plane and infinite depth), HI_{Ing} (kg a^{-1}) is an annual rate of inadvertent ingestion and C_{Dust} (kg m^{-3}) is the concentration of waste derived dust in the air.

The dose criterion applicable to this scenario is 1 mSv a^{-1}, however, a further safety factor of ten is also applied to reflect that more than one radionuclide may contribute significantly to the dose at any one time.

A.3.3.4 Additional Data for Screening Calculations

The dose coefficients for the screening calculations are adopted from Garisto (2002). Other data are provided in Table A.2 and are adopted from reference to internationally accepted sources and/or suitable cautious assumptions.

Table A.2: Non-Contaminant Dependent Data for Screening Calculations

Parameter	Units	Value	Justification
Groundwater Pathway			
Water volume in repository, V_R	m^3	418,000	Total void volume in Table 4.5
Water consumption rate, GW_{Ing}	$m^3\ a^{-1}$	0.84	Recommended 95th percentile value for adults from Clause 6.15.3.2 and Table 19 of CSA (2008)
Gas Pathway			
Annual release fraction for gas, F_{GAS}	-	0.1	Conservatively assumed that one tenth of the total inventory of gaseous radionuclides is released each year
Volume of building, V_H	m^3	228	Table 9.1 of Garisto et al. (2004)
Ventilation rate of the house, λ_H	a^{-1}	3060	Based on 0.35 h^{-1} from Table 9.1 of Garisto et al. (2004)
Fractional annual occupancy for gas pathway, O_{GAS}	-	1	Conservative assumption
Breathing rate for gas inhalation, BR_{GAS}	$m^3\ a^{-1}$	8400	Recommended value for adults from Clause 6.13.3 and Table 17 of CSA (2008), based on 95th percentile values
Human Intrusion Scenario			
Fractional annual occupancy for intrusion scenario, O_{HI}	-	0.005	Assuming occupancy of one working week (40 hours) per year
Annual rate of inadvertent ingestion, HI_{Ing}	$kg\ a^{-1}$	0.12	Based on recommended 95th percentile value for adults from Clause 6.15.2 and Table 18 of CSA (2008)
Concentration of waste derived dust in the air, C_{Dust}	$kg\ m^{-3}$	1.0E-7	95th percentile of distribution given in Section 3.2.1 of Amiro (1992), reflecting elevated dust levels.
Breathing rate for intrusion scenario, BR_{HI}	$m^3\ a^{-1}$	8400	As for the gas pathway

A.3.3.5 Implementation

The screening calculations for radionuclides are implemented in the AMBER 5.3 contaminant modelling software (QUINTESSA 2009). The calculations have been implemented in a single case file in which decay chains have been tracked, including branching decays (see Figure A.1). This results in a model that includes 1070 contaminants and 1160 decays (note that branching decays mean that contaminants can have more than one decay and that the decay rate is adjusted according to the branching ratio).

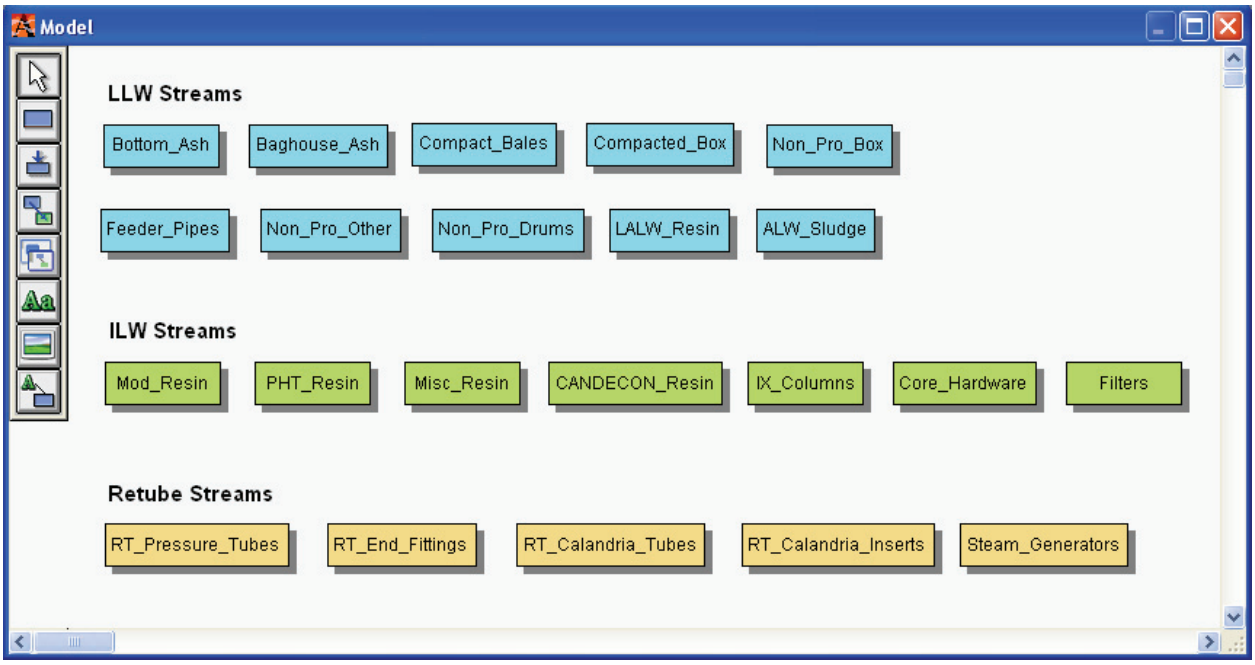

Figure A.1: Screenshot of the Radionuclide Screening Model Implemented in AMBER

Note that to minimize the risk of transcription errors, the half-lives, dose coefficients and used fuel scaling factors have all been implemented as 'Import Parameters' using a text-based file that is derived from Garisto (2002). In addition to these parameters, the inventory parameters are implemented as Import Parameters from a text file derived from the Reference L&ILW Inventory Report (OPG 2010).

A.3.3.6 Results of the Screening Calculations

The results of the radionuclide screening calculations described above are presented in Table A.3 for the reference period of institutional control (100 years) and for all of the 167 parent radionuclides. Table A.4 lists those radionuclides that are identified as warranting further consideration in the current SA for each of the three screening scenarios, resulting in:

- 34 radionuclides for the groundwater pathway;
- 9 radionuclides for the gas pathway; and
- 13 radionuclides for the human intrusion scenario.

Table A.3: Ratio of Screening Dose Rate to Conservative Screening Criteria for the Reference Period of Institutional Control (100 years)

Number	Radionuclide	Scenario		
		Ground Water	Gas[#]	Human Intrusion
1	Ac-225*	9.9E-19	-	5.2E-22
2	Ac-227*	7.5E-03	-	7.6E-07
3	Ag-108m*	2.6E+03	-	2.8E+03
4	Al-26	8.7E-23	-	3.9E-24
5	Am-241	2.7E+04	-	3.1E+00
6	Am-242m*	5.4E+01	1.7E-01	4.1E-03
7	Am-243	4.3E+01	-	5.5E-02
8	Ar-39	0.0E+00	1.0E-02	2.7E-07
9	Ar-42*	2.3E-10	5.7E-08	9.5E-12
10	Au-194	9.2E-32	-	1.3E-32
11	Ba-133	1.6E-04	-	9.9E-07
12	Be-10	8.4E-07	-	1.5E-11
13	Bi-207	8.5E-20	-	5.5E-21
14	Bi-208	2.8E-07	-	4.0E-08
15	Bi-210	1.3E-20	-	6.5E-26
16	Bi-210m*	5.7E-06	-	4.9E-09
17	Bk-247	4.3E-18	-	2.1E-22
18	C-14	2.3E+05	1.4E+09	6.2E+00
19	Ca-41	1.0E-03	-	4.4E-09
20	Cd-109	1.1E-22	-	7.0E-27
21	Cd-113	1.7E-13	-	8.8E-19
22	Cd-113m	2.1E-01	-	1.1E-06
23	Cf-249	1.6E-06	-	1.4E-10
24	Cf-250	1.0E-08	-	6.1E-13
25	Cf-251	5.3E-08	-	2.7E-12
26	Cf-252	4.7E-07	-	7.0E-11
27	Cl-36	8.8E+01	4.2E+05	1.2E-01
28	Cm-242	1.6E-01	7.6E-04	1.4E-05
29	Cm-243	4.2E+00	-	4.4E-04
30	Cm-244	6.4E+01	-	7.0E-02
31	Cm-245	3.8E-01	-	3.7E-05

Number	Radionuclide	Scenario		
		Ground Water	Gas[#]	Human Intrusion
32	Cm-246	7.3E-02	5.0E-07	6.3E-06
33	Cm-247*	3.9E-07	-	4.9E-11
34	Cm-248	9.0E-07	-	7.7E-11
35	Cm-250*	1.8E-12	-	1.7E-16
36	Co-60	4.0E-01	-	4.5E-01
37	Cs-134	6.9E-13	-	3.7E-14
38	Cs-135	4.9E-02	-	7.2E-06
39	Cs-137*	9.4E+03	-	2.1E+02
40	Dy-154	7.6E-21	-	2.0E-24
41	Eu-150	1.2E-08	-	6.9E-10
42	Eu-152	8.5E-01	-	4.1E-01
43	Eu-154	6.0E-03	-	1.4E-03
44	Eu-155	2.7E-07	-	8.9E-10
45	Fe-55	1.2E-08	-	2.9E-12
46	Fe-60*	1.3E-21	-	1.7E-24
47	Gd-148	5.3E-18	-	4.5E-22
48	Gd-150	1.2E-20	-	3.1E-24
49	Gd-152	2.4E-12	-	2.0E-16
50	H-3	4.4E+00	5.2E+03	2.3E-05
51	Hf-172	3.7E-31	-	1.7E-32
52	Hf-174	3.6E-12	-	9.4E-16
53	Hf-178m	2.9E-19	-	7.1E-21
54	Hf-182	1.1E-06	-	2.1E-08
55	Hg-194	1.8E-18	-	2.0E-21
56	Ho-163	2.3E-02	-	6.1E-06
57	Ho-166m	7.6E-03	-	3.5E-04
58	I-129	9.9E-01	1.9E+02	6.1E-05
59	In-115	1.5E-10	-	9.7E-16
60	Ir-192	1.9E-18	-	5.4E-20
61	Ir-192m	9.8E-01	-	1.3E+00
62	K-40	3.0E-06	-	4.5E-09
63	Kr-81	0.0E+00	1.6E-05	7.6E-09
64	Kr-85	0.0E+00	1.9E-01	4.3E-05

Number	Radionuclide	Scenario		
		Ground Water	Gas[#]	Human Intrusion
65	La-137	1.4E-06	-	1.8E-09
66	La-138	1.1E-10	-	7.1E-12
67	Lu-172	2.8E-31	-	2.3E-32
68	Lu-173	4.6E-32	-	6.3E-34
69	Lu-174	1.2E-27	-	2.2E-29
70	Lu-176	4.0E-11	-	4.9E-13
71	Mn-53	1.4E-25	-	6.5E-31
72	Mo-93	2.1E+02	-	4.1E-02
73	Na-22	4.0E-21	-	1.5E-22
74	Nb-91	5.7E-05	-	1.5E-08
75	Nb-92	3.4E-06	-	9.0E-10
76	Nb-93m	1.0E+00	-	4.3E-04
77	Nb-94	5.2E+05	-	1.3E+06
78	Nd-144	3.0E-07	-	7.8E-11
79	Ni-59	1.5E+02	-	2.8E-02
80	Ni-63	2.0E+04	-	2.5E+00
81	Np-235	4.5E-18	-	3.6E-22
82	Np-236	5.8E-06	-	1.3E-09
83	Np-237	5.7E+00	-	7.8E-04
84	Np-238	1.2E-05	5.4E-08	1.0E-09
85	Np-239	8.9E-05	-	7.9E-09
86	Os-186	1.1E-10	-	2.8E-14
87	Os-194*	7.9E-09	-	1.1E-11
88	P-32	7.2E-23	-	6.1E-27
89	Pa-231	4.6E-01	-	3.6E-05
90	Pa-232	4.5E-17	-	1.0E-20
91	Pa-233	4.9E-06	-	4.6E-10
92	Pb-202	3.1E-21	-	7.4E-24
93	Pb-205	5.4E-08	-	2.7E-13
94	Pb-210	1.8E+02	-	1.6E-03
95	Pd-107	1.0E-03	-	7.0E-09
96	Pm-145	2.1E-06	-	4.2E-09
97	Pm-146	1.4E-08	-	4.7E-10

Number	Radionuclide	Scenario		
		Ground Water	Gas[#]	Human Intrusion
98	Pm-147	1.9E-08	-	7.4E-13
99	Po-208	3.0E-25	-	2.9E-28
100	Po-209	1.1E-16	-	2.8E-20
101	Po-210	3.6E-19	-	1.8E-24
102	Pt-190	1.4E-10	-	3.8E-14
103	Pt-193	6.0E+00	-	1.7E-03
104	Pu-236	2.3E-05	-	5.3E-09
105	Pu-238	3.5E+03	1.6E+01	4.1E-01
106	Pu-239	1.5E+04	-	1.7E+00
107	Pu-240	2.2E+04	-	2.6E+00
108	Pu-241	1.9E+04	-	2.4E+00
109	Pu-242	2.2E+01	1.0E-02	2.4E-03
110	Pu-244*	1.4E-13	-	1.7E-17
111	Pu-246*	6.2E-20	-	5.3E-24
112	Ra-223*	5.8E-18	-	8.9E-22
113	Ra-224*	2.6E-16	-	3.4E-19
114	Ra-225	7.4E-18	-	8.9E-22
115	Ra-226	5.2E+02	5.6E+02	4.8E-02
116	Ra-228*	1.3E-07	-	3.1E-11
117	Rb-87	4.6E-06	-	2.3E-11
118	Re-186	1.0E-29	-	2.7E-33
119	Re-186m	3.3E-22	-	8.2E-26
120	Re-187	1.1E-10	-	4.8E-16
121	Rh-101	2.2E-27	-	4.3E-29
122	Rh-102	3.6E-19	-	1.6E-20
123	Rh-102m	5.2E-26	-	1.1E-27
124	Rn-222*	1.0E-08	7.5E-20	5.2E-14
125	Ru-106	7.3E-16	0.0E+00	1.7E-17
126	Sb-125	6.1E-10	-	2.4E-09
127	Sb-126	1.8E-17	-	1.1E-18
128	Se-79	2.4E+00	3.4E+03	9.9E-04
129	Si-32	1.4E-07	-	1.1E-11
130	Sm-146	2.9E-07	-	1.2E-11

Number	Radionuclide	Scenario		
		Ground Water	Gas[#]	Human Intrusion
131	Sm-147	6.3E-05	-	2.4E-09
132	Sm-148	4.6E-09	-	1.2E-12
133	Sm-151	6.2E-03	-	7.4E-06
134	Sn-121	2.5E-18	-	2.9E-23
135	Sn-121m	6.0E+02	-	2.4E+00
136	Sn-126*	2.5E-01	-	5.0E-02
137	Sr-90	1.0E+04	-	1.5E+00
138	Ta-179	1.1E-32	-	7.7E-35
139	Ta-182	1.4E-21	-	6.8E-23
140	Tb-157	1.0E-05	-	6.9E-09
141	Tb-158	7.4E-20	-	2.9E-21
142	Tc-97	7.8E-09	-	6.8E-13
143	Tc-98	1.3E-07	-	4.9E-09
144	Tc-99	2.6E+00	-	4.6E-04
145	Te-123	2.1E-14	-	3.0E-19
146	Te-125m	4.0E-16	-	5.1E-20
147	Th-227	1.0E-17	-	2.0E-21
148	Th-228	7.3E-14	-	5.1E-17
149	Th-229	7.8E-02	-	7.9E-06
150	Th-230	8.1E-02	7.8E-02	4.5E-06
151	Th-231	3.0E-07	-	2.4E-11
152	Th-232	2.8E-02	-	4.7E-06
153	Th-234*	6.3E-05	5.9E-05	3.5E-09
154	Ti-44*	5.7E-19	-	1.1E-20
155	Tl-202	9.9E-32	-	4.9E-33
156	Tl-204	1.4E-10	-	4.8E-15
157	Tm-171	3.2E-19	-	2.8E-23
158	U-232	4.2E+00	-	1.9E-03
159	U-233	2.0E+01	-	2.7E-03
160	U-234	1.4E+02	1.3E+02	1.0E-02
161	U-235	3.1E+00	-	3.3E-04
162	U-236	8.8E-01	-	4.2E-05
163	U-237	5.9E-07	-	6.3E-11

Number	Radionuclide	Scenario		
		Ground Water	Gas[#]	Human Intrusion
164	U-238	9.3E+02	8.5E+02	2.1E-02
165	V-50	1.1E-12	-	2.9E-16
166	Y-90	1.4E-12	-	2.0E-16
167	Zr-93	1.7E+04	-	5.1E+00

Notes:
Values highlighted in red and bold exceed the relevant screening criterion; values less than 10^{-10} are de-emphasized in grey. Note that the results are summed for all progeny resulting from the disposal of these radionuclides at 2062.

[#] The Gas Scenario results for actinides such as Ac-226 are because they can be sources of Rn-222.

* Indicates a radionuclide for which the effective dose coefficient includes contributions from progeny with half-lives less than 1 day.

Table A.4: Summary of Radionuclides Identified as Warranting Further Consideration as a Result of the Screening Calculations with the Reference Period of Institutional Control (100 years)

Scenario				
Groundwater (34)			Gas (9)	Human Intrusion (13)
H-3	Ag-108m	Pu-238	H-3	C-14
C-14	Sn-121m	Pu-239	C-14	Ni-63
Cl-36	Cs-137	Pu-240	Cl-36	Sr-90
Ni-59	Pt-193	Pu-241	Se-79	Zr-93
Ni-63	Pb-210	Pu-242	I-129	Nb-94
Se-79	Ra-226	Am-241	Ra-226 (Rn-222)	Ag-108m
Sr-90	Np-237	Am-242m	U-234 (Rn-222)	Sn-121m
Mo-93	U-232	Am-243	U-238 (Rn-222)	Cs-137
Zr-93	U-233	Cm-243	Pu-238 (Rn-222)	Ir-192m
Nb-93m	U-234	Cm-244		Pu-239
Nb-94	U-235			Pu-240
Tc-99	U-238			Pu-241
				Am-241

Notes: The disposed amounts of each radionuclide listed result in dose rates from themselves and their daughters that exceed the screening criteria and warrant more detailed consideration; i.e., the results are summed for all progeny resulting from the inventory of these radionuclides at 2062. For example, the Gas Scenario results for U-234, U-238 and Pu-238 are due to the in-growth of Rn-222, which is included as a gaseous radionuclide.

Tables A.5 and A.6 demonstrate the influence of the assumed period of institutional control by showing the list of radionuclides that exceed the screening criteria when no or 300 year periods of institutional control are used. When no period of institutional control is assumed, the radionuclides that exceed the screening criteria are:

- 48 radionuclides for the groundwater pathway (including shorter-lived radionuclides such as Fe-55, Co-60 and Cs-134);
- 10 radionuclides for the gas pathway (including Kr-85); and
- 20 radionuclides for the human intrusion scenario (including shorter-lived radionuclides such as Co-60 and Cs-134).

When the period of institutional control is extended to 300 years, the corresponding numbers are:

- 28 radionuclides for the groundwater pathway (losing H-3, Nb-93m, Pt-193, Pb-210, U-232 and Cm-243);
- 8 radionuclides for the gas pathway (losing H-3); and
- 9 radionuclides for the human intrusion scenario (losing Ni-63, Sr-90, Sn-121m and Ir-192m).

For the reference period of 100 years of institutional control, the full list of screened-in radionuclides comprises the following 36 radionuclides:

- H-3, C-14, Cl-36, Ni-59, Ni-63, Se-79, Sr-90, Mo-93, Zr-93, Nb-93m, Nb-94, Tc-99, Ag-108m, Sn-121m, I-129, Cs-137, Ir-192m, Pt-193, Pb-210, Ra-226, U-232, U-233, U-234, U-235, U-238, Np-237, Pu-238, Pu-239, Pu-240, Pu-241, Pu-242, Am-241, Am-242m, Am-243, Cm-243, Cm-244.
  Note that the all of these radionuclides have inventories reported in at least one waste stream in the Reference L&ILW Inventory Report (OPG 2010).

Table A.5: Summary of Radionuclides for which the Calculated Dose Rates Exceed the Screening Criteria assuming No Period of Institutional Control (0 years)

Scenario					
Groundwater (48)			Gas (10)	Human Intrusion (20)	
H-3	Cd-113m	U-234	H-3	C-14	Cs-134
C-14	Sn-121m	U-235	C-14	Co-60	Cs-137
Cl-36	Sb-125	U-238	Cl-36	Ni-63	Eu-152
Fe-55	Cs-134	Np-237	Se-79	Sr-90	Eu-154
Co-60	Cs-137	Np-239	Kr-85	Y-90	Ir-192m
Ni-59	Pm-147	Pu-238	I-129	Zr-93	Pu-239
Ni-63	Eu-152	Pu-239	Ra-226 (Rn-222)	Nb-94	Pu-240
Se-79	Eu-154	Pu-240	U-234 (Rn-222)	Ag-108m	Pu-241
Sr-90	Ir-192m Pt-193	Pu-241	U-238 (Rn-222)	Sn-121m	Am-241
Y-90	Pb-210	Pu-242	Pu-238 (Rn-222)	Sb-125	Cm-244
Mo-93	Ra-224	Am-241			
Zr-93	Ra-226	Am-242m			
Nb-93m	Th-228	Am-243			
Nb-94	U-232	Cm-242			
Tc-99	U-233	Cm-243			
Ag-108m		Cm-244			

Note: additional radionuclides over the reference period of institutional control are highlighted in red.

Table A.6: Summary of Radionuclides for which the Calculated Dose Rates Exceed the Screening Criteria assuming a 300 year Period of Institutional Control

Scenario					
Groundwater (28)			Gas (8)	Human Intrusion (9)	
H-3	Ag-108m	Np-237	H-3	C-14	Cs-137
C-14	Sn-121m	Pu-238	C-14	Ni-63	Ir-192m
Cl-36	Cs-137 Pt-193	Pu-239	Cl-36	Sr-90	Pu-239
Ni-59	Pb-210	Pu-240	Se-79	Zr-93	Pu-240
Ni-63	Ra-226	Pu-241	I-129	Nb-94	Pu-241
Se-79	U-232	Pu-242	Ra-226 (Rn-222)	Ag-108m	Am-241
Sr-90	U-233	Am-241	U-234 (Rn-222)	Sn-121m	
Mo-93	U-234	Am-242m	U-238 (Rn-222)		
Zr-93	U-235	Am-243	Pu-238 (Rn-222)		
Nb-93m	U-238	Cm-243			
Nb-94		Cm-244			
Tc-99					

Note: Items that are eliminated by the extra 200 years of institutional control in relation to the reference case are highlighted in grey.

For the reference period of 100 years of institutional control, the full list of screened-in radionuclides comprises the following 36 radionuclides:

- H-3, C-14, Cl-36, Ni-59, Ni-63, Se-79, Sr-90, Mo-93, Zr-93, Nb-93m, Nb-94, Tc-99, Ag-108m, Sn-121m, I-129, Cs-137, Ir-192m, Pt-193, Pb-210, Ra-226, U-232, U-233, U-234, U-235, U-238, Np-237, Pu-238, Pu-239, Pu-240, Pu-241, Pu-242, Am-241, Am-242m, Am-243, Cm-243, Cm-244.

Note that the all of these radionuclides have inventories reported in at least one waste stream in the Reference L&ILW Inventory Report (OPG 2010).

A.4 SCREENING NON-RADIOACTIVE SPECIES

The recommended approach for screening chemical substances in the L&ILW streams is implemented in this section. Appendix A.4.1 defines the initial inventory for non-radioactive species. Appendix A.4.2 implements the first step of screening, by eliminating species that are ubiquitous in the geosphere. Appendix A.4.3 describes the screening calculations for the groundwater and human intrusion scenarios.

A.4.1 Initial Inventory

The inventory information for each non-radioactive element or species considered is adopted from the Reference L&ILW Inventory Report (OPG 2010).

In particular, the non-radioactive species considered are:

- Elements: Al, Ag, As, Au, Be, Bi, B, Br, Ba, Ca, Ce, Cs, Cl, Cr, Co, Cd, Cu, F, Fe, Gd, Ga, Ge, Hf, Hg, I, In, K, La, Li, Mg, Mn, Mo, Nb, Ni, Na, Pb, Pt, P, Rb, Sn, Sc, Se, Si, Sb, Sr, S, Te, Th, Tl, Ta, Ti, U, V, W, Y, Zr and Zn; and
- Compounds: Cl-benzenes & Cl-phenols, dioxins & furans, polycyclic aromatic hydrocarbons (PAHs), polychlorinated biphenyl (PCB)s, ethylenediaminetetraacetic acid (EDTA), and asbestos.

Note that the data relates to emplaced waste only and not to containers, as described in Appendix A.2.2.2. Elements for which there is no inventory data are considered to be non-toxic (the organics C, H, O, N and the inert gases) and/or present in insignificant amounts (the lanthanides and rare earth elements Ru, Rh, Pd, Re, Os, Ir, Pr, Nd, Pm, Sm, Eu, Tb, Dy, Ho, Er, Tm, Yb and Lu).

A.4.2 Initial Screening

Of the non-radioactive species considered, the following can be screened out as not being of particular toxicological concern and as they are common elements in the geosphere at the repository site (NWMO 2011):

- Al, Ca, Cl, F, Fe, K, Mg, Na, P, S, Si and Ti.

Note that the organic species considered would be subject to microbial degradation. However, this degradation has conservatively been ignored for the purpose of these screening calculations.

A.4.3 Screening Calculations

The screening calculations for the groundwater pathway are described in Appendix A.4.3.1 and those for the Human Intrusion scenario are described in Appendix A.4.3.2.

A.4.3.1 Groundwater Screening

The groundwater screening has been undertaken by undertaking comparisons against surface water environmental quality criteria and drinking water guidelines. The relevant criteria have primarily been drawn from the acceptance criteria for non-radioactive contaminants (Table 7.12), which is primarily based upon the Ontario Ministry for the Environment standards (MoE 2009), supplemented by those presented in a chemical toxicity risk assessment undertaken for used CANDU fuel (Garisto et al. 2005). The criteria are presented in Table A.7 together with the screening comparisons.

No criteria are available for the following species, which can therefore be screened out because they are not notably hazardous in normal practice (as indicated by the lack of criteria) and because they are only present in minor amounts in the DGR (i.e., they are not present in any significant amount that would suggest more detailed assessment is appropriate):

- **Screened out** due to lack of water quality standard: Ga, Ge, Au, In, Rb, Ta, Th and EDTA.

An extremely cautious groundwater concentration is derived for the remaining elements by assuming that the disposed inventory is entirely dissolved in groundwater within the repository. The groundwater concentration, C_{GW} (μg L^{-1}), is therefore calculated with:

$$C_{GW} = \frac{I_W \, 10^6}{V_R} \qquad \text{(A-8)}$$

where I_W is the total inventory of the contaminant in the repository (kg), V_R is the volume of the void space in the disposed wastes, packages, overpacks and emplacement rooms (m^3) and the 10^6 is required to convert from kg m^{-3} to μg L^{-1}.

Note that the volume of groundwater is assumed to be the same as the void space within the repository (i.e., consistent with groundwater screening for radionuclides, see Appendix A.3.3 and Table A.2). Note also that the derived groundwater concentrations cautiously assume that all of the species are instantly available in a saturated facility (note that the DGR is expected to resaturate very slowly, over a period of hundreds of thousands of years). The calculation also ignores the significant dilution that would occur should contaminated groundwater migrate to the accessible environment and that would be required for the saline groundwater to be potable.

The resulting concentration is then compared against the criterion (see Table A.7), allowing the following elements to be screened out:

- **Screened out** due to not exceeding criteria: Bi, Ce, Cs, La, Pt, and Y.

Table A.7: Groundwater Screening Calculations for Non-Radioactive Species

Element/ Contaminant		Ref. Atomic Mass	Derived Groundwater Concentration	Criterion#	Derived Criterion*	Notes
		(g)	(μg L^{-1})	(μg L^{-1})	(μg L^{-1})	
Antimony	Sb	121.8	7.8E+3	1.5	0.15	
Arsenic	As	74.9	1.0E+3	13	1.3	
Barium	Ba	137.3	2.3E+4	610	61	
Beryllium	Be	9	3.2E+2	0.5	0.05	
Bismuth	Bi	209	2.6E+1	5000	500	
Boron	B	10.8	1.6E+4	1700	170	
Bromine	Br	79.9	3.1E+2	1700	170	
Cadmium	Cd	112.4	2.7E+4	0.5	0.05	
Cerium	Ce	140.1	6.8E-1	22.1	2.21	
Caesium	Cs	132.9	1.9E+0	100	10	
Chromium	Cr	52	2.4E+6	11	1.1	
Cobalt	Co	58.9	1.5E+3	3.8	0.38	
Copper	Cu	63.5	8.0E+6	5	0.5	
Gadolinium	Gd	157.3	1.3E+4	7.1	0.71	
Gallium	Ga	69.7	1.6E+2			No criterion
Germanium	Ge	72.6	7.2E+1			No criterion
Gold	Au	197	2.5E-1			No criterion
Hafnium	Hf	178.5	6.2E+2	4	0.4	
Indium	In	114.8	3.2E+2			No criterion
Iodine	I	126.9	1.6E+2	100	10	
Lanthanum	La	138.9	5.8E-2	10.1	1.01	
Lead	Pb	207.2	3.6E+6	1.9	0.19	
Lithium	Li	6.9	1.4E+4	2500	250	
Manganese	Mn	54.9	2.0E+6	200	20	
Mercury	Hg	200.6	1.6E+2	0.1	0.01	
Molybdenum	Mo	95.9	2.9E+3	23	2.3	
Nickel	Ni	58.7	4.0E+6	14	1.4	
Niobium	Nb	92.9	2.7E+4	600	60	

Element/ Contaminant		Ref. Atomic Mass	Derived Groundwater Concentration	Criterion[#]	Derived Criterion*	Notes
		(g)	(μg L^{-1})	(μg L^{-1})	(μg L^{-1})	
Platinum	Pt	195.1	1.2E+0	3000	300	
Rubidium	Rb	85.5	9.0E-1			No criterion
Scandium	Sc	45	5.6E+1	1.8	0.18	
Selenium	Se	79	2.1E+2	5	0.5	
Silver	Ag	107.9	1.7E+1	0.3	0.03	
Strontium	Sr	87.6	7.8E+3	1500	150	
Tantalum	Ta	180.9	3.7E+1			No criterion
Tellurium	Te	127.6	4.9E+2	20	2	
Thallium	Tl	204.4	1.3E+0	0.5	0.05	
Thorium	Th	232	1.8E+1			No criterion
Tin	Sn	118.7	6.0E+3	73	7.3	
Tungsten	W	183.8	3.6E+2	30	3	
Uranium	U	238	8.6E+2	8.9	0.89	
Vanadium	V	50.9	2.5E+3	3.9	0.39	
Yttrium	Y	88.9	3.4E-1	6.4	0.64	
Zinc	Zn	65.4	3.6E+5	160	16	
Zirconium	Zr	91.2	1.4E+6	4	0.4	
Cl-Benzenes & Cl-Phenols			6.6E+0	0.01	0.001	
Dioxins & Furans			2.2E-1	1.5E-5	1.5E-6	
PAH			8.2E+0	0.1	0.01	
PCB			3.1E-1	0.2	0.02	
EDTA			1.1E+5			No criterion

Notes:
Rows highlighted in grey text are screened out due to the cautious groundwater concentration calculation.

[#] Unless otherwise stated, criteria for elements are taken from Table 7.12; primarily these values correspond to groundwater values, with surface water values used in the absence of groundwater values, consistent with the approach recommended in Table 7.12. Others are taken from Garisto et al. (2005) for groundwater, with the lower criterion adopted where alternative numbers are available.

* 10% of the environmental criteria.

Note that the screening out of the lanthanide La and rare earth Ce here is consistent with the screening out of the rest of these elements as noted in Appendix A.4.1, as the rest of the lanthanide/rare earths are not expected to be present in any higher concentrations than these species, with the exception of Gd which is specifically accounted for.

As a result of these comparisons, the following 32 elements remain of potential interest for more detailed assessment of non-radioactive contaminants for the groundwater pathway because the results of simple screening calculations exceed water quality standards:

- **Screened in** due to exceeding criteria: Ag, As, B, Ba, Be, Br, Cd, Co, Cr, Cu, Gd, Hf, Hg, I, Li, Mo, Mn, Nb, Ni, Pb, Sb, Sc, Se, Sn, Sr, Te, Tl, U, V, W, Zn and Zr.

Several organic substances listed in the inventory also exceed the screening criteria, where water quality standards are available, and deserve some further consideration, particularly concerning whether they will degrade to non-toxic substances over the timescale of interest:

- **Screened in** due to exceeding criteria: Cl-benzenes & Cl-phenols, dioxins & furans, PAHs and PCBs.

A.4.3.2 Human Intrusion Screening

For the human intrusion scenario, it is assumed that a borehole intrusion through the waste containing the highest volumetric concentration of each contaminant occurs and distributes the resulting core over an area of soil. The resulting soil and air concentrations are compared against their associated environmental quality standards.

Comparison Against Environmental Quality Standards for Soil

No criteria are available for the following species, which are therefore screened out, consistent with the approach adopted for the groundwater pathway:

- **Screened out** due to lack of soil quality standard: Au, Cs, Ga, Ge, Hf, In, Mn, Pt, Rb, Sr, Ta, Th and EDTA.

The concentration in the soil, C_S (μg g^{-1}) can be calculated using:

$$C_S = \frac{C_W \; A_B \; L_B \; 10^6}{A_S \; D_S \; \rho_S} \tag{A.9}$$

where C_W is the highest concentration of the contaminant found in any of the waste streams (kg m^{-3}), A_B is the cross-sectional area of the borehole (m^2), L_B is the length of the borehole core (m), A_S is the area of soil over which the material is distributed, D_S is the depth of soil over which the material is distributed and ρ_S is the bulk density of the resulting soil (kg m^{-3}); the 10^6 is required to convert the value from kg kg^{-1} to μg g^{-1}. The assumed values for the new parameters required are given in Table A.8.

Table A.8: Non-Contaminant Dependent Parameters Required from Screening of Non-Radioactive Species for Human Intrusion Scenario

Parameter	Units	Value	Comment
Borehole cross-section, A_B	m^2	0.005	Hunter et al. (2006)
Length of core, L_B	m	16	Hunter et al. (2006)
Area over which dispersed, A_S	m^2	100	Assumed to be 10 m by 10 m
Depth to which mixed, D_S	m	0.2	Based on Clause 6.3.1.1 of CSA (2008)
Bulk density of soil, ρ_S	kg m^{-3}	1400	Based on value for clay soil given in Clause 6.3.2.2 of CSA (2008)

The results of this calculation are shown in Table A.9 for comparison against the environmental quality standards for the species, which are included in the same table. This screening suggests that the following 14 elements and two organic species can be screened out on this scenario:

- **Screened out** due to not exceeding criteria: Ag, As, Ba, Bi, Ce, Co, La, Sc, Se, Te, Tl, V, W, Y and PCBs.

Table A.9: Human Intrusion Screening Calculations for Non-Radioactive Species

Element/ Contaminant		Derived Soil Concentration	Criterion#	Derived Criterion*	Notes
		(µg g^{-1})	(µg g^{-1})	(µg g^{-1})	
Antimony	Sb	5.4E+0	1	0.1	
Arsenic	As	6.5E-1	11	1.1	
Barium	Ba	1.6E+1	210	21	
Beryllium	Be	7.5E-1	2.5	0.25	
Bismuth	Bi	3.4E-2	20	2	
Boron	B	2.6E+1	36	3.6	
Bromine	Br	1.4E+0	10	1	
Cadmium	Cd	4.3E+0	1	0.1	
Cerium	Ce	3.0E-3	50	5	
Cesium	Cs	9.7E-3			No criterion
Chromium	Cr	5.0E+2	67	6.7	
Cobalt	Co	6.5E-1	19	1.9	
Copper	Cu	1.1E+3	62	6.2	
Gadolinium	Gd	1.6E+2	50	5	
Gallium	Ga	8.0E-2			No criterion
Germanium	Ge	3.6E-2			No criterion
Gold	Au	1.8E-4			No criterion
Hafnium	Hf	2.8E-1			No criterion
Indium	In	2.0E+0			No criterion
Iodine	I	6.9E-1	4	0.4	
Lanthanum	La	2.8E-5	50	5	
Lead	Pb	1.2E+2	45	4.5	

Element/ Contaminant		Derived Soil Concentration ($\mu g\ g^{-1}$)	Criterion# ($\mu g\ g^{-1}$)	Derived Criterion* ($\mu g\ g^{-1}$)	Notes
Lithium	Li	2.1E+2	2	0.2	
Manganese	Mn	5.0E+2	0	0	No criterion
Mercury	Hg	1.1E-1	0.16	0.016	
Molybdenum	Mo	1.5E+0	2	0.2	
Nickel	Ni	1.8E+3	37	3.7	
Niobium	Nb	1.6E+2	10	1	
Platinum	Pt	5.5E-4			No criterion
Rubidium	Rb	2.5E-3			No criterion
Scandium	Sc	2.2E-1	50	5	
Selenium	Se	1.1E-1	1.2	0.12	
Silver	Ag	1.7E-2	0.5	0.05	
Strontium	Sr	5.8E+0	0	0	No criterion
Tantalum	Ta	2.3E-1			No criterion
Tellurium	Te	4.8E-1	1440	144	
Thallium	Tl	9.7E-3	1	0.1	
Thorium	Th	2.4E-2			No criterion
Tin	Sn	3.6E+1	5	0.5	
Tungsten	W	3.2E-1	400	40	
Uranium	U	2.1E-1	1.9	0.19	
Vanadium	V	1.1E+0	86	8.6	
Yttrium	Y	1.3E-3	50	5	
Zinc	Zn	2.2E+2	290	29	
Zirconium	Zr	6.4E+3	11	1.1	
Cl-Benzenes & Cl-Phenols		7.3E-2	0.01	0.001	
Dioxins & Furans		4.2E-4	7.0E-6	7.0E-7	
PAH		4.7E-2	0.05	0.005	
PCB		1.1E-3	0.3	0.03	
EDTA		4.9E+2			No criterion

Notes:
Rows highlighted in grey text are screened out due to the derived soil concentration being lower than 10% of the relevant environmental criteria.

Environmental criteria for soil from Table 7.12 and Garisto et al. (2005).

* 10% of the environmental criteria.

The results of the simple intrusion calculations exceed the screening criteria for the following 19 elements, which remain of potential interest for more detailed assessment of non-radioactive contaminants:

- **Screened in** due to exceeding criteria: B, Be, Br, Cd, Cr, Cu, Gd, I, Li, Hg, Mo, Nb, Ni, Pb, Sb, Sn, U, Zn and Zr.

With regards to the organic species, PCBs do not exceed the screening criteria for the human intrusion scenario, whereas the following compounds do, and deserve further consideration:

- **Screened in** due to exceeding criteria: Cl-benzenes & Cl-phenols, dioxins & furans, and PAHs.

Comparison Against Environmental Quality Standards for Air

Asbestos is present in the non-processible waste stream. No environmental quality standards are available for asbestos in either groundwater or soil in the references considered in Table 7.12. The primary concern for asbestos exposure is inhalation of fibres. An ambient air quality standard for asbestos is available for Ontario (MoE 2008), with a 24 hour average value of 0.04 fibres >5 μm cm^{-3}. Applying a safety factor of 10 provides a derived criterion of 0.004 fibres >5 μm cm^{-3}.

An ambient concentration of asbestos in the air can be calculated for the human intrusion scenario. The approach adopted for screening of radionuclides determines an air concentration from dust resuspension directly from the extracted waste material. This is considered inappropriate for comparison against the derived criterion for asbestos, which is expressed as a 24 hour ambient air concentration because:

- Individuals would not be exposed to such concentrations for a period of 24 hours; and
- The concentration immediately surrounding the extracted material is not representative of the ambient conditions.

Therefore, for the purpose of screening asbestos for postclosure assessment, an air concentration is calculated based on resuspension from soil that has been contaminated by the extracted material. Such a concentration is determined using:

$$C_{Air} = CF_{Asbestos}\, C_{Dust}\, 10^3\, C_S \qquad \text{(A.10)}$$

where the soil concentration, C_S (μg g^{-1}), is calculated as defined in Equation A.9, C_{Dust} (kg m^{-3}) is cautiously taken to be the same as that presented in Table A.2 (this is conservative because it is an elevated dust concentration[8]) and $CF_{asbestos}$ is a conversion factor from a mass concentration to a fibre concentration for asbestos with units of fibres >5 μm cm^{-3} per μg m^{-3}. The factor of 10^3 is required to convert the soil concentration from μg g^{-1} to μg kg^{-1}.

There is a range of methods available for measuring asbestos concentrations in the air. Phase contrast microscopy (PCM) enumerates fibres longer than 5 μm (USEPA 1986). USEPA (1986) gives a range of 5 to 150 for the conversion factor from μg m^{-3} per fibre >5μm cm^{-3}. The smallest of these conversion factors conservatively gives the highest conversion factor from mass to fibres of 0.2 fibres >5 μm cm^{-3} per μg m^{-3}.

The above calculation generates an air concentration of asbestos of 0.00026 fibres >5 μm cm^{-3}. This does not exceed the derived criterion of 0.004 fibres >5 μm cm^{-3}. Asbestos is therefore **screened out** from the postclosure assessment on the basis of this calculation.

[8] The 10 m x 10 m area is unlikely to be large enough to locally maintain a high concentration of fibres in air.

A.4.4 Summary of Screening for Non-Radioactive Species

As a result of the screening of non-radioactive species against the groundwater pathway and human intrusion, the following 36 species remain of potential interest for more detailed non-radioactive assessment (see also Table A.10):

- **Screened in**: Ag, As, B, Ba, Be, Br, Cd, Co, Cr, Cu, Gd, Hf, Hg, I, Li, Mo, Mn, Nb, Ni, Pb, Sb, Sc, Se, Sn, Sr, Te, Tl, U, V, W, Zn, Zr, Cl-benzenes & Cl-phenols, dioxins & furans, PAHs and PCBs.

Table A.10: Summary of Non-Radioactive Species Identified as Warranting Further Consideration as a Result of the Screening Calculations

Scenario				
Groundwater (36)			Human Intrusion (22)	
Ag	I	Te	B	Nb
As	Li	Tl	Be	Ni
B	Mo	U	Br	Pb
Ba	Mn	V	Cd	Sb
Be	Nb	W	Cr	Sn
Br	Ni	Zn	Cu	U
Cd	Pb	Zr	Gd	Zn
Co	Sb	Cl-benzenes & Cl-phenols	I	Zr
Cr	Sc	Dioxins & furans	Li	Cl-benzenes & Cl-phenols
Cu	Se	PAHs	Hg	Dioxins & furans
Gd	Sn	PCBs	Mo	PAHs
Hf	Sr			
Hg				

A.5 DISCUSSION

As a result of simple cautious screening calculations, based primarily on the characteristics of the wastes themselves, many radioactive and non-radioactive contaminants can be screened out as not likely to cause any significant impact from placement in the DGR. The following radioactive and non-radioactive contaminants exceed the simple and cautious screening criteria and warrant further consideration in the quantitative safety assessments.

Adopting the reference period of institutional control (100 years) results in the following 36 radionuclides exceeding the screening criteria for the three screening scenarios considered:

- H-3, C-14, Cl-36, Ni-59, Ni-63, Se-79, Sr-90, Mo-93, Zr-93, Nb-93m, Nb-94, Tc-99, Ag-108m, Sn-121m, I-129, Cs-137, Ir-192m, Pt-193, Pb-210, Ra-226, U-232, U-233, U-234, U-235, U-238, Np-237, Pu-238, Pu-239, Pu-240, Pu-241, Pu-242, Am-241, Am-242m, Am-243, Cm-243, Cm-244.

The following 36 non-radioactive species exceed the screening criteria for the scenarios considered and warrant further consideration:

- 32 elements: Ag, As, B, Ba, Be, Br, Cd, Co, Cr, Cu, Gd, Hf, Hg, I, Li, Mo, Mn, Nb, Ni, Pb, Sb, Sc, Se, Sn, Sr, Te, Tl, U, V, W, Zn and Zr; and
- 4 groups of organic species: Cl-benzenes & Cl-phenols, dioxins & furans, PAHs and PCBs.

In comparing the above results with the corresponding outcomes in other major assessments, it should first be noted that any set of results is dependent on the wastes to be disposed of and the scope of each assessment. Some of the screening exercises reviewed apply to spent fuel and high-level waste: such wastes have radioactive inventories greatly in excess of the wastes intended for the DGR and do not contain hazardous organic species. Such assessments might be expected to have larger numbers of radionuclides and smaller numbers of non-radioactive species screened in compared with the DGR project.

The screening calculations for the DGR are particularly wide-ranging, encompassing human intrusion and gas, as well as the groundwater pathway. Other assessments typically omit the first or second of these, which tends to decrease the number of species screened in. However, it is noteworthy that consideration of the gas pathway and human intrusion for radioactive species each led to the inclusion of one additional radionuclide (I-129 and Ir-129m, respectively). Consideration of human intrusion for nonradioactive species did not result in the inclusion of any additional contaminants.

It can be concluded therefore that no precise comparisons with other assessments can be made for either radioactive or non-radioactive contaminants.

Considering radioactive contaminants in greater detail, the lists of priority radionuclides can be conveniently divided into (a) fission and activation products and (b) actinides in the 4N+1, 4N+2 and 4N+3 series. Table A.11 compares the results for the radionuclide screening for the DGR project with those included in other assessment studies. The table shows that the list derived for the actinide series is similar to those found in other assessments.

Table A.11: Comparison of Radionuclide Screening for the DGR Project with those included in Other Assessments

Assessment	DGR Project (Canada)	SFR 1 (Sweden) [1]	LLWR (UK) [2]	Nagra (Switzerland) [3]	Nirex (UK) [4]	SR-Can (Sweden) [5]
Context	Deep geological L&ILW	Near surface L&ILW	Surface LLW	Deep geological SF, HLW & ILW	Deep geological ILW and HLW/SF	Deep geological HLW/SF
Fission and Activation Products	H-3, C-14, Cl-36, Ni-59, Ni-63, Se-79, Sr-90, Mo-93, Zr-93, Nb-93m, Nb-94, Tc-99, Ag-108m, Sn-121m, I-129, Cs-137, Ir-192m, Pt-193	H-3, C-14, Cl-36, ***Co-60***, Ni-59, Ni-63, Se-79, Sr-90, Mo-93, Nb-94, Tc-99, Ag-108m, ***Sn-126***, I-129, ***Cs-135***, Cs-137, ***Ho-166m***	H-3, C-14, Cl-36, ***Co-60***, Ni-63, Sr-90, Zr-93, Nb-94, ***Nb-95***, Mo-93, Tc-99, ***I-125***, I-129, ***I-131***, ***Cs-135***, Cs-137	H-3, ***Be-10***, C-14, Cl-36, ***Ca-41***, Co-60, Ni-59, Ni-63, Se-79, Sr-90, Zr-93, Nb-93m, Nb-94, Mo-93, Tc-99, ***Pd-107***, Ag-108m, Sn-121m, ***Sn-126***, I-129, ***Cs-135***, Cs-137, ***Sm-151***, Eu-154, Ho-166m	C-14, Cl-36, Ni-59, Ni-63, Se-79, Sr-90, Zr-93, Nb-93m, Nb-94, Mo-93, Tc-99, ***Pd-107***, Ag-108m, Sn-121m, ***Sn-126***, I-129, ***Cs-135***, Cs-137, ***Sm-151***, ***Eu-152***, ***Ho-166m***	C-14*, Cl-36, ***Ca-41***, Ni-59, Ni-63, Se-79, Sr-90, Zr-93, Nb-94, Tc-99, ***Pd-107***, Ag-108m, ***Sn-126***, I-129, ***Cs-135***, Cs-137, ***Sm-151***, ***Ho-166m***
4N Series	Cm-244, Pu-240, U-232	Cm-244, Pu-240	***Cm-248***, Cm-244, Pu-240, ***Th-232***	Cm-244, Pu-240, ***U-236***, U-232, ***Th-232***, ***Th-228***, **Ra-228**	Cm-244, Pu-240, ***U-236***, U-232, ***Th-232***, ***Th-228***, ***Ra-228***	Cm-244, Pu-240, ***U-236***, ***Th-232***
4N+1 Series	Pu-241, Am-241, Np-237, U-233	Am-241, Pu-241, Np-237	***Cm-245***, Am-241, Pu-241, Np-237, U-233	***Cm-245***, Pu-241, Am-241, Np-237, U-233, ***Th-229***	***Cm-245***, Am-241, Pu-241, Np-237, U-233, ***Th-229***	***Cm-245***, Am-241, Np-237, U-233, ***Th-229***
4N+2 Series	Am-242m, Pu-242, Pu-238, U-238, U-234, Ra-226, Pb-210		***Cm-246***, Am-242m, Pu-242, Pu-238, U-238, U-234, ***Th-230***, Ra-226, Pb-210	***Cm-246***, Am-242m, Pu-242, Pu-238, U-238, U-234, ***Th-230***, Ra-226, Pb-210, ***Po-210***	***Cm-246***, Am-242m, Pu-242, Pu-238, U-238, U-234, ***Th-230***, Ra-226, Pb-210	***Cm-246***, Pu-242, U-238, U-234, ***Th-230***, Ra-226, Pb-210
4N+3 Series	Cm-243, Am-243, Pu-239, U-235	Am-243, Pu-239	Cm-243, Am-243, Pu-239, ***Pa-231***, U-235	Cm-243, Am-243, Pu-239, U-235, ***Pa-231***, ***Ac-227***	Cm-243, Am-243, Pu-239, U-235, ***Pa-231***, ***Ac-227***	Am-243, Pu-239, U-235, ***Pa-231***
Total	36	24	39	54	49	38

Notes:
(1) Appendix B of Thomson et al. (2008); (2) Section 7.3.2 of Randall (2008); (3) Appendix A5 of NAGRA (2002); (4) Thorne (2006); (5) Section 3.1 of Avila and Ekström (2006).

* C-14 is recognized as being a potentially important radionuclide, but was excluded from the SR-Can study as the associated models were being updated.

Radionuclides in *italic bold* are evaluated but not screened in for the DGR postclosure safety assessment.

The list of fission and activation products derived here is again mostly similar in composition and length to those found in other assessments. Ir-192m and Pt-193 are notable exceptions that are screened in this study but are not included in the other assessments reviewed.

The list derived for non-radioactive species is notably longer than those for other assessments, and encompass 32 elements and 4 groups of organic species (see Table A.12). The starting point is the inventory of 57 metals and 13 compounds. Mallants et al. (2000) started with a list of 41 species that was reduced to 11. Nirex's screening within a generic repository assessment (Hunter et al. 2006) led to 38 initial species being reduced to 10. The results from the SAFIR 2 assessment were closer numerically to the DGR project: of 54 initial elements identified, 24 remained after screening (ONDRAF/NIRAS 2001). However, only about half of the 24 are common to the DGR list.

Table A.12: Comparison of Non-Radioactive Species Screening for the DGR Project with those included in Other Assessments

Assessment	DGR Project (Canada)	Nirex (UK) [1]	SCK•CEN (Belgium) [2]	SAFIR 2 (Belgium) [3]
Context	Deep geological L&ILW	Deep geological ILW and HLW/SF	Surface LLW	Deep geological HLW
Elements	As, Ag, B, Ba, Be, Br, Co, Cr, Cu, Cd, Gd, Hf, Hg, I, Li, Mo, Mn, Nb, Ni, Pb, Se, Sc, Sb, Sr, Sn, Te, Tl, U, V, W, Zn and Zr	***Al***, Be, Cr, ***Fe***, Mn, Pb, U	B, Be, Cr, Cd, ***Cl***, Hg, I, Nb, Pb, Sb, Zn	As, B, Ba, Br, Cd, Co, Cr, ***Cs***, ***Ge***, Hg, ***In***, Mn, Mo, Ni, Pb, ***Rb***, Sb, ***Sm***, Sr, ***Tc***, U, W, ***Y***, Zn
Organic Species	Cl-benzenes & Cl-phenols, Dioxins & furans, PAHs PCBs	Benzene, Phenol, **Vinyl chloride monomer**	*	*

Notes:
(1) Hunter at al. (2006); (2) Mallants et al. (2000); (3) Section 11.6 of ONDRAF/NIRAS (2001)
* Only consider inorganic species.
Non-radioactive species in *italic bold* are evaluated but not screened in the DGR postclosure safety assessment.
Vinyl chloride monomer, a degradation product of PVC, is not evaluated in the DGR project.

There is no accepted method for conducting the screening. Under these circumstances, it could be considered prudent to go forward with a priority list that may be a little long. The list of priority non-radioactive contaminants derived in this study is therefore considered suitably conservative.

Finally, the screening nature of this assessment is emphasized. The calculations are deliberately simple and very cautious, and are largely based on the characteristics of the wastes themselves, without consideration of the containment, retardation and dispersion of the geosphere and biosphere. They do not reflect the expected impact of the DGR and are intended only as an extreme bounding assessment to ensure that effort during the subsequent, more detailed, analyses focuses on the key species.

REFERENCES FOR APPENDIX A

Amiro, B.D. 1992. The Atmosphere Submodel for the Assessment of Canada's Nuclear Fuel Waste Management Concept. AECL Research Report AECL-9889. Pinawa, Canada.

Avila, R. and P.-A. Ekström. 2006. Development of Landscape Dose Factors for Dose Assessments in SR-Can. Swedish Nuclear Fuel and Waste Management Company Technical Report TR-06-15. Stockholm, Sweden.

CSA. 2008. Guidelines for Calculating Derived Release Limits for Radioactive Material in Airborne and Liquid Effluents for Normal Operation of Nuclear Facilities. Canadian Standards Association, CSA-N288.1. Toronto, Canada.

Garisto, F. 2002. Radionuclide and Element Specific Data for the Radionuclide Screening Model Version 1.1. Ontario Power Generation Report 06819-REP-01200-10038-R01. Toronto, Canada.

Garisto, F., A. D'Andrea, P. Gierszewski and T. Melnyk. 2004. Third Case Study – Reference Data and Codes. Ontario Power Generation Report OPG 06819-REP-01200-10107-R00. Toronto, Canada.

Garisto, F., T. Kempe, P. Gierszewski, K. Wei, C. Kitson, T. Melnyk, L. Wojciechowski, J. Avis and N. Calder. 2005. Horizontal Borehole Concept Case Study: Chemical Toxicity Risk. Ontario Power Generation Report 06819-REP-01200-10149-R00. Toronto, Canada.

Hunter, F.M., C.P. Jackson, M. Kelly and S.J. Williams. 2006. A Post-closure Toxicity Screening Assessment for the Nirex Phased Geological Disposal Concept. Serco Assurance Report SA/ENV-0854. Harwell, United Kingdom.

ICRP. 2008. Nuclear Decay Data for Dosimetric Calculations. International Commission on Radiological Protection Publication 107, Annals of the ICRP 38(3).

Mallants, D., G. Volckaert, J. Marivoet and B. Neerdael. 2000. Disposal of Low-level Radioactive Waste in Belgium, a Safety Analysis for Inorganic Chemotoxic Elements. International Conference on the Safety of Radioactive Waste Management, Contributed Papers, IAEA/CN/78/15, Cordoba, Spain.

MoE. 2008. Ontario's Ambient Air Quality Criteria. Standards Development Branch, Ontario Ministry of the Environment PIBS # 6570e. Toronto, Canada.

MoE. 2009. Soil, Ground Water and Sediment Standards for Use Under Part XV.1 of the Environmental Protection Act. Toronto, Canada.

NAGRA. 2002. Project Opalinus Clay: Models, Codes and Data for Safety Assessment. Nagra Technical Report 02-06. Wettingen, Switzerland.

NWMO. 2011. Geosynthesis Report. Nuclear Waste Management Organization Report DGR-TR-2011-11 R000. Toronto, Canada.

ONDRAF/NIRAS. 2001. SAFIR 2: Safety Assessment and Feasibility Interim Report 2. ONDRAF/NIRAS Report NIROND 2001-06E. Belgium.

OPG. 2010. Reference Low and Intermediate Level Waste Inventory for the Deep Geologic Repository. Ontario Power Generation Report 00216-REP-03902-00003-R003. Toronto, Canada.

QUINTESSA. 2009. AMBER 5.3 Reference Guide. Quintessa Ltd. report QE-AMBER-1. Henley-on-Thames, United Kingdom.

Randall, M. 2008. LLWR Lifetime Plan: Inventory and Near Field. LLW Repository Ltd. Report 10003 LLWR LTP Volume 3 Issue 01. Holmrook, United Kingdom.

Thomson, G., A. Miller, G. Smith and D. Jackson. 2008. Radionuclide Release Calculations for SAR-08. Svensk Kärnbränslehantering AB Report R-08-14. Stockholm, Sweden.

Thorne, M.C. 2006. Screening of Radionuclides for Inclusion in Post-closure Biosphere Assessment Calculations. Mike Thorne and Associates Ltd. report for United Kingdom Nirex Ltd. MTA/P0011c/2006-3: Issue 2. Halifax, United Kingdom.

USEPA. 1986. Airborne Asbestos Health Assessment Update. United States Environmental Protection Agency report EPA/600/8-84/OO3F. Washington, DC, USA.

THIS PAGE HAS BEEN LEFT BLANK INTENTIONALLY

APPENDIX B: HENRY'S LAW CONSTANTS AND GAS SOLUBILITIES

An illustration of gas partitioning data is shown in Table B.1. The data shows the general trend for decreasing solubility with temperature (increasing K_H) and with salinity. It also shows that the influence of pressure is smaller. The influence of higher salt concentrations is to significantly decrease solubility relative to freshwater.

Table B.1: Henry's Law Constant (K_H) variation with Temperature, Pressure and Salinity

K_H (CH_4) atm per mole fraction	K_H (CO_2) atm per mole fraction	K_H (H_2) atm per mole fraction	K_H (N_2) atm per mole fraction	Reference
Fresh water: 2.24×10^4 (0°C) 2.97×10^4 (10°C) 3.76×10^4 (20°C) 4.49×10^4 (30°C)	0.73×10^3 (0°C) 1.04×10^3 (10°C) 1.42×10^3 (20°C) 1.86×10^3 (30°C)	5.79×10^4 (0°C) 6.36×10^4 (10°C) 6.83×10^4 (20°C) 7.29×10^4 (30°C)		Wilhelm et al. (1977)
3.20×10^4 (15°C) 3.56×10^4 (20°C) 3.92×10^4 (25°C) 4.26×10^4 (30°C)				CRC (2006)
			5.6×10^4 (1 atm N_2, 0°C) 1.1×10^5 (1 atm N_2, 40°C)	Sun et al. (2001)
3.01×10^4 (10°C) 3.40×10^4 (15°C) 3.79×10^4 (20°C) 4.17×10^4 (25°C)	1.03×10^3 (10°C) 1.18×10^3 (15°C) 1.47×10^3 (20°C) 1.63×10^3 (25°C)			Recalculated from Perry et al. (1984)
5.12×10^4 (3.1 atm CH_4, 30°C) 4.63×10^4 (5.3 atm CH_4, 30°C) 4.17×10^4 (7.7 atm CH_4, 30°C) 3.91×10^4 (9.1 atm CH_4, 30°C)				Duffy et al. (1961)
4.2×10^4 (24 atm CH_4, 25°C) 4.3×10^4 (37 atm CH_4, 25°C) 4.6×10^4 (51 atm CH_4, 25°C)				Stoessell and Byrne (1982)
0.5M NaCl: 5.56×10^4 (14 atm CH_4, 30°C) 5.11×10^4 (27 atm CH_4, 30°C) 5.34×10^4 (35 atm CH_4, 30°C)				Duffy et al. (1961)

K_H (CH_4) atm per mole fraction	K_H (CO_2) atm per mole fraction	K_H (H_2) atm per mole fraction	K_H (N_2) atm per mole fraction	Reference
2.77×10^4 (0°C) 5.25×10^4 (30°C)				Yamamoto et al. (1976) [seawater, ~0.5 M NaCl]
4.7×10^4 (24 atm CH_4, 25°C) 5.0×10^4 (37 atm CH_4, 25°C) 5.3×10^4 (51 atm CH_4, 25°C)				Stoessell and Byrne (1982)
4M NaCl (230 g L^{-1}): 1.2×10^5 (24 atm CH_4, 25°C) 1.3×10^5 (37 atm CH_4, 25°C) 1.4×10^5 (51 atm CH_4, 25°C)				Stoessell and Byrne (1982)
			1.4×10^5 (1 atm N_2, 0°C) 1.8×10^5 (1 atm N_2, 20°C) 1.9×10^5 (10 atm N_2, 20°C)	Sun et al. (2001)
2M $CaCl_2$ (220 g L^{-1}): 1.1×10^5 (24 atm CH_4, 25°C) 1.2×10^5 (37 atm CH_4, 25°C) 1.2×10^5 (51 atm CH_4, 25°C)				Stoessell and Byrne (1982)

Since the exact chemical conditions in the DGR will vary with location and with time, approximate values are recommended here as representative for brine conditions. These are listed in Table B.2. The units can be converted using 1 mol L^{-1} MPa^{-1}=$(10/K_H)$*55.5/$(1-10/K_H)$, where K_H is the Henry's Law constant expressed in atm per mol fraction. The factor 10 arises in this conversion because 1 MPa = 10 atm, and 55.5 is the molality of water.

Table B.2: Suggested Values for Henry's Constant for Repository Gases, at P_{gas} = 1 MPa, T = 20-25 ºC and brine (TDS >100 g L^{-1}) salinity

Gas	Henry's Constant (atm per mole fraction)	Henry's Constant (m^3 @STP m^{-3} Pa^{-1})	Henry's Constant (mol L^{-1} MPa^{-1})
CH_4	1.4E+05	8.9E-08	4.0E-03
CO_2	8.0E+03	1.6E-06	6.9E-02
H_2	2.5E+05	5.0E-08	2.2E-03
He	4.5E+05	2.8E-08	1.2E-03
N_2	1.9E+05	6.5E-08	2.9E-03
O_2	6.2E+04	2.0E-07	9.0E-03
H_2S	1.1E+03	1.1E-05	5.1E-01

The reference value for methane is based on the value for 4 M NaCl from Stoessell and Byrne (1982) and the more recent thermodynamic model provided in Duan and Mao (2006). The value for O_2 is at 1 M NaCl (Battino et al. 1983). The reference value for H_2S is from Duan et al. (2007) for 4M NaCl.

The dissolution of CO_2 is a special case as it is part of a pH-dependent speciation equilibrium for dissolved inorganic carbon:

$$CO_{2(g)} \leftrightarrow CO_{2(aq)} \leftrightarrow H_2CO_3 \leftrightarrow HCO_3^- \leftrightarrow CO_3^{2-} \quad \text{(B.1)}$$

and hence the value of K_H (CO_2), if measured on the basis of total dissolved inorganic carbon (TIC), would vary with pH. However if the TIC speciation is correctly modelled to obtain the 'actual' CO_2(aq) concentration, then K_H (CO_2) should vary with pressure and salinity in a similar way to the other gases although the polar nature of CO_2 will cause deviation from this behaviour at high salinities.

Thermodynamic models for calculating carbon dioxide solubility over a wide range of temperatures, pressures and salinities have been published by Duan and Sun (2003) and Portier and Rochelle (2005). The latter shows that CO_2 solubility decreases linearly with ionic strength in NaCl solutions, from ~0.035 mol kg^{-1} H_2O for pure water to ~0.02 mol kg^{-1} H_2O for an ionic strength of 3 molal and a CO_2 pressure of 0.1 MPa. The slope of increase of CO_2 solubility with increasing pressure decreases at higher pressures, i.e., above 5 MPa, for 1M NaCl and $CaCl_2$ solutions whereas the slope is fairly uniform for solubility in pure water. The decrease of slope, i.e., increasing Henry's Law constant (when defined as K_H = solubility/pressure), is most marked for $CaCl_2$ solutions (Portier and Rochelle 2005). As a general estimate for DGR conditions, the value in Table B.2 is suggested.

The effect of salinity on H_2 solubility has been modelled using the Setschenow equation. The solubility of H_2 in pure water at 25°C and 1 atm (Table B.1) was adjusted using a salting out coefficient for H_2 in NaCl brine conditions from Onda et al. (1970).

The effect of salinity on He solubility was also modelled using the Setschenow equation. The solubility of He in pure water at 25°C and 1 atm (1.43×10^5 atm per mole fraction, CRC 2006) was adjusted using a salting out coefficient for He in 5 molal NaCl from Smith and Kennedy (1983). The resulting values are given in Table B.2.

REFERENCES FOR APPENDIX B

Battino, R., T.R. Rettich and T. Tominaga. 1983. The Solubility of Oxygen and Ozone in Liquids. Journal of Physical Chemistry Reference Data 12, 163-178.

CRC. 2006. Handbook of Chemistry and Physics. 87th edition, Chemical Rubber Company Press. Boca Raton, USA.

Duan Z.H. and S.D. Mao. 2006. A thermodynamic model for calculating methane solubility, density and gas phase composition of methane-bearing aqueous fluids from 273 to 523 K and from 1 to 2000 bar. Geochimica et Cosmochimica Acta, 70(13), 3369-3386.

Duan, Z. and R. Sun. 2003. An improved model calculating CO_2 solubility in pure water and aqueous NaCl solutions from 273 to 533 K and from 0 to 2000 bar. Chemical Geology 193, 257-271.

Duan, Z., R. Sun, R. Liu and C. Zhu. 2007. Accurate thermodynamic model for the calculation of H_2S solubility in pure water and brines. Energy & Fuels 21, 2056-2065.

Duffy, J.R., N.O. Smith and B. Nagy. 1961. Solubility of natural gases in aqueous salt solutions – I. Geochimica et Cosmochimica Acta 24, 23-31.

Onda, K., E. Sada, T. Kobayashi, S. Kito and K. Ito. 1970. Salting-out parameters of gas solubility in aqueous salt solutions. Journal of Chemical Engineering of Japan 3(1), 18-24.

Perry, R.H., D.W. Green and J.O. Maloney. 1984. Chemical Engineer's Handbook. 7th edition. McGraw-Hill, New York, USA.

Portier, S. and C.A. Rochelle. 2005. Modelling CO_2 solubility in pure water and NaCl-type waters from 0 to 300 °C and from 1 to 300 bar, Application to the Utsira Formation at Sleipner. Chemical Geology 217(3-4), 187-199.

Smith, S.P. and B.M. Kennedy. 1983. The solubility of noble gases in water and in NaCl brine. Geochimica et Cosmochimica Acta 47, 503-515.

Stoessell, R. and P. Byrne. 1982. Salting-out of methane in single-salt solutions at 25°C and below 800 psia. Geochimica et Cosmochimica Acta 46, 1327-1332.

Sun, R., W. Hu and Z. Duan. 2001. Prediction of nitrogen solubility in pure water and aqueous NaCl solutions up to high temperature, pressure and ionic strength. Journal of Solution Chemistry 30(6).

Wilhelm, E., R. Battino and R.J. Wilcock. 1977. Low pressure solubility of gases in liquid water. Chemical Reviews 77, 219-262.

Yamamoto, S., J.B. Alcauskas and T.E. Crozier. 1976. Solubility of methane in distilled water and seawater. Journal of Chemical Engineering Data 21(1), 78-80.

APPENDIX C: DETERMINATION OF REPRESENTATIVE WATER COMPOSITIONS AND SOLUBILITY LIMIT CALCULATIONS FOR SELECTED ELEMENTS

C.1 INTRODUCTION

Preliminary safety assessment calculations indicated that potentially important radionuclides for the long-term safety of the DGR include C-14, Cl-36, Ni-59, Zr-93, Nb-94, I-129, Ra-226, Np-237, U-238 and Pu-239. The significance of these radionuclides is largely determined by a combination of their half-life, amount in inventory, and/or mobility. Also, non-radioactive Cd, Cr, Cu and Pb, were identified as potentially important hazardous elements.

This appendix discusses possible solubility limiting compounds containing these elements and provides calculated solubility limits for representative water compositions. In order to undertake such calculations, representative water chemistries were first identified and then aqueous speciation calculations were carried out.

C.2 METHODS

C.2.1. Determination of Representative Water Compositions (Aqueous Speciation Calculations)

In order to determine the major solute activities and $pCO_{2(g)}$ required to construct phase diagrams, aqueous speciation calculations were undertaken using the geochemical modelling software PHREEQC (Parkhurst and Appelo 1999; Box 1) and the "Pitzer" thermodynamic database "data0.ypf.R2". This database was produced initially in EQ3/6 format by the Yucca Mountain Project (YMP) (USDOE 2007) and was converted to PHREEQC format by Quintessa for NWMO. The database was considered to be the best available for the calculations undertaken, because it is the most complete and most fully-documented "Pitzer" database in the public domain. It has been developed by USDOE under a well-documented regime specifically for application to a radioactive waste management project (USDOE 2007). The calculations were based upon groundwater and porewater compositions given in Table 5.4 of this report. A porewater composition from the Cobourg Formation in DGR3 and an opportunistic groundwater sample from the Guelph Formation in DGR3 were used (Table C.1). The Cobourg Formation water was selected because it comes from the host rock for the DGR. The Guelph Formation water was selected because it is the most saline water encountered within the Intermediate and Deep Bedrock Groundwater Zones and so can be used to investigate the impact of salinity on solubility.

Inevitably any analysis of a groundwater or porewater sample from deep underground will differ from the composition of the natural in-situ water, owing to varied chemical processes that occur during sampling and analysis. These perturbations can never be entirely eliminated, even though they are typically minimized by various sampling and data correction procedures. Furthermore, the chemistry of sampled porewater is particularly susceptible to perturbations by the chemical and physical processes that occur during porewater extraction. For these reasons, in the present work, the Cobourg and Guelph water compositions in Table C.1 were not used directly to calculate solubilities, but rather used as a basis for estimating in-situ water compositions by theoretical modelling.

Given that neither directly measured pH data nor dissolved bicarbonate data are available for the Cobourg limestone, a "model" Cobourg limestone porewater was calculated from the composition reported in Table C.1, using the following staged approach.

Box 1: PHREEQC QA Information

Introduction

PHREEQC version 2 is a United States Geological Survey code written in the C programming language that can perform a wide variety of low-temperature aqueous geochemical calculations. PHREEQC has capabilities for (1) speciation and saturation-index calculations; (2) batch-reaction and one-dimensional (1D) transport calculations involving reversible reactions, (aqueous, mineral, gas, solid-solution, surface-complexation, and ion-exchange equilibria) and irreversible reactions; and (3) inverse modelling (Parkhurst and Appelo 1999).

User manual

A user manual for the core part of PHREEQC has been published by Parkhurst and Appelo (1999) and is available online at: http://wwwbrr.cr.usgs.gov/projects/GWC_coupled/phreeqc/. FAQs are also provided online with additional example calculations and release notes. Additional material on the Windows GUI ("PHREEQC for Windows" is available from http://www.falw.vu/~posv/phreeqc/index.html.

Verification

The code is distributed with a large number of worked examples (documented in Parkhurst and Appelo 1999) the input files for which are distributed with the software. A selection of these was used to verify the software.

Version Tracking

Calculations were undertaken using Version 2.17 of PHREEQC for Windows running on a standard PC (http://www.falw.vu/~posv/phreeqc/download.html).

Reference

Parkhurst, D.L. and C.A.J. Appelo. 1999. User's guide to PHREEQC (version 2) - a computer program for speciation, batch-reaction, one-dimensional transport, and inverse geochemical calculations. Water-Resources Investigations Report 99-4259, US Department of the Interior, US Geological Survey, Denver, USA.

Table C.1: Values of Geochemical Parameters in Selected Groundwater and Porewater from the DGR Site (based on Table 5.4)

Formation	Guelph	Cobourg
% Drill Water Contamination	0.3	
pH	6.5	
Eh (mV)	-141.9	
DO (mg L^{-1})	0.23	
Sulphide (mg L^{-1})	0	
Calculated TDS (mg L^{-1})	375468	260362
Fluid Density (kg m^{-3})	1210	
Na (mg L^{-1})	99133	59514
Ca (mg L^{-1})	31597	9530
Mg (mg L^{-1})	7901	22099
K (mg L^{-1})	3665	17303
Sr (mg L^{-1})	589.3	1868
Fe (mg L^{-1})	29.6	
Mn (mg L^{-1})	4.27	
Cl (mg L^{-1})	229635	178956
Br (mg L^{-1})	1715	1824
F (mg L^{-1})	0.3	
I (mg L^{-1})	0.5	
Si (mg L^{-1})	987	
SO_4 (mg L^{-1})	211	1415
NO_3 (mg L^{-1})	<5	
B (mg L^{-1})		177
Alkalinity as $CaCO_3$ (mg L^{-1})	42.5	

Note:
Porewater concentrations (apart from TDS) were reported in the original source in units of mmol kg^{-1} water. These concentrations have been converted to mg L^{-1} based on1 kg L^{-1} water density.

1. The reported Cobourg limestone composition was speciated at pH values of 5.0, 6.0, 6.5 and 7.0, using PHREEQC. The log *p*CO2(g) of the atmosphere is –3.5 (resulting in rainwater pH of ~ 5.5), whereas groundwater log $pCO_{2(g)}$ values are typically between -3 to -2, due to $CO_{2(g)}$ being absorbed from soil.
   PHREEQC calculations show that a pH of 6.5 gives a plausible log $pCO_{2(g)}$ value of -2.78 (based on total dissolved carbonate activity being buffered by calcite solubility using a measured Ca^{2+} concentration). This value is significantly higher than the atmospheric value of -3.5, as expected due to the biogenic input of CO_2 to any water that recharges through a soil zone. The calculated log $pCO_{2(g)}$ value at pH 5 was 0.2. In the absence of CO_2 sources such as volcanic degassing or the degradation of organic sludges, this value appears to be unrealistically high (also see Hutcheon et al. 1993). At a pH of 7, log $CO_{2(g)}$ = -3.78, a value which is unrealistically low (less then atmospheric).

2. Taking a pH of 6.5, a model pO_2(g) value for Cobourg porewater was determined by considering a number of potential buffer reactions using Geochemist's Workbench (Bethke 2008; Box 2) (see Table C.2). Based on reported mineralogy of the Cobourg Limestone at the Bruce nuclear site (INTERA 2011, Sections 3.7 and 3.8.6.1) and the theoretical stability of these minerals in log pO_2(g) - pH space (Figure C.1) it was apparent that from an equilibrium thermodynamic standpoint, in-situ $pO_{2(g)}$ could be buffered by pyrite-hematite or pyrite-siderite equilibrium at pH of 6.5. An aqueous speciation calculation with these minerals redox buffer using the total measured dissolved sulphate concentration gave log $pO_{2(g)}$ = -65.23. However, at very low temperatures, like those in the Cobourg Formation (~ 20 to 25 ^{o}C), this mineral pair is unlikely to be at equilibrium. It is more likely that iron (II) carbonate would participate in equilibrium buffering reactions at this temperature. At a pH of 6.5. pyrite-siderite equilibrium gave a similar log $pO_{2(g)}$ of -66.3. These values appear to be reasonable given that sulphate reduction to sulphide is unlikely in the absence of significant microbial activity. Given the likely pH and redox conditions, and the lithologies present at the Bruce nuclear site, a preliminary reduced (low-pe, corresponding to the calculated log $pO_{2(g)}$) model Cobourg water composition was produced for pH = 6.5, log $pO_{2(g)}$ = -65.2 (the dissolved carbonate concentration was set at the equilibrium solubility of calcite). The activities of dissolved silica species and dissolved Al species were fixed by SiO_2 (amorphous) equilibrium and illite equilibrium respectively. The dissolved Fe^{2+} activity corresponds to siderite equilibrium. The predominant sulphur-bearing aqueous species in the model output generated using the Pitzer approach is SO_4^{2-}. The calculated fluid composition is supersaturated with respect to gypsum, anhydrite and dolomite.

3. An initial model Cobourg water composition (Model 1, Table C.3) was produced considering the results of the previous speciation calculation. For the Model 1 composition, pH and pe were maintained at the same values as before, but dissolved Mg, Sr and S species activities were set at dolomite, celestite and anhydrite saturation respectively. With the exception of celestite, these are all minerals that occur within the Cobourg Formation (INTERA 2011, Sections 3.7.1.1, 3.7.1.2, 3.10.2 and 3.10.3). The activities of Sr species were set at celestite solubility as speciation calculations suggested slight oversaturation with respect to this mineral (saturation index of 0.09). As with the previous speciation calculations, there is a significant average charge imbalance of -15% associated with the calculated water composition. Therefore, a Model 2 water composition was produced by adjusting the total Cl^- concentration in Model 1 to achieve electrical neutrality (Table C.3). This resulted in the total Cl^- concentration being reduced from 5 to 3.5 mol L^{-1}.

Table C.2: Preliminary $pO_{2(g)}$ Values for Potential Redox Buffers

Buffer	Equilibrium Expression	log K (25°C, 1 bar)	Calculated log $pO_2(g)$[1] ($\log pCO_2(g) = -2.78$; pH = 6.5; log activity SO_4 = -1.8 (as total S))
Siderite-hematite	$FeCO_3 + 0.25\ O_{2(g)} = 0.5\ Fe_2O_3 + CO_{2(g)}$	15.33	-72.45
Magnetite-hematite	$Fe_3O_4 + 0.25\ O_{2(g)} = 1.5\ Fe_2O_3$	18.07	-72.30
$H_2O_{(l)}$-$H_{2(g)}$	$H_2O_{(l)} = H_{2(g)} + 0.5\ O_{2(g)}$	-41.55	-83.11
Pyrite-siderite	$FeS_2 + 2\ H_2O + 3.5\ O_{2(g)} + CO_{2(g)} = 4\ H^+ + 2\ SO_4^{2-} + FeCO_3$	199.64	-66.31
Pyrite-hematite	$FeS_2 + 2\ H_2O + 3.75\ O_{2(g)} = 4\ H^+ + 2\ SO_4^{2-} + 0.5\ Fe_2O_3$	214.97	-65.23
Pyrite-magnetite	$FeS_2 + 2\ H_2O + 3.667\ O_{2(g)} = 4\ H^+ + 2\ SO_4^{2-} + 0.333\ Fe_3O_4$	208.94	-65.05

Note:
[1] Geochemist's Workbench reports gas fugacity values, which at 1 bar are taken to be equal to partial pressure.

Box 2: Geochemist's Workbench QA Information

Introduction

Geochemist's Workbench is a set of commercial geochemical modelling programs distributed by Rockware http://www.rockware.com/). Geochemist's Workbench "Standard" includes the following codes: Act2 (for drawing thermodynamic phase/predominance diagrams); SpecE8 (aqueous speciation); Tact (for drawing temperature-activity diagrams); RXN (reaction writing and rearranging); React (for batch reaction modelling and simple kinetic simulations); GTPlot (for plotting React output).

User manual

The software is supplied with four user guides: Bethke and Yeakel (2007a, 2007b, 2000c, 2000d). Examples of geochemical calculations undertaken using Geochemist's Workbench are also given in Bethke (2008). A number of example calculations are provided.

Verification

Verification can be undertaken using provided example calculations.

Version Tracking

Calculations were undertaken using a verified version of Geochemist's Workbench Standard (version 7.0) on a standard PC.

References

Bethke, C.M. and S. Yeakel. 2007a. The Geochemist's Workbench GWB Release 7.0. Essentials Guide. Hydrogeology Program, University of Illinois.

Bethke, C.M. and S. Yeakel. 2007b. The Geochemist's Workbench Reaction Modeling Guide. Release 7.0. Hydrogeology Program, University of Illinois.

Bethke, C.M. and S. Yeakel. 2007c. The Geochemist's Workbench Reaction Transport Modeling Guide. Release 7.0. Hydrogeology Program, University of Illinois.

Bethke, C.M. and S. Yeakel. 2007d. The Geochemist's Workbench. Release 7.0. Reference Manual. Hydrogeology Program, University of Illinois.

Bethke, C.M. 2008. Geochemical and Biogeochemical Reaction Modelling (2nd Ed.) Cambridge University Press.

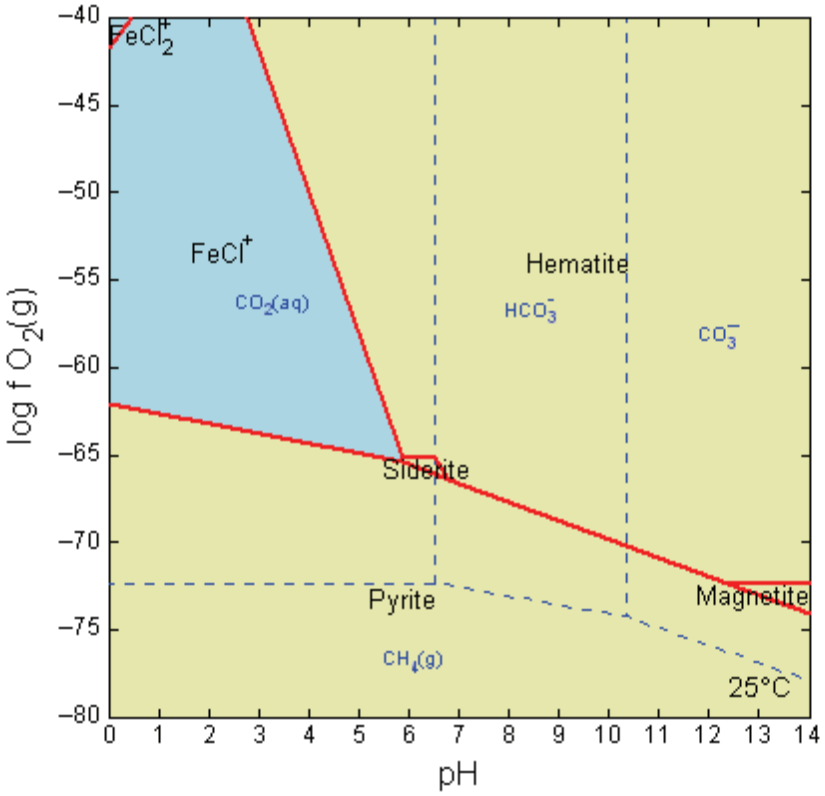

Note: Based on Model 2 data from Table C.4.

Figure C.1: Mineral Stability Diagram Showing the Stability of Redox-sensitive Minerals in the Cobourg Formation

Table C.3: Calculated Model 1 and Model 2 Compositions for the Cobourg Formation Porewaters

Parameter	Model 1 Concentration (molality)	Model 2 Concentration (molality)
Ionic Strength	4.56E+00	3.80E+00
pH	6.5	6.5
pe	-1.994	-2.002
Eh (V)	-0.12	-0.12
Na	2.59E+00	2.59E+00
Ca	2.38E-01	2.38E-01
Mg	8.38E-03	9.72E-03
K	4.43E-01	4.43E-01
Sr	1.98E-03	1.91E-03
Cl	5.05E+00	3.48E+00
Br	2.28E-02	2.28E-02
SO4	1.09E-02	1.94E-02
B	1.64E-02	1.64E-02
C	2.93E-04	6.10E-04
Al	6.88E-11	6.22E-11
Si	6.43E-04	9.98E-04
% charge error	-17.73	0
log $pCO_2(g)$	-2.77	-2.43
log $pO_2(g)$	-65.23	-65.23
Saturation Indices		
Anhydrite	0	0
Calcite	0	0
Dolomite	0	0
Gypsum	0.03	0.06
Halite	-0.65	-0.88
Strontianite	-0.12	-0.12
Sylvite	-0.95	-1.11
Celestite	0	0
Illite	0	0
$SiO_2(am)$	0	0

In order to investigate the impact of high pH conditions (for example those found in cementitious waste packages) on solubility limits in the DGR, a compositional model of high pH cement porewater was produced by equilibrating the Model 2 Cobourg porewater composition with cement phases. The equilibrium solubility of a cement phase was specified to control the solute activity/concentration of a given solute as follows:

- Portlandite equilibrium constrained aqueous Ca;
- Hydrotalcite equilibrium constrained aqueous Mg;
- Al-ettringite equilibrium constrained aqueous S;
- Jennite compositional CSH end-member equilibrium constrained aqueous Si; and
- Hydrogarnet equilibrium constrained aqueous Al.

The total concentration of inorganic carbon was set to correspond to the equilibrium solubility of calcite. The calculations were undertaken using PHREEQC. A combination was used of the "Pitzer" thermodynamic database "data0.ypf.R2" and equilibrium constants (log K values) for the hydrolysis reactions of cement solid phases calculated using solids data (ΔG_f) from the GEMS-compatible database (Thoenen and Kulik 2003). This database includes cement data from Lothenbach et al. (2008) and standard molal aqueous species data from the 1996 revision of the SUPCRT92 database (Johnson et al. 1992).

The Lothenbach et al. (2008) data compilation includes an ideal solid-solution treatment of calcium-silica-hydrate gel, which includes "jennite" and "tobermorite" compositional end-members. Given that fresh Ordinary Portland Cements (OPC) will have CSH with a relatively higher Ca/Si ratio (prior to significant leaching) than the CSH in "aged" OPC, it was specified that the CSH consists entirely of the jennite compositional solid solution end-member (Table C.4). The water composition that was calculated by this approach is given in Table C.5.

Table C.4: Equilibrium Constants for the Hydrolysis Reactions of Cement Solid Phases (Used to Calculate a Cement Porewater Composition)

Solids		Hydrolysis Reaction	log K (25°C, 1 bar)
CSH (Jennite)	ideal solid solution	$(CaO)_{1.6666}(SiO_2)(H_2O)_{2.1} + 3.3332\ H^+ = 1.6666\ Ca^{2+} + SiO_2 + 3.7666\ H_2O$	29.301
CSH (Tobermorite)		$(CaO)_{0.8333}(SiO_2)(H_2O)_{1.3333} + 1.6666\ H^+ = 0.8333\ Ca^{2+} + SiO_2 + 2.1666\ H_2O$	11.137
Hydrotalcite		$Mg_4Al_2(OH)_{14}{:}3H_2O + 14\ H^+ = 4\ Mg^{2+} + 2\ Al^{3+} + 17\ H_2O$	75.108
Portlandite		$Ca(OH)_2 + 2\ H^+ = + Ca^{2+} + 2\ H_2O$	22.800
Al-Ettringite		$Ca_6Al_2(OH)_{12}(SO_4)_3{:}\ 26H_2O + 12\ H^+ = 6\ Ca^{2+} + 2\ Al^{3+} + 3\ SO_4^{2-} + 38\ H_2O$	58.225
Hydrogarnet		$Ca_3Al_2(SiO_4)_{0.8}(OH)_{8.8} + 12\ H^+ = 3\ Ca^{2+} + 2\ Al^{3+} + 0.8\ SiO_{2(aq)} + 10.4\ H_2O$	69.905

Table C.5: Composition of Water Produced by Equilibrating Model 2 Cobourg Formation Porewater with Cement Minerals

Parameter	Cement-Equilibrated Model Concentration (molality)
Ionic Strength	3.77
pH	11.9 (calculated)
pe	-7.419
Eh (V)	
Na	2.59E+00
Ca	2.34E-01
Mg	3.14E-07
K	4.430E-01
Sr	3.580E-02
Cl	3.480E+00
Br	2.280E-02
SO4	1.046E-03
B	1.640E-02
C	1.037E-05
Al	5.025E-07
Si	9.169E-07
% charge error	0
log $pCO_2(g)$	-13.17
log $pO_2(g)$	-65.23
Saturation Indices	
Anhydrite	-1.36
Calcite	0
Dolomite	-4.81
Gypsum	-1.30
Halite	-0.88
Strontianite	1.25
Sylvite	-1.12
Celestite	0
Illite	-17.84
$SiO_{2(am)}$	-5.92

C.2.2 Phase Diagram Construction

Phase diagrams (mostly solubility diagrams) were constructed in order to identify the potential solubility-limiting phases of the elements of interest. This task was undertaken using the commercial software package, "Geochemist's Workbench" supplied by Rockware (Bethke 2008), which is supplied with a number of thermodynamic databases. Among these databases are "Pitzer" databases (including the one distributed as standard with PHREEQC), but these contain only relatively small numbers of solid phases compared to the most recent Geochemist's Workbench database "thermo.com.V8.R6+" (distributed by Rockware, http://www.rockware.com/product/data.php?id=132) which is designed for use with the Debye-Hückel approach for calculating activity coefficients. The diagrams are expressed as functions of aqueous species activities rather than concentrations and therefore a non-Pitzer database can be used. To undertake the calculations reported here, the database "thermo.com.V8.R6+" was used for solubility diagram construction. It should be noted that a PHREEQC version of this database is also available ("llnl.dat"; Parkhurst and Appelo 1999), some data from which was used for solubility calculations. Major element species activities were set at values representing those calculated using PHREEQC.

During the construction of the phase diagrams, major ion activities and gas fugacities were set at the values determined by aqueous speciation. Phase diagrams were constructed for Ni, Zr, Np, Cd, Cr, Cu, Pb, Pu, Ra and U in the presence of water with the same major solute concentrations as the Model 2 Cobourg Formation porewater (Table C.3) and cement porewater produced by equilibrating this porewater with solid phases present in young cement (Table C.5).

Data for Nb species are not included in either the "thermo.com.V8.R6+" database or the "data0.ypf.R2" database. Therefore, this element was not considered further and was conservatively taken to be solubility-unlimited. For Cl^- and dissolved C species, the calculated solute concentrations were taken to represent effective limits to the solubility of these elements and therefore phase diagrams were not required.

In groundwater studies, I is normally regarded as a conservative (non-reactive) element and for this reason is often used as a tracer (e.g., as KI; NIREX 1997). I is associated with various organic materials present in many soils and rocks (e.g., Fuge and Johnson 1986; Sheppard and Thibault 1992) and is often highly enriched in oilfield brines compared to other waters; indeed oilfield brines are a major commercial source of I. In these cases the release of I to the aqueous phase appears to be governed predominantly by the slow breakdown of the organic matter within which the I is located during diagenesis. For these reasons, iodine is treated as being solubility unlimited and therefore phase diagrams were not required.

It should be noted that the solubility diagrams presented in Appendix C.3 represent the stabilities of aqueous species and minerals over wide ranges of pH. That is, although the major solute concentrations are the same as those in modelled in-situ Cobourg porewater and cement-equilibrated Cobourg porewater, the solubility diagrams cover a much wider range of conditions than those of these waters.

In systems where Fe minerals may buffer solubilities, diagrams were constructed with dissolved Fe being buffered by the solubility of goethite. Magnetite or siderite could also have been used. However, the difference this makes to the diagrams is very minor. Geochemist's Workbench produces diagrams that have the most stable mineral assemblage (system-wide free energy minimization). For elements that may exist in solid sulphide compounds, diagrams were constructed both with and without sulphide minerals, given that in natural systems, sulphate

reduction to sulphide if often kinetically inhibited. Diagrams were also produced that excluded the most stable solubility-limiting phase, in order to identify possible metastable and therefore more soluble solids (which in some cases, may act as precursor phases, in accordance with Ostwald's step rule).

C.2.3 Solubility Limit Calculations

Calculations of elemental solubilities were undertaken using the solubility-limiting phases identified by the construction of representative phase diagrams and through literature review for Ni, Zr, Np, Cd, Cr, Cu, Pb, Pu, Ra and U. Calculations were carried out using PHREEQC (Parkhurst and Appelo 1999), together with the "Pitzer" thermodynamic database "data0.ypf.R2"

In undertaking this task, the completeness of the data0.ypf.R2 database was reviewed. In cases where data for solid phases were missing from the data0.ypf.R2 database, mostly data were taken from either the "thermo.com.V8.R6+" or "llnl.dat" databases, depending on what basis elements were required by the "data0.ypf.R2" database, given that PHREEQC and Geochemist's Workbench often use different equilibrium constant "basis" expressions. However, this makes no difference to the final result of solubility calculations, as the same parent standard molal thermodynamic data were used to assemble both databases. The minerals for which thermodynamic data were not available in the data0.ypf.R2 database included: bunsenite (NiO), $Ni(OH)_2$, trevorite ($NiFe_2O_4$), vaesite (NiS_2), millerite (NiS), $CaZrO_3$, chromite ($FeCr_2O_4$) $RaSO_4$, coffinite ($USiO_4$). In addition, data for CaU_2O_7 were taken from the NDA "HATCHES" database (Heath 2007), as this phase is not included in the llnl.dat, thermo.com.V8.R6+ or data0.ypf.R2 databases. In the case of Cr, data from Rai et al. (1986) were also included for $Cr(OH)_3$ as it was identified by Hunter et al. (2006) to be a potential solubility-limiting phase.

Instead of editing the "data0.ypf.R2" database, the extra data required were inserted into the PHREEQC input files, using the "PHASES" command (Parkhurst and Appelo 1999). Where data were available for solid phase hydrolysis reactions in both the Pitzer and Geochemist's Workbench databases, calculations were undertaken using both sets of data for comparison. However, it should be noted that it was beyond the scope of this work to determine whether data added to the "data0.ypf.R2" database were thermodynamically consistent with those data already present.

C.3 RESULTS AND DISCUSSION

Seven of the elements considered are taken to be solubility unlimited. As noted above, I is normally regarded as a conservative (non-reactive) element in groundwater studies and is treated as being solubility-unlimited. In addition, Cu, Cd, Nb, Pb and Ra are cautiously taken to be solubility unlimited due to the absence of suitable data in the "data0.ypf.R2" database. Bruno et al. (2001) note that solubility controls for Ni are not well understood and so Ni is also cautiously taken to be solubility unlimited.

The seven remaining elements (C, Cl, Cr, Zr, U, Np and Pu) are solubility limited. Their solubility-limiting phases and solubility limits for both 'Model 2' Cobourg porewater and cement porewater compositions are discussed below and, in the case of Cr, Zr, U, Np and Pu, are also summarized in Tables C.6 and C.7.

Table C.6: Calculated Solubility Limits and Solubility-limiting Phases for the Elements Considered in the Presence of Model 2 Cobourg Porewater

Element	Solubility-limiting Phases[1]	Notes	Total Concentration (molal)[2] Pitzer (YMP)	Total Concentration (molal)[2] Extended D-H (llnl)
Cr	Eskolaite (Cr_2O_3)	Stable in the absence of iron	1.50E-11	1.08E-12
	Eskolaite (Cr_2O_3)(YMP)	Stable in the absence of iron	4.13E-11	
	Chromite ($FeCr_2O_4$)	Stable in Fe bearing systems (siderite solubility limit)	8.34E-13	1.13E-13
	$Cr(OH)_3$ (YMP)	Metastable	6.20E-06	
	$Cr(OH)_3$(Hatches)	Metastable	4.11E-03	
Zr	$CaZrO_3$	Stable	0	0
	SrZrO3	Metastable	0	0
	Zircon ($ZrSiO_4$)	Metastable	4.83E-39	9.36E-15
	Baddelyite (ZrO_2)	Metastable	2.59E-34	5.46E-10
	Baddelyite (ZrO_2) (YMP)	Metastable	1.64E-28	
	$Zr(OH)_4$ (Hatches)	Metastable	1.30E-31	
U	Uraninite (UO_2)	Stable in the absence of $SiO_{2(am)}$	1.05E-13	3.39E-10
	UO_2(cr) YMP	Stable in the absence of $SiO_{2(am)}$	1.15E-13	
	UO_2(am)	Metastable	9.26E-09	2.97E-05
	$U(OH)_4$(am) (YMP)	Metastable	3.43E-07	
	Coffinite ($UsiO_4$)	Stable ($SiO_{2,am}$ buffer)	3.57E-14	1.10E-10
Np	NpO_2	Stable	8.02E-17	2.90E-18
	NpO_2(cr) (YMP)	Stable	1.17E-16	
	$Np(OH)_4$	Metastable	4.33E-08	1.49E-09
	$Np(OH)_4$(am) (YMP)	Metastable	1.53E-09	
Pu	PuO_2	Stable	8.23E-13	5.49E-13
	PuO_2(cr) (YMP)	Stable	2.20E-13	
	$Pu(OH)_4$	Metastable	1.44E-04	9.11E-05
	$Pu(OH)_4$(am) (YMP)	Metastable	9.07E-08	

Notes:
(1) YMP = thermodynamic data taken from "data0.ypf.R2" rather than “llnl.dat” or where labelled as such, Hatches; cr = crystalline, am = amorphous
(2) Total concentration of element in solution; NA = database insufficient; (-) = PHREEQC could not find a numerical solution

Table C.7: Calculated Solubility Limits and Solubility-limiting Phases for the Elements Considered in the Presence of Cement-equilibrated Model 2 Cobourg Porewater

Element	Solubility-limiting Phases[1]	Notes	Total Concentration (molal)[2] Pitzer (YMP)	Total Concentration (molal)[2] Extended D-H (llnl)
Cr	Eskolaite (Cr_2O_3)	Metastable	2.77E-12	5.84E-12
	Eskolaite (Cr_2O_3)(YMP)	Metastable	7.64E-12	
	Magnesiochromite ($MgCr_2O_4$)	Stable	1.19E-13	2.56E-13
	Chromite ($FeCr_2O_4$)	Metastable	8.19E-13	1.72E-12
	$Cr(OH)_3$(am)(YMP)	Metastable	1.17E-06	
Zr	$CaZrO_3$	Stable	0.00E+00	0.00E+00
	$SrZrO_3$	Metastable	0.00E+00	0.00E+00
	Zircon ($ZrSiO_4$)	Metastable	0.00E+00	8.09E-09
	Baddelyite (ZrO_2)	Metastable	0.00E+00	5.50E-10
	Baddelyite (ZrO_2) (YMP)	Metastable	0.00E+00	
	$Zr(OH)_4$ (Hatches)	Metastable	0.00E+00	
U	$CaUO_4$	Stable	3.83E-14	3.68E-12
	$Ca(UO_2)_6O_4(OH)_6$:$8H_2O$ (YMP)	Metastable	4.82E-04	
	CaU_2O_7 (Hatches)	Metastable	1.04E-05	1.01E-03
	$U(OH)_4$(am) (YMP)	Metastable	1.15E-05	
	$U(OH)_2$(am)	Metastable	3.11E-07	
	UO_2(cr) YMP	Metastable	3.85E-12	
	Uraninite (UO_2)	Metastable	3.52E-12	3.40E-10
Np	NpO_2	Stable	6.35E-17	2.88E-18
	NpO_2(cr) (YMP)	Stable	9.28E-17	
	$Np(OH)_4$	Metastable	3.39E-08	1.48E-09
	$Np(OH)_4$(am) (YMP)	Metastable	1.21E-09	
Pu	PuO_2	Stable	4.37E-16	1.13E-17
	PuO_2(cr) (YMP)	Stable	1.17E-16	
	$Pu(OH)_4$	Metastable	7.54E-08	1.88E-09
	$Pu(OH)_4$(am) (YMP)	Metastable	4.81E-11	

Notes:
(1) YMP = thermodynamic data taken from "data0.ypf.R2" rather than “llnl.dat” or where labelled as such, Hatches; cr = crystalline, am = amorphous
(2) Total concentration of element in solution; NA = database insufficient; (-) = PHREEQC could not find a numerical solution

C.3.1 Carbon

The solubility limit for inorganic C is governed by carbonate mineral equilibria. For the Cobourg porewater, total dissolved C concentrations were calculated by specifying equilibrium with calcite. In Table C.4 (Cobourg porewater) two different C concentrations were calculated, depending on whether or not the solution composition was corrected to achieve electrical neutrality. The C concentration for Cobourg porewater equilibrated with cement is given in Table C.5, while the value for the Guelph water is given in Table C.8.

C.3.2 Chlorine

Calculated saturation indices suggest that Cobourg porewater is undersaturated with respect to halite (NaCl) (Table C.3). It is highly probable that a maximum limit on dissolved Cl concentration would be given by halite saturation since halite has been observed to occur in the Cobourg Formation (INTERA 2011, Section 3.7.1.2). One approach is to use the reported Cl^- concentration for the Cobourg Formation (Table C.1) and speciate the solution so that the total Na+ concentration is adjusted to result in a halite saturation index of 0. However, this approach does not alter the Cl^- concentration. Another option is to use the reported Na^+ concentration and adjust the Cl^- concentration to produce a halite saturation index of 0. However, this results in PHREEQC either failing to find a solution or producing a solution with an exceedingly large charge imbalance. Therefore, a theoretical halite-saturated saline water composition was derived using PHREEQC (and the "data0.ypf.R2" Pitzer database). The following parameters were set:

- Log $pO_2(g)$ = -65.2;
- Log $pCO_2(g)$ = -2.22 (a value that gives a pH of 6.5 with the specified mineral assemblage); and
- Equilibrium with the following minerals: halite, siderite, dolomite, calcite, anhydrite, illite, sylvite, celestite, SiO_2(am).

Initial input that included Br and B data from Table C.1 led to PHREEQC's solver not being able to converge. Therefore, these elements were excluded. Since they are present at only trace concentrations, this approach will not have a significant impact on the calculated solubility-limited Cl concentration. The resulting calculated solution composition ("Model 3") is given in Table C.9.

C.3.3 Chromium

Chromium solubility diagrams for the Model 2 Cobourg Formation porewater composition are given in Figure C.2. Where there is sufficient dissolved iron to result in the occurrence of discrete iron phases there is a chromite ($FeCr_2O_4$) stability field at all pH > 5.5. Decreasing pH would result in firstly eskolaite (Cr_2O_3) and then brezinaite (Cr_3S_4) becoming the stable solubility limiting phases. In Fe-free systems (or where iron is not in sufficient quantities to form discrete phases), the eskolaite field expands to cover a wider pH range, between pH values of approximately 4 and 8, and magnesiochromite ($MgCr_2O_4$) becomes stable instead of chromite. For the Model 2 porewater, eskolaite or chromite are the most stable phases, depending upon dissolved iron availability.

Table C.8: Model Guelph Water Composition

Parameter	Concentration (molality)
Ionic Strength	7.20E+00
pH	6.5
pe	-1.97
Eh (V)	-0.117
Na	4.57E+00
Ca	7.88E-01
Mg	2.28E-02
K	9.37E-02
Sr	8.18E-03
Cl	6.48E+00
Br	2.15E-02
SO4	4.60E-03
C	7.42E-05
Al	1.13E-10
Si	5.87E-04
av. % charge error	-1.6
log $pCO_2(g)$	-3.7
log $pO_2(g)$	-65.2
Saturation Indices	
Anhydrite	0.00
Calcite	0.00
Dolomite	0.00
Gypsum	-0.09
Halite	0.00
Strontianite	-0.12
Sylvite	-1.34
Celestite	0.00

Table C.9: Summary of "Model 3" Cobourg Formation Porewater (Halite-saturated)

	Conc. (mol L^{-1})	Species	Conc. (molal)	Log Act.	Species	Conc. (molal)	Log Act.	Species	Conc. (molal)	Log Act.	Species	Conc. (molal)	Log Act.
Ionic Strength	7.39	AlOH+2	4.45E-11	-12.616	Ca+2	3.77E-02	-0.949	FeCl+	7.88E-03	-2.497	K+	2.15E+00	0.238
pH	6.5	AlO2-	1.87E-11	-11.178	CaSO4	2.38E-03	-2.623	Fe+2	4.14E-04	-3.027			
pe	-2.031	HAlO2	5.87E-12	-11.231	CaCl+	1.92E-05	-1.048	FeHCO3+	1.40E-05	-5.247	Mg+2	1.20E-03	-2.205
Eh(V)	-0.12	AlO+	4.38E-12	-11.752	CaCO3	7.52E-06	-5.124	FeCO3	8.03E-06	-5.095	MgHCO3+	3.66E-05	-4.83
log $pO_2(g)$	-65.5	Al+3	1.61E-14	-14.018	CaOH+	9.40E-08	-7.421	FeOH+	1.64E-06	-6.178	MgCO3	1.89E-07	-6.724
log $pCO_2(g)$	-2.22				CaCl2	8.25E-17	-16.084	Fe(CO3)2-2	9.75E-09	-10.95	MgOH+	6.58E-08	-7.519
		HCO3-	8.35E-04	-3.69				Fe(OH)2	1.21E-11	-10.919			
Al	7.34E-11	CO2	5.04E-05	-3.683	Cl-	7.21E+00	0.667	Fe(OH)2+	5.47E-12	-11.656	Na+	5.08E+00	0.901
C	9.56E-04	MgHCO3+	3.66E-05	-4.83	FeCl+	7.88E-03	-2.497	Fe+3	3.72E-12	-18.074			
Ca	0.0401	FeHCO3+	1.40E-05	-5.247	CaCl+	1.92E-05	-1.048	FeOH+2	2.81E-12	-13.815	O2	0.00E+00	-68.399
Cl	7.22	FeCO3	8.03E-06	-5.095	FeCl+2	1.37E-14	-16.127	Fe(OH)3	5.05E-14	-13.297			
Fe	8.32E-03	CaCO3	7.52E-06	-5.124	FeCl2+	6.51E-16	-15.58	FeCl+2	1.37E-14	-16.127	SO4-2	4.72E-02	-3.369
K	2.15	CO3-2	4.41E-06	-7.542	CaCl2	8.25E-17	-16.084	Fe(OH)4-	6.23E-15	-14.938	CaSO4	2.38E-03	-2.623
Mg	0.00124	MgCO3	1.89E-07	-6.724	ClO4-	0.00E+00	-151.859	FeCl2+	6.51E-16	-15.58	HSO4-	3.46E-08	-7.864
Na	5.08	Fe(CO3)2-2	9.75E-09	-10.95				FeSO4+	1.66E-17	-17.173	HS-	2.45E-11	-11.344
S	0.0496				SiO2	5.06E-04	-2.749	Fe(SO4)2-	1.07E-18	-18.702	SO3-2	1.42E-13	-15.787
Si	5.10E-04	Sr+2	3.72E-04	-3.263	HSiO3-	3.19E-06	-6.228				FeSO4+	1.66E-17	-17.173
Sr	3.72E-04							H2	9.19E-13	-12.037	Fe(SO4)2-	1.07E-18	-18.702

Chromium solubility diagrams for cement-equilibrated Model 2 Cobourg Formation porewater are given in Figure C.3. When there is sufficient dissolved iron present for discrete Fe-bearing phases to form, the most likely solid phases to control aqueous chromium concentrations are chromite (at pH <11) and magnesiochromite (at pH > 11). Under the highly alkaline conditions calculated for cement-equilibrated Cobourg Formation porewater (pH 12) magnesiochromite would be the most likely solubility-limiting phase in Fe-bearing systems. If neither chromite nor magnesiochromite form, for kinetic reasons or because aqueous iron and magnesium concentrations are too low, then the most likely solubility-limiting solid phase is eskolaite, over the entire pH range that is plausible in natural porewaters and cement porewaters. It is noteworthy that in the Fe-bearing system, solubility limitation of chromium concentrations is predicted to be several orders of magnitude greater in cement than in the surrounding natural rock. In contrast, in the Fe-free system, solubility limitation by eskolaite results in similar aqueous chromium concentrations to those in the natural porewater.

Eskolaite (Cr_2O_3) has been previously considered as a solubility-limiting phase for chromium (III) present in stainless steel (e.g., Wilson et al. 2009). However, Hunter et al. (2006) used $Cr(OH)_3$ which is metastable (and therefore, of a higher solubility) for similar purposes (Beverskoy and Puigdomenech 1997).

C.3.4 Zirconium

Solubility diagrams for Zr are given in Figures C.4 and C.5. These figures show that throughout the considered pH range, the most stable potential solubility limiting phase is $CaZrO_3$ in water with the composition of either Model 2 Cobourg Formation water, or cement-equilibrated Model 2 Cobourg Formation water. This phase has an extremely low solubility (PHREEQC reports this as 0).

If $CaZrO_3$ does not precipitate for kinetic reasons then in the presence of water with the composition of the model natural porewater, the next most stable phase is $SrZrO_3$. This phase would buffer aqueous zirconium concentrations at concentrations approximately 25 orders of magnitude greater than would $CaZrO_3$, although still at extremely low levels. Again, $CaZrO_3$ could control aqueous zircon concentrations across the considered pH range. If both $CaZrO_3$ and $SrZrO_3$ did not precipitate, then zircon ($ZrSiO_3$) would be the most likely solubility-limiting phase. The solubility of this solid is much greater than that of the other phases and would be the same across the considered pH range. Baddleyite (ZrO_2) is also a possible solubility-limiting phase, which would buffer concentrations at around 5 orders of magnitude greater than zircon, again at similar levels across the pH range.

Zirconium solubility-limiting phases which have previously been considered for safety assessment calculations include: ZrO_2 (Kristallin-I, Nagra, SKB-91 and SKI-90, McKinley and Savage 1994; Bruno et al. 1997; Skagius et al. 1999) and $Zr(OH)_4$ PNC /H-3 (McKinley and Savage 1994). $Zr(OH)_4$ was also identified as a solubility-limiting phase in the SRCan assessment (Duro et al. 2006).

C.3.5 Uranium

Uranium solubility diagrams for the Model 2 Cobourg Formation porewater are given in Figure C.6. The most thermodynamically stable potential solubility-controlling phase at the calculated in-situ pH of 6.5 is coffinite ($USiO_4$). If this phase does not precipitate, owing to kinetic reasons or because the dissolved activity of dissolved silica is too low, then uraninite (UO_2) would be the next most stable solubility-controlling phase. However, the solubility of uraninite is very similar to that of coffinite. For water of this overall composition, at lower pH than about 5,

US_3 would be the most stable solubility-controlling phase, while at pH greater than about 8, haiweeite ($Ca(UO_2)_2(Si_2O_5)3{:}5H_2O$) would be the most stable phase. If this phase too does not form, owing to unfavourable kinetics, then $CaUO_4$ could be the most stable solubility-limiting phase under these alkaline conditions.

In the presence of cement-equilibrated water, at pH 12, $CaUO_4$ is the most stable solid U phase (Figure C.7). If this phase does not form, then metastable uraninite will be the most likely solubility-limiting phase. It is noteworthy that the solubility of both these phases is rather similar and would buffer the aqueous uranium concentration at a value similar to that in the natural porewater, when either coffinite or uraninite is the solubility-limiting phase.

It should be borne in mind that uranium solubility is strongly dependant on solution redox conditions (as well as pH). This should be recognized while considering U concentrations in light of any updated redox data.

UO_2 (crystalline or amorphous) has been identified as a potential near-field solubility-limiting phase, especially in low Eh groundwaters (McKinley and Savage 1994; Langmuir 1997). Under high Eh conditions, uranophane ($Ca(H_3O)_2(UO_2)_2(SiO_4)_2{:}\ 3H_2O$) has been considered (Langmuir 1997) as it forms as a secondary mineral in massive uranium ore deposits. It has been suggested that schoepite ($UO_3{:}2H_2O$) is metastable with respect to uranophane and that kinetic considerations mean that it is more likely to occur in the short term (Bruno et al. 1997).

Under oxidising conditions, a U(VI)-Ca(II) oxide called becquerelite ($CaU_6O_{19}{:}11H_2O$) has been observed and this too could be a solubility-limiting phase (Duro et al. 2006).

Bruno et al. (2001) found in a blind modelling study of natural analogue sites, that under reducing conditions, uranium concentrations in nature are controlled by uranium oxides and coffinite.

$CaUO_4$ has also been previously identified as a U solubility-limiting phase under highly alkaline cementitious porewater conditions (BNFL 2002; Wilson et al. 2009). However, it has been suggested that under highly alkaline cementitious conditions, CaU_2O_7 may be the U solubility-limiting phase (Hunter et al. 2006). In addition, the YMP database includes $Ca(UO_2)_6O_4(OH)_6{:}8H_2O$.

C.3.6 Neptunium

A neptunium solubility diagram for the Model 2 Cobourg Formation water is given in Figure C.8. A similar diagram for cement-equilibrated water is given in Figure C.9. In both cases, the solubility diagrams are dominated by NpO_2 across the full range of pH; this phase would be the stable solubility-limiting phase at the estimated in-situ pH of the Cobourg Formation water and in cement-equilibrated porewater. If this phase is excluded, metastable $Np(OH)_4$ appears, again across the full pH range; this would be the metastable solubility-limiting phase in both the natural porewater and in cement-equilibrated porewater.

It is apparent from a comparison of Figures C.8 and C.9 that if NpO_2 solubility controls the concentration of aqueous neptunium in both cement-equilibrated water and natural porewater, both kinds of water would have similar neptunium concentrations. Similarly, if $Np(OH)_4$ controls the solubility of neptunium, then both cement-equilibrated water and natural porewater would have similar aqueous neptunium concentrations. Therefore, only if there are different solubility-controlling phases in the presence of each water, would the cement-equilibrated porewater and natural porewater have substantially different neptunium concentrations. In this case, the

NpO_2-equilibrated water would have a neptunium concentration around 10 orders of magnitude lower than the $Np(OH)_4$-equilibrated water.

A number of programs have considered neptunium and, generally, NpO_2 or $Np(OH)_4$ are assumed to be the main solubility-limiting phases (McKinley and Savage 1994). Under higher Eh/pe conditions, Np_2O_5 has also been identified (Duro et al. 2006).

C.3.7 Plutonium

Plutonium solubility diagrams for the Model 2 Cobourg Formation porewater are given in Figure C.10. The most stable phase that could control plutonium solubility is PuO_2 under all conditions. If this phase is excluded from the diagrams, it is replaced by metastable $Pu(OH)_4$, which would buffer dissolved plutonium at a concentration around six orders of magnitude greater than in the case where PuO_2 is the dominant solubility-controlling phase. At the estimated pH of the in-situ porewater, 6.5, the solubility of both phases is pH-dependent, with solubility falling as pH increases to about 7.5; at higher pH, the solubilities are constant.

The solubilities of plutonium-bearing phases in the presence of water with the composition of cement-equilibrated Model 2 Cobourg Formation porewater are illustrated in Figure C.11. This figure shows that the most likely solubility controlling phases are the same as in the presence of the natural porewater. However, at the high pH of the cement-equilibrated porewater, pH12, the solubility of plutonium would be around 5 orders of magnitude lower than in the natural porewater, assuming that the same solubility-limiting phase is present in each case.

A number of programs have considered Pu, and in general, PuO_2 or $Pu(OH)_4$ are assumed to be the main solubility-limiting phases (e.g., McKinley and Savage 1994; Duro et al. 2006).

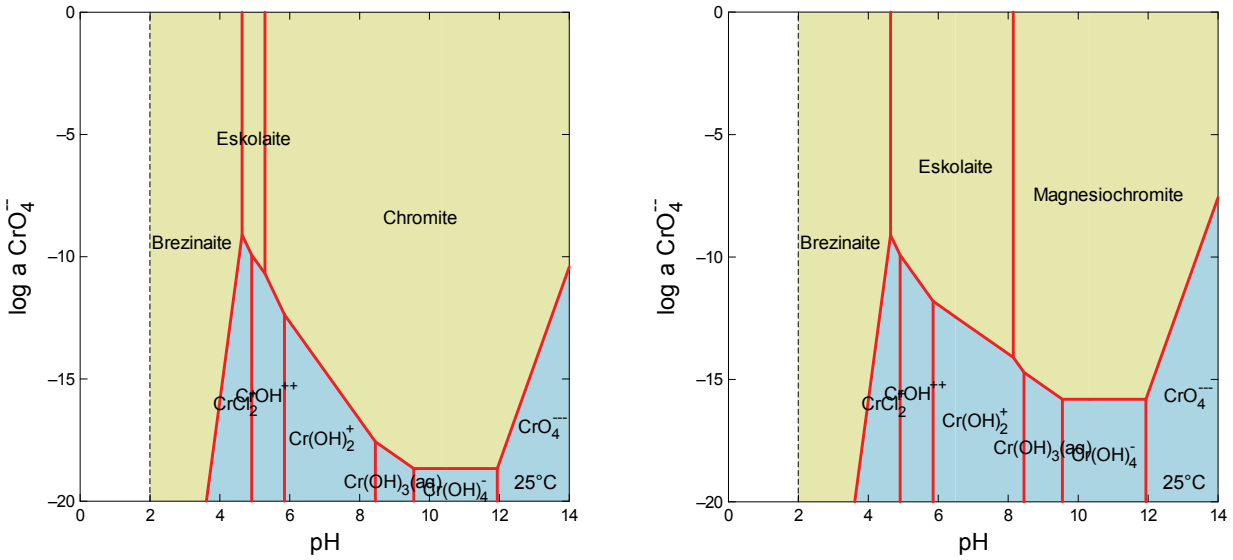

Note: for all phase diagrams: solid phases are coloured kaki and aqueous species are blue.

Left: All stable Cr minerals and aqueous species in the thermodynamic database allowed. Right: As for Left, but aqueous Fe concentration reduced to a trivial level (<1E-6 mol m^{-3}). Brezinaite is Cr_3S_4. Eskolaite is Cr_2O_3. Magnesiochromite is $MgCr_2O_4$. Chromite is $FeCr_2O_4$.

Figure C.2: Chromium Solubility Diagrams for Cobourg Formation "Model 2" Porewater (T = 25°C, P = 1 bar)

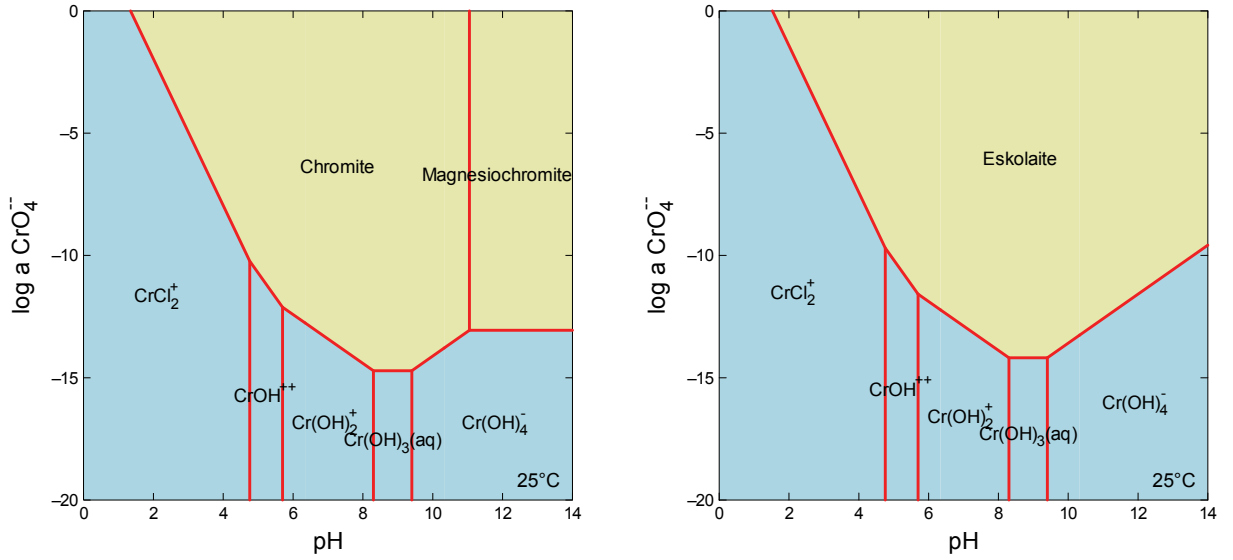

Note: Left: All stable Cr minerals and aqueous species in the thermodynamic database allowed. Right: As for Left, but chromite ($FeCr_2O_4$) and magnesiochromite ($MgCr_2O_4$) are suppressed. Eskolaite is Cr_2O_3.

Figure C.3: Chromium Solubility Diagrams for Cement-equilibrated Cobourg Formation "Model 2" Porewater (T = 25°C, P = 1 bar)

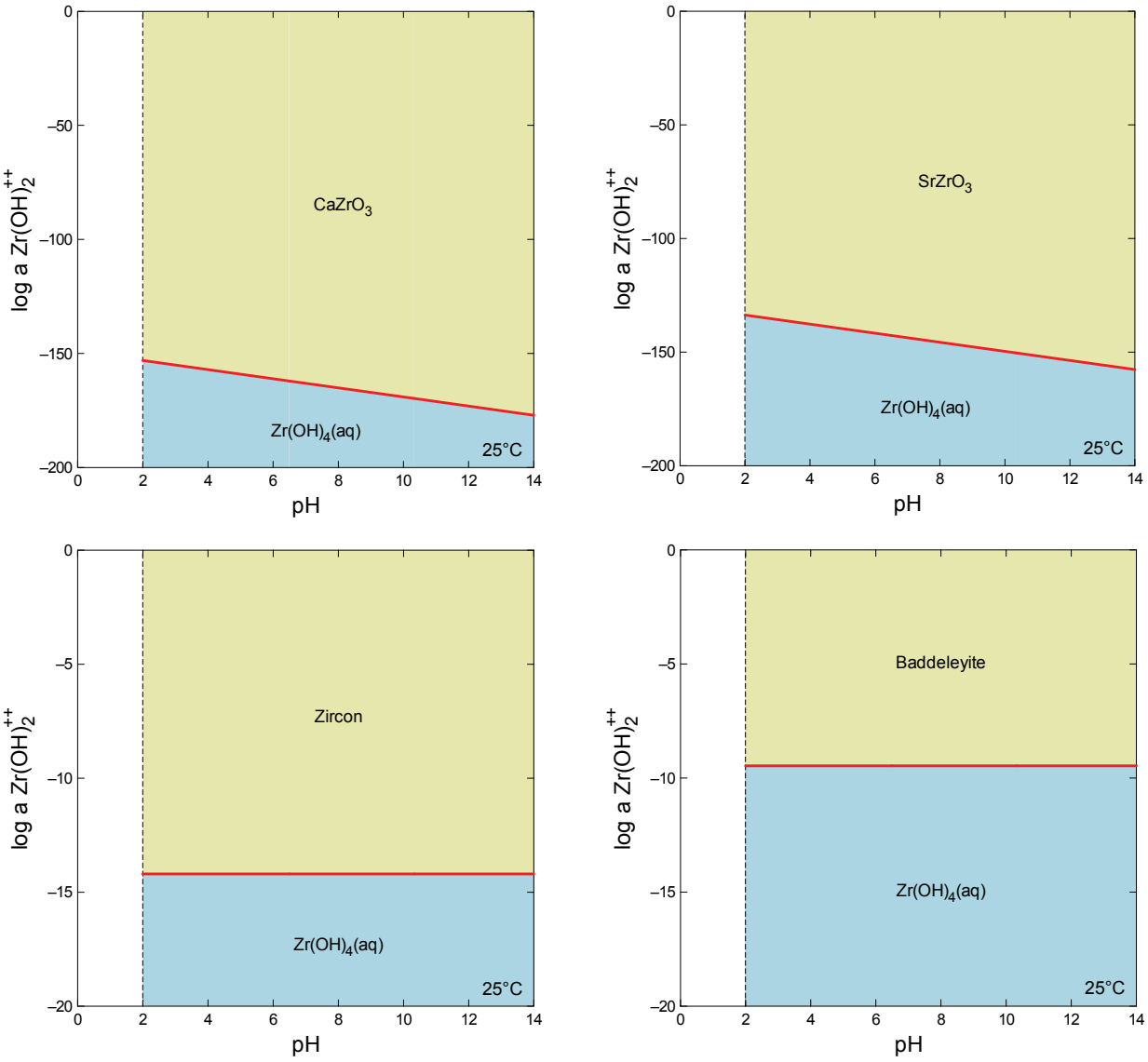

Note: Upper Left: All stable Zr minerals and aqueous species in the thermodynamic database allowed. Upper Right: As for Upper Left, but $CaZrO_3$ is suppressed. Bottom Left: As for Upper Left, but $CaZrO_3$ and $SrZrO_3$ are suppressed. Bottom Right: As for Upper Left, but $CaZrO_3$, $SrZrO_3$ and Zircon are suppressed. Zircon is $ZrSiO_4$ and Baddleyite is ZrO_2.

Figure C.4: Zirconium Solubility Diagrams for Cobourg Formation "Model 2" Porewater (T = 25°C, P = 1 bar)

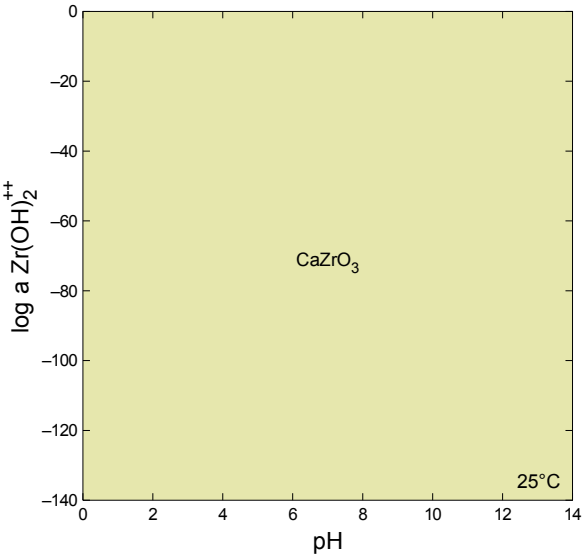

Note: All stable Zr minerals and aqueous species in the thermodynamic database allowed.

Figure C.5: Zirconium Solubility Diagram for Cement-equilibrated Cobourg Formation "Model 2" Porewater (T = 25°C, P = 1 bar)

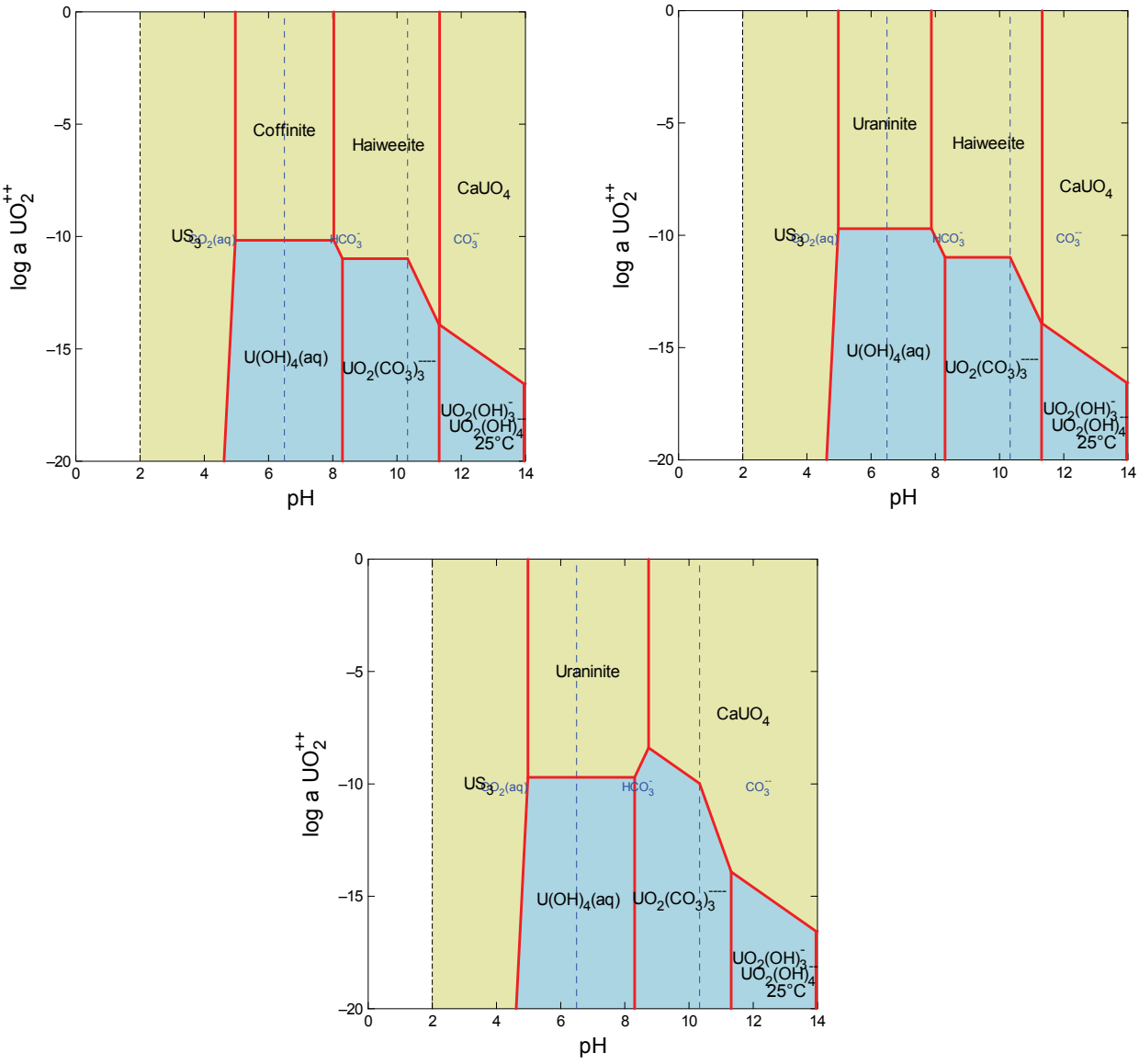

Note: Upper Left: All stable U minerals and aqueous species in the thermodynamic database allowed. Upper Right: As for Upper Left, but Coffinite ($USiO_4$) is suppressed. Lower: As for Upper Left, but Haiweeite ($Ca(UO_2)_2(Si_2O_5)_3{:}5H_2O$) is suppressed. Uraninite is UO_2.

Figure C.6: Uranium Solubility Diagrams for Cobourg Formation "Model 2" Porewater (T = 25°C, P = 1 bar)

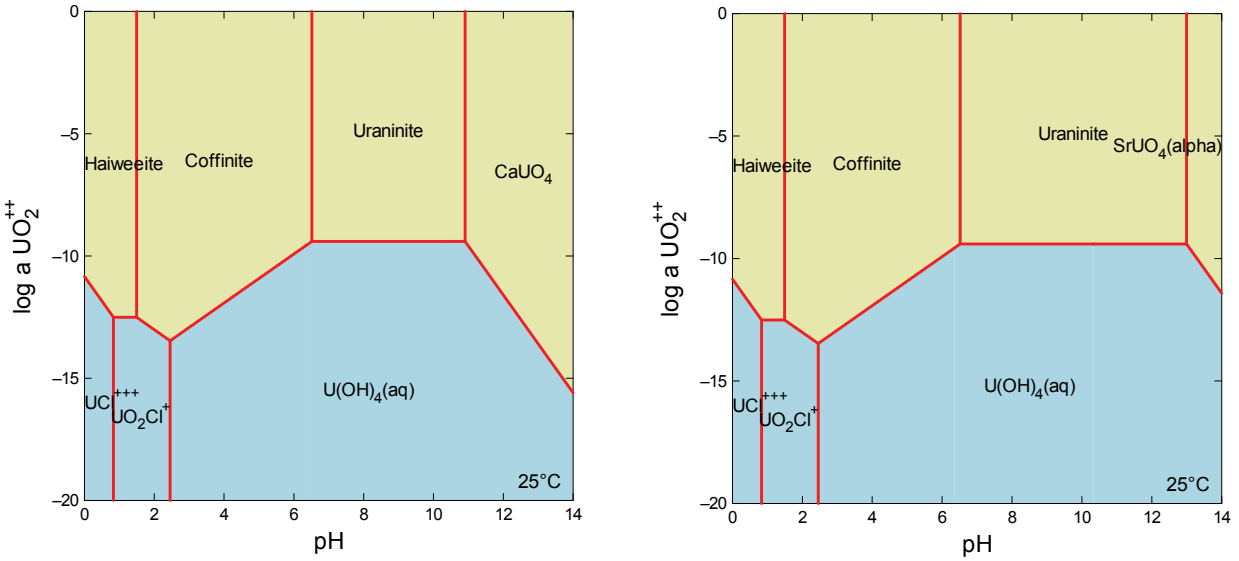

Note: Left: All stable U minerals and aqueous species in the thermodynamic database allowed. Upper Right: As for Left, but $CaUO_4$ is suppressed. Haiweeite is $Ca(UO_2)_2(Si_2O_5)_3{:}5H_2O$. Coffinite is $USiO_4$. Uraninite is UO_2.

Figure C.7: Uranium Solubility Diagrams for Cement-equilibrated Cobourg Formation "Model 2" Porewater (T = 25°C, P = 1 bar)

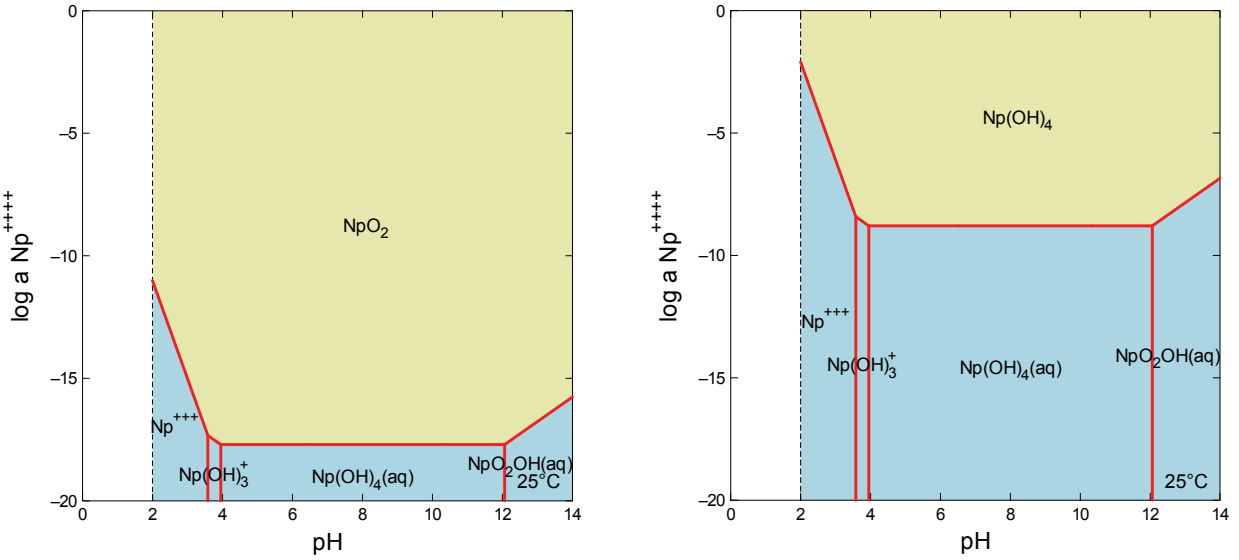

Note: Left: All stable Np minerals and aqueous species in the thermodynamic database allowed. Right: As Left, but NpO_2 is suppressed.

Figure C.8: Neptunium Solubility Diagrams for Cobourg Formation "Model 2" Porewater (T = 25°C, P = 1 bar)

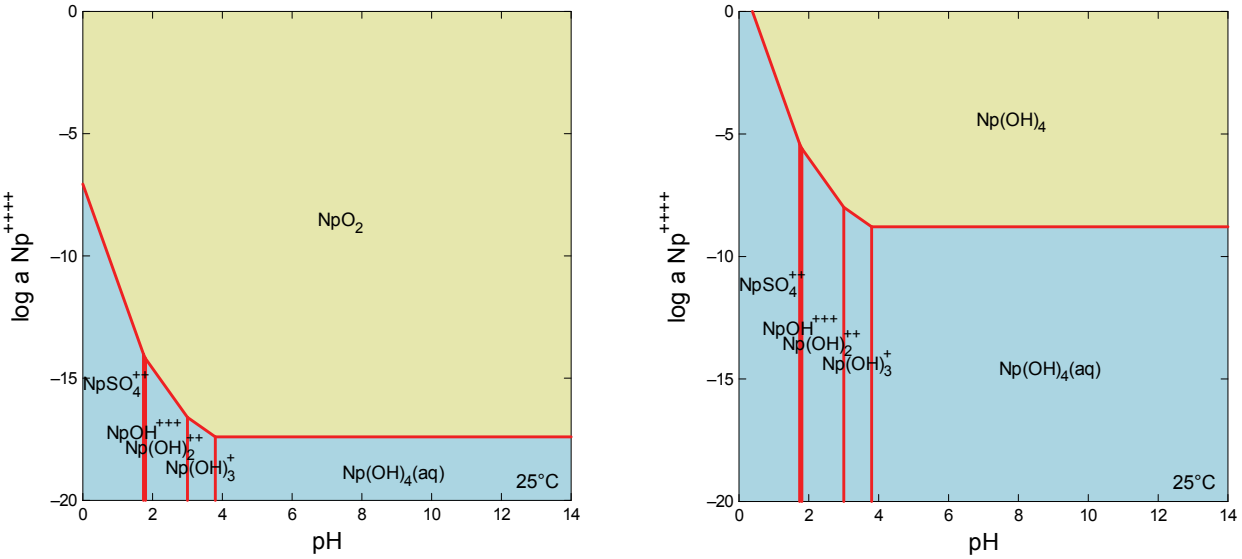

Note: Left: All stable Np minerals and aqueous species in the thermodynamic database allowed. Right: As Left, but NpO_2 is suppressed.

Figure C.9: Neptunium Solubility Diagrams for Cement-equilibrated Cobourg Formation "Model 2" Porewater (T = 25°C, P = 1 bar)

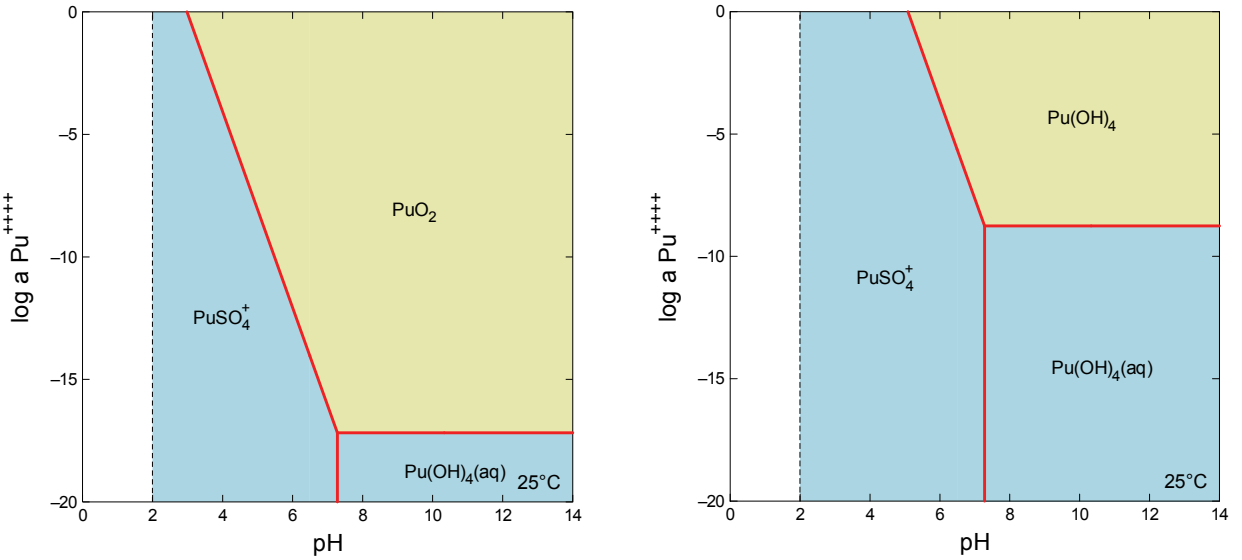

Note: Left: All stable Pu minerals and aqueous species in the thermodynamic database allowed. Right: As for Left, but PuO_2 is suppressed

Figure C.10: Plutonium Solubility Diagrams for Cobourg Formation "Model 2" Porewater (T = 25°C, P = 1 bar)

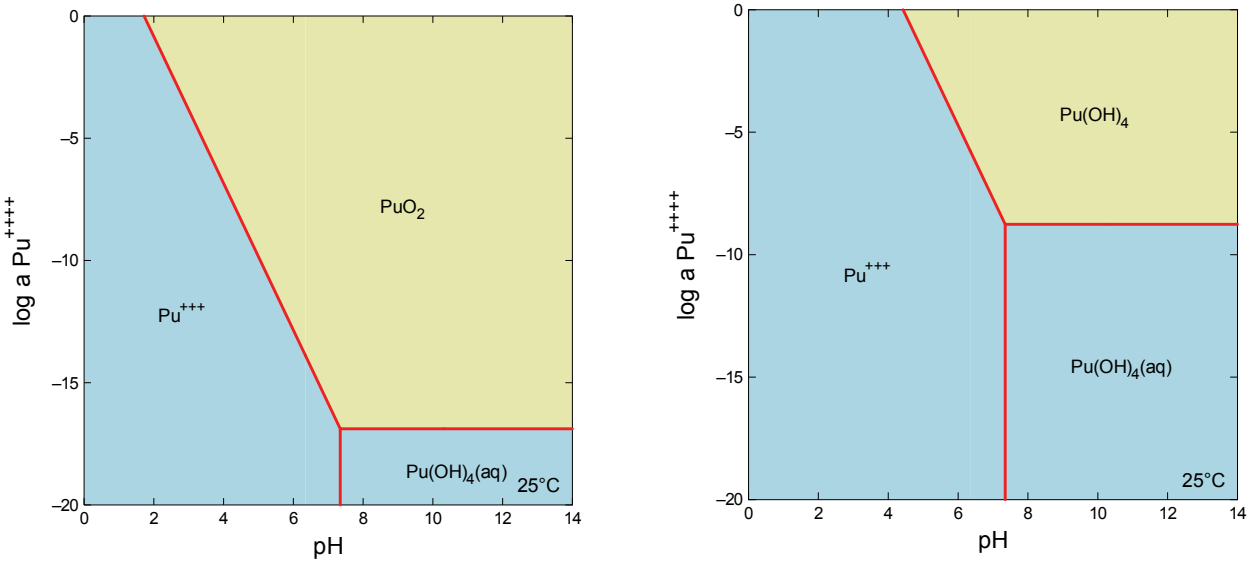

Note: Left: All stable Pu minerals and aqueous species in the thermodynamic database allowed. Right: As for Left, but PuO_2 is suppressed.

Figure C.11: Plutonium Solubility Diagrams for Cement-equilibrated Cobourg Formation "Model 2" Porewater (T = 25°C, P = 1 bar)

C.3.8 Effect of Water Composition Variation on Calculated Solubilities

In order to determine the possible effect of composition variation (especially with regard to salinity) on solubility limits, the higher salinity (NaCl saturated) Guelph water composition (Table C.1) was subjected to aqueous speciation calculations using the same approach as that previously described for Cobourg porewater. The speciation indicated that water composition was relatively close to equilibrium with respect to a number of minerals, namely: anhydrite (SI = -0.31); halite (SI = 0.04); celestite (SI = -0.38). In addition, the water composition was oversaturated with respect to dolomite (SI = 1.15); SiO_2(amorphous) (SI = 1.77). The calculated log $pO_{2(g)}$ for this water (using the measured Eh as input) is -66.99, a value that is relatively similar to that adopted for the Model 2 Cobourg porewater (log $pO_{2(g)}$ = 65.2). The pH of the Guelph is the same as that associated with Cobourg porewater (pH 6.5), although the $pCO_{2(g)}$ is lower (-3.8 log units, rather than -2.4 log units).

A 'model' Guelph porewater composition was produced, by setting total solute activities to be at equilibrium with specified solid phases: illite (Al); calcite (HCO_3^-); dolomite (Mg); halite(Na); anhydrite (S); $SiO_{2(am)}$(Si), Celestite (Sr). Calculated solubility limits for this water composition are compared to those calculated for Cobourg (Model 2) porewater in Table C.8. Calculated total solute concentrations are given in Table C.10. The effects of variation in salinity and $pCO_{2(g)}$ (and to a lesser extent, $pO_{2(g)}$) between the two water compositions resulted in calculated solubility limits varying by values of up to approximately two orders of magnitude (e.g., uranium). However, many values are within an order of magnitude.

Table C.10: Calculated Solubility Limits for Guelph and Cobourg (Model 2) Waters (Pitzer Database)

Element	Solubility-limiting Phases[1]	Total Conc. (molal)[2] Guelph	Total Conc. (molal)[2] Cobourg M2
Cr	Eskolaite (Cr_2O_3)	1.63E-11	1.50E-11
	Eskolaite (Cr_2O_3)(YMP)	4.49E-11	4.13E-11
	Chromite ($FeCr_2O_4$)	3.77E-12	8.34E-13
	$Cr(OH)_3$ (YMP)	8.71E-06	6.20E-06
	$Cr(OH)_3$(Hatches)	5.76E-03	4.11E-03
Zr	$CaZrO_3$	0	0
	SrZrO3	0	0
	Zircon ($ZrSiO_4$)	6.81E-39	4.83E-39
	Baddelyite (ZrO_2)	3.65E-39	2.59E-34
	Baddelyite (ZrO_2) (YMP)	2.31E-28	1.64E-28
U	Uraninite (UO_2)	1.27E-15	1.05E-13
	UO_2(cr) YMP	1.39E-15	1.15E-13
	UO_2(am)	1.12E-10	9.26E-09
	$U(OH)_4$(am) (YMP)	5.85E-09	3.43E-07
	Coffinite ($USiO_4$)	4.33E-16	3.57E-14
Np	NpO_2	5.69E-17	8.02E-17
	NpO_2(cr) (YMP)	8.33E-17	1.17E-16
	$Np(OH)_4$	4.29E-08	4.33E-08
	$Np(OH)_4$(am) (YMP)	1.53E-09	1.53E-09
Pu	PuO_2	1.02E-13	8.23E-13
	PuO_2(cr) (YMP)	2.72E-14	2.20E-13
	$Pu(OH)_4$	2.47E-05	1.44E-04
	$Pu(OH)_4$(am) (YMP)	1.58E-08	9.07E-08

Notes:
(1) Thermodynamic data for solid phase hydrolysis reactions were taken from *llnl.dat* unless otherwise specified as YMP (*data0.ypf.R2*) or "Hatches" database; cr = crystalline, am = amorphous
(2) Total concentration of element in solution

C.4. SUMMARY AND CONCLUSIONS

Aqueous speciation calculations were carried out for a model in-situ Cobourg Formation porewater (Table C.4) and a water composition produced by equilibrating this porewater with cement (Table C.5), using the Yucca Mountain Project (YMP) Pitzer database, "data0.ypf.R2" (USDOE 2007). Calculations were also undertaken for a model in-situ Guelph Formation water composition (Table C.8). There are limits to the YMP Pitzer database; however it is deemed to be the best available at present for simulating the very saline waters at the Bruce nuclear site.

Solubility calculations were then carried out for these model waters for C, Cl, Cr, Zr, U, Np and Pu, primarily using the YMP database (Ni, Cu, Nb, Cd, I, Pb and Ra were taken to be solubility-unlimited). Thermodynamic modelling was used to determine possible solubility limiting phases for each porewater considered. The results of this modelling were compared against the solubility limiting phases identified in previous work by other radioactive waste organizations.

Both **carbon** and **chlorine** are relatively soluble elements that are major solutes within the porewaters. These elements were specified to be solubility-limited by calcite and halite respectively, since these minerals have been identified in host rocks of the DGR (INTERA 2011, Sections 3.7.1.1 and 3.7.1.2).

For the Model 2 porewater, eskolaite (Cr_2O_3) is the most stable **chromium** solid. In the presence of large amounts of iron (in the vicinity of steel containers), chromite ($FeCr_2O_4$) could be a stable solubility-limiting phase. However, the solubility of this phase is similar to, or lower than, that of eskolaite, depending upon the pH. It is likely that if chromium is present mainly as a component of steel, or other alloys, it will probably have a very low solubility, as represented by eskolaite. However, some safety assessments in other radioactive waste programs have conservatively used the much more soluble $Cr(OH)_3$ as the solubility-limiting phase. This conservative approach is also taken here.

With regard to **zirconium**, the most stable phase was calculated to be $CaZrO_3$, which is effectively insoluble. Metastable ZrO_2 (baddleyite) may be considered as a reasonable solubility-limiting phase. The solubilities calculated using the YMP and thermo.com.V8.R6+ databases for the Cobourg Formation porewater are comparable; both sets of calculations reveal that zirconium is effectively insoluble. However, for cement porewater the solubility calculated using the YMP database is very low (effectively zero) compared to that calculated using the thermo.com.V8.R6+ database (5.50E-10 molal). These differing solubilities calculated with the two databases appear to reflect the differing thermodynamic data present. Whereas Zr^{4+} is the only aqueous zirconium species present in the YMP database, the thermo.com.V8.R6+ database contains a wide range of Zr-hydroxy species. Since these latter species become more important as pH increases, zirconium is calculated to be more soluble in the cement porewater when the thermo.com.V8.R6+ database is used than when the YMP database is used. The higher solubility at high pH calculated using the former database is the most reasonable value. It is uncertain how rapidly zirconium at this higher solubility limit would precipitate after migrating from a high-pH cement-buffered porewater into the surrounding lower-pH natural porewater, i.e., assuming that its aqueous concentration was controlled by its solubility rather than by sorption. In view of these considerations, a value of 6E-10 molal is recommended conservatively as the solubility limit for zirconium in both Cobourg Model 2 and cement-equilibrated Cobourg porewater compositions.

With regard to **uranium**, coffinite ($USiO_4$) is the most likely stable solubility phase in the natural porewater. A reasonable choice for a metastable solubility-limiting phase would be UO_2(am) or uraninite (UO_2). However, the calculations showed that $U(OH)_4$ has a much higher solubility than any of these phases and therefore the solubility limit for $U(OH)_4$ is cautiously adopted. Under highly alkaline cementitious conditions, $CaUO_4$ is the most likely stable solubility-limiting phase. However, metastable UO_2 could plausibly limit the concentration of dissolved uranium. The YMP database also includes $Ca(UO_2)6O_4(OH)_6{:}8H_2O$ (becquerelite) which, if metastably present would limit uranium concentrations at around eight orders of magnitude greater than for UO_2 limitation. However, naturally $Ca(UO_2)6O_4(OH)_6{:}8H_2O$ is a weathering product of uraninite and there is no evidence that it would form within a cementitious environment. Consequently, UO_2(cr) is taken as the solubility-limiting phase.

Metastable $Np(OH)_4$ is a reasonable (and conservative) solubility-limiting phase for **neptunium**. The calculated solubility is the same in both the natural porewater and cement-equilibrated water. Therefore, little variation in solubility-limited concentrations would be expected between cementitious and non-cementitious areas of the DGR.

For **plutonium**, the most stable possible solubility-limiting phase is PuO_2. However, $Pu(OH)_4$ (especially of low crystallinity) is a reasonable metastable solubility-limiting phase. The cement pore fluid is likely to have the lowest concentration of Pu in solubility-limited cases.

REFERENCES FOR APPENDIX C

Bethke, C.M. 2008. Geochemical and Biogeochemical Reaction Modelling (2nd Ed.) Cambridge University Press. Cambridge, United Kingdom.

Beverskoy B and I. Puigdonenech. 1997. Revised pourbaix diagrams for chromium at 25-300°C. Corrosion Science 39 (1), 43-57.

BNFL. 2002. Drigg Post-Closure Safety Case: Near-Field Biogeochemistry. British Nuclear Fuels. Risley, United Kingdom.

Bruno, J., E. Cera, J. de Pablo, L. Duro, S. Jordana and D. Savage. 1997. Determination of Solubility Limits to be Used in SR 97. Swedish Nuclear Fuel and Waste Management Company Technical Report 97-33. Stockholm, Sweden.

Bruno, J., L. Duro and M. Grivé. 2001. The Applicability and Limitations of the Geochemical Models and Tools Used in Simulating Radionuclide Behaviour in Natural Waters. Lessons Learned from the Blind Predictive Modelling Exercises Performed in Conjunction with Natural Analogue Studies. Swedish Nuclear Fuel and Waste Management Company Technical Report TR-01-20. Stockholm, Sweden.

Duro, L., M. Grive, E. Cera, C. Domenech and J. Bruno. 2006. Determination and Assessment of the Concentrations Limits to be Used in SR-Can. Swedish Nuclear Fuel and Waste Management Company Technical Report TR-06-32. Stockholm, Sweden.

Fuge, R. and C.C. Johnson. 1986. The Geochemistry of Iodine — A Review. Environmental Geochemistry and Health 8, 31-54.

Heath, T. 2007. The Hatches User Manual. Serco Assurance, Harwell, United Kingdom.

Hunter, F.M.I., C.P. Jackson, M. Kelly and S.J. Williams. 2006. A Post-Closure Toxicity Screening Assessment for the Nirex Phased Geological GDF Concept. Serco Assurance Report SA/ENV-0854. Harwell, United Kingdom.

Hutcheon, I., M. Shevalier and H.J. Abercrombie. 1993. pH buffering by metastable mineral-fluid equilibria and evolution of carbon dioxide fugacity during burial diagenesis. Geochimica et Cosmochimica Acta 57, 1017-1027.

INTERA. 2011. Descriptive Geosphere Site Model, Deep Geologic Repository Bruce Site. Intera Engineering Ltd. report for the Nuclear Waste Management Organization DGR-TR-2011-24 R000. Toronto, Canada.

Johnson, J.W., E.H. Oelkers and H. Helgeson. 1992. SUPCRT92: a software package for calculating the standard molal thermodynamic properties of minerals, gases, aqueous species, and reactions for 1–5000 bar and 0–1000ºC. Computers & Geosciences 18, 899–947.

Langmuir, D. 1997. Aqueous Environmental Geochemistry. Prentice Hall, New Jersey.

Lothenbach B., T. Matschei, G. Moschner and F.P. Glasser. 2008. Thermodynamic modelling of the effect of temperature on the hydration and porosity of Portland cement. Cement and Concrete Research 38 (1), 1-18.

McKinley, I.G. and D. Savage. 1994. Comparison of solubility databases used for HLW performance assessment. Fourth International Conference on the Chemistry and Migration Behaviour of Actinides and Fission Products in the Geosphere, 657-665.

NIREX. 1997. Hydrogeological Investigations: The Hydrochemistry of Sellafield, 1997 Update. Nirex Report S/97/089. Harwell, United Kingdom.

Parkhurst, D.L. and C.A.J. Appelo. 1999. User's guide to PHREEQC (Version 2) – a computer program for speciation, batch reaction, one-dimensional transport, and inverse geochemical calculations. Water-Resources Investigations Report 99-4259.

Rai, D., B.M. Sass and D.A. Moore. 1986. Chromium (III) hydrolysis constants and solubility of chromium (III) hydroxide. Inorganic Chemistry 26, 345-349.

Sheppard, M.I. and D.H. Thibault. 1992. Chemical behaviour of iodine in organic and mineral soils. Applied Geochemistry 7, 265-272.

Skagius, K., M. Pettersoon, M. Wiborgh, Y. Albinsson and S. Holgersson. 1999. Compilation of Data for the Analysis of Radionuclide Migration from SFL 3-5. Swedish Nuclear Fuel and Waste Management Company Report 99-13. Stockholm, Sweden.

Thoenen, T. and D. Kulik. 2003. Nagra/PSI Chemical Thermodynamic Data Base 01/01 for the GEM-Selektor (V.2-PSI) Geochemical Modeling Code: Release 28-02-03. PSI Technical Report TM-44-03-04. Paul Scherrer Institut, Villigen, Switzerland.

USDOE. 2007. In-Drift Precipitates/Salts Model. United States Department of Energy ANL-EBS-MD-000045 REV 03. Las Vegas, USA.

Wilson, J., M. Thorne and G. Towler. 2009. Treatment of chemotoxic species (I) quantitative human health risk assessment. Quintessa Report QRS-1378M-R1 for the Nuclear Decommissioning Authority. NDA RWMD, Harwell, United Kingdom.

APPENDIX D: SORPTION CHARACTERISTICS OF SELECTED ELEMENTS

D.1 INTRODUCTION

Preliminary safety assessment calculations indicated that potentially important radionuclides for the long-term safety of the DGR include C-14, Cl-36, Ni-59, Zr-93, Nb-94, I-129, Ra-226, Np-237, U-238 and Pu-239. The significance of these radionuclides is largely determined by a combination of their half-life, amount in inventory, and/or mobility. Also, non-radioactive Cd, Cr, Cu and Pb, were potentially important chemically hazardous elements.

This appendix provides data with respect to sorption for these species, as this may be a significant natural retardation mechanism. Appendix D.2 comments on the most important retardation processes for each element of interest and Appendix D.3 presents recommended sorption values. Since there are very few sorption data appropriate to the brines present in and around the DGR's host rocks, this appendix necessarily focuses on data for low-salinity to moderately saline groundwater systems. The aim is to use these data to inform a general discussion of sorption, and hence a judgment of those elements that undergo ion exchange and those elements that undergo surface complexation.

The appendix focuses on sorption in bentonite-bearing seals within the shafts and in the host rocks. Sorption on concrete and asphalt is conservatively taken to be zero since there are no reliable data for relevant geochemical conditions in the DGR and its shafts. Additionally, concrete waste packages are unlikely to provide an effective long-term barrier function, while concrete monoliths and bulkheads in the shafts are likely to be bypassed by radionuclide migration through the surrounding EDZ. For these reasons, any sorption that does occur on these concrete components is unlikely to be significant for overall safety. In addition, it is assumed that there is no sorption onto the engineered fill.

D.2 SORPTION BEHAVIOUR OF KEY ELEMENTS

D.2.1 Key Factors Controlling Sorption

Sorption is affected by several geochemical factors:

- Rock type (encompassing mineralogy, surface chemistry, specific surface area, etc.);
- Ionic strength of the water;
- Chemical composition of the water, notably the concentration of ligands such as carbonate species;
- pH; and
- Redox (for redox-sensitive solutes and solid phases).

There are limited sorption data available for many of the radionuclides and non-radioactive elements of interest, under the conditions that prevail in the DGR. However, it is possible to estimate the likely significance of sorption under these conditions, first by using data obtained under different conditions, and second by applying theoretical knowledge of sorption mechanisms (e.g., Crawford et al. 2006; Vilks 2009).

Of particular relevance to the Postclosure Safety Assessment are the very high salinities of the deep porewaters and groundwaters at the Bruce nuclear site (up to ~ 375 g L^{-1}; Table 5.4) compared to the salinities of water in water-solid systems for which there are published sorption data. Additionally, there are relatively few data for relevant solid materials that will be present in and around the DGR, notably the limestone host rock. The most relevant published data are

those for radionuclide sorption on sedimentary formations at the Gorleben site, Germany (e.g., Warnecke et al. 1994) and for sorption onto dolomitic limestones in the WIPP site, New Mexico (USEPA 1998). The German literature includes data for NaCl brines with TDS as high as 159 g L^{-1}. Actinide sorption on dolomite in the presence of NaCl brines with TDS up to 338 g L^{-1} has been described for the WIPP site, New Mexico. Information from these programs, combined with our current understanding of sorption mechanisms indicates that in brine solutions the mass action effects of Na^+ and Ca^{2+} will significantly reduce or eliminate the sorption of elements that are sorbed by non-specific coulombic sorption in the diffuse layer and coulombic sorption in the Stern layer. In contrast, elements that hydrolyze at pH > 6 will be sorbed by surface complexation, in which the effects of TDS will be minimal. The sorption of neutral species by physical sorption (which is due to long-range attractive forces involving whole electron shells of the sorbate and sorbent (Van der Waals forces)) might not be affected significantly by the high salt concentration. Neutral species could include complexes with OH^-.

It can be concluded that alkali and alkali earth elements that sorb mainly by coulombic attraction are likely to have their sorption reduced to close to zero under highly saline conditions. Transitional elements that may sorb by both coulombic and specific chemical sorption may have their sorption significantly reduced. Since the lanthanides and actinides sorb mainly through surface complexation, the mass action effect of brine may be negligible to their sorption properties. However, most available data are for lithologies dissimilar to the Cobourg Formation. Consequently, the extent to which the surfaces of limestone constituents in this formation are conducive to sorption is uncertainty.

Although this information provides valuable background knowledge, existing sorption databases can only be adapted to high salinity solutions after one has acquired an understanding of sorption processes in Na-Ca-Cl brine solutions with Canadian sedimentary and crystalline rocks.

D.2.2 Carbon

In natural porewaters and groundwaters, inorganic carbon exists as $H_2CO_3^0$, HCO_3^- and CO_3^{2-}, depending on the solution pH (Appelo and Postma 2005). The presence of abundant calcium in cement waste packages, in groundwater, and in the host rock, means that calcite precipitation will impact upon carbon concentrations in near-field pore fluids. Calcite precipitation is relatively rapid even at low temperatures and precipitation/dissolution of $CaCO_3$ is often found to control the level of inorganic carbon in natural systems (Appelo and Postma 2005). It is therefore inappropriate to use the Kd approach to model retardation of dissolved carbon in the porewaters and groundwaters of the DGR. In any case, sorption of dissolved inorganic carbon is generally very weak under most groundwater conditions, probably reflecting the fact that at near-neutral pH, dissolved inorganic carbon is generally in an anionic form (Linklater et al. 2003). Under strongly reducing conditions, the oxidized forms of carbon can be reduced to methane, $CH_4(g)$, although the reduction process can be slow and may require microbial mediation. However, $CH_4(g)$ is also not expected to sorb significantly (Linklater et al. 2003).

D.2.3 Chlorine

A useful review of chlorine chemistry and its role in the risk assessment of deep radioactive waste disposal is given by Jones (1992). Chlorine exists in aqueous solution as the chloride ion, Cl^-, although complexes of chlorine with metal ions are possible, for example at low pH values where metal hydrolysis is limited. Most chlorides are highly soluble and in groundwater environments other than those containing solid chloride salts (halite, KCl etc.) it is unlikely that

chlorine-bearing solids will be precipitated. Chlorine shows no real tendency to sorb to solids through ion exchange, since most minerals do not possess a significant anion exchange capacity (Linklater et al. 2003). For these reasons, chlorine is generally regarded as a non-sorbing element.

D.2.4 Chromium

There are two common redox states in natural groundwater systems, Cr(III) and Cr(VI). There are few sorption data available for conditions similar to those in the deep groundwater system of the DGR. USEPA (1999) reports some data for soils. In these materials, Cr(III) concentrations are typically solubility limited and sorption is relevant only for the Cr(VI) form. This sorption is inversely related to pH over the pH range 4 to 10. Fendorf et al. (1994) report that Cr(III) sorbs on silica via formation of monodentate surface complexes, but again under conditions that are more relevant to soils than to the deep porewaters at the DGR site. Additionally, Cr(VI) can be reduced by ferrous Fe in Fe-oxyhydroxides (e.g., Brigatti et al. 2000), while Cr(III) can be oxidized by Mn-oxides (e.g., Tan et al. 2005). Consequently, at least in soils, the extent to which migration of chromium is controlled by sorption depends upon the presence or absence of Fe- and Mn- oxides and oxyhydroxides.

D.2.5 Nickel

Nickel can exist in oxidation states ranging from -1 to +4, although in natural groundwaters the dominant form is Ni(II) and it is not readily affected by redox reactions (Krauskopf 1967; Wedepohl 1978). In aqueous solutions nickel may readily form an aquo complex, $[Ni(H_2O)_6]^{2+}$ and complexes with many other organic and inorganic ligands such as Cl^-, CO_3^{2-}, SO_4^{2-} (Brookins 1988; Stenhouse 1995; Linklater et al. 2003); nickel forms salts with almost all common inorganic anions. Below pH 9, speciation is likely to be dominated by Ni^{2+}, but contributions from $NiOH^+$, $Ni(OH)_2^0$, and $Ni(OH)_3^-$ increase with increasing pH.

Nickel sorption onto Fe/Mn oxides and hydroxides is generally strongest, but sorption onto clays and micas also occurs. In contrast sorption onto feldspar and quartz is weak. Sorption is thought to take place by a combination of cation exchange and surface complexation mechanisms (Stenhouse 1995; Linklater et al. 2003).

Since the aqueous speciation of nickel and the charges on mineral surfaces vary with pH, nickel sorption is also pH-dependent (Stenhouse 1995; Linklater et al. 2003). As with many elements, the sorption is low at acidic pH (where mineral surfaces will tend to be positively charged and therefore repel Ni^{2+}) and at very high pH (where negatively charged nickel species such as $Ni(OH)_3^-$ become increasingly abundant and mineral surfaces tend to develop a net negative charge).

Owing to the relative stability of the Ni^{2+} valence state compared with other valence states, variations in redox conditions are unlikely to affect nickel sorption significantly. In contrast, there is more variable evidence that the presence of ligands may affect nickel sorption (Stenhouse 1995; Linklater et al. 2003). The presence of organic complexants, such as citrate or oxalate appears to significantly reduce the proportion of nickel that is sorbed. On the other hand, the presence of CO_3^- does not seem to significantly influence sorption, possibly owing to ligand exchange with solid-phase carbonate.

Competition between Ni^{2+} and alkaline earth cations (Ca^{2+} and Mg^{2+}) may have a particularly strong influence on nickel sorption (Linklater et al. 2003, referring to Ticknor 1994). High aqueous concentrations of these alkaline earth cations will tend to decrease nickel sorption.

However, except under acidic conditions when cation exchange is expected to be an important sorption mechanism, ionic strength does not appear to influence nickel sorption significantly. The reason is believed to be that at neutral to alkaline pH, the dominantly inner-sphere nickel sorption mechanism is relatively insensitive to ionic strength (Linklater et al. 2003).

Under neutral to alkaline pH conditions, nickel is expected to sorb strongly to Fe/Mn-oxides and Fe/Mn-oxyhydroxides and clays. Under the highly saline porewater conditions in the host rock of the DGR, competition between aqueous Ca^{2+} and possibly Mg^{2+} may cause sorption to be less than would occur in the presence of less Ca-rich waters.

D.2.6 Copper

Copper is a transition metal that occurs predominantly in either the Cu(I) or Cu(II) oxidation states. It is unusual among metals in that it may occur in the free (native) state in nature.

Rybicka et al. (1995) measured heavy metal (Cd, Cu, Pb, Zn and Ni) sorption on illite at pH 5.5. Unfortunately the data cannot be used since no information was given on the water chemistries. The only semi-quantitative conclusion which could be drawn from this study was the sequence of adsorption affinities for illite, i.e., Pb > Cd ~ Cu > Ni > Zn.

In summary there appears to be no reliable sorption data for copper under conditions that are relevant to the DGR. The available information suggests that sorption is a plausible retardation mechanism, but that natural levels of dissolved copper could also be controlled by formation of a solid copper-bearing compound.

D.2.7 Zirconium

Zirconium has oxidation states of 0, II, III, and IV, but in nature it occurs predominantly in the 4+ valence state. Although analyses of Zr in rocks are widely used as a petrogenetic indicator, there is a dearth of information relating to concentrations of Zr in groundwater. Zr-bearing minerals such as zircon, have very low solubilities. Nevertheless, small, though detectable concentrations of Zr are present in at least some natural waters (e.g., Zr in oilfield waters of the USA is in the range < 10-20 μg L^{-1}, Rittenhouse et al. 1969). In a survey of alkaline thermal waters in granites in southern Europe, Alaux-Negrel et al. (1993) concluded that zirconium (along with other tri- and tetravalent elements) was associated with a particulate fraction (< 450 nm) in groundwaters. This indicates that Zr was sorbed on the particulate fraction in the groundwaters and not in true solution.

Although there are limited data concerning the precise nature of zirconium sorption, a number of observations can be made on the basis of its known solution chemistry and the properties of typical mineral surface groups (Linklater et al. 2003).

- Given its strong tendency to hydrolyze, it is unlikely that IX mechanisms will be important in zirconium sorption. Surface complexation reactions are more likely to prevail.
- A strong tendency to hydrolyze is often linked with strong sorption, particularly when oxide/hydroxide surfaces are involved. This suggests that zirconium sorption will be strong.
- At high pH values (e.g., > 10), most mineral oxide surfaces will be negatively charged. The predominant aqueous zirconium species is expected to be $Zr(OH)_5^-$, and therefore sorption should decrease with increasing pH.

D.2.8 Niobium

Niobium has valence states of 2+, 3+, 4+, and 5+, but the last is the most common in natural systems.

Although niobium is a trace element which is routinely analyzed in rocks for petrogenetic studies, groundwater analyses of this element are extremely rare. In aqueous solutions, at near-neutral pH values, $Nb(OH)_5^0$ is expected to dominate. The anionic species $Nb(OH)_6^-$ dominates speciation at higher pH values (Cross et al. 1995). At lower pH values, the extent of niobium hydrolysis decreases, and significant complexation by acid stable anions may occur (e.g., SO_4^{2-}, Cl^-, PO_4^{3-}, etc.). Niobium also has a tendency to form polymeric oxo-anions in aqueous solution (Cotton and Wilkinson 1980).

Regarding sorption behaviour, given its strong tendency to hydrolyze, it is unlikely that IX mechanisms will be important in niobium sorption, so that surface complexation reactions are more likely to prevail. A very strong tendency to hydrolyze is often linked with strong sorption, particularly when oxide/hydroxide surfaces are involved (James and Healy 1972), which suggests that niobium sorption should be strong. At high pH values (pH > 10), most mineral oxide surfaces will be negatively charged. The fact that the predominant aqueous niobium species under these conditions is expected to be $Nb(OH)_6^-$, suggests that sorption should decrease with increasing pH.

D.2.9 Cadmium

The following summary of cadmium geochemistry is taken predominantly from Carbol and Enkvist (1997) and USEPA (1999).

In low-temperature natural groundwater systems, cadmium is not redox-sensitive in so far as it is present in the divalent state. However, its behaviour is affected by redox conditions owing to its ability to combine with sulphide to form solid CdS; reduction of SO_4 to S^{2-} will therefore tend to favour precipitation of cadmium.

In low-salinity aqueous solutions at pH < 6 and with < $10^{-2.5}$M SO_4 dissolved cadmium occurs entirely as the uncomplexed Cd^{2+} cation. At higher pH, between 6 and 8.2, carbonate species, ($CdHCO_3^+$ and $CdCO_3^0$(aq)) become increasingly important, though Cd^{2+} remains dominant (Carbol and Enkvist 1997; USEPA 1999). At more alkaline pH, up to around 10, almost all the cadmium is in the form of $CdCO_3^0$ (aq), although there will be much smaller concentrations of $CdCl^+$, $CdCl_3$ and $CdCl_4^2$, $CdSO_4^0$(aq), $CdHCO_3^+$, and $CdOH^+$. There may also be complexes with I^- and Br^-, although these will be present in very low concentrations. No aqueous speciation data have been identified for highly saline conditions such as those occurring within the deep groundwater system at the DGR site, but it is to be expected that the chloride species would be relatively more abundant compared to the other species.

There are almost no reliable sorption data for cadmium under conditions that are relevant to deep groundwaters. Bradbury and Baeyens (2003a, 2003b) used sorption data for nickel, which they considered to be an analogue for cadmium. However, they decreased their measured nickel values to correct for the fact that cadmium may form stronger complexes with chloride than does nickel.

At concentrations of cadmium >10 mg L^{-1}, cadmium undergoes cation exchange with calcium and magnesium on soils (USEPA 1999). This exchange is possible because Cd^{2+}, Ca^{2+} and Mg^{2+} have similar ionic radii. However, when cadmium is less concentrated it may sorb to

calcite and Fe-Al oxyhydroxides by a surface complexation mechanism.

The sorption of cadmium, like that of other metal cations, is strongly pH-dependent. The concentrations of ligands that may complex with cadmium and competing cations also affect the tendency of cadmium to sorb. In soils, cadmium sorption by Fe-oxides, Mn-oxides and Al-oxides is reduced by the presence of calcium, magnesium and trace metals. Sorption of cadmium may also occur onto organic matter present in soils. The occurrence of zinc significantly reduces cadmium sorption to Fe-oxides, suggesting that these metals compete for the same sorption sites. However, the presence of trace lead and copper reduces the tendency for cadmium to sorb on Fe-oxides only slightly implying that these lead and copper are sorbed largely on different sites to cadmium.

When cadmium has a low aqueous concentration there are sharp sorption edges where the proportion of sorbed cadmium changes from 0 to 100% over a very small pH range. The occurrence of these edges suggests that there is specific adsorption. Under low-pH conditions cadmium appears to sorb less strongly than chromium, which in turn is not as strongly sorbed as lead.

Sorption is likely to be specific and occur by a surface complexation mechanism. Consequently, sorption will not be affected directly by variations in salinity. Cadmium is also present only in the divalent form and its behaviour will be affected only indirectly by redox processes, principally by reduction and/or oxidation of sulphur species.

D.2.10 Iodine

There are few data available with which to judge whether iodide sorption could be significant in the presence of the brines present at the site of the DGR. Iodide is often used as a conservative tracer in groundwater investigations because it is considered to be relatively unreactive (e.g., NIREX 1997). However, sorption has been proposed to occur on organic matter, aluminum oxides, iron oxides and clay minerals in soils (e.g., Fuge 1996 and references therein; Kaplan et al. 2000). Sorption of iodide onto cement phases has also been investigated (Toyohara et al. 2002). However, owing to the ability of iodide to react with organic matter and certain cement minerals, there must be some doubt about whether studies of iodine sorption on these materials have truly investigated sorption. Measurements reported by Bradbury and Baeyens (2003b) reveal that in the Opalinus Clay, Switzerland, iodide sorption is extremely limited; these authors proposed a Kd value of only 3.5×10^{-5} m^3 kg^{-1}. Furthermore, Kaplan et al. (2000) reported no evidence for iodide sorption on calcite, while chloride was found to cause desorption of iodine from illite. This latter observation suggests that iodide sorption would become less important in increasingly Cl-rich waters. For these reasons, transport of this element is not expected to be limited by sorption under the groundwater conditions of interest.

D.2.11 Lead

The following summary of the chemical characteristics of lead under low-temperature conditions is taken from USEPA (1999).

Lead is a metal that lies in Group 13 of the periodic table and has common oxidation states of II and IV. For water with the major ion composition of typical river water (Cl^- 2.2×10^{-4} mol L^{-1}) under acidic conditions, with pH values < 6.5, Pb^{2+} is the dominant aqueous species of lead. At higher pH $PbCO_3(aq)$ becomes the dominant species, but with increasing pH, $Pb(OH)^+$ and $Pb(OH)_2$ also become successively more important. In brines $PbCl^+$ or $PbCl_4^{2-}$ are expected to

be dominant over a wide range of pH, unless dissolved carbonate is sufficiently high to cause $PbCO_{3(aq)}$ or $Pb(CO_3)_2^{2-}$ to dominate at intermediate to alkaline pH. Complexes with other species are also possible, such as PO_4^{2-} and certain organic ligands.

The range of measured K_d values is very wide, varying from about 0.01 $m^3 kg^{-1}$ to >10^2 $m^3 kg^{-1}$ (Linklater et al. 2003). However, Bradbury and Baeyens (2003a,b) note that except for studies of lead sorption in soils, almost no reliable sorption data are available in the literature. Bradbury and Baeyens (2003a) reviewed published data for lead sorption on montmorillonite, but concluded that they are not relevant for constraining Kd values for compacted bentonite. The reasons are that either the data were obtained under pH conditions different from those in bentonite, or else the chemistry of the water was not reported.

Lead has been found to sorb strongly to oxides and hydroxides (particularly those of iron and manganese). There is also significant sorption onto other minerals, particularly micas, feldspar, clay and silica. In the cases of sorption onto Fe/Mn-oxides and oxyhydroxides and silica, there is a strong pH-dependency which is consistent with a surface complexation mechanism. At low pH, mineral surfaces tend to be positively charged and the dominant aqueous species (at least in low-chloride waters) is Pb^{2+}, which means that little sorption occurs. As pH increases, hydrolysis of the dissolved lead also increases, producing successively monovalent cationic, neutral and monovalent anionic complexes. However, at intermediate pH, the surface charge remains positive resulting in strong sorption. This sorption decreases at even higher pH owing to the development of negative surface charges.

Surface complexation is also likely to be the dominant mechanism when sorption occurs on micas or clays. There is again a pH-dependence, reflecting the varying charge on exposed silanol (Si-OH) and aluminol (Al-OH) species with varying pH. However, significant ion exchange also seems to occur on these minerals, due partly to the similar ionic radius of Pb^{2+} and the alkaline and alkaline earth metals. The occurrence of ion exchange means that sorption onto micas or clays is less pH-dependent than that onto Fe/Mn oxides and oxyhydroxides or silica.

Owing to the dominant surface complexation sorption mechanism, lead is bound to mineral surfaces mostly as an inner-sphere complex. This phenomenon means that there is relatively little direct effect of variations in ionic strength on sorption. However, the ability of lead to form aqueous complexes with a wide range of species means that sorption can be reduced if the aqueous concentrations of these other species are sufficiently high. Additionally, sorption to micas and clays, which show a significant amount of cation exchange, is likely to show a greater degree of influence due to variations in ionic strength.

In summary there are no reliable sorption data for lead under conditions that are relevant to the DGR. The available information suggests that sorption is a plausible retardation mechanism. Sorption that does occur is controlled by an inner-sphere mechanism and is therefore relatively insensitive to variations in porewater salinity.

D.2.12 Radium

The following summary is based on Linklater et al. (2003) and USEPA (2004).

Radium is an alkaline earth metal which is produced by the radioactive decay of uranium and thorium. In natural aqueous solutions Ra^{2+} is the dominant species at pH < 10. However radium can also form complexes with several different anions, but notably chloride, phosphate and carbonate. The aqueous complexes $RaOH^+$, $RaCl^+$, $RaCO_3(aq)$, and $RaSO_4$ (aq) are known,

but thermodynamic data for these species have not been established.

The element is not redox sensitive and occurs only in the divalent state. However, where it occurs as a trace constituent in sulphate minerals, there is a possibility that reduction of sulphate could lead to the release of radium (USEPA 2004).

Sulphates and carbonates are potential solubility-limiting phases. However, it is highly unlikely that pure radium phases will control radium solubility in natural systems (USEPA 2004). It is much more likely that any solubility control will be exerted by solid solutions of radium in sulphates (gypsum, anhydrite, barite), carbonates (calcite) or phosphates (apatite). There is also a possibility that mixed radium-Fe/Mn oxides might control radium solubility.

There are relatively few sorption data for radium (USEPA 2004; Bradbury and Baeyens 2003a,b; Wieland and Van Loon 2002). Reported high sorption values are questionable owing to the possibility that radium may have co-precipitated in solids such as $(Ba,Ra)SO_4$ during the measurements (USEPA 2004; Bradbury and Baeyens 2003b). However, broadly, radium is thought to sorb in a similar fashion to barium (Bradbury and Baeyens 2003a) and strontium (USEPA 2004; Bradbury and Baeyens 2003b; Wieland and Van Loon 2002). Bradbury and Baeyens (2003a) used sorption data for barium to estimate K_d values for compacted MX-80 bentonite. In contrast, Bradbury and Baeyens (2003b) used strontium as an analogue in order to estimate K_d values for radium in the Opalinus Clay.

Sorption of radium ranges from very weak to very strong, reflecting the fact that, depending upon the nature of the sorbent, it occurs by both cation exchange and surface complexation mechanisms (Linklater et al. 2003; USEPA 2004). The former mechanism is dominant in minerals with high cation exchange capacities, such as clays and zeolites, which have a strong affinity for Ra^{2+}. This cation is able to exchange for alkali metals (principally Na^{+}) and alkaline earth metals (principally Ca^{2+}) that are located between layers of the clay lattice. Since IX is affected by competition for exchange sites between aqueous ions, increases in ionic strength will cause a decrease in Ra^{2+} sorption. In saline solutions, Ra^{2+} sorption may be negligible in consequence.

The relative ability of the different alkaline earth elements to exchange for one another is:

$$Ra^{2+} > Ba^{2+} > Sr^{2+} > Ca^{2+} > Mg^{2+}$$

That is, Ra^{2+} has the strongest tendency to partition onto the surface of a solid while Mg^{2+} has the weakest tendency. The alkali metals generally show larger selectivity coefficients than alkaline earth metal ions. However, radium is unlikely to become ‘fixed’ in interlayer sites.

Sorption of radium on other minerals, principally oxides and oxyhydroxides, is likely to be dominated by a surface complexation sorption mechanism. However, compared to clays and zeolites, sorption to oxide/hydroxides is only moderate. In these cases, reflecting the dominant complexation mechanism, there is a strong pH-dependency to sorption. There is little sorption at low pH owing to Ra^{2+} being the dominant radium species and the surfaces of the solids being positively charged. As pH increases, the solid surfaces become negatively charged, resulting in a sharp increase in sorption. However, the alkaline earths are believed to sorb by means of outer-sphere complexes, which are weakly combined to the surface compared with inner-sphere complexes. As a result, radium sorption by surface complexation is decreased by competing cations and by increasing the ionic strength of the solution that contacts the surface.

The results of some studies also suggest that radium may be strongly adsorbed by organic

material in soils (USEPA 2004).

In summary, radium may be retarded in the geosphere by sorption. On minerals with high cation exchange capacities, sorption is likely to be dominated by a cation exchange mechanism whereas on other minerals sorption is likely to take place by an outer-sphere surface complexation mechanism. In either case, sorption will depend upon the concentrations of both competing ions and the ionic strength of the solution. In very high-salinity porewaters, sorption is expected to be significantly less than in lower salinity waters.

D.2.13 Uranium

Sorption of actinides such as uranium generally varies according to aqueous speciation behaviour, pH, the predominance field of actinide-hydroxy complexes, and the presence of complexing ligands such as carbonate (Turner et al. 2002). Actinides act as 'hard acids' and form strong complexes with oxygen-donating ligands such as OH^-, CO_3^{2-}, and PO_4^{3-}, and less stable complexes with F^- and SO_4^{2-}, and only weak complexes with Cl^- and NO_3^-. Although hydrolysis dominates the speciation behaviour of actinides, carbonate concentrations at neutral pH are generally sufficient to form mixed actinide hydroxocarbonate and pure carbonate aqueous complexes. The resulting negatively-charged solution species dominate as pH increases and are responsible for increased solubility in the more alkaline region.

Under low pH conditions, actinide sorption tends to be weak, except for cation exchangers such as montmorillonite or zeolites. With increasing pH, actinide sorption increases, with a maximum where hydroxy complexes dominate.

In carbonate-free systems (e.g., unweathered cements), actinide sorption continues to increase with pH and increasing hydrolysis. In the presence of carbonate however, sorption tends to decrease with increasing pH and/or carbonate concentration (Bertetti et al. 1998; LaFlamme and Murray 1987; Sanchez et al. 1985; Pabalan et al. 1998). Sorption for all actinides tends to decrease in the sequence iron oxyhydroxides > clay >> sand (quartz) (Runde 2002).

The effect of pH upon actinide sorption is similar for a wide range of minerals such as quartz, alumina, clinoptilolite, montmorillonite, amorphous silica, kaolinite, and titanium oxide, which suggests a relative insensitivity to surface charge characteristics of the sorbent (Turner et al. 2002). In all cases, sorption is at a maximum at near-neutral pH (6.0 – 6.8) and decreases towards more acidic or more alkaline conditions.

Ionic strength effects up to about 1M are limited for actinide surface complexation reactions (Turner et al. 2002), although ionic strength may be important where ion exchange is the principal mechanism.

Uranium has valence states between 2+ and 6+ in nature, but only the 4+ and 6+ valence states are important in the natural environment. In solutions without carbonate, soluble U^{VI} species include UO_2^{2+}, UO_2OH^+, $(UO_2)_3(OH)_5^+$, and $(UO_2)_3(OH)_7^-$ (Zhang et al. 2002). Carbonate in solution tends to cause conversion of hydroxyl U^{VI} species to dissolved U^{VI} carbonate species such as UO_2CO_3, $UO_2(CO_3)_2^-$, and $UO_2(CO_3)_3^{4-}$. The anionic carbonate species dominate above neutral pH and tend to cause the desorption of U^{VI} from mineral surfaces and dissolution of U^{VI} solids (Zhang et al. 2002). In addition to carbonate complexes, soluble U-species include sulphate, fluoride and phosphate complexes.

To summarize uranium sorption behaviour (e.g., Linklater et al. 2003).

- Uranium sorption is lowest at acidic pH values, increasing sharply as pH increases, reaching a maximum at near-neutral pH values and then decreasing as pH becomes more alkaline, especially if carbonate is present.
- Uranium(IV) sorption is considerably stronger than that of uranium(VI). Uranium oxidation state is a function of Eh and other aspects of the system, such as the presence of complexing ligands and properties of the contacting mineral surfaces (some minerals can catalyze redox reactions).
- Uranium forms aqueous complexes with carbonate, and increased carbonate concentrations are associated with reduced sorption.
- At near-neutral pH values, uranium sorption is unaffected by ionic strength. However, at acidic pH values, high ionic strength is likely to be associated with a reduction in sorption.

D.2.14 Neptunium

Neptunium redox behaviour in aqueous systems is complex; five oxidation states exist, III,

IV, V, VI and VII. For most groundwater conditions only the oxidation states IV and V will be important. At near-neutral pH, the predicted neptunium (IV)/(V) transition occurs at approximately +200 mV (Lieser and Mühlenweg 1988). The presence of complexing ligands such as carbonate may alter the Eh at which this transition takes place.

The main mechanism of sorption for neptunium, in oxidation states IV and V, is believed to be surface complexation. Sorption of neptunium(IV) is significantly stronger than that of neptunium(V) (Lieser and Mühlenweg 1988). Sorption onto most minerals and rocks is observed to be strongly pH dependent (Linklater et al. 2003). Typically, sorption is lowest at acidic pH values and then increases sharply as the pH is increased, reaching a maximum in the near-neutral pH range. At more alkaline pH values (pH > 9) sorption appears to decrease again. This pH dependence can be explained by considering the pH dependence of the charge on the aqueous species and the mineral surface (Linklater et al. 2003):

- At acidic pH values the charge on both the mineral surface and the dominant aqueous species (likely to be Np^{4+} under reducing conditions, and NpO_2^+ under oxidising conditions) is positive leading to repulsion and low sorption;
- The sharp increase in sorption corresponds to the onset of hydrolysis (formation of species such as $Np(OH)_3^+$, $Np(OH)_2^{2+}$ and $NpO_2(OH)^0$) and also a change in the charge on the mineral surface, which becomes increasingly negative as the pH increases; and
- The decrease in sorption at alkaline pH values can be explained by the formation of negatively-charged aqueous species, e.g., $NpO_2(OH)_2^-$, or carbonate complexes if significant carbonate concentrations are present. At alkaline pH values, the mineral surface would also be negatively charged causing repulsion of these species.

The importance of the surface complexation mechanism is consistent with the observation that high neptunium sorption is observed onto iron and manganese oxides. These phases are known to interact strongly with solution species via this mechanism.

D.2.15 Plutonium

The following summary of the chemical characteristics of plutonium under low-temperature conditions is taken mostly from Carbol and Enkvist (1997), USEPA (1999), Linklater et al. (2003) and Choppin (2005).

Plutonium is a transuranic element belonging to the actinide series. Plutonium redox behaviour is complex and four oxidation states may exist, III, IV, V and VI. In natural systems with organic carbon concentrations >10 mg kg^{-1}, plutonium exists mainly in trivalent and tetravalent redox states. Depending upon the composition of the water, the dominant aqueous species are hydroxides, sulphates, carbonates and fluoride complexes. Plutonium will also form complexes with a wide range of organic materials. Humic substances and carboxylate in particular will combine strongly with plutonium. Plutonium may also bind strongly with certain colloids (e.g., Yelton et al. 1996; Kersting et al. 1999; Lu et al. 2003).

Under reducing conditions and pH up to about 7.5, the Pu(III) species in most groundwater would be typically Pu^{3+}, $PuCO_3^+$, and $PuOH_2^+$, depending upon the concentration of carbonate in the water and the pH. In contrast, under more oxidising and/or alkaline conditions, the dominant soluble species in most groundwater is expected to be $Pu(OH)_4(aq)$. This latter species has been reported to be dominant for most natural groundwater environments (Runde 2002).

Measurement of K_d values for plutonium are complicated by the very low concentrations that will be present in solution and by the complex redox behaviour, allied to the difficulty of maintaining stable redox conditions during experiments. Plutonium reduction may be catalyzed by the surfaces of Fe(II)-bearing minerals while Pu(IV) may be stabilized by the presence of carbonate. For these reasons, many published data are of uncertain quality (Linklater et al. 2003).

Most K_d values measured under aerobic conditions are < 1 $m^3\,kg^{-1}$, whereas those measured under 'anaerobic' conditions are typically greater (Linklater et al. 2003). The Nirex Safety Assessment Research Programme found that sorption onto hematite, ilmenite and chlorite is greater than sorption onto other minerals, such as calcite, feldspar, and quartz. However, Linklater et al. (2003) noted that some studies have reported strong sorption to calcite compared to sorption on oxides, micas, clays and feldspars. They interpreted these different results to reflect differences in plutonium oxidation states in the different experiments. They were confident that the Nirex results are appropriate for Pu(IV), but in the other studies it was possible that plutonium had been present in mixed IV, V and VI oxidation states, or dominantly as plutonium(V). Based on theoretical modeling they considered that Pu(IV) would be the stable oxidation state in the deep saline groundwaters at Sellafield (UK). They evaluated Na-Cl dominated groundwaters with TDS contents up to about 55 g L^{-1}.

Bradbury and Baeyens (2003b) considered that Pu(III) would be the dominant oxidation state in porewaters from the Opalinus Clay. However, they were unable to find sorption data for these conditions and therefore used Am(III) as an analogue for Pu(III); the K_d values that they recommended were Am(III) values that had been corrected to allow for the different aqueous speciation of Am(III) and Pu(III). They did not take into account the small proportion of Pu(IV) that they thought would be present in the Opalinus Clay porewaters, thereby ensuring that the Pu(III) K_d values they used would be conservative.

Sorption of plutonium (III) or (IV) is stronger than sorption of plutonium (V) or (VI). Except possibly at very low pH (<4) that is not attained in most natural groundwaters, sorption of plutonium is insensitive to a solid's cation exchange capacity. Consequently, ion exchange is not thought to be a significant contributor to plutonium sorption. Instead the main sorption mechanism reported in the literature is surface complexation, which is reflected in a strong pH-dependence. Generally there is least sorption at low pH but a sharp increase in sorption as pH increases through near-neutral values. Sorption at more alkaline pH is high. These variations are caused by the pH-dependent changes in solid surface charges and plutonium

speciation. At acidic pH, both the solid surface and dominant aqueous species (Pu^{4+}, PuO_2^{+} or PuO_2^{2+} depending on redox state) are positively charged, causing repulsion of the aqueous species from the surface and consequently little sorption. Plutonium hydrolysis at near-neutral pH causes the progressive dominance of species such as $Pu(OH)_3^{+}$, $Pu(OH)_2^{2+}$ and $PuO_2(OH)^0$) and an increasingly negative solid surface charge. This change is reflected in the occurrence of a sorption edge, across which sorption increases dramatically towards more alkaline pH over a relatively small pH range.

Linklater et al. (2003) also report that sorption of plutonium IV and V is not greatly affected by the ionic strength of the solution. This finding is consistent with sorption involving inner-sphere complexes. However, the formation of complexes between plutonium and ligands such as acetate and fulvate will reduce plutonium adsorption (USEPA 1999).

Sorption on plutonium on a wide range of colloids may occur (e.g., Yelton et al. 1996; Kersting et al. 1999; Lu et al. 2003). However, the significance of colloidal transport under highly saline porewater conditions like those at the Bruce nuclear site is less clear. Lu et al. (2003) found that sorption of Pu(V) onto colloids of hematite and montmorillonite tended to decrease as the ionic strength of the coexisting aqueous solution increased, but the investigated solutions were all less concentrated than the porewaters at the site. It seems likely that in the extremely low-permeability rocks around the DGR, colloids would be effectively filtered and hence immobile.

Sorption is likely to be the most important retardation mechanism in the geosphere and this will occur via an inner-sphere surface complexation mechanism. Consequently, sorption will be relatively insensitive to variations in porewater salinity.

D.3 SORPTION VALUES FOR REPOSITORY MATERIALS AND GEOSPHERE

D.3.1 Selection of Sorption Data

D.3.1.1 Published Literature Values

Many studies of sorption have been made in recent years. These studies range from reviews of published K_d values (e.g., Stenhouse 1995; Savage and Stenhouse 2002), to state-of-the-art experimental studies designed to obtain sorption isotherms (Wieland and Van Loon 2002; Bradbury and Baeyens 2003a,b).

The more relevant published values for K_d are given in Tables D.1 and D.2.

In addition to the data summarized in Tables D.1 to D.2, a large compilation of data produced by the Japan Atomic Energy Agency (JAEA) (Tachi et al. 2009) was also reviewed. This compilation has been developed specifically to support radioactive waste management and is part of a larger database termed the “Nuclide Migration Database”. This database is freely accessible via the worldwide web at:

http://migrationdb.jaea.go.jp/nmdb/index.jsp

The sorption data in Tables D-1 and D-2 have been carefully selected by the authors of the source documents to be relevant for specific radioactive waste-related safety assessments. In contrast, the JAEA database contains a large collection of data for varied solid materials and water compositions obtained from wide-ranging sources, not all of which is relevant to deep geological repositories for radioactive wastes. However, the database contains information from

which it is possible to deduce the relevance and quality of the data. To support the selection of Kd data for the Postclosure Safety Assessment, Kds for relevant materials and groundwater samples were selected from the JAEA database. These data were then compiled and statistics calculated, as summarized in Table D.3.

Table D.1: Summary of K_d Values from Selected Literature (Limestone and Argillaceous Rocks)

Source	Stenhouse (1995)	Bradbury and Baeyens (2003b)	USEPA (1998)	Linklater et al. (2003)	Linklater et al. (2003)	Linklater et al. (2003)	Linklater et al. (2003)
Description of estimate	Realistic/ Conservative	Range from experiments and literature review	Range based on experiments	Range, based on batch experiments	Literature review	Literature review	Laboratory measurement
Rock type	Marl	Opalinus Clay	Culebra Dolomite	Carboniferous Limestone	Calcareous sediment	Varied mudrocks	London Clay
Water composition	Na-Cl	Na-Cl	Na-Cl	Not reported	Not reported	Not reported	Not reported
Salinity	Saline	Saline	Brine	Not reported	Not reported	Not reported	Not reported
TDS (g L^{-1})	~ 30	~ 13	~ 325	Not reported	Not reported	Not reported	Not reported
Comment		R_d reported[a]		Range of salinities at Sellafield, U.K., R_d reported[a]	R_d reported[a]	R_d reported[a]	R_d reported[a]
Element	**m^3 kg^{-1}**	**m^3 kg^{-1}**	**m^3 kg^{-1}**	**m^3 kg^{-1}**	**m^3 kg^{-1}**	**m^3 kg^{-1}**	**m^3 kg^{-1}**
C	0.001 / 0	0.00013 – 0.006					
Cl	0 / 0	0					0.0003 – 0.0038
Ni	0.5 / 0.05	0.29 – 1.9			0.2 - 1000	0.0065 - 290	
Zr	0.5 / 0.05	4.7 – 40					
Nb	0.5 / 0.05	4					0.240 - >10
U (oxidation state unstated)	1 / 0.05						
U(IV)		0.55 – 48	0.7 - 10				4.3 - >10
U(VI)			0.00003 – 0.020	<0.001			0.1 - 29
Np (oxidation state unstated)	1 / 0.05						
Np(IV)		22 – 55	0.7 – 10		10 - 100		
Np(V)			0.001 - 0.200		1 - 5		
Cd		0.057 – 0.37					
Cr							
Cu							
Pb	0.5 / 0.05	0.8 – 6.7					1 - >100
Pu	5 / 0.5[b]	1.1 – 75.[c]	0.02 – 0.40[d]	0.33 – 0.47			>0.15 - >10
Ra	0.1 / 0.01	0.00069 – 0.00076		0.001 – 0.007			0.14 – 3.6

Table D.2: Summary of K_d Values from Selected Literature (Bentonite)

Source	Stenhouse (1995)	Bradbury and Baeyens (2003a)	Linklater et al. (2003)	Linklater et al. (2003)	Linklater et al. (2003)	Linklater et al. (2003)	Linklater et al. (2003)
Description of estimate	Realistic/ conservative	Range from experiments and literature review	Measurement on Japanese samples	Range, based on literature review	Los Alamos laboratory measurement	Range, based on literature review	Swedish research
Rock type	Bentonite	MX-80 Bentonite	Bentonite	Bentonite	Bentonite	Bentonite/ sand	Bentonite/ quartz
Water composition	Na-Cl	Na-Cl	Not reported	Not reported	Not reported	Not reported	Not reported
Salinity	Brackish	Saline	Not reported	Not reported	Not reported	Not reported	Not reported
TDS (g L^{-1})	~ 5	~ 20	Not reported	Not reported	Not reported	Not reported	Not reported
Comment			R_d reported[a]	R_d reported[a]	R_d reported[a]	Oxidizing conditions, R_d reported[a]	R_d reported[a]
Element	**m^3 kg^{-1}**	**m^3 kg^{-1}**	**m^3 kg^{-1}**	**m^3 kg^{-1}**	**m^3 kg^{-1}**	**m^3 kg^{-1}**	**m^3 kg^{-1}**
C	0	0.000027 – 0.00032					0.0028 – 0.0078
Cl	0	0					
Ni	1 / 0.1	0.14 – 0.58					
Zr	1 / 0.1	33. - 135				0.05 – 1.6	
Nb	1 / 0.1	30			0.84-1.7		
U (oxidation state unstated)	5 / 0.5						
U(IV)		2.8 – 63					
U(VI)		0.01		0.008 – 0.33			
Np (oxidation state unstated)	5 / 0.5						
Np(IV)		63	4.5 – 5.7				
Np(V)		0.018					
Cd		0.055 - 0.23					
Cr							
Cu							
Pb	0.01 / 0.001	4.7 - 62					
Pu	5 / 0.5	6.6 - 105					
Ra	0.01 / 0.001	0.0021					

Table D.3: Summary of K_d Values from the JAEA Sorption Database

(1) Sorbent – Expandable clays/rocks and mixtures with expandable clays						
Element	**Redox**	**No of SINGLE* measurements**	**Kd (m^3 kg^{-1}) (5 percentile)**	**Kd (m^3 kg^{-1}) (95 percentile)**	**Average**	**Standard Deviation**
Np	Redox to consider – Np (IV) and Np(V)	388	3.9E-03	6.1E+00	1.3E+00	5.3E+00
Np	Only reducing (anoxic) waters included	161	4.7E-03	8.8E+00	2.0E+00	7.6E+00
Pb	All data	47	1.2E-02	6.1E+01	1.1E+01	2.7E+01
Pu	Redox to consider – Pu(III), Pu(IV) and Pu(VI)	119	1.2E-01	6.3E+01	1.4E+01	2.4E+01
Pu	Only reducing (anoxic) waters included	24	2.0E+00	1.2E+02	3.1E+01	3.9E+01
Ra	All data	243	4.0E-02	1.7E+01	3.3E+00	5.6E+00
U	Redox to consider – U(IV) and U(VI)	257	2.5E-03	7.6E+01	1.6E+01	7.0E+01
U	Only reducing (anoxic) waters included	48	1.1E-01	4.2E+02	7.9E+01	1.5E+02
Zr	All data	36	9.5E-02	8.7E+02	1.8E+02	3.9E+02

*Where values are reported as minima, maxima or ranges, they are excluded from the statistics
Removed from the list of all "Bentonite (Clay minerals)" data, those entries that did not relate to materials relevant to bentonite (i.e., kaolinite, illite), or which are of uncertain nature ("clay")
Removed from the list of all "Bentonite (Clay minerals)" data, those entries that had water not clearly similar to groundwater (e.g., cement porewater, $NaClO_4$)
Values reported to have been obtained under reducing conditions are highlighted in yellow.

(2) Sorbent – Mudstone (Sedimentary rocks, including Soils, Alluvium, Mudrock)

Element	Redox	No of SINGLE* measurements	Kd (m^3 kg^{-1}) (5 percentile)	Kd (m^3 kg^{-1}) (95 percentile)	Average	Standard Deviation
Nb	All +5	30	9.6E-02	6.3E+00	3.2E+00	4.5E+00
Np	Redox to consider - Np (IV) and Np(V)	95	3.5E-03	3.1E+00	6.4E-01	1.1E+00
Np	Only reducing (anoxic) waters included	11	2.1E-01	2.3E+00	1.0E+00	8.7E-01
Pb	All +2	34	3.4E-02	4.4E+02	6.5E+01	1.8E+02
Pu	Redox to consider - Pu(III), Pu(IV) and Pu(VI)	97	2.3E-01	8.6E+01	2.3E+01	3.0E+01
Ra	All +2	39	1.2E-02	5.5E+01	9.7E+00	3.4E+01
U	Redox to consider - U(IV) and U(VI)	99	1.4E-03	6.3E+00	2.6E+00	1.8E+01
U	Only reducing (anoxic) waters included	18	1.4E-03	5.7E+00	1.0E+00	2.3E+00
Zr	All +4	57	8.8E-02	4.3E+01	9.5E+00	1.6E+01

*Where values are reported as minima, maxima or ranges, they are excluded from the statistics

Removed from the list of all "Mudstone (sedimentary rocks)" data, those entries that had water not clearly similar to groundwater (e.g., $NaClO_4$, $NaNO_3$)

All values for Pu were obtained for oxidizing conditions

(3) Sorbent - Calcite

Element	Redox	No of SINGLE* measurements	Kd (m^3 kg^{-1}) (5 percentile)	Kd (m^3 kg^{-1}) (95 percentile)	Average	Standard Deviation
Np	Redox to consider - Np (IV) and Np(V)	54	3.9E-02	7.0E+00	3.3E+00	2.2E+00
Pu	Redox to consider - Pu(III), Pu(IV) and Pu(VI)	6	1.9E-02	4.6E-01	2.0E-01	2.0E-01
U	Redox to consider - U(IV) and U(VI)	6	1.4E-02	3.0E-01	1.2E-01	1.2E-01

*Where values are reported as minima, maxima or ranges, they are excluded from the statistics

D.3.1.2 Sorption at High Salinity

Sorption measurements under DGR-relevant conditions are underway as part of the NWMO technical program, but results are not presently available (Vilks 2009). Published sorption data are generally not reported at conditions relevant to the DGR, notably the groundwater salinities are much lower than those occurring at the depth of the DGR (estimated to be up to about 375 g L^{-1} TDS; Table 5.4).

Probably the most thorough reported investigations of sorption are those of Weiland and Van Loon (2002) and Bradbury and Baeyens (2003a,b). However, these investigations were conducted only for about 13 g L^{-1} TDS for natural waters and about 20 g L^{-1} TDS for cement porewaters.

Stenhouse (1995) excluded sorption data obtained from experiments where the solution had NaCl > 1M (~ 58 g L^{-1}). Consequently, the data in this compilation are for substantially lower salinities. Unfortunately, the sources of data for higher salinities that were excluded are not reported by Stenhouse (1995).

The most relevant data are those obtained by the US DOE during the WIPP program (USEPA 1998). Here, the salinity and composition of the groundwater in the rocks of the Rustler Formation, which immediately overlies the repository host rock, is very similar to those of the groundwater thought to occur at the depth of the DGR. Furthermore, the most transmissive formation within the Rustler Formation is the Culebra Dolomite, the mineral surfaces of which are expected to have generally similar sorption characteristics to the Ordovician limestones that form the host rock of the DGR (although it should be noted that the Culebra Dolomite is very much more porous and permeable than the Cobourg Formation). However, the WIPP is a repository for Transuranic (TRU) waste and hence the investigations there have focussed on obtaining sorption data for uranium and trans-uranic elements. Consequently, there are no reported K_d values for Ni, Zr, Nb, Cd, Cr, Cu, Pb, Ra, C, or Cl. Other work by the USDOE on brine-saturated mudstone, carbonate and halite from Texas focussed on U (Voudrias et al. 1993, Voudrias and Means 1993). The results indicated significant retardation on the carbonates; results on halite and mudstone were ambiguous.

The German program has also produced sorption data under very high-salinity conditions (e.g., Warnecke et al. 1994). However, these data are not reported with supporting chemical information and consequently no use was made of them in the WIPP program (USEPA 1998). Also the source documents are not readily available. For this reason, they have not been considered in the present review.

Luckscheiter and Nesovic (2002) measured sorption of actinides and rare earths on glass and synthetic smectites, in both 5 M NaCl and $MgCl_2$ rich brines at 80°C. The results indicated relatively little effect of NaCl brine on clay sorption, but the $MgCl_2$ brine reduced sorption.

It can be concluded that alkali and alkali earth elements that sorb mainly by coulombic attraction are likely to have their sorption reduced to close to zero under highly saline conditions. Transitional elements that may sorb by both coulombic and specific chemical sorption may have their sorption significantly reduced. Since the lanthanides and actinides sorb mainly through surface complexation, the mass action effect of brine may be negligible to their sorption properties. However, most available data are for lithologies dissimilar to the Cobourg Formation. Consequently, the extent to which the surfaces of limestone constituents in this formation are conducive to sorption is uncertainty.

D.3.2 Recommended K_d Values

D.3.2.1 Approach to Recommending K_d Values

The review of the available data shows that it is reasonable to specify C, Cl and I to be non-sorbing.

Elements that are likely to sorb by cation exchange over at least a significant part of the relevant pH range, Ni and Ra, are conservatively specified to have Kd = 0. This approach is justified because Kd data are available only for lower water salinities and/or water compositions that are dissimilar to the deep groundwater and porewater at the Bruce nuclear site. Thus, it is likely that the sorption of Ni and Ra in these latter waters will be lower than the reported values, none of which can therefore be used to estimate conservative Kd values.

In the cases of Cr and Cu, the sorption mechanism is uncertain and therefore it cannot be deduced whether any reported Kd values can reasonably be used to estimate minimum values for in-situ deep groundwaters and porewaters at the Bruce nuclear site. For this reason, it is also conservatively specified that these elements have Kd = zero.

In contrast, Zr, Nb, Np, Cd, Pb, U and Pu are believed to sorb by surface complexation mechanisms. Consequently, sorption of these elements is not likely to be affected significantly by ionic strength. However, when deducing plausible conservative Kd values for the higher salinity waters present at the Bruce nuclear site, it is necessary to take into account the possibility that complexing by ligands would reduce sorption at high salinities compared to lower salinities. The review of chemical sorption suggests that this process is likely to occur in the cases of Nb, Np, Cd, Pb, U and Pu, depending upon the pH and the precise composition of the water.

Except for Nb, these elements may all form complexes with aqueous carbonates. If it occurs, formation of these complexes would tend to reduce sorption. However, the deep porewaters at the Bruce nuclear site have relatively high Ca concentrations, reflecting the presence of calcite and anhydrite in the rock. Consequently it is believed that TIC concentrations are relatively low, owing to an approach to equilibrium with calcite, which also occurs in the rock. For this reason, and bearing in mind that many of the published Kd data were obtained for rocks that contain calcite, it is likely that complexing with carbonate species will not significantly reduce Kd values of these elements compared to published ones. A particular problem concerns sorption of Pb onto carbonate minerals. Since Pb complexes with carbonate and may form a distinct carbonate mineral phase (cerrusite, $PbCO_3$) if present at a sufficiently high concentration the limited available data for sorption are of questionable quality. Consequently, Pb is treated conservatively as not sorbing on limestone.

Niobium may form complexes with SO_4, Cl and PO_4, but only at lower pH. Over the pH range of interest, ~ 5 to ~ 12.5 (in cement), these complexes will probably not cause actual sorption in the presence of Bruce groundwaters to depart significantly from reported values.

Lead may complex with Cl if carbonate concentrations are sufficiently low, while complexes with SO_4^{2-}, PO_4^{2-} and certain organic ligands are also possible. Similarly, U may form complexes with Cl and PO_4^{2-} if carbonate concentrations are sufficiently low. As for niobium, it is similarly likely that these complexes will not significantly reduce Kd in the presence of Bruce groundwaters compared to published values.

For these reasons, for Zr, Nb, Np, Cd, Pb, U and Pu the minimum Kd reported for each relevant material from among the values in Tables D-1 to D-3 (5th percentile in the last case) is conservatively recommended. Values are reported for bentonite, argillaceous lithologies, and limestone lithologies. Data for marl (especially Stenhouse 1995), clays and mudstones were used for argillaceous lithologies, while data for calcite, dolomite and limestone were used for the limestone lithology.

D.3.2.2 Recommended K_d Values

The Deep and Intermediate Bedrock Groundwater Zones of the Bruce nuclear site are reducing (see Table 5.4). Consequently, K_d values are recommended only for reduced forms of the elements of interest. Recommended values are tabulated in Table D.4.

Sorption values are provided for bentonite, for argillaceous lithologies, and for limestone/calcite. Argillacious lithologies have an appreciable amount of clay, and include shales, mudrock and marls. The Ordovician shales at the DGR site have 20-40% clay, and the values for argillaceous rocks are appropriate.

Although there is limited sorption data for specific DGR materials and salinities, there is a substantive knowledge base to indicate that some elements of interest will have non-negligible sorption under DGR conditions. The recommended values in Table D.4 are cautious estimates of the sorption – actual values are likely to be similar or higher. They are also consistent with preliminary and as yet unpublished measurements by NWMO. Nonetheless, the importance of the uncertainty in these values can be tested by also considering a case in which all sorption is set to zero.

Table D.4: Summary of Recommended K_d Values

Element	Argillaceous Lithologies (m^3 kg^{-1})	Limestone Lithologies (m^3 kg^{-1})	Bentonite (m^3 kg^{-1})
C	0	0	0
Cl	0	0	0
Cr	0 (1)	0 (1)	0 (1)
Ni	0	0	0
Cu	0 (1)	0 (1)	0 (1)
Zr	0.01	0 (1)	0.05
Nb	0.05	0 (1)	0.1
Cd	0.05	0 (1)	0 (1)
I	0	0	0
Pb	0.03	0 (1)	0.001
Ra	0	0	0
U	0.001	0.001	0.01
Np	0.03	0.001	0.004
Pu	0.2	0.02	0.5

Note:
(1) No relevant data for sorbent; no sorption is conservatively assumed.

REFERENCES FOR APPENDIX D

Alaux-Negrel, G., C. Beaucaire, G. Michard, P. Toulhoat and G. Ouzounian. 1993. Trace-metal behaviour in natural granitic waters. Journal of Contaminant Hydrology 13, 309-325.

Appelo, C.A.J. and D. Postma. 2005. Geochemistry, groundwater and pollution, 2nd edition, A.A. Baelkema Publishers, Amsterdam, Netherlands.

Bertetti, F.P., R.T. Pabalan and M.G. Almendarez. 1998. Studies of Neptunium V Sorption on Quartz, Clinoptilolite, Montmorillonite, and α-alumina. Adsorption of Metals by Geomedia. Academic Press, New York, USA.

Bradbury, M. and B. Baeyens. 2003a. Near Field Sorption Data Bases for Compacted MX-80 Bentonite for Performance Assessment of a High-level Radioactive Waste Repository in Opalinus Clay Host Rock. PSI Report 03-07/Nagra Report NTB-02-18. Wettingen, Switzerland.

Bradbury, M. and B. Baeyens. 2003b. Far Field Sorption Data Bases for Performance Assessment of a High-level Radioactive Waste Repository in an Undisturbed Opalinus Clay Host Rock. PSI Report 03-08/Nagra Report NTB-02-19. Wettingen, Switzerland.

Brigatti, M.F., C. Lugli, G. Cibin, A. Marcelli, G. Giuli, E. Paris, A. Mottana and Z. Wu. 2000. Reduction and sorption of chromium by Fe(II)-bearing phyllosilicates: chemical treatments and X-ray absorption spectroscopy studies. Clays and Clay Minerals 48, 272-281.

Brookins, D.G. 1988. Eh-pH Diagrams for Geochemistry. Springer-Verlag, New York, USA.

Carbol, P. and I. Enkvist. 1997. Compilation of Radionuclide Sorption Coefficients for Performance Assessment. SKB Report R-97-13. Stockholm, Switzerland

Choppin, G.R. 2005. Actinide Science: Fundamental and Environmental Aspects. Journal of Nuclear and Radiochemical Sciences 6. 1-5.

Cotton, F.A. and G. Wilkinson. 1980. Advanced Inorganic Chemistry - A Comprehensive Text, 4th Edition. John Wiley & Sons, New York, USA.

Crawford J., I. Neretnieks and M. Malmström. 2006. Data and Uncertainty Assessment for Radionuclide Kd Partitioning Coefficients in Granitic Rock for Use in SR-Can Calculations. SKB Report R-06-75. Stockholm, Sweden.

Cross, J.E., A.D. Moreton and C.J. Tweed. 1995. Thermodynamic Modelling of Radioactive Waste Disposal: Assessment of Near-field Solubility. UK Nirex Report NSS/R311. Harwell, United Kingdom.

Fendorf, S.E., G.M. Lambie, M.G. Stapleton, M.J. Kelley and D.L. Sparks. 1994. Mechanisms of chromium(III) sorption on silica. 1. Chromium(III) surface structure derived by extended x-ray absorption fine structure spectroscopy. Environmental Science and Technology 28, 284–289.

Fuge, R. 1996. Geochemistry of iodine in relation to iodine deficiency diseases. Environmental Geochemistry and Health, Geological Society Special Publication, 113, 201-211.

James, R.O. and T.W. Healy. 1972. Adsorption of hydrolyzable metal ions at the oxide-water interface. III. A thermodynamic model of adsorption. Journal of Colloid and Interface Science 40, 65-81.

Jones, M.A. 1992. The treatment of iodine and chlorine chemistry in the risk assessment of deep radioactive waste disposal. UK DOE Report DoE/HMIP/RR/92.069, UK Department of the Environment, London, United Kingdom.

Kaplan, D.I., R.J. Serne, K.E. Parker and I.V. Kutnyakov. 2000. Iodide Sorption to Subsurface Sediments and Illitic Minerals. Environmental Science and Technology, 34, 399–405.

Kersting, A.B., D.W. Efurd, D.L. Finnegan, D.J. Rokop, D.K. Smith and J.L. Thompson. 1999. Migration of plutonium in groundwater from the Nevada Test Site. Nature 397, 56-58.

Krauskopf, K.B. 1967. Introduction to Geochemistry. McGraw-Hill, New York, USA.

LaFlamme, B.D. and J.W. Murray. 1987. Solid-solution interaction: the effect of carbonate alkalinity on adsorbed thorium. Geochimica et Cosmochimica Acta 51, 243-250.

Lieser, K.H. and U. Mühlenweg. 1988. Neptunium in the hydrosphere and in the geosphere. Radiochimica Acta 43, 27-35.

Linklater, C.M., A.D. Moreton and C.J. Tweed. 2003. Analysis and interpretation of geosphere sorption data for a Nirex performance assessment. UK Nirex Report N/083. Harwell, United Kingdom.

Lu., N., P.W. Reimus, G.R. Parker, J.L.Conca and I.R. Triay. 2003. Sorption kinetics and impact of temperature, ionic strength and colloid concentrations on the adsorption of plutonium-239 by inorganic colloids. Radiochimica Acta 91, 713-720.

Luckscheiter, B. and M. Nesovic. 2002. Sorption behaviour of Am on precorroded HLW glass in water and brines. Radiochimica Acta 90, 537-541.

NIREX. 1997. Sellafield Geological and Hydrogeological Investigations: The Hydrochemistry of Sellafield, 1997 Update. United Kingdom Nirex Ltd. Science Report No. S/97/089.

Pabalan, R.T., D.R. Turner, F.P. Bertetti and J.D. Prikryl. 1998. UraniumVI sorption onto selected mineral surfaces. In: E.A. Jenne (Editor), Adsorption of Metals by Geomedia. Academic Press. New York, USA.

Rittenhouse, G., R.B. Fulton, R.J. Grabowski and J.L. Bernard. 1969. Minor elements in oilfield waters. Chemical Geology 4, 189-209.

Runde, W. 2002. Geochemical interactions of actinides in the environment. In: P.-C. Zhang and P.V. Brady (Editors), Geochemistry of Soil Radionuclides. Soil Science Society of America, Madison. USA.

Rybicka, E.H., W. Calmano and A. Breeger. 1995. Heavy metals sorption/desorption on competing clay minerals; an experimental study. Applied Clay Science 9, 369-381.

Sanchez, A.L., J.W. Murray and T.H. Sibley. 1985. The adsorption of plutonium IV and V on goethite. Geochimica et Cosmochimica Acta 49, 2297-2307.

Savage, D. and M. Stenhouse. 2002. SFR 1 Vault Database. SKI Report 02:53. Stockholm, Sweden.

Stenhouse, M.J. 1995. Sorption databases for crystalline rock, marl and bentonite for performance assessment, Nagra Technical Report NTB 93-06, Wettingen, Switzerland.

Tachi, Y., Y. Tochigi, T. Suyama, Y. Saito, M. Ochs and M. Yui. 2009. Development of the sorption and diffusion database system for safety assessment of geological disposal. JAEA Report, JAEA-Data/Code 2008-034. Japan.

Tan, W., F. Liu, X. Feng, Q. Huang and X. Li. 2005. Adsorption and redox reactions of heavy metals on Fe–Mn nodules from Chinese soils. Journal of Colloid and Interface Science, 284, 600–605.

Ticknor, K.V. 1994. Sorption of Nickel on Geological Materials, Radiochimica Acta 66/67, 341-348.

Toyohara, M., M. Kaneko, M. Mitsutsuka, H. Fujihara, N. Saito and T. Murase. 2002. Contribution to Understanding Iodine Sorption Mechanism onto Mixed Solid Alumina Cement and Calcium Compounds. Journal of Nuclear Science and Technology, 39, 950-956.

Turner, D.R., F.P. Bertetti and R.T. Pabalan. 2002. Role of radionuclide sorption in high-level waste performance assessment: approaches for the abstraction of detailed models. In: P.-C. Zhang and P.V. Brady (Editors), Geochemistry of Soil Radionuclides. Soil Science Society of America, Madison, USA.

USEPA. 1998. Technical support document for Section 194.14: Assessment of Kds used in the CCA. United States Environmental Protection Agency DOCKET NO: A-93-02 V-B-4. USA.

USEPA. 1999. Understanding variation in partition coefficient, Kd, values, Vol II. United States Environmental Protection Agency Report EPA 402-R-99-004B. USA.

USEPA. 2004. Understanding variation in partition coefficient, Kd, values, Vol III. United States Environmental Protection Agency Report EPA 402-R-04-002C. USA.

Vilks, P. 2009. Sorption in highly saline solutions – state of the art science review. Nuclear Waste Management Organization report TR-2009-18. Toronto, Canada.

Voudrias, E., J. Means and J. Kittel. 1993. Retardation of tritium and cesium in brine-saturated mudstone, halite and carbonate porous media. Ground Water 31(4), 605.

Voudrias, E., and J. Means. 1993. Sorption of uranium by brine-saturated halite, mudstone and carbonate minerals. Chemosphere 26(10), 1753-1765.

Warnecke, E., A. Hollman, G. Tittel and P. Brennecke. 1994. Gorleben Radionuclide Migration Experiments: More Than 10 Years of Experience. In: Fourth International Conference on the Chemistry and Migration Behavior of Actinides and Fission Products in the Geosphere, 821-827, R. Oldenbourg Verlag, Munich, Germany.

Wedepohl, K.H. (ed). 1978. Handbook of Geochemistry II-3. Springer-Verlag, Berlin, Germany.

Wieland, E. and Van Loon, L.R. 2002. Cementitious near-field sorption data base for Performance Assessment of an ILW repository in Opalinus Clay. PSI Report 03-06/Nagra Report NTB 02-20. Wettingen, Switzerland.

Yelton, W.G., Y.K. Behl, J.W. Kelly, M. Dunn, J.B. Gillow, A.J. Francis and H.W. Papenguth. 1996. Laboratory evaluation of colloidal actinide transport at the Waste Isolation Pilot Plant (WIPP): 1. Crushed-dolomite column flow experiments. Sandia Report SAND96-2894C. Albuquerque, USA.

Zhang, P.-C., J.L. Krumhansl and P.V. Brady. 2002. Introduction to properties, sources and characteristics of soil radionuclides. In: P.-C. Zhang and P.V. Brady (Editors), Geochemistry of Soil Radionuclides. Soil Science Society of America, Madison, USA.

APPENDIX E: REVIEW OF CORROSION RATES

E.1 INTRODUCTION

The corrosion behaviour of the metallic containers and waste forms is determined by the nature of the repository environment. Given that the temperature of the repository is relatively constant, the environmental factors that have the most influence on the corrosion behaviour are the availability of water (H_2O) and oxygen (O_2), and the presence of chloride (Cl^-) ions.

Water is required for all aqueous corrosion processes, serving a number of different roles, including:

1. Providing an electrolyte to support the electrochemical reactions that constitute the overall corrosion reaction;
2. Participating in hydrolysis and film formation reactions; and
3. In the absence of O_2, serving as an oxidant for base metals, such as steel, nickel, and zirconium alloys.

It is possible that the rate of corrosion could be limited by the availability of water in the repository if the rate of saturation is sufficiently slow. In practice, the availability of water can be related to the relative humidity (RH) in the atmosphere. It is typically found that corrosion does not occur at an RH of less than 60-80% (Leygraf and Graedel 2000, Shreir et al. 1993). Below this range, there is insufficient water on the surface to support electrochemical reactions. At higher moisture contents, the water layer thickness increases with increasing RH.

Oxygen acts as an oxidant, the electrochemical reduction of which is coupled to the anodic dissolution of the metal. Oxygen is a more powerful oxidant than H_2O and shifts the corrosion potential (E_{CORR}) of the metal surface to more positive values. In turn, this can, in the presence of an aggressive species such as Cl^-, lead to localized breakdown of the protective surface layer (see below). Under some circumstances, the rate of reduction of O_2 (and of the overall corrosion process) can become limited by its rate of supply to the corroding surface. However, given that the repository is likely to be unsaturated during the aerobic phase, this is unlikely to be so here because of rapid O_2 transport across the thin water film.

Chloride ions affect the formation and stability of protective (oxide) layers that would otherwise form on the corroding surface. The range of effects include:

1. Increased solubility of dissolved metal ions, slowing or preventing the precipitation of protective oxide or oxyhydroxide surface layers;
2. Localized attack on passive films, leading to pitting or crevice corrosion;
3. In the presence of stress, environmentally assisted cracking of susceptible materials such as austenitic stainless steels; and
4. Extensive dissolution of pre-existing passive films leading to de-passivation.

The consequences of these various effects include:

1. Increased rates of general corrosion;
2. Localized corrosion in the form of pits or crevice attack; and
3. Stress corrosion cracking.

Since no credit is taken in the post-closure safety assessment for the effect of the container as mass-transport barrier to the release of radionuclides, the only consequence of high salinity here is the effect on the rate of general corrosion.

Corrosion rates for the four groups of metallic materials (carbon and galvanized steel, passivated carbon steel, passive alloys such as stainless steel and nickel-based alloys, and zirconium alloys) are required for both aerobic and anaerobic conditions and in saturated and unsaturated phases. Values were selected from various literature studies.

The rates given below are best estimates, with the upper and lower bounds given below each value as a range in parentheses.

E.2 CARBON AND GALVANIZED STEEL

The presence of O_2 under aerobic conditions leads to relatively rapid corrosion of C-steel. Under unsaturated (vapour-phase) conditions, a wide range of rates has been reported. Rates of 10 to several 100's of $\mu m \cdot a^{-1}$ (ASM 1987, DECHEMA 1990) have been found under various atmospheric conditions, the higher rates found close to oceans where the effect of salinity is compounded by the action of wind and precipitation, which tends to prevent the formation of a stable oxide film. The best-estimate value is defined as 10 $\mu m \cdot a^{-1}$ because of a greater tendency for the precipitation of a protective film in thin liquid films in the stagnant air of the repository. However, the relative ease of access of O_2 to the corroding surface through the thin surface water film can lead to increased rates of corrosion, which is reflected in a larger range of values under aerobic unsaturated conditions.

Under anaerobic conditions, C-steel corrodes at a lower rate with relatively little difference between the rates under saturated and unsaturated conditions. The rates are lower under anaerobic conditions because the electrochemical potential is less positive as H_2O is a less powerful oxidant than O_2. There should be little difference in saturated and vapour-phase corrosion rates as there is little difference in the rate of supply of oxidant (H_2O) except at very low RH. There is extensive evidence that the rate of corrosion decreases with time because of the build-up of a protective surface film (King 2008). This effect can be clearly seen if the rate of corrosion is followed by measuring the rate of H_2 evolution (Blackwood et al. 2002). Under saturated conditions, the film comprises a duplex magnetite (Fe_3O_4) structure, with ion transport across the inner barrier layer thought to be rate determining. The best estimate rate for saturated conditions of 2 $\mu m\ a^{-1}$ reflects both the long-term effect of the corrosion product (which leads to a decrease in corrosion rate) and the effect of the saline groundwater (which tends to increase the corrosion rate). For C-steel, increasing Cl^- ionic concentration lead to an increase in corrosion rate up to a concentration of several 10's of $g\ L^{-1}$, but there is relatively little further increase at higher salinity (King 2005).

Under unsaturated conditions, the formation of a protective surface film is favoured by the limited volume of solution, resulting in faster saturation of the liquid with dissolved metal ions. This is reflected in slightly lower corrosion rates compared with saturated conditions. Recent measurements of the anaerobic corrosion rate of C-steel under unsaturated conditions (Newman et al. 2010) confirm both the threshold RH range for corrosion and the lower corrosion rates in humid atmospheres relative to saturated conditions. Newman et al. (2010) reports very low corrosion rates (<0.1 $\mu m \cdot a^{-1}$) for clean surfaces (without salt contaminants) and for salt-coated surfaces at RH below the threshold value range of 60-80% RH. However, salt-coated surfaces exposed to 75% and 100% RH atmospheres did exhibit measurable corrosion at rates of ~1 $\mu m\ a^{-1}$ (Table E.1).

The effects of variations in the groundwater composition are captured within the ranges given in Table E.1.

E.3 PASSIVATED CARBON STEEL

Carbon steel is passivated by the high pH of the porewater in cementitious materials. Provided the pH is maintained in the range pH 12-13, there is no evidence that the potentially high Cl^- concentration in the groundwater will induce a loss of passivity and a consequent increase in corrosion rate. Under alkaline conditions, the corrosion rate is anodically controlled by the properties of the passive oxide (Fe_3O_4) film. Smart et al. (2004) have summarized results from an extensive UK program on the corrosion of carbon and stainless steels in such environments, from which the best-estimate values and ranges in Table E.2 are taken.

Table E.1: Corrosion Rates of Carbon and Galvanized Steels under Aerobic and Anaerobic Conditions

Redox Conditions	Saturated Conditions ($\mu m\ a^{-1}$)	Vapour Phase Conditions ($\mu m\ a^{-1}$)*
Aerobic	30 (5-50)	10 (1-100)
Anaerobic	2 (0.1-10)	1 (0.1-10)

Note: * The vapour-phase corrosion rates assume a relative humidity greater than the threshold value range of 60-80%.

Table E.2: Corrosion Rates of Passivated Carbon Steel under Aerobic and Anaerobic Conditions.

Redox Conditions	Saturated Conditions ($\mu m\ a^{-1}$)	Vapour Phase Conditions ($\mu m\ a^{-1}$)*
Aerobic	0.1 (0.05-5)	0.1 (0.05-5)
Anaerobic	0.1 (0.01-1)	0.1 (0.01-1)

Note: * The vapour-phase corrosion rates assume a relative humidity greater than the threshold value range of 60-80%.

A similar best-estimate value is adopted for both aerobic and anaerobic conditions, as corrosion is likely to occur under anodic-limiting conditions (at a rate determined by the properties of the passive film). The range of rates is shifted towards smaller values for anaerobic conditions to account for the possible lower corrosion rate as a result of the smaller potential drop across the passive film. Corrosion rates would be expected to be similar under both saturated and unsaturated conditions as the rate is determined primarily by the properties of the passive film, not by transport in solution.

E.4 PASSIVE ALLOYS

Passive alloys will also exhibit low rates of corrosion in the repository environment. Some of these wastes will be in contact with cementitious materials, whereas others will be exposed to the groundwater. This range of environments is reflected in the ranges in the corrosion rates given in Table E.3, with the best-estimate values representing mean values.

Saline groundwaters may lead to relatively high rates of corrosion, which are reflected by the upper bounds of the ranges quoted. However, there is no evidence that stainless steel will de-passivate in saline anaerobic groundwaters (the most likely conditions under which this might occur). White et al. (1966) report a rate of 0.8 $\mu m\ a^{-1}$ for anoxic seawater after 120 days exposure at 24-40 ^{o}C. This value is within the range of values reported for more-dilute solutions and does not indicate any increase due to de-passivation of the alloy.

Table E.3: Corrosion Rates of Stainless Steels and Nickel-Based Alloys Under Aerobic and Anaerobic Conditions.

Redox Conditions	Saturated Conditions ($\mu m \cdot a^{-1}$)	Vapour Phase Conditions ($\mu m \cdot a^{-1}$)
Aerobic	0.1 (0.05-5)	0.1 (0.05-5)
Anaerobic	0.1 (0.01-1)	0.1 (0.01-1)

As noted above, although Cl^- ions may induce localized corrosion of stainless steel under aerobic conditions, this is not of interest here as this will not significantly increase the rate of release of radionuclides from the waste form.

Values for stainless steels in cementitious materials were taken from Smart et al. (2004), with values for near-neutral pH taken from BSC (2004), Casteels et al. (1986), and White et al. (1966). These latter studies encompass a range of salinities, temperatures, and exposure periods, with corrosion rates that vary between 0.01 $\mu m\ a^{-1}$ and 5 $\mu m\ a^{-1}$. There are relatively few studies under anaerobic conditions, with most studies performed in aerated solution.

In Table E.3, the same rates, and ranges of rates, have been used to represent the expected corrosion rates under saturated and unsaturated conditions. The corrosion rate of passive materials is controlled by the properties of the passive oxide layer, which would not be expected to strongly affected by the availability of water (assuming a relative humidity sufficient to form a thin electrolyte layer on the surface). The range of rates selected for anaerobic conditions is lower than that for aerobic environments as, although the corrosion rate is primarily anodically limited, the concentration of dissolved oxygen will affect the extent to which the corrosion potential of the surface is polarized and, consequently, may have a slight effect on the passive current density. However, the mean corrosion rate is the same for both aerobic and anaerobic conditions as the effect on the passive current density will be small.

E.5 ZIRCONIUM ALLOYS

Zirconium is one of the more corrosion-resistant alloys and can be expected to corrode slowly in the DGR environment. Rates of 0.0001 to 2 $\mu m\ a^{-1}$ have been reported at temperatures of 24-40 ^{o}C and pH values ranging from neutral to pH 14 (Hansson 1985, McDeavitt et al. 1998, Videm 1981, Wada et al. 1999). Shoesmith and Zagidulin (2010) recently reviewed the literature and recommended an upper limit of 0.02 $\mu m\ a^{-1}$ and a reasonable value of 0.005 $\mu m\ a^{-1}$ for passive corrosion, with some studies suggesting less than 0.001 $\mu m\ a^{-1}$.

The lower rates tend to be from long-term studies, possibly indicating that the higher rates do not fully take into account the protective properties of the oxide film that will be present on the Zr alloys in the repository. Because of the inherent stability of the ZrO_2 film, greater emphasis is placed here on the results of the longer-term studies in selecting the best estimate and range of corrosion rates.

The range of rates given in Table E.4 reflects the possible variation in groundwater composition.

Table E.4: Corrosion Rates of Zirconium Alloys Under Aerobic and Anaerobic Conditions.

Redox Conditions	Saturated Conditions ($\mu m\ a^{-1}$)	Vapour Phase Conditions ($\mu m\ a^{-1}$)
Aerobic	0.01 (0.005-0.05)	0.01 (0.005-0.05)
Anaerobic	0.01 (0.005-0.05)	0.01 (0.005-0.05)

REFERENCES FOR APPENDIX E

ASM. 1987. Metals Handbook, Ninth edition, Volume 13, Corrosion. American Society for Metals International, Metals Park, USA.

Blackwood, D.J., L.J. Gould, C.C. Naish, F.M. Porter, A.P. Rance, S.M. Sharland, N.R. Smart, M.I. Thomas and T. Yates. 2002. The localized corrosion of carbon steel and stainless steel in simulated repository environments. AEA Technology Report, AEAT/ERRA 0318. Harwell, United Kingdom.

BSC. 2004. Aqueous corrosion rates for waste package materials. Bechtel SAIC Company ANL-DSD-MD-000001. Las Vegas, USA.

Casteels, F., G. Dresselaars and H. Tas. 1986. Corrosion Behaviour of Container Materials for Geological Disposal of High Level Waste, 3-40, Commission of the European Communities Report EUR 10398 EN. Brussels, Belgium.

DECHEMA. 1990. Corrosion Handbook: Corrosive Agents and their Interaction with Materials, Volume 7, Atmosphere. VCH, Weinheim, Germany.

Hansson, C.M. 1985. The corrosion of steel and zirconium in anaerobic concrete. Materials Research Society Symposium 50, 475-482.

King, F. 2005. Overview of the corrosion behaviour of copper and steel used fuel containers in a deep geologic repository in the sedimentary rock of the Michigan Basin, Ontario. Ontario Power Generation Report OPG 06819-REP-01300-10101-R0. Toronto, Canada.

King, F. 2008. Corrosion of carbon steel under anaerobic conditions in a repository for SF and HLW in Opalinus clay. Nagra Technical Report NTB 08-12. Wettingen, Switzerland.

Leygraf, C. and T.E. Graedel. 2000. Atmospheric Corrosion. Wiley Interscience. New York, USA.

McDeavitt, S.M., D.P. Abraham and J.Y. Park. 1998. Evaluation of stainless steel-zirconium alloys as high level nuclear waste forms. Journal of Nuclear Material 257, 21-34.

Newman, R.C., S. Wang and G. Kwong. 2010. Anaerobic Corrosion Studies of Carbon Steel Used Fuel Containers. Nuclear Waste Management Organization Report, TR-2010-07. Toronto, Canada.

Shoesmith, D. and D. Zagidulin. 2010. The Corrosion of Zirconium Under Deep Geological Repository Conditions. Nuclear Waste Management Organization Report, TR-2010-19. Toronto, Canada.

Shreir, L.L., R.A. Jarman and G.T. Burstein. 1993. Corrosion. Volume 1 Metal/Environment Reactions, 3rd Edition. Butterworth-Heinemann. Oxford, United Kingdom.

Smart, N.R., D.J. Blackwood, G.P. Marsh, C.C. Naish, T.M. O'Brian, A.P. Rance and M.I. Thomas. 2004. The Anaerobic Corrosion of Carbon and Stainless Steels in Simulated Repository Environments: A Summary Review of Nirex Research. UK Nirex report AEAT/ERRA-0313. Harwell, United Kingdom.

Videm, K. 1981. Corrosion studies of candidate materials for permanent storage of nuclear waste. In Proceedings International Congress on Metallic Corrosion (8th) Mainz, Germany.

Wada, R., T. Nishimura, K. Fujiwara, M. Tanabe and M. Mihara. 1999. Experimental study of hydrogen gas generation rate from corrosion of Zircaloy and stainless steel under anaerobic alkaline condition. Proceedings of the Radioactive Waste Management and Environmental Remediation Conference, September 26-30, Nagoya, Japan.

White, J.H., A.E. Yanic and H. Schick. 1966. The corrosion of metals in the water of the Dead Sea. Corrosive Science 6, 447.

APPENDIX F: REVIEW OF MICROBIAL DEGRADATION DATA

F.1 INTRODUCTION

This appendix presents a review and assessment of microbial degradation data of organic wastes. Within the repository, the organic wastes are classified as cellulose, resin, and plastic and rubber.

The majority of data available on degradation of these waste materials is in the form of gas generation rates. In order to transform this data into a polymer degradation rate, a first order kinetic relationship is employed as outlined in Equation F.1 (Rittmann and McCarty 2001)

$$-\frac{dC}{dt} = V.C \qquad (F.1)$$

where *C* is the concentration of the substrate, and V is the degradation rate constant for the substrate.

The rate constant can be calculated from the integration of the rate equation (Equation F.2).

$$\ln\left(\frac{C_t}{C_0}\right) = -V.t \qquad (F.2)$$

where C_t is the concentration of substrate at time t, and C_0 is the concentration of substrate at time 0.

In cases where only gas generation rates or production profiles are available, substrate concentrations are calculated from the stoichiometry of the gas generation reactions (e.g., Equation F.3 for methane generation from cellulose). This approach was employed to generate cellulose degradation rates from experimental data (Beadle 2001, 2002) for the Drigg 2002 PCSC (BNFL 2002a).

$$C_6H_{10}O_5 + H_2O \rightarrow 3CO_2 + 3CH_4 \qquad (F.3)$$

The data sources used to generate polymer degradation rates are described below. Assumptions employed in the derivation of these rates are also highlighted along with any relevant data on the environmental conditions the data was collected under, e.g., temperature, degree of saturation.

Appendix F.2, F.3 and F.4 summarize literature data on the degradation of cellulose, ion exchange resin, and plastic and rubber, respectively.

F.2 CELLULOSE DEGRADATION

F.2.1 Drigg Technical Programme

The Drigg Technical Programme carried out a number of long-term (>3 a) LLW degradation experiments (Beadle 2001, 2002) aimed at deriving degradation rates for source term modelling studies. These programs included small-scale laboratory-based experiments (10 L, ~20^{o}C, fully saturated) containing 1 kg of simulated LLW waste (40 wt% paper, 50 wt% mixed plastic and rubber, 10 wt% carbon steel) and larger-scale field experiments (~200 L, 5-15^{o}C, fully saturated) containing a similar simulated waste mixture (180 kg of cellulosic material per vessel) to the small-scale experiments. Both sets of experiments were filled with rainwater and maintained a

pH of >6.0 throughout their operation. Gas generation rate and gas composition data (CO_2, CH_4) was collected allowing cellulose degradation rates to be calculated. Both sets of experiments exhibited biphasic gas generation profiles with an initial faster rate giving way to a slower long-term gas generation rate. Average cellulose degradation rates from these experiments can be found in Table F.1.

Table F.1: Cellulose Degradation Rates from the Drigg Waste Degradation Experiments

Experiments	Conditions	Average Rate (a^{-1})
Small-scale laboratory experiments	Aerobic rate	$1.5x10^{-2}$
	Initial anaerobic rate	$1.2x10^{-1}$
	Final anaerobic rate	$2.7x10^{-2}$
Large-scale field experiments	Aerobic rate	$3.0x10^{-4}$
	Initial anaerobic rate	$2.9x10^{-2}$
	Final anaerobic rate	$1.0x10^{-2}$

Note: From Beadle (2001 and 2002).

The aerobic degradation rates were estimated from the CO_2 generation curves. The anaerobic rates were calculated from the methane generation curves and assume that all methane is derived from cellulose degradation. This assumption neglects methane derived from the consumption of corrosion hydrogen; consequently the calculated rates are likely to be overestimates of the actual cellulose degradation rate. There is insufficient data available to adjust the rates to take into account the impact of methane generation from corrosion hydrogen. The calculated aerobic rates assume the end of the aerobic phase is indicated by the onset of methane production. This assumption will underestimate the aerobic degradation rate since there is likely to be a lag between the end of oxygen consumption and the onset of methane generation.

F.2.2 NIREX Gas Generation Studies

UK Nirex Ltd commissioned a number of studies in order to test its gas generation model GAMMON (Agg et al. 1997; 2002a,b). These experiments were similar to those described above; however they generally had a wider range of scales and experimental conditions. A series of laboratory experiments were carried out at 1.5-L scale and below (Agg et al. 2002a,b) using a simulated waste mix (~79 wt% carbon steel, 8 wt% cellulose, 13wt% mixed plastics and rubber). These experiments investigated a range of atmospheres, saturation levels, chemical compositions and pH values. A series of larger-scale experiments (220 L) were also run (Agg et al. 1997) at a range of moisture contents and starting pH, again using a simulated waste mix representative of UK LLW. Unfortunately the data provided by Agg et al. (1997) are not sufficient to calculate cellulose degradation rates. Of the smaller-scale experiments reported by Agg et al. (2002a,b), only one experiment generated sufficient gas to be suitable for the calculation of a cellulose degradation rate (Table F.2). The experiment in question was carried out under saturated conditions with an anaerobic atmosphere. No details are given as to the temperature of the experiment; it is taken to be at laboratory temperature (20 to 25 °C). Two degradation rates have been derived from these data in the same manner as those derived from the Drigg experiments.

Table F.2: Cellulose Degradation Rates Derived from the Nirex Experimental Program

Experiments	Conditions	Rate (a^{-1})
Small-scale laboratory experiments	Initial anaerobic rate	1.9×10^{-1}
	Final anaerobic rate	3.1×10^{-2}

Note: From Agg et al. (2002a,b).

The calculated rates are of the same order of magnitude of those calculated from the Drigg experiments. The assumptions inherent in these calculations are the same as those outlined for the Drigg data above.

F.2.3 Gas Generation from the German Radioactive Waste Disposal Program

A number of papers originating from the German radioactive waste disposal program were reviewed for waste degradation rates (Kannen and Muller 1999, Bracke and Muller 2003, Bracke et al. 2004, Bracke and Muller 2007). Bracke et al. (2004) report a range of gas generation rates for mixed wastes and ion exchange resins under a range of environmental conditions. The data appears to come from a combination of real waste packages and laboratory-based experiments. The rates are expressed in terms of m^3 of gas generated per tonne of waste per year. This data was converted to a range of waste degradation rates (Table F.3) using the stoichiometry of the reaction, a temperature of 20°C, and taking the cellulose content of mixed waste to be 30% (Kannen and Muller 1999).

Table F.3: Waste Degradation Rates

Waste	Environment	Water Content	pH	Rate (a^{-1})
Mixed	Aerobic	Dry	6-8	1.5×10^{-3} to 3.7×10^{-3}
	Aerobic	Dry	9-11	5.2×10^{-3} to 5.2×10^{-2}
	Anaerobic	Dry	6-8	7.5×10^{-5} to 6.0×10^{-3}
	Anaerobic	Dry	9-11	3.7×10^{-5}
	Anaerobic	Humid	6-8	5.2×10^{-3} to 6.4×10^{-3}
Resins	Anaerobic	Dry	6-8	1.6×10^{-5} to 6.5×10^{-4}
	Anaerobic	Humid	6-8	7.6×10^{-5} to 2.7×10^{-4}

Note: Derived from Bracke et al. (2004).

Further gas generation rates are presented by Kannen and Muller (1999) and Bracke and Muller (2003). However, in these publications the rates are expressed per unit volume (e.g., per drum) and there is no data provided on the mass of waste per unit volume. However, by assuming a 30% cellulose content (Kannen and Muller 1999) and a cellulose density of 1.6 g cm^{-3} (Sun 2005), it is possible to calculate rate values from these sources (Table F.4).

Table F.4: Waste Degradation Rates

Source	Waste	Data	Rate (a^{-1})
Kannen and Muller (1999)	Compacted mixed waste	Mean values from a range of sources.	$1.3x10^{-4}$
	Mixed waste		$2.0x10^{-4}$
	Experimental systems		$4.8\ x10^{-5}$
	Real compacted waste		$1.2\ x10^{-5}$
Bracke and Muller (2003)	Compacted mixed waste	Mean Rate	$2.4\ x10^{-4}$
		Maximum Rate	$2.0\ x10^{-3}$
	Cemented mixed waste	Mean Rate	$2.4x10^{-5}$
		Maximum Rate	$4.0x10^{-4}$

Note: Derived from Kannen and Muller (1999) and Bracke and Muller (2003).

F.2.4 WIPP-related Data

A range of gas generation experiments to support the WIPP program have been reported (Caldwell et al. 1988, Francis et al. 1997, Felicione et al. 2003). Caldwell et al. (1998) investigated gas generation from simulated WIPP waste and plywood sawdust under aerobic and anaerobic conditions in the presence of water or brine at a range of temperatures. The experimental data indicate that only carbon dioxide was detected in aerobic and anaerobic experiments. The lack of methane generation in anaerobic experiments suggests that cellulose degradation is not proceeding to completion. In view of this, cellulose degradation rates calculated from carbon dioxide production rates assume that cellulose is degraded via fermentation to acetic acid (Equation F.4).

$$C_6H_{10}O_5 + 5H_2O \rightarrow CH_3COOH + 8H_2 + 4CO_2 \qquad (F.4)$$

A further complication arising from using carbon dioxide production to calculate cellulose degradation rates is that it is difficult to take carbon dioxide solubility into account. Consequently calculated rates may be underestimates of the actual rate. Cellulose degradation rates calculated from the degradation of simulated WIPP waste incubated at 24°C can be found in Table F.5. Caldwell et al. (1998) also published carbon dioxide generation data from previous studies carried out at low water contents (1%), these data are also presented in Table F.5.

Table F.5: Cellulose Degradation Rates

Environment	% Water Content	Rate (a^{-1})
Aerobic	100	$3.5x10^{-3}$
Aerobic	100 (Brine)	$2.2x10^{-3}$
Aerobic	1	$2.0x10^{-3}$
Anaerobic	100	$9.9x10^{-3}$
Anaerobic	100 (Brine)	$2.2x10^{-4}$
Anaerobic	1	$5.6x10^{-3}$

Note: Derived from the WIPP Gas Generation Experiments of Caldwell et al. (1988).

Francis et al. (1997) reported a similar series of experiments which looked at the degradation of cellulose and irradiated plastics at a range of water contents, nutrient levels and environmental conditions. The experiments were carried out at 30°C in 160 mL serum bottles using WIPP brines. The majority of these experiments generated low volumes of gas which may be due to the fact that the experiments often developed acidic conditions not favourable for gas generation. In general those experiments with nitrate present and/or bentonite present to buffer the system generated sufficient gas to allow cellulose degradation rates to be calculated (Table F.6). As with the other experimental data discussed above, gas generation in these experiments demonstrated a biphasic profile with an initial faster rate followed by a slower gas generation rate.

Felicione et al. (2003) reported on a 6.5 year experiment investigating gas generation from contact-handled transuranic wastes. The waste was inundated with simulated brine and incubated at 30°C under anoxic conditions. In common with other WIPP-related studies (Caldwell et al. 1988, Francis et al. 1997), the majority of these experiments did not produce significant amounts of methane suggesting that the carbon dioxide measured reflects incomplete cellulose degradation (Equation F.4). Cellulose degradation rates derived from this study are summarized in Table F.7.

Table F.6: Cellulose Degradation Rates

Conditions	Bentonite Present	Water (Brine) Content	Rate (a^{-1})	
Aerobic (inoculated + nutrients)	Yes	Humid (RH = 70-74%)	1.8×10^{-2}	
Aerobic + Nitrate	No	Saturated	Max	4.8×10^{-3}
			Min	5.6×10^{-4}
	Yes		Max	8.6×10^{-3}
			Min	3.6×10^{-4}
Anaerobic (inoculated + nutrients)	No	Humid (RH = 70-74%)	3.0×10^{-3}	
	Yes		1.5×10^{-2}	
Anaerobic (inoculated + nutrients)	No	Saturated	1.3×10^{-3}	
	Yes	Saturated	3.6×10^{-3}	

Note: Derived from the WIPP Gas Generation Experiments (Francis et al. 1997).

Table F.7: Cellulose Degradation Rates

	Degradation Rate (a^{-1})		
	Average	**Maximum**	**Minimum**
Initial Rate (up to 200 days)	$1.6x10^{-4}$	$4.1x10^{-4}$	$5.1x10^{-5}$
Overall Rate (> 4 years)	$3.5x10^{-5}$	$8.4x10^{-5}$	$1.0x10^{-5}$

Note: Derived from the WIPP Gas Generation Experiments (Felicione et al. 2003).

F.2.5 Finnish Large-Scale Gas Generation Experiment

The Finnish nuclear power generating company Teollisuuden Voima Oy (TVO) operates a large-scale Gas Generation Experiment (GGE) in its VLJ Repository at the Olkiluoto site (Small et al. 2005). The primary objective of the GGE is to quantify rates of gas generation from actual LLW and it has been producing data on gas generation rates and composition data since operation started in 1997. Methane generation data taken from Small et al. (2005) was used to calculate a cellulose degradation rate of $3.8x10^{-1}$ a^{-1}. In the absence of any data on the mass of waste in the experiment, starting and final cellulose concentrations were calculated from the methane generation curve. It is understood that an operating temperature of $10^{o}C$ was employed. The calculated cellulose degradation rate is likely to be an overestimate since the methane generation curve will also include methane produced via the oxidation of corrosion hydrogen. Significant amounts of corrosion hydrogen were detected early in the lifetime of the experiment suggesting that hydrogen consumption is a significant route of methane generation.

F.2.6 Gas Generation Modelling Studies

EPRI (Yim and Simonson 1997) developed a gas generation model for performance assessment studies. The model was populated with a range of hydrolysis rates for a range of polymeric substrates (Table F.8). These rates appear to be derived from generic literature data from non-nuclear sources.

NAGRA (2004) and SKB (Skagius et al. 1999) report gas modelling of L&ILW repositories. They used a reference value of 0.7 and 0.05 mol gas a^{-1} kg^{-1} for cellulosic wastes and for other organics (plastics, rubber, bitumen) respectively. Assuming 50% CO_2 and CH_4, and a formula of $C_6H_{10}O_5$ for cellulose and C_8H_8 for other organics, the equivalent degradation rate is listed in Table F.8. NAGRA (2004) notes that these values are about an order of magnitude higher than measurements.

Table F.8: Waste Degradation Rates (a^{-1}) from Modelling Studies

	Paper	**Plastic, Rubber and Wood**
EPRI	$3.1x10^{-2}$	$2.3x10^{-3}$
Nagra, SKB	$1.9x10^{-2}$	$6.5x10^{-4}$

F.2.7 Summary of Cellulose Waste Degradation Rates

A summary of the cellulose waste degradation data reported in this section is outlined in Table F.9. In general, the data show higher degradation rates under saturated conditions. The impact of temperature is less obvious due to the considerable scatter seen in the data. Degradation rates would be expected to increase with temperature up to a maximum temperature determined by the organisms present.

Table F.9: Summary of Cellulose Waste Degradation Rates

Aerobic Degradation Rates (a^{-1})				
Water Content		**Temperature (^oC)**		
		10	**20-25**	**≥30**
Saturated	Brine		$2.2x10^{-3}$	$3.6x10^{-4}$ to $8.6x10^{-3}$
	Water	$3.0x10^{-4}$	$1.5x10^{-2}$ $3.5x10^{-3}$	
Humid			[a] $2.0x10^{-3}$	[b] $1.8x10^{-2}$
Dry		1.5 $x10^{-3}$ to 3.7 $x10^{-3}$		
Anaerobic Degradation Rates (a^{-1})				
Water Content		**Temperature (^oC)**		
		10	**20-25**	**≥30**
Saturated	Brine		$2.2x10^{-4}$	$1.3x10^{-3}$ to $3.6x10^{-3}$ $3.5x10^{-5}$ to $1.6x10^{-4}$
	Water	$2.9x10^{-2}$ to $1.0x10^{-2}$ $3.8x10^{-1}$ $3.1x10^{-2}$	$2.7x10^{-2}$ to $1.2x10^{-1}$ $3.1x10^{-2}$ to $1.9x10^{-1}$ $9.9x10^{-3}$	
Humid		[c] $5.2x10^{-3}$ to $6.4x10^{-3}$	[a] $5.6x10^{-3}$	[b] $3.0x10^{-3}$ to $1.5x10^{-2}$
Dry		$7.5x10^{-5}$ to $6.0x10^{-3}$		

Notes: [a] 1 wt% water present, [b] RH=70-74%, [c] water content not specified

Considering the wide range of rates and conditions summarized in Table F.9, in order to derive best estimates and ranges, emphasis is given to the rates from studies at less than 25 ^oC and, where possible, to those produced in the presence of brine and with lower water content. The aerobic rates ranged from $1.5x10^{-2}$ to $3x10^{-4}$ a^{-1}. Consequently, a rate of $1.5x10^{-3}$ a^{-1} is taken as the midpoint (best estimate) with an order of magnitude variation either side to reflect the spread seen in the data. There are more anaerobic rates so emphasis is placed on those that might better reflect repository conditions, i.e., those from brine experiments and low water content. This gives a range of $5.2x10^{-3}$ to $7.5x10^{-5}$ a^{-1}. Consequently, a rate of $5.0x10^{-4}$ a^{-1} is taken as the midpoint (best estimate) with an order of magnitude uncertainty either side.

F.3 ION EXCHANGE RESIN DEGRADATION

Bowerman et al. (1988) published some of the earliest data on the degradation of ion exchange resins. Data on carbon dioxide evolution from dewatered resins incubated at 37°C are provided in the report. The resins concerned were taken from filter units of the High Flux Beam reactor at BNL and consisted of Amberlite IR-200 cation exchange resins and a mixed resin composed of Amberlite IR-200 and IRA-400. Although not explicitly stated in the report it appears that these resins were incubated under aerobic conditions. Consequently the degradation rate was calculated using the aerobic degradation of the polystyrene backbone of the resins. Taking the average values published, calculated rates of resin degradation are 9.8×10^{-4} a^{-1} for cation exchange resins and 4.3×10^{-4} a^{-1} for the mixed resins.

Resin degradation data on OPG stored resins is provided by Husain and Jain (2003) who provided both carbon dioxide and methane generation rates. Taking the geometric mean values quoted and assuming complete resin degradation, it was possible to calculate resin degradation rates of 1.8×10^{-9} a^{-1} (based on the methane generation rate) and 1.09×10^{-7} a^{-1} (based on the carbon dioxide generation rate).

Data on resin degradation has also been generated by the German radioactive waste disposal program (Kannen and Muller 1999, Bracke and Muller 2003, Bracke et al. 2004, Bracke and Muller 2007). The data appears to come from a combination of real waste packages and laboratory-based experiments. The rates are expressed in terms of m^3 of gas generated per tonne of waste per year. This data was converted to resin degradation rates (Table F.10) using the stoichiometry of the reaction, a temperature of 20°C.

Data on IX resin degradation under anaerobic conditions are given in Wiborgh et al. (1986) as part of a review of gas formation and transport for the Swiss radioactive waste disposal program. Wiborgh et al. (1986) note that the porous structure of the resins increases the surface available to microorganisms. They give a resin degradation rate of up to 0.01 moles of gas kg^{-1} a^{-1}.

A summary of the resin degradation rates calculated in this section is given in Table F.10.

Table F.10: Resin Degradation Rates

Source	Degradation Rate (a^{-1})	
	Aerobic	Anaerobic
Bowerman et al. (1988)	4.3×10^{-4} to 9.8×10^{-4}	
Wiborgh (1986)		0 to 3.0×10^{-4}
Husain and Jain (2003)		1.0×10^{-7} to 1.8×10^{-9}
Bracke et al. (2004)		1.6×10^{-5} to 6.5×10^{-4}

In conclusion, there is a limited amount of data available for resin degradation and these data require more assumptions in order to calculate rates of degradation from the gas generation values provided. In the case of aerobic degradation only one data set was available covering two types of resin. In this case a rate of 5.0×10^{-4} a^{-1} with a range of 1.0×10^{-4} to 1.0×10^{-3} a^{-1} is recommended for modelling and sensitivity studies. In the case of anaerobic resin degradation, the recommended rate is 5.0×10^{-5} a^{-1} which is an order of magnitude lower than that employed

for aerobic degradation and lies within the range of data from Bracke et al. (2004) and Wiborgh et al. (1986). A range of values from $5.0x10^{-6}$ to $5.0x10^{-4}$ a^{-1} would be appropriate for sensitivity studies. This reflects the added uncertainty in the values indicated by the rates derived from the work of Husain and Jain (2003) (although the very low rates reported by Husain and Jain (2003) have not been included in this range).

F.4 PLASTIC AND RUBBER DEGRADATION

The plastic and rubber components of radioactive waste represent a heterogeneous mix of materials such as PVC, polyethylene, neoprene, nitrile, and latex. The heterogeneous nature of this waste category makes it difficult to model since the degradation of each material would have to be modelled explicitly with an individual inventory and reaction scheme for each component.

A number of authors have suggested that plastic waste components such as PVC and polyurethane are recalcitrant under repository conditions (Grant et al. 1997, BNFL 2002b). BNFL (BNFL 2002b) stated in documentation supporting the 2002 Drigg safety case that: "*The current available information would suggest that the majority of the higher molecular weight polymers would remain undegraded for a considerable length of time, particularly addition polymers*." This position is supported by the work of Francis et al. (1997) who found no evidence of biodegradation of electron beam irradiated plastic and rubber.

A more recent review by Cohen (2006) for the WIPP project concluded that some degradation of plastics and rubbers "*may occur over 10,000 years in the WIPP repository*." This conclusion appears to be based on the fact that oxidation and radiation damage may enhance biodegradation of these materials or generate soluble intermediates amenable to microbial attack. The authors point out that much of the evidence for the microbial degradation of these materials comes from aerobic systems, but they do not rule out the possibility of anaerobic microbial degradation.

NAGRA (2004) uses a gas generation rate of 0.05 mol kg^{-1} a^{-1} for general plastics, resin and bitumen in LLW, equivalent to a degradation rate of about $7x10^{-4}$ a^{-1}, but noted that these are about a factor of ten higher than measurements. Yim and Caron (2006) propose rates of $9x10^{-4}$ a^{-1} for moderately biodegradable plastics, and $3.5x10^{-4}$ a^{-1} for recalcitrant organics.

In order to assess the impact of potential plastic and rubber degradation on the overall gas generation in the repository these components are modelled in the same manner as ion exchange resins. This allows their impact to be assessed without the need for detailed degradation pathways for each component.

F.5 BIOMASS DEGRADATION

Microbial biomass generated through the degradation of waste components may itself be subject to further degradation. In order to allow for this biomass recycling, it is necessary to partition biomass into a degradable and a recalcitrant fraction. A wide variety of biodegradation fractions can be found in the literature mainly derived for sewage treatment and algal biomass studies (Table F.11). However, it should be noted that many of these studies have been carried out over timescales that are much shorter than those associated with radioactive waste disposal. Consequently they may underestimate the degradability of microbial biomass by not taking into account the slowly degradable biomass constituents.

Table F.11: Biomass Recycle Fractions

Conditions	% Degradability	Reference
Aerobic	68	Arnarson and Keil (2005)
Aerobic	82	Caradec et al. (2004)
Aerobic	90	Harvey and Macko (1997)
Aerobic	92	Henze et al. (2000)
Anoxic	71	Harvey and Macko (1997)
Anoxic	77	Caradec et al. (2004)
Anaerobic	40 to 60	Foree and McCarthy (1970)

REFERENCES FOR APPENDIX F

Agg, P.J., R.S. Billington and Y. Gunn. 1997. Preliminary Testing of the Gas Generation Model GAMMON using Data from Drums Containing Low-Level Waste Simulant. UK Nirex Report NSS/R299. Harwell, United Kingdom.

Agg, P.J., A. Arcus, D. Blackwood, P.L. FitzGerald, G.J. Holtom, T.R. Lineham, A. Rosevear and N.R. Smart. 2002a. The Gas Generation Programme GAMMON : I. Model Calibration. UK Nirex Report AEAT/ERRA-0307. Harwell, United Kingdom.

Agg, P.J., A. Arcus, D. Blackwood, P.L. FitzGerald, G.J. Holtom, T.R. Lineham, A. Rosevear and N.R. Smart. 2002b. The Gas Generation Programme GAMMON : II. A Blind Validation Test. UK Nirex Report AEAT/ERRA-0320. Harwell, United Kingdom.

Arnarson, T.S. and R.G. Keil. 2005. Influence of Organic-mineral Aggregates on Microbial Degradation of the Dinoflagellate Scrippsiella trochoidea. Geochimica et Cosmochimica Acta 69(8), 2111-2117.

Beadle, I. 2001. Gas Monitored Trench Simulants, Progress Report. DTP 01/02 TN106. Drigg Technical Programme, BNFL, United Kingdom.

Beadle, I. 2002. Long Term Trench Experiment, Progress Report. DTP 02/03 TN120. Drigg Technical Programme, BNFL, United Kingdom.

BNFL. 2002a. Drigg Post-Closure Safety Case. British Nuclear Fuels plc, September 2002. BNFL, United Kingdom.

BNFL. 2002b. Potential for the Degradation of High Molecular Weight Synthetic Organic Polymers DTP/90. BNFL, United Kingdom.

Bowerman, B.S., J.H. Clinton and S.R. Cowdery. 1988. Biodegradation of Ion Exchange Media. NUREG/CR-5221, BNL-NUREG-52163, Brookhaven National Laboratory, New York, USA.

Bracke, G. and W. Muller. 2003. Modelling Gas Generation of Intermediate and Low Level Radioactive Wastes. Proceedings of the Radioactive Waste Management and Environmental Remediation Conference. Sept 21-25, 2003, Oxford, United Kingdom.

Bracke, G. and W. Muller. 2007. Considerations on the Release of C-14 from a Closed Final Repository for Low-Level Radioactive Waste. Proceedings of WM'07, Tucson, USA.

Bracke, G., W. Muller and K. Kugel. 2004. Derivation of Gas Generation Rates for the Morsleben Radioactive Waste Repository. Proceeding of the Proceeding of the DisTec Conference, April 26-28, Berlin, Germany.

Caldwell, D.E., R.C. Hallet, M.A. Molecke, E. Martinez and B.J. Barnhart. 1988. Rates of CO_2 Production from the Microbial Degradation of Transuranic Wastes under Simulated Geologic Isolation Conditions. Sandia Report SAND87-7170, Sandia National Laboratory Albuquerque, USA.

Caradec, S., V. Grossi, F. Gilbert, C. Guigue and M. Goutx. 2004. Influence of various redox conditions on the degradation of microalgal triacylglycerols and fatty acids in marine sediments. Organic Geochemistry 35, 277-287.

Cohen, S. 2006. Preliminary review of the degradation of cellulosic, plastic, and rubber materials in the Waste Isolation Pilot Plant, and possible effects on magnesium oxide safety factor calculations. Contract Number EP-D-05-002. Work Assignment No. 2-09, S. Cohen & Associates, Vienna, USA.

Felicione, F.S., K.P. Carney, C.C. Dwight, D.G. Cummings and L.E. Foulkrod. 2003. Gas-Generation Experiments for Long-Term storage of TRU Wastes at WIPP. Proceedings Waste Management WM'03, Tucson, USA.

Foree, E.G. and P.L. McCarthy. 1970. Anaerobic Decomposition of Algae. Environmental Science and Technology 4(10), 842-849.

Francis, A.J., J.B. Gillow and M.R. Giles. 1997. Microbial Gas Generation Under Expected Waste Isolation Pilot Plant Repository Conditions. Sandia report SAND96-2582. Sandia National Laboratory, Albuquerque, USA.

Grant, W.D., G.J. Holtom, A. Rosevear and D. Widdowson. 1997. A review of environmental microbiology relevant to the disposal of radioactive waste in a deep underground repository. UK Nirex Report NSS R329. Harwell, United Kingdom.

Harvey, H.R. and S.A. Macko. 1997. Kinetics of phytoplankton decay during simulated sedimentation: changes in lipids under oxic and anoxic conditions. Organic Geochemistry 27(3/4), 129-140.

Henze, M., W. Gujer, T. Mino and M. von Loosdrecht. 2000. Activated Sludge Models ASM1, ASM2D and ASM3. Scientific and Technical Report No 9, IWA Publishing, London, United Kingdom.

Husain, A. and D. Jain. 2003. Chemical Radiochemical and Microbiological Characterisation of the Contents of Resin Liners Sampled at the Western Waste Management Facility in 2002. Kinectrics Report 9820-090-RA-0001-R00. Toronto, Canada.

Kannen, H. and W. Muller. 1999. Gas Generation of Radioactive Wastes – Comparison Between Laboratory Experiments and Measurements on Real Wastes. Proceedings of the Radioactive Waste Management and Environmental Remediation Conference, September 26-30, Nagoya, Japan.

NAGRA. 2004. Effects of Post-disposal Gas Generation in a Repository for Spent Fuel, High-level Waste and Long-lived Intermediate Level Waste Sited in Opalinus Clay. Nagra Technical Report 04-06. Wettingen, Switzerland.

Rittmann, B.E. and P.L. McCarty. 2001. Environmental Biotechnology: Principles and Applications. McGraw –Hill. USA.

Skagius, K., M. Lindgren and K. Pers. 1999. Gas Generation in SFL 3-5 and Effects on Radionuclide Release. SKB report R-99-16. Stockholm, Sweden.

Small, J.S., M. Nykyri, N. Paaso, U. Hovi, M. Itavaara and T. Sarlin. 2005. Testing of a Near-Field Biogeochemical Model Against Data From a Large-Scale Gas Generation Experiment. Proceedings, MRS Scientific Basis of Nuclear Waste Management, Ghent, Belgium.

Sun, C. 2005. True Density of Microcrystalline Cellulose. Journal of Pharmaceutical Science 94 (10), 2132-2134.

Wiborgh, M., L.O. Höglund and K. Pers. 1986. Gas Formation in a L/ILW Repository and Gas Transport in the Host Rock. Nagra Technical Report 85-17. Baden, Switzerland.

Yim, M.S. and F. Caron. 2006. Life cycle and Management of Carbon-14 from Nuclear Power Generation. Progress in Nuclear Energy 48, 2–36.

Yim, M.S. and S. Simonson. 1997. Technical Issues and Low Level Waste Performance Assessment: ^{14}C in Disposal Facilities. EPRI Report TR-107995. Palo Alto, USA.

APPENDIX G: GAS-WATER PARTITION COEFFICIENTS FOR VOLATILE CONTAMINANTS

G.1. INTRODUCTION

Iodine, chlorine and selenium released from the wastes will dissolve in water in the repository. These radionuclides may subsequently be volatilized, and enter the gas phase prior to complete resaturation of the repository. Volatilization can be described using gas-water partition coefficients which are derived by taking the concentration of the element in gas and dividing it by the concentration in water. These coefficients are derived from the literature reviews described below.

G.2. IODINE AND CHLORINE

ANDRA (2005a,b) state that chlorine and iodine are not volatile under repository conditions. Any iodine or chlorine gases rapidly hydrolyze to form non-volatile and stable iodide and chloride ions. They have similar considerations for methylated chloride and iodide. This concurs with the treatment by Nagra (cited by ANDRA).

Lemire et al. (1981) details gas-water partition coefficients for iodine based on thermodynamic calculations for iodine solutions and literature reviews. The peak partition coefficient from thermodynamic calculations for repository conditions is 10^{-5} (volumetric concentration in gas/volumetric concentration in water) at pH 5, falling to 10^{-7} at pH 7. However, the thermodynamic calculations do not include organic compounds such as methylated iodine. Slightly greater partition coefficients have been observed for marine systems due to methylation of iodine, and large-scale reactor accident simulations indicate that methyl-iodine is the dominant airborne species. A partition coefficient of 10^{-4} has often been used for safety analysis of nuclear reactor accidents. Conservatively, this value is chosen for the DGR assessment.

Chlorine is much less volatile than iodine and this can be understood in terms of the difference between the electrochemical potentials for chlorine and iodine oxidation (CRC 2006):

$$2Cl^- = Cl_2 + 2e^- \qquad E° = -1.36V$$

$$2I^- = I_2 + 2e^- \qquad E° = -0.54V$$

A partition coefficient of 10^{-6} is chosen.

G.3. SELENIUM

In the absence of oxygen, i.e., under repository conditions, selenium may be present in the elemental form or as selenides. Selenium may be methylated and volatilized as dimethylselenide $Se(CH_3)$ or dimethyldiselenide $Se_2(CH_3)_2$ as a result of biological reduction, whereas inorganic volatilization is unlikely.

The generation of methylated forms of selenium appears to be a detoxification process employed by a wide range of microorganisms to deal with the toxic oxianions of selenium namely selenate and selenite (Stolz et al. 2006). Although the generation of methylated selenium compounds has been attributed to both aerobic and anaerobic environments, generation under anaerobic conditions can be considerably reduced and often undetectable (Hapuarachchi et al. 2004; Haudin et al. 2007; Zannoni et al. 2008) even though bacteria able to generate methylselenium can be cultured from these or similar environments (Chasteen and Bentley 2003; Dungan and Frankenberger 2000; Meyer et al. 2007).

Under anaerobic conditions the fate of selenium is determined by competing reduction and methylation reactions with the dominant form of selenium being elemental selenium (Se^0) generated by the microbial reduction of oxidized forms such as selenate and selenite (Stolz et al. 2006; Zannoni et al. 2008; Stolz and Oremland 1999). Stolz and Ormland (1999) suggest that bacteria capable of selenium reduction are abundant in nature. In anaerobic experiments containing selenite undertaken by Hapuarachchi et al. (2004), <0.1% of added selenium was lost in a volatile organic form. Anaerobic soil experiments funded by ANDRA (Haudin et al. 2007) demonstrated that added selenium was strongly immobilized within the system. In this study the reduction and immobilization of selenium was enhanced by the addition of a cellulose source (straw), a situation comparable (to a limited extent) with cellulose containing radioactive waste. Pure culture experiments with selenite (Dungan and Frankenberger 2000) demonstrated that the partitioning between methylation and reduction is inversely dependent on the starting concentration with methylated forms being enhanced at low selenite concentrations (10 μM) and reduction more dominant at higher concentrations (1 mM).

Not only is selenium reduction the dominant process in anaerobic environments it is also likely that selenium methylation and reduction are mutually exclusive processes (Zannoni et al. 2008) with the highly insoluble selenium metal being a stable sink for selenium within anaerobic systems (Knotek-Smith et al. 2006). The stability of reduced selenium appears to be further enhanced by reactions with iron corrosion products (Knotek-Smith et al. 2006), a situation which has similarities with the environment present in a radioactive waste disposal site.

The published data on selenium suggests that although the formation of methylated selenium compounds cannot be ruled out, the dominant process under anaerobic conditions is more likely to be selenium reduction with enhanced immobilization occurring through interactions with anaerobic corrosion products. Conservatively, it is assumed that the gas-water partition coefficient for selenium is the same as for iodine, i.e., 10^{-4}.

REFERENCES FOR APPENDIX G

ANDRA. 2005a. Dossier Argile. Phenomenological Evolution of a Geological Repository. Paris, France.

ANDRA. 2005b. Dossier Argile. Safety Evaluation of a Geological Repository. Paris, France.

Chasteen, T.G. and R. Bentley. 2003. Biomethylation of Selenium and Tellurium: Microorganisms and Plants. Chemical Reviews 103(1), 1-25.

CRC. 2006. Handbook of Chemistry and Physics. 87th edition, Chemical Rubber Company CRC Press. Boca Raton, USA.

Dungan, R.S. and W.T. Frankenberger. 2000. Factors Affecting the Volatilization of Dimethylselenide by Enterobacter Cloacae SLD1a-1. Soil Biology & Biochemistry 32(10), 1353-1358.

Hapuarachchi, S., J. Swearingen and T.G. Chasteen. 2004. Determination of Elemental and Precipitated Selenium Production by a Facultative Anaerobe Grown under Sequential Anaerobic/aerobic Conditions. Process Biochemistry 39, 1607-1613.

Haudin, C.S., M.L. Fardeaud, L. Amenc, P. Renault, B. Ollivier, E. Leclerc-Cessac and S. Staunton. 2007. Responses of Anaerobic Bacteria to Soil Amendment with Selenite. Soil Biology & Biochemistry 39, 2408-2413.

Knotek-Smith, H.M., D.L. Crawford, G. Möller and R.A. Henson. 2006. Microbial Studies of a Selenium-contaminated Mine Site and Potential for On-site Remediation. Journal of Industrial Microbiology and Biotechnology 33, 897-913.

Lemire, R., J. Paquette, D.F. Torgerson, D.J. Wren and J.W. Fletcher. 1981. Assessment of Iodine behaviour in Reactor Containment Buildings from a Chemical Perspective. Atomic Energy of Canada Ltd. Report AECL-6812. Pinawa, Canada.

Meyer, J., A. Schmidt, K. Michalke and R. Hensel. 2007. Volatilization of Metals and Metalloids by the Microbial Population of an Alluvial Soil. Systematic and Applied Microbiology 30, 229-238.

Stolz, J.F., P. Basu, J.M. Santini and R.S. Oremland. 2006. Arsenic and Selenium in Microbial Metabolism. Annual Review of Microbiology 60, 107-130.

Stolz, J.F. and R.S. Oremland. 1999. Bacterial Respiration of Arsenic and Selenium. FEMS Microbial Reviews 23, 615-627.

Zannoni, D., F. Borsetti, J.J. Harrison and R. Turner. 2008. The Bacterial Response to the Chalcogen Metalloids Se and Te. Advances in Microbial Physiology 53, 1-72.

THIS PAGE HAS BEEN LEFT BLANK INTENTIONALLY

APPENDIX H: CALCULATION OF PACKAGING VOIDAGE

H.1 INTRODUCTION

Most of the containers and overpacks (packaging) used for OPG's wastes will involve a degree of "void" space in the total volume that it occupies in the repository. For example, many containers have 4" risers at their base which are accounted for in the total height occupied by the container. As this unused space is an important part of the total voidage of the repository, it is necessary to determine an estimate of the packaging voidage.

The packaging voidage can be calculated by taking the emplaced volume (Table 4.6) and subtracting the sum of the raw waste volume (Table 3.11) and the packaging volume (derived below). The packaging (container and overpack) volume can be calculated in a number of ways, for example:

- By subtracting the internal volume from the external volume quoted by OPG (2010) for each waste package; or
- By calculating the volume of the container from its surface area and wall thickness, and subtracting this from the reported external volume.

In the current assessment, the latter approach is used, except where the wall is thick in comparison to the overall waste packaging dimensions (as is the case for overpacks and retube waste containers). For overpacks and retube waste containers, the volume of the container is calculated using the former approach (i.e., the difference of the external and internal volume of the container).

H.2 CONTAINER VOLUME

The calculated volume associated with waste containers is presented in Table H.1. Here, the surface area and wall thickness relate to the reference waste containers described in Section 3.2 of the main text, with the container numbers being obtained from OPG (2010). Steam generators and "other" non-processible wastes are assumed to be emplaced directly and therefore no waste container volume is calculated and these wastes are not included in the table.

H.3 OVERPACK VOLUME

Some wastes are to be overpacked prior to placement in the DGR, specifically: all ash waste; LLW resins; ALW sludges; and ILW resins. The overpacks are intended to provide additional shielding and facilitate operational management of the wastes. As the overpacks are characterized by thick walls and simple geometry, the approach to calculating the volume of overpacks is the same as that applied to retube waste containers – i.e., the difference between the external and internal volume reported in OPG (2010). Table H.2 presents the volume of overpacks calculated with this method.

Table H.1: Emplaced Container Volume

Waste Category	Surface Area (m^2)	Wall Thickness (m)	Containers	Total Container Volume# (m^3)
Bottom ash	10.9	0.0034	882	32.7
Baghouse ash	10.9	0.0034	218	8.1
Compacted wastes (bales)	14.0	0.0016	1,383	31.0
Compacted wastes (boxes)	11.8	0.0046	6,135	333.0
Non-processible (drums)	11.9	0.0065	7,840	606.5$
Non-processible (boxes)	13.0	0.0027	24,190	849.1
LLW resins and ALW resins	11.4	0.0016	2,165	39.5
ALW sludges	11.9	0.0027	1,709	54.9
CANDECON resins	13.4	0.0063	503	42.5
Moderator resins	13.4	0.0063	430	36.3
PHT resins	13.4	0.0063	301	25.4
Misc. resins	13.4	0.0063	403	34.0
Irradiated core components, Filters and filter elements, IX columns	20.8	0.01	4,459	927.5
Waste Category	**Internal Volume (m^3)**	**External Volume (m^3)**	**Containers**	**Total Container Volume~ (m^3)**
Retube Wastes (Pressure Tubes)	0.8	7.7	242	1669.8
Retube Wastes (End Fittings)	2.7	10.9	899	7371.8
Retube Wastes (Calandria Tubes)	0.8	7.7	167	1152.3
Retube Wastes (Calandria Tube Inserts)	0.8	7.7	45	310.5

Notes:
Steam generators and "Other" non-processible wastes are assumed to be emplaced directly and therefore no waste package voidage is calculated and these wastes are not included in the table.

Container volume calculated as *surface area x thickness x number of containers*.
~ Container volume calculated as (external volume – internal volume) x number of containers.
^ Weighted average wall thickness, assuming 5 mm for the drum bin and 2.6 mm for the drums.
$ Accounts for 6 drums in one drum bin.

Table H.2: Overpack Volume

Waste	Internal Volume (m^3)	External Volume (m^3)	Overpacks	Total Overpack Volume~ (m^3)
Bottom ash	6.56	8.5	882	1711.1
Baghouse ash	6.56	8.5	218	422.9
Non-processible (drums)	6.56	8.5	323~	625.7
LLW resins	6.56	8.5	80#	155.2
ALW sludges	6.56	8.5	1709	3315.5
CANDECON resins	6	16.2	256*	2565.3
Moderator resins	6	16.2	430	2193.0
PHT resins	6	16.2	301	1535.1
Misc. resins	6	16.2	403	2055.3

Notes:
~ 10% of drum racks are overpacked in LLW container overpacks (see Table 2.1 of OPG 2010). There are 3,225 drum racks (see Table 2.9 of OPG 2010).
* Two CANDECON resin containers can be contained in each resin overpack.
\# Low level resin boxes are overpacked in LLW container overpacks (see Table 2.1, OPG 2010). There are 80 low level resin boxes (see Table 2.9, OPG 2010).

H.4 PACKAGING VOIDAGE

The above calculations yield a total volume of containers of 13,525 m^3 and a total volume of overpacks of 14,579 m^3. As noted above, the total additional voidage in the wastes associated with waste packaging can be calculated as the difference between the emplaced volume, and the sum of the raw waste volume, container and overpack volumes.

For waste emplaced in Panel 1, this gives a total packaging voidage of:

- 68,153 m^3 - (37,118 m^3 + 8,173 m^3 + 7,032 m^3) = 15,830 m^3

For waste emplaced in Panel 2, this is gives a total packaging voidage of:

- 132,490 m^3 - (78,454 m^3 + 5,351 m^3 + 7,547 m^3) = 41,138 m^3

REFERENCES FOR APPENDIX H

OPG. 2010. Reference Low and Intermediate Level Waste Inventory for the Deep Geologic Repository. Ontario Power Generation Report 00216-REP-03902-00003-R003. Toronto, Canada.